Influenza vaccine development: immunogenicity and correlates of protection

Alexander I. Makarkov
Division of Experimental Medicine
McGill University, Montreal
August 2018

A thesis submitted to McGill University in partial fulfillment of the requirements of the degree of Doctor of Philosophy

Abstract

Influenza viruses cause significant morbidity and mortality worldwide. Vaccines are the best tools available to reduce the disease burden; however, vaccine effectiveness varies significantly between years, target populations and strains. Medicago Inc. has developed a highly efficient platform to produce plant-derived virus-like particle (VLP) vaccines bearing influenza hemagglutinin (HA) that have been shown to elicit strong humoral and $CD4^+$ T cell responses in both pre-clinical and clinical studies. To better understand the immunogenicity of these vaccines, we studied the early interactions of VLPs with antigen-presenting cells (APC) *in vitro*. We demonstrated that VLPs bind to human monocytoid U-937 cells and monocyte-derived macrophages (MDMs) in a sialic acid-dependent manner. VLP attachment to the cell surface led to internalization, trafficking to acidic cell compartments and fusion of the VLP lipid envelope with endosomal membranes. Incubation of MDMs with VLPs bearing H1 (HA sequence from A/California/07/2009 (H1N1) strain) but not H5 (HA sequence from A/Indonesia/05/2005 (H5N1) induced proliferation of autologous lymphoid cells suggesting antigen processing by MDMs and stimulation of a memory T cell response. Pulse-exposure of MDMs with H1-VLPs resulted in a rapid and massive intracellular accumulation of HA that was driven by clathrin-mediated and clathrin-independent endocytosis as well as macropinocytosis/phagocytosis. The H1-VLPs endosomal distribution pattern suggested that HA delivered by VLP had entered both high-degradative late (supporting major histocompatibility complex (MHC) II-restricted antigen presentation) and low-degradative static early and/or recycling (favoring MHC I-restricted antigen cross-presentation) endosomal pathways. High-resolution tandem mass spectrometry identified a large number of HA-derived peptides associated with MHC I in the H1-VLP-treated MDMs. In addition, many host-derived MHC I peptides were identified in VLP-treated samples. These peptides were mainly processed by matrix metalloproteinases and cathepsins. The host proteins associated with these peptides were primarily involved in pathways modulating inflammation (i.e. stimulation and attenuation), innate and adaptive immunity, clathrin-mediated endocytosis, protein synthesis and endo-lysosomal degradation. Finally, tools we used while studying endosome-lysosome fusion led to the development of a novel serological assay for influenza based on 1,1'-dioctadecyl-3,3,3',3'-tetramethylindodicarbocyanine perchlorate (DiD) fluorescence dequenching. This assay measures 'functional' influenza antibody titers, is free from observer bias and has the potential to be fully automated. In summary, we demonstrated

that HA delivery to APCs in a form of plant-derived VLPs facilitates antigen uptake, endosomal processing, presentation and cross-presentation. These observations may help to explain the broad and cross-reactive immune responses generated by VLP vaccines. The new DiD fluorescence dequenching assay we developed may give new insights into the spectrum of antibodies produced in response to influenza infection or vaccination.

Résumé

Les virus grippaux entraînent une morbidité et une mortalité significatives dans le monde entier. Les vaccins sont les meilleurs outils disponibles pour réduire le fardeau de cette maladie; cependant, l'efficacité du vaccin varie de manière significative entre les années, les populations cibles et les souches. Medicago Inc. a développé une plate-forme hautement efficace pour produire des vaccins à particules pseudo-virales (VLP) d'origine hémagglutinine (HA) dérivées de plantes qui ont démontré une forte réponse humorale et lymphocytaire T $CD4^+$ dans les études précliniques et cliniques. Pour mieux comprendre l'immunogénicité de ces vaccins, nous avons étudié les interactions précoces des VLP avec des cellules présentatrices d'antigènes (APC) in vitro. Nous avons démontré que les VLP se lient aux cellules monocytaires humaines U-937 et aux macrophages dérivés des monocytes (MDM) d'une manière dépendante de l'acide sialique. La fixation des VLP à la surface cellulaire a conduit à l'internalisation, au trafic vers les compartiments cellulaires acides et à la fusion de l'enveloppe lipidique VLP avec les membranes endosomales. L'incubation des MDM avec des VLP portant H1 (séquence HA de la souche A/California/07/2009 (H1N1) mais pas H5 (séquence HA de A/Indonesia/05/2005 (H5N1) induit une prolifération de cellules lymphoïdes autologues suggérant un traitement antigénique par MDMs et la stimulation d'une réponse lymphocytaire mémoire L'exposition pulsatile des MDM aux H1-VLP a entraîné une accumulation intracellulaire rapide et massive d'HA causée par l'endocytose induite par la clathrine et la clathrine ainsi que par la macropinocytose/phagocytose. La distribution endosomale de VLP suggérait que la HA délivrée par VLP était entrée à la fois dans les voies endosomiques tardives à haute dégradation (soutenant la présentation d'antigènes restreints au complexe majeur d'histocompatibilité (CMH) II) et dans les voies endosomiques statiques et/ou de recyclage statiques à faible dégradation (favorisant la présentation croisée de l'antigène du CMH I). La spectrométrie de masse en tandem à haute résolution a permis d'identifier un grand nombre de peptides dérivés de HA associés au CMH I dans les MDM H1-VLP traités. Les peptides du CMH I ont été identifiés dans des échantillons traités par VLP. Ces peptides ont été principalement traités par des métalloprotéinases matricielles et des cathepsines. Les protéines hôtes associées à ces peptides étaient principalement impliquées dans les voies modulant l'inflammation (c'est-à-dire la stimulation et l'atténuation), l'immunité innée et adaptative, l'endocytose médiée par la clathrine, la synthèse protéique et la dégradation endo-lysosomale. Enfin, les outils que nous avons utilisés lors de l'étude de la fusion endosome-

lysosome ont conduit au développement d'un nouveau test sérologique de la grippe basé sur l'extinction de fluorescence 1,1'-dioctadécyl-3,3,3 ', 3'-tétraméthylindodicarbocyanine perchlorate (DiD). Ce test mesure les titres d'anticorps de la grippe 'fonctionnels', est exempt de biais observateur et a le potentiel d'être entièrement automatisé. En résumé, nous avons démontré que la délivrance de HA aux CPA dans une forme de VLP dérivée de plantes facilite l'absorption d'antigène, le traitement endosomal, la présentation et la présentation croisée. Ces observations peuvent aider à expliquer les réponses immunitaires larges et réactives croisées générées par les vaccins VLP. Le nouveau test d'extinction de fluorescence DiD que nous avons développé pourrait donner de nouvelles perspectives sur le spectre des anticorps produits en réponse à une infection grippale ou à la vaccination.

Acknowledgments

First and foremost, I would like to thank my supervisor Dr. Brian J. Ward. Thank you for always believing in me. I know it was not an easy decision, but you gave me a chance to step in the same river a second time. Thank you for the continuous support of my study, for your patience, motivation, and immense knowledge. Thank you for giving me the freedom to explore the diverse aspects of the project, learn different experimental approaches and techniques. It was a great privilege and an honor for me to work in your lab and become a member of the extraordinary team.

I would like to thank my colleagues and friends Dr. Sabrina Chierzi, Dr. Makan Golizeh, Aakash Patel and Ian Noel Costas Cancelas for our collaborative work, helpful and encouraging discussions, our crazy experiments, and for time spent together. I am sincerely grateful to all the members of the Ward/Ndao lab. You became my true family in these four years!

I would also like to thank my committee members Drs. Connie Krawczyk, Jerry Aldridge, Salman Qureshi, Martine Culty and Giovanni Di Battista. Our meetings let me look critically at my work, and your guidance helped me to move forward with the project. My sincere thank you also goes to Drs. Isabelle Rouiller, Paul Wiseman and Angelica Gopal who generously supported key steps of the study.

I greatly appreciate the encouragement and support from my dear friends and colleagues Drs. Natalia P. Sanina, Tobias Schmidt and Ilia V. Baskakov who made this amazing endeavor possible.

I am grateful to the scientists and managers at Medicago, Inc. who developed a striking product and let me study it, explore its exciting features, present and publish the results of our experiments. Thank you for your encouraging attitude, kindness and support for my work.

Almost 30 years ago, I made my first diffident steps in research, and I think it is the right moment to express my deep and sincere gratitude to my teachers and mentors at the Russian State Medical University, Drs. Valery S. Kurmangaliev, Andrey N. Samsonov, Jean M. Salmasi, Yuri S. Sverdlov and Gennady V. Poriadin. Time is relentless, and not all of them are with us today.

Last but not the least, I would like to thank my dear parents, my brother and my friends-for-life for helping me, listening to me and being with me, and just for my life.

Thank you all for everything!

Contribution of authors

The candidate has chosen to present a manuscript-based thesis. This thesis contains four manuscripts and is in accordance with the 'Preparation of a Thesis' guidelines provided by the Faculty of Graduate and Postdoctoral Studies of McGill University. The candidate is recognized as the principal author and has performed the majority of the work in the manuscripts presented. The manuscripts included in this thesis are:

Chapter 2: Alexander I. Makarkov, Sabrina Chierzi, Stéphane Pillet, Keith K. Murai, Nathalie Landry, Brian J. Ward. Plant-made virus-like particles bearing influenza hemagglutinin (HA) recapitulate early interactions of native influenza virions with human monocytes/macrophages. *Vaccine* 2017;35(35 Pt B):4629-4636.

Chapter 3: Alexander I. Makarkov, Makan Golizeh, Angelica A. Gopal, Ian N. Costas-Cancelas, Sabrina Chierzi, Stephane Pillet, Nathalie Charland, Nathalie Landry, Isabelle Rouiller, Paul W. Wiseman, Momar Ndao, Brian J. Ward. Plant-derived virus-like particle vaccines drive cross-presentation of influenza A hemagglutinin peptides by human monocyte-derived macrophages. Submitted to *npj Vaccines.*

Chapter 4: Makan Golizeh[†], Alexander I. Makarkov[†], Brian J. Ward, Momar Ndao. MHC I-restricted immunopeptidomics analysis of human monocyte-derived macrophages exposed to biological nanoparticles bearing influenza hemagglutinin. Submitted to *Molecular & Cellular Proteomics.*

[†] These authors contributed equally.

Chapter 5: Alexander I. Makarkov[†], Aakash Patel[†], Valentine Bainov, Brian J. Ward. A novel serological assay for influenza based on DiD fluorescence dequenching that is free from observer bias and potentially automatable - A proof of concept study. *Vaccine* 2018;36(30):4485-4493.

[†] These authors contributed equally.

For Chapter 2, the candidate and Dr. Brian J. Ward developed the concept and designed the study. The candidate and Dr. Sabrina Chierzi performed imaging experiments and analyzed imaging data; other experiments were performed and analyzed by the candidate. The candidate wrote the manuscript with significant editorial assistance from Dr. Brian J. Ward. All authors provided editorial input and approved the final version of the article prior to its submission.

For Chapter 3, the candidate and Dr. Brian J. Ward developed the concept and designed the study. The endocytic mechanisms studies, confocal imaging and conventional image analysis were performed by the candidate. The proteomics experiments were planned, performed and analyzed by the candidate and Dr. Makan Golizeh at Dr. Momar Ndao/Dr. Brian J. Ward lab. The image cross-correlation spectroscopy analysis was performed by Dr. Angelica A. Gopal at Dr. Paul W. Wiseman lab. The electron microscopy imaging was performed by Ian N. Costas-Cancelas at Dr. Isabelle Rouiller lab. The candidate wrote the manuscript with significant editorial assistance from Dr. Brian J. Ward. All authors provided editorial input and approved the final version of the article prior to its submission.

For Chapter 4, the candidate, Dr. Makan Golizeh and Dr. Brian J. Ward developed the concept and designed the study. The experiments were planned, performed and analyzed by the candidate and Dr. Makan Golizeh. Dr. Makan Golizeh and the candidate wrote the manuscript. All authors provided editorial input and approved the final version of the article prior to its submission.

For Chapter 5, the candidate and Dr. Brian J. Ward developed the concept and designed the study. The experiments were planned, performed and analyzed by the candidate and Aakash R. Patel. Valentine Bainov developed algorithm and performed computational analysis of DiD fluorescence dequenching results. The candidate wrote the manuscript with significant editorial assistance from Dr. Brian J. Ward. All authors provided editorial input and approved the final version of the article prior to its submission.

Contribution to original knowledge

The work presented in this thesis contributes to original knowledge in the fields of the mechanisms of immunogenicity of plant-derived VLP-based influenza vaccines and serological correlates of protection induced by influenza vaccination. The specific contributions are as follows:

1. We showed that plant-derived VLPs recapitulate key interactions of influenza virions with human monocyte/macrophage cells such as sialic acid-dependent surface binding and internalization, trafficking to acidic cell compartments and fusion of the VLP lipid envelope with endosomal membranes.
2. We provided evidence that influenza HA delivered in a form of plant-derived VLPs is processed by human MDMs, and HA-derived antigenic peptides are presented to the memory pool of immune cells *in vitro*.
3. We showed a rapid and massive internalization of HA-bearing VLP by human MDM through multiple endocytic pathways, including clathrin-mediated and clathrin-independent endocytosis, macropinocytosis and phagocytosis.
4. We demonstrated bidirectional endosomal trafficking of HA-bearing VLP in human MDM towards both high-degradative late endosomes that favor the MHC II-restricted antigen presentation and low-degradative static early and/or recycling endosomes that support the MHC I-restricted antigen cross-presentation.
5. Using advanced proteomics techniques, we demonstrated robust cross-presentation of influenza HA delivered in a form of plant-derived VLP by human MDM *in vitro*.
6. We showed that treatment of human MDM with VLP induces a massive up-regulation of the endogenous (host) protein-derived peptides presentation in the MHC I context. These proteins are primarily involved in cellular, metabolic and regulatory processes and activate several pathways including inflammation stimulation and attenuation, response to stimuli, innate and adaptive immunity, clathrin-mediated endocytosis, protein synthesis and endo-lysosomal degradation.
7. We developed a novel serological assay for influenza based on DiD fluorescence dequenching upon fusion of DiD-labelled influenza virions with target cell membranes.

List of abbreviations

Å	angstrom
a.u.	arbitrary unit
AA	amino acid
ADCC	antibody-dependent cell-mediated cytotoxicity
ADP	adenosine-5′-diphosphate
alum	aluminium hydroxide
ANOVA	analysis of variance
AP-2	adaptor protein-2
APC	antigen-presenting cell
ATP	adenosine-5'-triphosphate
BM2	influenza B matrix protein 2
BrDU	5-bromo-2'-deoxyuridine
BSA	bovine serum albumin
CAGR	compound annual growth rate
CBER	Center for Biologics Evaluation & Research
CCL	CC chemokine ligand
CD	cluster of differentiation
Cdc42	Cell division control protein 42
CID	collision-induced dissociation
CIE	clathrin-independent endocytosis
CLEC12A	C-type lectin domain family 12 member A
CLEC9A	C-Type Lectin Domain Family 9 Member A
CLIP	class-II-associated invariant chain peptide
CM2	influenza C matrix protein 2
CME	clathrin-mediated endocytosis
CO	control
cRNA	complementary RNA
CRTAM	class I-restricted T cell-associated molecule
CTL	cytotoxic T lymphocyte
CXCL	chemokine (C-X-C motif) ligand

DAPI	4′,6-diamidino-2-phenylindole
DC	dendritic cell
DCIR	dendritic cell immunoreceptor
DC-SIGN	dendritic cell-specific intercellular adhesion molecule-3 grabbing non- integrin
DDX21	DEAD (Asp-Glu-Ala-Asp) box helicase 21
DiD	1,1-dioctadecyl-3,3,3,3-tetramethylindodicarbocyanine
DNA	deoxyribonucleic acid
dsRNA	double-stranded RNA
EDTA	ethylenediaminetetraacetic acid
EEA1	early endosomal antigen-1
eGFP	enhanced green fluorescent protein
EGFR	epidermal growth factor receptor
ELISA	enzyme-linked immunosorbent assay
EM	electron microscopy
ER	endoplasmic reticulum
ERAP	endoplasmic reticulum aminopeptidase
ERGIC	endoplasmic reticulum-Golgi intermediate compartment
ERp57	endoplasmic reticulum-resident protein 57
ESCRT	endosomal sorting complex required for transport
eV	electron-volt
EV	empty vesicle
Fas	first apoptosis signal receptor
FBS	fetal bovine serum
Foxp3	forkhead box P3
gag-p24	group-specific antigen core protein of 24 kDa
GDP	gross domestic product
GMT	geometric mean titer
GnRHR	gonadotropin-releasing hormone receptor
GO	gene ontology
GRAVY	grand average of hydropathy
GTP	guanosine-5'-triphosphate

HA	hemagglutinin
HAI	hemagglutination inhibition assay
HBSS	Hank's balanced salt solution
HCl	hydrochloric acid
HEF	hemagglutinin-esterase-fusion protein
HEPES	4-(2-hydroxyethyl)-1-piperazineethanesulfonic acid
HIV	human immunodeficiency virus
HLA	human leukocyte antigen
Hobit	Homolog of Blimp-1 in T cells
HR	high resolution
ICCS	image cross-correlation spectroscopy
IEDB	Immune Epitope Database
IFITM	interferon-induced transmembrane protein
IFN	interferon
IFNAR	interferon-α/β receptor
IFNLR	interferon-λ receptor
Ig	immunoglobulin
Ii	invariant chain
IIV	inactivated influenza vaccine
IL	interleukin
ILV	intraluminal vesicle
IP	inhibitory peptide
IRAP	insulin-regulated aminopeptidase
ISG	interferon-stimulated gene
IU	international unit
JAK	Janus kinase
LAIV	live attenuated influenza vaccine
LAMP	lysosome-associated membrane protein
LC	liquid chromatography
LDH	lactate dehydrogenase
LEPR	leptin receptor

LOD	limit of detection
LOX-1	lectin-like oxidized low-density lipoprotein receptor-1
L-SIGN	liver/lymph node-specific intercellular adhesion molecule-3-grabbing integrin
M1	matrix 1 protein
M2	matrix 2 protein
MAPK	mitogen-activated protein kinase
MAVS	mitochondrial antiviral-signaling protein
MDA5	melanoma differentiation-associated protein 5
MDCK	Madin-Darby canine kidney cell
MDDC	monocyte-derived dendritic cell
MDM	monocyte-derived macrophage
MDN1	Midasin AAA ATPase 1
MGL	macrophage galactose-type lectin
MHC	major histocompatibility complex
MLKL	mixed lineage kinase domain-like protein
MMP	matrix metalloproteinase
MN	microneutralization assay
MR	mannose receptor
mRNA	messenger RNA
MS	mass spectrometry
MS/MS	tandem mass spectrometry
MVB	multivesicular body
MxA	human myxovirus resistance protein 1
MyD88	myeloid differentiation primary response 88
NA	neuraminidase
nAChR	nicotinic acetylcholine receptor
NADPH	nicotinamide adenine dinucleotide phosphate
NEP	nuclear export protein
NK cell	natural killer cell
NKp44	natural killer cell p44-related protein
NKp46	natural killer cell p46-related protein

NLR	nucleotide oligomerization domain (NOD)-like receptor
NLRP3	NLR Family Pyrin Domain Containing 3
NLS	nuclear localization sequence
NP	nucleoprotein
NS1	non-structural protein 1
NS2	non-structural protein 2
OVA	ovalbumin
PA	polymerase acidic protein
PAMP	pathogen-associated molecular pattern
PB1	polymerase basic protein 1
PB1-F2	Polymerase basic protein 1 frame 2
PB2	polymerase basic protein 2
PBMC	peripheral blood mononuclear cell
PBS	phosphate-buffered saline
pdmH1N1	H1N1 pandemic influenza virus
PEP	posterior error probability
pH	potential of hydrogen
PI	propidium iodide
PIGO	GPI ethanolamine phosphate transferase 3
PLC	peptide-loading complex
PRR	Pattern recognition receptor
QIV	quadrivalent influenza vaccine
R (>t)	Pearson coefficient for pixels whose intensity falls above a threshold value
R	Pearson correlation coefficient
Rab	Ras-associated binding protein
Rac1	Ras-related C3 botulinum toxin substrate 1
RBC	red blood cell
RDE	receptor destroying enzyme
RIG-I	retinoic acid-inducible gene-I
RIP1	receptor-interacting protein kinase 1
RIP3	receptor-interacting protein kinase 3

RLR	RIG-I-like receptor
RNA	ribonucleic acid
RNP	ribonucleoprotein
ROI	region of interest
ROS	reactive oxygen species
RPMI	Roswell Park Memorial Institute medium
RT	room temperature
S.E.M.	standard error of the mean
SCR	seroconversion rate
SNARE	soluble *N*-ethylmaleimide-sensitive factor attachment protein receptor
SPR	seroprotection rate
SRH	single radial haemolysis
ssRNA	single-stranded RNA
STAT	signal transducer and activator of transcription
STING	stimulator of interferon genes
TAP	transporter associated with antigen processing
TCID50	50% tissue culture infective dose
Th1	type 1 T helper cell
Th2	type 2 T helper cell
TIV	trivalent influenza vaccine
TLR	toll-like receptor
tM1	Manders above threshold colocalization coefficient 1
tM2	Manders above threshold colocalization coefficient 2
TNF	tumor necrosis factor
TPCK	tolylsulfonyl phenylalanyl chloromethyl ketone
Tpn	tapasin
Treg	regulatory T cell
Trf	transferrin
TRIF	TIR-domain-containing adapter-inducing interferon-β
TRIM	tripartite motif-containing protein
TUFM	Tu elongation factor, mitochondrial

UHPLC	ultra-high-performance liquid chromatography
US$	United States dollar
USA	United States of America
v-ATPase	vacuolar-type H^+-ATPase
VE	vaccine effectiveness
VLP	virus-like particle
vRNP	viral ribonucleoprotein
WHO	World Health Organization

Table of contents

List of Tables

List of Figures

Chapter 1

Chapter 2

Chapter 3

Chapter 6

Chapter 1: Literature review and research objectives

1.1. INFLUENZA: MEDICAL AND SOCIO-ECONOMIC ASPECTS

1.1.1. Social and economic burden of seasonal and pandemic influenza

Despite undeniable progress in influenza prevention and treatment, this infection remains a major public health threat. The World Health Organization (WHO) estimates that 3 to 5 million cases of severe illness caused by influenza viruses occur every season and lead to 290,000 to 650,000 deaths worldwide (1). In developed countries, most influenza-related deaths occur in individuals ≥75 years of age but up to 99% of the influenza-related deaths in those 5 years old or younger happen in the developing world (2,3). In 2016-2017 influenza season, an estimated 30.9 million people became sick with influenza in the United States, 14.5 million visited their health care provider, and ~600,000 required hospitalization (4). Influenza may cause exacerbation or worsening of chronic diseases such as chronic obstructive pulmonary disease, atherosclerosis and ischemic heart disease leading to myocardial infarction or stroke. Influenza also increases the risk of miscarriage in pregnant women and is strongly associated with secondary bacterial infections, although the influenza virus itself is often undetectable when these complications occur (5–8).

The socio-economic impact of influenza is massive. The total (direct and indirect) annual cost of seasonal influenza is reported to be as high as $19,8 billion in the USA, which means ~$63 per capita or 0.14% of gross domestic product (GDP). Similar figures for per capita costs ($27-$52) and GDP impact (0.04%-0.13%) are reported for the European countries (9). A recent European study reported that influenza had the highest burden (30% of the total burden) of the disability-adjusted life years - 81.8 per 100,000 population - among 31 communicable diseases included in the analysis (10). It is likely that both the prevalence and the economic burden of influenza in developing countries are greatly underestimated (11,12).

Although the burden of seasonal influenza cases is already large, influenza viruses also have the potential for sustained national and international spread leading to infection of a large proportion of the world's population, or a 'pandemic' (13). Since 1510, at least 14 pandemics have been caused by influenza viruses; in the past 120 years, influenza pandemics occurred in 1889, 1918, 1957, 1968, 1977, and 2009 (14). The catastrophic 'Spanish' influenza pandemic of

1918-1920 affected one third of the world population (about 500 million people) with case/fatality rates exceeding 2.5%, compared to less than 0.1% for other influenza pandemics, and 50 to 100 million people died (15). A number of influenza viruses that cause severe disease and high mortality in humans have emerged in the last two decades, including H5N1 virus, first detected in 1997, and the H7N9 and H10N8 viruses, first reported in 2013 (16).

The most recent influenza pandemic was caused by an 'new' H1N1 virus that was first reported in 2009 (pdmH1N1) (17). The WHO reported 18,632 deaths associated with laboratory-confirmed 2009 pdmH1N1 influenza (18). However, a computational modelling study argued that there were at least 201,200 respiratory deaths with an additional 83,300 cardiovascular deaths globally were caused by pdmH1N1 in 2009-2010. Furthermore, this study estimated that 80% of the respiratory and cardiovascular deaths were in people younger than 65 years of age and that 51% of them occurred in South-East Asia and Africa (19). High mortality in the younger age groups resulted in a much greater loss of life-years compared to seasonal influenza epidemics (18).

1.1.2. Influenza etiology, pathogenesis and clinical presentations in humans

The causative agents of human influenza are influenza A, B or C viruses that belong to the *Orthomyxoviridae* family (20). Recently characterized influenza D viruses have not been found in humans to date (21,22). Influenza type A viruses can infect people, birds, pigs, horses, seals, whales, and other animals, but wild birds are the natural hosts for these viruses. Influenza type A viruses can cause human epidemics and pandemics. Influenza B viruses are normally found only in humans, although they have also been isolated from seals. Although influenza type B viruses can cause human epidemics, they have not yet caused a pandemic. Influenza type C viruses cause mild illness in humans and do not cause epidemics or pandemics (20,23,24).

Influenza A, B and C viruses are distinguished on the basis of their core proteins, which are specific for each viral type (25). Subtypes of influenza A virus are classified according to their hemagglutinin (HA) and neuraminidase (NA) surface proteins. There are 18 HA subtypes and 11 NA subtypes known to date (26). The WHO recommended nomenclature of influenza viruses includes the type of virus (A, B, or C), the host (if nonhuman), place of isolation, isolation number, and year of isolation (separated by slashes). For influenza A viruses, HA and NA subtypes are specified in parentheses (14,25). Influenza B viruses initially formed a

homogenous group. During the mid-1980's, evolutionary changes in the HA gene separated influenza B viruses into two antigenically distinct lineages represented by B/Yamagata/16/88 and B/Victoria/2/87 (27–29).

1.1.2.1. Structure and life cycle of influenza viruses

Influenza viruses are enveloped negative-strand RNA viruses with segmented genomes containing 8 (type A and B viruses) or 7 (type C viruses) gene segments. Influenza A and B viruses are represented by two morphological forms: spherical and filamentous. Spherical virions have diameters of 80–120 nm. Filamentous virions exhibit elongated morphology with the length sometimes upwards of 20 μm; these are predominantly found in freshly isolated clinical samples (30–32). Influenza C viruses can form long (up to 500 μm) cord-like structures on the surface of infected cells (33). In all cases, the viral envelope is derived from the host cell membrane acquired when the virion buds from an infected cell. HA (in the form of trimers) and NA (in the form of tetramers) spikes, as well as matrix 2 (M2) transmembrane envelope proteins are exposed on the surface of influenza A virions (34–36). Matrix 1 (M1) protein lies on the inner side of viral envelope (37). The core of the influenza A virion is formed by 8 viral ribonucleic acid (RNA) segments associated with multiple copies of nucleoprotein (NP) and polymerase complexes of PA, PB1, and PB2 proteins (38). Influenza A virus RNA also encodes a nonstructural protein (NS1) and the nuclear export protein NS2/NEP (39–41). In addition, other viral proteins can be produced using alternative translation initiation sites, ribosomal frameshift or alternative mRNA splicing (42). Together, the 8 segments of influenza A virus genome can be translated into up to 20 viral proteins (Table 1.1) (43). Influenza B virion structure is similar to influenza A; however, it has four transmembrane proteins on the surface: HA, NA, NB (acts as an ion channel) and BM2 (like the M2 protein of influenza A, BM2 acts as a proton channel) (44,45). The influenza C virus has an envelope hemagglutinin-esterase-fusion (HEF) protein that combines the functions of HA and NA; another protein unique to influenza C is CM2 that acts as an ion channel (46,47).

The influenza virus life cycle consists of the following steps: entry into the host cell; entry of viral ribonucleoproteins (RNPs) into the nucleus; transcription and replication of the viral genome; export of the viral RNPs from the nucleus; and assembly and budding at the host cell plasma membrane (Fig. 1.1) (48).

Upon binding to host cell sialic acid residues, influenza virions enter the host cell predominantly through clathin-mediated endocytosis; however, other internalization mechanisms also contribute to cell entry (49–51). Endosomes containing influenza virions undergo maturation and acidification, and when pH reaches 5-6, fusion of the viral and endosomal membranes occurs. Low pH induces a conformational change in the HA molecule, exposing a fusion peptide that mediates merging of the viral envelope and endosomal membrane by bringing them into close proximity. Next, local destabilization of the lipid bilayers occurs, and membranes fuse causing mixing of the lipids and formation of a fusion pore in endosomal membrane (24,52,53). At the same time, protons from the endosomal milieu are pumped into the virus particle via the M2 ion channel. Internal acidification of the influenza virion disrupts internal protein-protein interactions, allowing viral RNPs to be released from the viral core into the host cell cytoplasm (54). Influenza viral transcription and replication occurs in the nucleus. The NP, PA, PB1, and PB2 viral proteins all have nuclear localization sequences that bind to the cellular nuclear import machinery. The viral RNA-dependent RNA polymerase complex - a component of the RNPs imported into the nucleus - uses the negative-sense viral RNA as a template to synthesize two positive-sense RNA species: messenger RNA (mRNA) templates for viral protein synthesis and complementary RNA (cRNA) intermediates from which the RNA polymerase subsequently transcribes more copies of negative-sense, genomic viral RNA (55). The envelope proteins HA, NA, and M2 are translated from messenger RNA of viral origin in the endoplasmic reticulum (ER). All three proteins have apical sorting signals that subsequently direct them to lipid rafts in the cell membrane for virion assembly. Influenza virus budding occurs at cell membrane, where viral RNA segments and proteins form complete viral particles (56). When budding is complete, HA spikes continue to bind the virions to the sialic acid residues on the cell surface until the particles are released by the sialidase activity of the NA protein (48,57).

1.1.2.2. Antigenic drift and antigenic shift of influenza viruses

The influenza viruses are constantly evolving pathogens, and their ability to evade multiple defense mechanisms allows them to be a continual threat to their hosts and to survive in populations with considerable prior exposure. These viruses have two major mechanisms for antigenic change, antigenic drift and antigenic shift (58). Antigenic drift occurs in all influenza viruses and is a gradual evolution of the viral strains, due to frequent mutations, primarily in the

surface protein genes. For example, in the H3N2 influenza A viruses, a mutation frequency of less than 1 % per year in the amino acid sequences of HA and NA results in so-called antigenic clusters that emerge and replace each other every 2 to 8 years (59,60). The infection of a person with specific influenza virus strain leads to development of adaptive immunity against that strain during the course of disease. The infection with a newly-emerged strain can occur when these immune defenses targeting the previously circulated strains are unable to recognize the new virus (61).

To address these drifted viruses, influenza vaccine content is reviewed annually to ensure maintenance of protection, despite the emergence of new variants. Indeed, a network of global surveillance has been established to monitor the evolution of human influenza viruses and select the appropriate strains that should be included in the annual influenza vaccines (62).

Antigenic shift is only seen in influenza A viruses, and results from the exchange of one or more genome segments between two related viruses which infect a host cell at the same time. During such a double infection, the various components of each virus are generated and, at the stage of assembling the progeny virions, mistakes in the combination of the independent gene segments happen because the budding mechanism cannot differentiate between RNA segments the two parent viruses. The reassortment of complete gene segments results in the formation of mosaic viruses known as ‘reassortants’. When genetic reassortment results in the exchange of segments encoding the viral surface proteins HA and NA, the progeny virus gains a new antigenic pattern (61). Reassortment can therefore result in the emergence of a new virus that has never circulated in humans before or may not have circulated for decades. Such viruses can have significant impact on the disease burden, causing worldwide pandemics and resulting in hundreds of thousands, or possibly millions of influenza-related deaths (63). Pandemic viruses are often genetic reassortants of human and avian/swine influenza A virus subtypes. Antigenic shifts occur all of the time in nature but truly pandemic viruses emerge approximately three times every 100 years (64). For example, three major antigenic shifts with resulting pandemics occurred during the 20th century (14). Rapid production of large quantities of a vaccine offering protection against the new pandemic strain remains a major challenge for influenza vaccine manufacturers (65,66).

1.1.2.3. Clinical manifestations and consequences of influenza

The clinical manifestations of seasonal influenza range from asymptomatic infection to a fulminant illness, depending on the characteristics of both the host and the virus. In typical cases, the 'flu' is an acute respiratory disease characterized by the sudden onset of fever (body temperature can rise up to 41°C in the first 24 h of illness), headache, prostration, malaise, accompanied by respiratory symptoms, including non-productive cough, nasal discharge, and sore throat. Ocular symptoms can also be present and include photophobia, conjunctivitis, lacrimation, and pain with eye movement. Arthralgias are also quite frequent, but symptoms of true arthritis are not present. Some patients can exactly define the precise hour of disease onset. The incubation period is short (from a few hours up to 2 days). The fever is mostly continual, but it can be intermittent when the patient is taking antipyretic medications. The fever typically lasts 1–5 days - very rarely longer - and goes down gradually. Complete recovery in an otherwise healthy individual usually takes 1-2 weeks; however, cough, weakness and malaise may last longer, particularly in the elderly (32,67).

Importantly, influenza is often complicated by secondary bacterial or viral infections, causing severe morbidity and mortality. Approximately one in four patients (adult and children) admitted to intensive care units with confirmed influenza A infection in 2009 had a bacterial or viral co-infection. *Staphylococcus aureus, S. pneumoniae* and *Haemophilus influenzae* were among the most frequently identified pathogens (68). Bacterial infection may be concurrent with influenza, and the resulting co-infection can lead to enhanced lung injury. By another mechanism, prior influenza infection can alter both host immunity and pulmonary architecture (e.g. sloughing of the epithelial barrier), leading to increased susceptibility to secondary bacterial pneumonia (69,70).

Disease severity, risk of complications, hospital admission and death are higher in some age groups. Typically, children younger than 5 years (particularly children <2 years of age) and individuals older than 65 years are at risk of increased morbidity and mortality from influenza. This is not always the case however. For example, in both the 2018-19 and 2009-10 pandemics, there was an unusual increased risk of mortality in young adults (71–73). 'Sero-archeology' studies suggest this unusual pattern of susceptibility may be attributable to early life experience with prior pandemic viruses (74).

A number of comorbidities significantly increase the risks associated with influenza, including chronic obstructive pulmonary disease, cardiovascular diseases, renal and liver diseases, diabetes and obesity (5,75–78). Pregnant women are also at elevated risk of pregnancy complications and poor fetal outcomes, hospitalizations and death caused by both pandemic and seasonal influenza (79–81).

1.2. IMMUNE RESPONSES DURING THE NATURAL INFLUENZA

1.2.1. Innate immunity to influenza virus

During the first days of infection with a new influenza strain, innate immune mechanisms form the first line of defense, limiting massive pathogen invasion and excessive tissue damage, slowing viral replication and spread, and laying the groundwork for an effective adaptive response (82–84). Innate immunity refers to genetically determined host defense mechanisms that do not require prior exposure to the pathogen. Instead, the innate response relies on recognition of evolutionary formed pathogen-associated molecular patterns (PAMPs) that distinguish them from healthy mammalian cells or commensal organisms (82,85).

1.2.1.1. Mucosal factors preventing the invasion of influenza viruses

A large number of innate immune defense mechanisms play key roles at different stages of the infectious process. Soluble factors termed γ inhibitors prevent the interaction of influenza HA with the sialic acid residues on the surface of host cells that act as attachment factors for influenza virions. These factors are present in oral cavity, nasopharynx and the respiratory tract, and include a collectin family member (i.e. surfactant protein A), mucins, gp-340, pentraxins and ficolins (86,87). Other molecules called β inhibitors act through calcium-dependent binding to carbohydrates present on viral proteins. β inhibitors found in human airway secretions include the collectins, surfactant protein D and mannose-binding lectin, H-ficolin and galectin (88,89). Several other components of healthy respiratory fluids also contribute to early antiviral defense, including the hydrophobic surfactant protein C and surfactant lipids. Anti-microbial peptides such as α- and β-defensins, cathelicidins may also help to combat the influenza infection (90,91). The complement system is activated early in influenza by mannose-binding lectin or H-ficolin (92). Finally, the high mobility group box protein I is released from necrotic cells, and acts as an

'alarmin', signaling through various receptors on immune cells and causing release of pro-inflammatory cytokines and chemoattractants at the site of invasion (93,94). Altogether, these soluble factors block the initial interactions between influenza virions and host cells and help to eliminate infected cells (83).

1.2.1.2. Innate recognition of the influenza viruses

Healthy respiratory epithelial cells form an effective mechanical barrier against invasion by bacterial and viral pathogens. These cells have been shown to produce granulocyte macrophage colony-stimulating factor as well as type I and type III interferons (IFNs), which trigger a cascade of the antiviral effector mechanisms (83,95–97). There are at least three pattern recognition pathways through which respiratory epithelial cells respond to influenza virus infection: (i) toll-like receptors (TLRs) that recognize viral RNA at the cell surface or in the endosomal compartment; (ii) cytoplasmic nucleic acids recognition RIG-I-like receptors (RLRs); and (iii) nucleotide oligomerization domain (NOD)-like receptors (NLRs) that trigger the inflammasome pathway leading to caspase 1 activation and interleukin (IL)-1β and IL-18 production (Fig. 1.2) (82,84,97,98).

1.2.1.2.1. Toll-like receptors and influenza

TLRs are expressed either on the plasma membrane or in endosomal compartments in epithelial and immune cells, and act as initial sensors of the pathogen- or damaged cell-associated structural patterns. TLR7 is endosomal receptor that is thought to play a major role in the recognition and control of influenza virus infection. TLR7 detects single-stranded RNA (ssRNA) of the viral particles, and the sensing event does not require viral replication (99). Influenza infection also causes an increase of TLR8 expression in human monocytes and dendritic cells (DCs) (100). Stimulation of TLR8 with ssRNA triggers production of Th1-polarizing proinflammatory cytokine IL-12 but not IFN-α (101). The role of TLR3 in protection against influenza virus infection is still not fully understood but treatment of the host cells with TLR3 ligand suppresses influenza virus replication (102). This is odd because TLR3 is thought to act as a sensor of double-stranded RNA (dsRNA) present in the endosomal compartment (103), and influenza A virus, like other negative-sense RNA viruses, does not generate dsRNA in infected cells (104,105). TLR3 may detect an unidentified dsRNA-containing substrate released

from the influenza A virus-infected cell upon phagocytosis of damaged/dying cells by neighbouring phagocytes (84). The role of other TLRs in influenza infection remains debatable. Influenza virus infection causes an increase of the expression of TLR9, a DNA sensor, in human pharyngeal epithelial cells, and treatment with a TLR9 ligand can suppress viral replication (102). TLR10 is thought to detect functional protein-RNA complexes of the influenza virus in infected cells (106). Influenza A virus caused a dramatic increase of the TLR10 expression in human macrophages, and down-regulation of TLR10 expression results in suppression of proinflammatory cytokines and type I and type III IFNs secretion (106). In addition, stimulation of 'bacterial' sensors TLR2 and TLR4 can also potentiate innate and adaptive antiviral immune responses (107,108).

1.2.1.2.2. RIG-I-like receptors and influenza

Whereas TLRs are membrane-associated structures that generally recognize extracellular or compartmentalized in endosomes PAMPs of non-replicating viruses, RLRs are located in the cytosol and detect the products of viral replication (109). RLRs are expressed in almost all tissues, and their expression level is greatly increased after exposure to viral pathogens or IFNs (84). Cytosolic sensing of the influenza viruses appears to be an important function of RIG-I system (110). RIG-I sensor detects phosphorylated 5' terminus of ssRNA viral genomes, and the cytoplasmic presence of RNA containing 5'-phosphates allows recognition of viral RNA vs. host cell RNAs (111). Stimulation of RLRs results in activation of downstream cell signaling pathways that lead to production of type I and type III IFNs, proinflammatory cytokines and other antiviral factors (109,112).

1.2.1.2.3. Nucleotide oligomerization domain (NOD)-like receptors and influenza

The anti-infective function of NLRs is primarily associated with their contribution to the formation of inflammasomes, multi-molecular complexes assembled in response to invading pathogens or other danger signals (113–115). Proinflammatory factors induce expression of the inactive pro-forms of IL-1β and IL-18. Maturation of these pro-cytokines requires proteolytic cleavage of pro-caspase-1. Once activated, caspase-1 cleaves the inactive pro-IL1β and pro-IL18 to their active forms, which then signal through target cell receptors to induce a broad spectrum of proinflammatory and antiviral cytokines, including IL-6, tumor necrosis factor (TNF)-α, and

IFN-γ (113,116). Inflammasome activation during influenza virus infection could be explained by at least three mechanisms. First, transfection of ssRNA isolated from influenza virions into target cells can directly trigger IL-1β production; second, proton flux through the influenza virus-encoded M2 ion channel in the trans-Golgi network triggers NLRP3 activation, formation of the inflammasome and cleavage of pro-IL-1β and pro-IL-18; and, finally, high-molecular-weight aggregates of the influenza virus virulence protein PB1-F2 stimulates the activation of the NLRP3 inflammasome (82,84).

1.2.1.3. Type I and type III interferons, and interferon-stimulated genes in influenza

The potent anti-viral state created at the site of influenza virus invasion is largely attributable to type I IFNs, such as IFN-α and IFN-β, and type III IFNs also known as interferon lambdas (IFN-λ1, IFN-λ2, IFN-λ3, IFN-λ4). Infection of airway epithelial cells with influenza viruses induces robust production of type I and type III IFNs (95,96,117). IFN-α and IFN-β interact with IFN-α/β receptors (IFNAR), while IFN-λs interact with IFNL receptors (IFNLR) in an autocrine or paracrine manner, which both trigger downstream cell signalling pathways resulting in the transcription of numerous interferon-stimulated genes (ISGs) (82,95,118). ISGs target different steps of influenza virus life cycle. For example, interferon-induced transmembrane (IFITM) proteins restrict replication of the influenza A virus by blocking virus-host cell membrane fusion following viral attachment and endocytosis (119). Similarly, cholesterol 25-hydroxylase enzymatic activity converts cholesterol to soluble 25-hydroxycholesterol, which is involved in antiviral defense by blocking endosomal fusion (120,121). Tripartite motif-containing protein (TRIM) 22 blocks viral genome encapsidation and degrades nucleoprotein of the influenza virus by polyubiquitination (122). TRIM32 binds to influenza PB1 RNA polymerase, reduces the polymerase activity, and thus restricting viral replication (123). ISG15 is a ubiquitin-like protein that targets newly translated viral proteins (124). Human myxovirus resistance protein 1 (MxA) retains incoming viral RNP in the cytoplasm and blocks the amplification of viral RNA from cRNA copies (secondary transcription), possibly via cytoplasmic sequestering of newly synthesized NP and PB2 (125,126). A large number of other ISGs such as protein kinase R, 2',5'-oligoadenylate (2-5A) synthetases, DEAD-Box Helicase 21 (DDX21), cyclophilins A and E, zinc finger antiviral

protein, Tu elongation factor, mitochondrial (TUFM), viperin, tetherin also contribute to restricting the replication of influenza viruses (82,95,118).

1.2.1.4. Cells of the innate immune system involved in immunity to influenza

Airway epithelial cells are the first target of influenza viruses and they rapidly produce many inflammatory cytokines and chemokines, such as IL-1β, IL-6, IL-8 TNF-α, CCL2, CCL3, and CXCL10 that recruit other immune cells (84,98,117,127–129). Alveolar macrophages, neutrophils and monocytes recruited from the bloodstream are critical for limiting the infection. Once activated, macrophages enhance their pro-inflammatory cytokine response, including production of IFNs, IL-6, and TNF-α. In addition, activated macrophages phagocytose influenza virus-infected cells and thus limit viral spread and regulate the developing adaptive immune response (130–132). Natural killer (NK) cells are important cytotoxic and effector cells of the innate immunity. Cells infected with influenza A virus have HA protein on their surface that is recognized by NK cells via their receptors NKp44 and PKp46 leading to lysis of the infected cells (133,134).

1.2.1.5. Programmed cell death as an innate antiviral mechanism

When the host fails to control influenza virus replication through the innate immune mechanisms discussed above, the individual infected cell can still execute a final desperate antiviral response via programmed death – apoptosis, necroptosis or pyroptosis (131,135–137). Apoptosis is generally considered to be immunologically silent and non-inflammatory, whereas pyroptosis and necroptosis are pro-inflammatory modes of programmed cell death (135). Apoptosis of influenza virus infected cells is a well-characterised phenomenon. Pathogen sensors and ISGs such as RIG-I, MDA5, protein kinase R recognize accumulating viral RNA and activate apoptotic machinery that directs the fate of infected cells. The apoptotic cascade results in mitochondria membrane permeabilization followed by cytochrome C release, apoptosome activation, ATP degradation, and eventually cell death (131,138,139). As the initial trigger of this process, the concentration of viral RNA is a critical factor in timing. Indeed, if the viral load is high enough, apoptosis can be initiated at the stage of virus entry (118,140,141). The initiation of apoptosis in infected cells may also result from upregulation of surface expression of Fas and Fas ligand; a death receptor and its ligand (142). Apoptotic cells are rapidly phagocytosed both

by neighbouring cells and newly-recruited phagocytes responding to 'find-me/eat-me' signals (proteins, lipids, and nucleotides, phosphatidylserine surface exposure etc.) released from dying infected cells. Apoptosis-dependent phagocytosis by 'professional' antigen-presenting cells (APCs) such as DCs and macrophages is thought to be an important mechanism for the phenomenon of cross-presentation, when the presentation of microbial antigens is performed by APCs that are apparently not infected with the corresponding pathogens (143–145). APCs that are not infected by influenza virus engulf virus-infected cells undergoing apoptosis, process viral proteins, and present viral antigens to induce and activate cytotoxic T lymphocytes. Once activated, these cytotoxic T lymphocytes can, in turn, induce further apoptosis of cells infected with the same virus. Therefore, the phagocytosis of virus-infected cells is a critical link between innate and adaptive immune responses (131,146,147).

Another form of cell death, necroptosis, or regulated necrosis, can be activated by ligation of death receptors and stimulation of death receptor ligand expression under apoptotic deficient conditions. Activation of necroptosis requires the kinase activity of RIP1, which mediates the activation of RIP3 and MLKL, two critical downstream mediators of necroptosis (148). RIPK1 and RIPK3 auto- and transphosphorylate each other, leading to the formation of a microfilament-like complex called the necrosome which then activates the pro-necroptotic protein MLKL via phosphorylation. Phosphorylated MLKL molecules form a homotrimer, which inserts into the bilipid membranes of organelles and the plasma membrane, leading to leakage of cellular contents into the extracellular space (149). Replicating influenza A viruses appear to be capable of driving assembly of the necrosome and MLKL phosphorylation independent of signaling by the RNA-sensing innate immune receptors (RLRs, TLRs, protein kinase R) or type I IFNs and TNF-α. Such necroptotic death has been reported in many different infected cells including alveolar epithelial cells, fibroblasts, and DCs (150–153). Pyroptosis is a highly inflammatory form of programmed cell death and the end result of the NLR-inflammasome pathway activation. Although inflammasome formation and pro-inflammatory cytokine release in influenza-infected cells are well-documented, pyroptosis has not been directly reported in the context of influenza virus infection yet (83,135).

The sections above should make it clear that multiple innate immune mechanisms are activated to limit influenza virus infection. These diverse elements combine to form a hierarchical defense structure that begins by interfering with the virion binding to host cells,

endosomal fusion and release of the viruses into cytosol, their replication and budding the progeny virions from infected cells. If these relatively subtle and targeted mechanisms of control fail, the infected host cells die through one or another programmed death pathway. Importantly, many of these innate immune mechanisms also contribute to the development of effective anti-viral adaptive immunity.

1.2.2. Adaptive immune responses to influenza virus

Simultaneous with the initial innate defensive effort, activation of the adaptive immune system in initiated. While innate mechanisms are needed to keep us alive in the short term, in most instances it is the adaptive response that plays the central role in viral clearance, host recovery, and establishment of immunological memory (154–156). The adaptive immune response consists of cell-mediated ($CD4^+$ and $CD8^+$ T cells) and humoral (virus-specific antibodies) branches (85,98,157). APCs, in the first instance DCs and macrophages, serve as bridges between the innate and adaptive immune responses (158–160).

1.2.2.1. Processing and presentation of influenza virus-derived antigens

APCs can acquire viral antigens in three ways: (i) by being directly infected with the influenza virus (161–163), (ii) through phagocytosis of infected neighbouring cells/apoptotic bodies (131,164) or (iii) by internalization of non-infectious viral components (e.g. the mechanism of most vaccines) (165,166). They then process and present the pathogen-derived peptides in the context of major histocompatibility complex (MHC) class I (for $CD8^+$ T cells) or MHC class II (for $CD4^+$ T cells) to the naive or memory T cells (167,168).

1.2.2.1.1. Cell surface attachment factors and entry receptors for influenza viruses

The form of antigen presentation - MHC I or MHC II-restricted - depends on multiple factors, and APC surface receptors serve as the initial sorting mechanism that shifts the balance towards one or another antigen processing/presentation pathway (169–171). More than a decade ago, mannose receptor (MR) was found to be essential for the **MHC I-restricted presentation** of soluble ovalbumin by mouse DCs and bone marrow-derived macrophages (172,173). The HIV gag-p24 protein targeted with a monoclonal antibody to DEC-205 receptor on monocyte-derived DCs caused robust proliferation and IFN-γ production by antigen-specific $CD8^+$ T cells (174).

The HIV gag-p24 fusion constructs with antibodies against Langerin, DEC-205, and C-Type Lectin Domain Family 9 Member A (CLEC9A) greatly enhanced antigen cross-presentation by the mouse DCs (175). A number of other receptors on APCs such as macrophage galactose-type lectin (MGL) 2, lectin-like oxidized low-density lipoprotein receptor-1 (LOX-1), C-type lectin domain family 12 member A (CLEC12A), Dectin-1, DC immunoreceptor (DCIR), CD11c and CD40 were shown to facilitate the cross-presentation pathway (176–182).

Targeting LOX-1 and Dectin-1 on human monocyte-derived DCs resulted in a predominantly **MHC II-restricted antigen presentation** and eliciting $CD4^+$ T cell responses (182). Fcγ receptors and DEC-205 facilitated internalization of model antigens by mature bone marrow-derived DCs, their processing in MHC II-enriched endosomal compartment and efficient presentation to $CD4^+$ T cells in mice (171). TLR5 serves as an endocytic receptor for flagellin and facilitates its MHC II-restricted presentation and stimulation of flagellin-specific $CD4^+$ T cells (183). Endocytic function of surface lysosome-associated membrane protein-2 (LAMP-2) on human monocyte-derived DCs has been reported recently (184). Surface ligation of LAMP-2 induced rapid internalization of the receptor and its trafficking to the MHC class II peptide-loading compartment. Despite this, DCs pulsed with antigens conjugated to anti-LAMP-2 antibody evoked only modest $CD4^+$ T cell proliferation. Instead, antigens internalized with LAMP-2 were selectively routed into highly immunogenic exosomes that stimulated robust proliferation of $CD4^+$ T cells (184).

Antigen processing appears to be impacted not only by the type of endocytic receptor, but also by the **receptor's targeted domain**. Ligand binding to carbohydrate recognition domain of DC-SIGN (for dendritic cell-specific intercellular adhesion molecule-3 grabbing non-integrin) resulted in a rapid internalization of the ligand-receptor complexes, leading to $CD4^+$ and $CD8^+$ T cells responses (185,186). However, targeting the DC-SIGN neck region led to ~1000-fold greater antigen cross-presentation compared to 'free' antigen (187).

Thus, engagement of one or another endocytic receptor can influence the MHC restriction of an antigen processing/presentation. Expanding our knowledge of these mechanisms is essential for understanding the pathogen-elicited immune responses. It may also help to develop vaccines with predicted and desirable immunogenic properties.

The initial step in the influenza virus interaction with a human being is binding of the HA spike to N-acetylneuraminic (sialic) acids on the surface of a respiratory epithelial cell. The carbon-2 of the terminal sialic acid can be attached to either the carbon-3 or carbon-6 of galactose, forming α-2,3- or α2,6-linkages; these linkages result in unique steric configurations of the terminal sialic acids (188). The α-2,6-linkages predominate in human upper respiratory tract (nasopharynx, paranasal sinuses, trachea and bronchi), while α-2,3-linkages are more common in duck gastrointestinal tract epithelium. Sialic acids with terminal α-2,3-linkages are also present in human lower respiratory tract (bronchioles and alveoli) epithelium (189–191). Thus, humans can be infected only with difficulty by most avian influenza viruses (i.e. they must somehow access the deep respiratory tissues) (23,192,193). Both α2,3- and α2,6-linked sialic acids are present in varying densities on human immune cells such as alveolar macrophages, peripheral blood monocytes, monocyte-derived macrophages and DCs, creating a widely underappreciated variable in the immune responses against different influenza strains and vaccines (194–196).

The HA - sialic acid interaction is based on recognition of the unique amino acid sequence of HA but can be greatly impacted by the glycosylation pattern of HA (197). Pre-treatment of target cells with bacterial sialidases can strip sialic acids from their surface and prevent binding of influenza viruses and subsequent infection (198–201). Blocking sialic acid residues with proteins engineered based on sialic acid-binding domain from *V. cholerae* or *S. pneumoniae* sialidases can mask the cell-surface receptor recognized by the influenza virus and protected mice from a lethal challenge with 2009 pandemic H1N1 influenza virus (202). However, it has been shown that influenza viruses can also infect desialylated mammalian cells in some experimental models (189,203). Although Lec1 cells, a mutant CHO cell line deficient in terminal N-linked glycosylation, are refractory to infection by several strains of influenza virus due to the lack of sialoglycoproteins, surface binding mediated by the normally-expressed sialoglycolipids is not impaired (199). Thus, although the influenza HA - sialic acid interaction is an important component of the infectious process, sialic acids presence on the surface of target cells are not an absolute requirement for virus entry and sialic acid-deficient cells can sometimes be infected by alternate mechanisms. These observations led to the hypothesis of a more supportive role for sialic acid residues that they serve as attachment factors rather than fully-featured entry receptors on target cells (204). In other words, sialic acids may help to concentrate

influenza virions on the surface but other putative receptors such as transmembrane protein(s) are necessary for executing target cell entry by influenza virions. The entry step is essential for the infectious process, allowing viral replication and spread. It is not yet known if the sialic acid residues are structural components of the entry receptors themselves or act as coreceptors by brining influenza virions into close proximity with the entry receptors and facilitating their interactions (205).

Although the specific molecules mediating influenza virus entry into macrophages and DCs have not yet been defined, several receptor candidates have been proposed to date. Cell entry of influenza viruses binding to 2,6- but not 2,3-linked sialic acids can be mediated by host **fibronectin** in epithelial cells (206). The ability of several influenza strains to infect murine alveolar and peritoneal macrophages as well as the macrophage-derived cell line J774 is markedly inhibited by mannan, a competitive ligand of mannose receptor (**MR)**, suggesting an important role for this receptor in influenza virus binding and/or entry into macrophages (207). Influenza viruses directly bind to the carbohydrate recognition domains of MR and **MGL** in Ca^{2+}-dependent manner but independently of sialic acids (208). Multivalent blocking ligands of the MR and MGL inhibit the influenza virus infection of macrophages in a manner that correlates with expression of these receptors on different macrophage populations (208). In Lec1 cells that are largely resistant to influenza infection despite abundant expression of sialic acids and surface binding of influenza virions (199), transfection with C-type lectin MGL1 enhances Ca^{2+}-dependent influenza A virus binding and restores permissivity to infection (209). Sialic acid-deficient Lec2 cells, a mutant CHO cell line, are resistant to influenza virus infection; however, transfection of Lec2 cells with C-type lectin receptor **Langerin** restores their susceptibility to influenza A virus infection (210). Infection of Langerin-transfected Lec2 cells depends on lectin-mediated recognition of the virus, which is inhibited by mannan and modulated by the degree of glycosylation of the viral HA (210). Transfection of Lec2 cells with either **DC-SIGN** or **L-SIGN** make them susceptible to influenza virus infection (211). DC-SIGN-expressing B-THP-1/DC-SIGN and T-THP-1/DC-SIGN cells show enhanced susceptibility to H5N1 virus particles (pseudotyped or generated by reverse-genetics). DC-SIGN expression facilitates virus transport to recipient cells via B-THP-1/DC-SIGN and human DCs; this action is blocked by anti-DC-SIGN monoclonal antibodies (212). Mutant influenza viruses bearing HA that cannot interact with sialic acids can infect mammalian epithelial cells

transfected with DC-SIGN in sialic acid-independent manner (200). Sialidase treatment of target cells greatly reduces the infection efficiency by a number of influenza viruses bearing fully-functional HA; however, DC-SIGN transfection restores susceptibility of desialylated cells to infection. The infection rates are reduced in the presence of anti-DC-SIGN blocking antibodies or mannose. Perhaps most importantly, influenza A viruses infect human DCs in DC-SIGN-dependent manner (200).

In summary, a number of C-type lectins and non-lectin proteins have been shown to act as fully-featured binding and/or entry receptors for influenza viruses. However, the primary influenza receptor(s), if a singular 'receptor' exists, remains unidentified. It is of great importance to further explore influenza virus entry mechanisms in APCs because these may have a major impact on magnitude and diversity of the immune responses against the pathogen and because such mechanisms may be 'targetable' for anti-influenza drug development.

1.2.2.1.2. Internalization mechanisms of influenza viruses

The diversity of viral entry/antigen uptake mechanisms by APCs creates another level of cargo sorting that can influence the immune response. DCs and macrophages are 'professional' phagocytes with exceptionally high phagocytic activity. In addition, these cells internalize antigen through macropinocytosis and endocytosis. Further, endocytic pathways can be divided into relatively well-characterised clathrin-mediated endocytosis (CME) and the less well-defined clathrin-independent endocytosis processes (CIE). Indeed, CIE encompasses a large group of endocytic routes that include caveolae-, Arf6-, flotillin-dependent, and several other poorly characterized mechanisms. Despite the fact that all of these processes execute intracellular delivery of exogenous cargo, they are initiated through the engagement of different receptor structures and utilize diverse intracellular networks, which result in distinct antigen processing mechanisms and diverse immunologically relevant outcomes (Fig. 1.3) (213,214).

1.2.2.1.2.1. An overview of the internalization mechanisms that can affect the outcome of antigen processing/presentation

Processing of an exogenous antigen internalized through phagocytosis, macropinocytosis, CME and CIE has been shown to facilitate both MHC I- and MHC II-restricted antigen presentations (215–217). However, there is a rapidly growing body of evidence suggesting that

employment of specific internalization pathways may increase the probability of one or another antigen processing and presentation mechanism. Phagocytosis and macropinocytosis often result in the uptake of large amounts of the antigenic material that favors its cross-presentation by APCs and stimulation of $CD8^+$ T cells (218,219). Caveolae-mediated endocytosis typically delivers cargo into non-degradative and non-acidifying endosomal compartment that retain antigenic material for prolonged periods, favoring its cross-presentation (220–223). In contrast, antigens internalized through CME are most often delivered into rapidly maturing endosomes that undergo acidification and lysosomal fusion (218,222–224). Lysosomal enzymes facilitate proteolysis of antigenic material and formation of 13-25 amino acid (AA) peptides that are optimal for MHC II loading (225). This last endocytic pathway typically results in stimulation of $CD4^+$ T cells and support of antibody production (223,226) .

1.2.2.1.2.2. Diversity of the internalization mechanisms utilized by influenza viruses

Live influenza virus internalization pathways are well-studied in epithelial cells. CME has been shown to be the major uptake mechanism for human and avian influenza strains (51,227–229). CIE and macropinocytosis also play a role in influenza virus cell entry (230–232). Filamentous influenza viruses use macropinocytosis as the primary entry mechanism (49). However, little is known about the endocytic routes favored by influenza viruses to enter APCs. DC-SIGN, which has been considered as a putative entry receptor for influenza viruses, colocalizes with clathrin in immature human DCs, suggesting that CME may play a role in influenza virus internalization by these cells (233). Influenza A virus entry in murine RAW 264.7 macrophages is reduced upon cholesterol depletion, suggesting that CIE contributes to virion uptake in this model (234). Further studies are needed to explore the role of the different endocytic pathways in the influenza virus – APC interactions and care must be taken to study primary human cells rather than murine cells.

1.2.2.1.3. Endosomal trafficking, processing and presentation of influenza virus antigens

Endosomes play a central role in controlling the re-utilization or degradation of cell components such as membrane lipids and membrane-associated receptors, as well as internalized

exogenous cargo. Endosomal trafficking regulates many fundamental processes in a living cell, including nutrients uptake, adhesion, development, immunity and signaling (235). High complexity and diversity of endosomal trafficking machinery support different modalities of antigen processing and presentation by APCs (236,237).

1.2.2.1.3.1. An overview of the endosomal trafficking pathways

The endosomal pool can generally be divided into three large intracellular compartments: early, late and recycling endosomes (Fig. 1.4) (238,239). Early endosomes are defined as a highly dynamic first endocytic compartment to accept incoming cargo internalized from the cell surface. They are often considered as the major intracellular sorting station from which endocytosed cargo can be either recycled back to the cell membrane or targeted for degradation in the lysosomes (240–242). Early endosomes form intracellular functional networks due to high capacity to undergo homotypic fusion, or to fuse with other components of the endocytic system (243). The early endosome milieu is moderately acidified with a pH ~6.3-6.8 that favors dissociation of the ligands from their endocytic receptors and further recycling. At the same time, the early endosome lumen is not acidic enough to cause an extensive denaturation and degradation of the cargo (240). Within minutes, a substantial portion of cargo accumulated in early endosomes recycles back to the plasma membrane, directly or via recycling endosomes in the perinuclear region (244). Another group of early endosomes undergo maturation as they move towards the perinuclear space where they give rise to the late endosomes that inherit the vacuolar domains of the early endosomal network. These maturing endosomes carry a selected subset of the endocytosed cargo and lower their intralumenal pH to ~6.0–4.9 *en route* with newly synthetized lysosomal hydrolases (242,245). The fusion of an endosome with a lysosome generates a transient hybrid organelle, the endolysosome, in which active degradation takes place (246,247). Late endosomes typically contain a number of intraluminal vesicles, adopting the morphology of multivesicular bodies (248). These intraluminal vesicles and the proteins and lipids associated with them can be either degraded or secreted as exosomes to the extracellular environment upon fusion of late endosomes with the plasma membrane (245,249,250).

A number of proteins that execute key functions of specific endosome types are widely used for their morphological characterization and visualization including a group of endocytic regulators called Ras-associated binding (Rab) proteins. Rabs are small GTP-binding proteins

that cycle between a GTP-bound active state and a GDP-bound inactive state. In their active state, Rab proteins localize to intracellular membranes where they can interact with and recruit a variety of proteins known as Rab effectors. Rab proteins regulate a wide range of endosomal trafficking, maturation, fusion processes, and serve as hallmarks of distinct endosomal pools. More than 60 Rab proteins have been characterized to date (240,251,252).

Rab5 is the most extensively studied protein of the early endocytic pathway and is often targeted for phenotypical or functional characterization of early endosomes. Rab5 regulates entry of the cargo from the plasma membrane to the early endosomes, controls the lipid composition of early endosomes, their homotypic fusion and the motility of early endosomes on actin and microtubules tracks. Rab5 follows early endosomes through the various stages of their maturation and serves as the main regulator of the conversion to late endosomes (235,252). Early endosomal antigen-1 (EEA1) is a well-characterized effector of Rab5 that controls membrane docking/fusion, and is another widely-used marker for early endosomes (252,253).

In the course of endosome maturation, replacement of Rab5 by Rab7 occurs, a process called Rab conversion (254). Rab conversion is an essential step in late endosomes formation and in the transport of cargo to lysosomes. As the result of repetitive endosomal fusion and fission events, endocytosed cargo in early endosomes becomes concentrated in fewer and larger endosomes, which progressively move to the perinuclear region. During this movement, the levels of Rab5 peak, and then the complete loss of Rab5 and its replacement with Rab7 occurs. Thus, conversion of Rab5 to Rab7 designates the transition of cargo from early to late endosomes (245,252). Importantly, Rab5 and Rab7 proteins can sometimes be co-expressed on the same endosomal vesicles. These ‘double positive’ endosomes comprise about 14% of the early endosomal pool and identify a subset that undergoes rapid maturation. Stimulation of cell endocytic machinery can lead to a further increase in the number of $Rab5^{+}Rab7^{+}$ endosomes up to 35% (224). However, a large portion of early endosomes remains $Rab5^{+}Rab7^{-}$, therefore representing the pool of slowly maturing early endosomes (224). With further maturation, late endosomes acquire lysosomal-associated membrane protein 1 (LAMP-1), another marker commonly used for characterization of the end-stage degradative endosomal route. At steady stage, LAMP-1 is presented on late endosomes, lysosomes and endolysosomes (245). However, LAMP-1 can also be found at low levels at the plasma membrane and even detected in the early endocytic compartment (255).

Recycling endosomes form another highly heterogeneous intracellular compartment. Rapidly recycling endosomes bear Rab4 marker, whereas slowly recycling vesicles are characterized by Rab11 expression (244). Diverse recycling endosome subtypes can also be distinguished based on Rab35, Arf6 or transferrin receptors presence (256).

Functionally, non-acidified early and/or recycling endosomes bearing the markers Rab5, Rab14, Rab3b/3c, EEA1 and enriched with MHC class I molecules serve as a cross-presentation compartment favoring antigen processing for MHC I-restricted presentation (223,257,258). As noted above, these endosomal markers are of great use in characterizing the various intracellular vesicles that arise from different forms of endocytosis, macropinocytosis and phagocytosis by APCs (235,251,252).

1.2.2.1.3.2. Endocytic mechanisms of MHC II-restricted antigen presentation

MHC II molecules are expressed on immune cells such as B cells, monocytes, macrophages, and DCs, and on epithelial cells following inflammatory signals (237). MHC II-restricted antigen presentation is primarily based on processing within endosomes (223) where acidification followed by fusion with lysosomes favor for MHC II-restricted antigen presentation (Fig. 1.5) (226). Such antigens can be acquired from the extracellular environment or imported from the nucleo-cytosolic space (259). Captured antigens in the endosomal route are degraded by proteases and loaded onto MHC II molecules for cell surface display. The peptides produced are of variable length but are typically longer than those suitable for the MHC I-restricted presentation: usually 13-25 AA-long due to the open configuration of the MHC II binding groove (225). MHC II is composed of two chains – α-chain and β-chain that are already fully assembled in the ER. However, they capture peptides only after arriving at the endocytic pathway. Premature peptide loading is prevented by the invariant chain (Ii) that blocks the binding groove with its domain called CLIP (for class-II-associated invariant chain peptide) (225,260). In late endosomes/endolysosomes Ii is degraded by proteases, except the CLIP segment that is protected due to its binding to MHC II. CLIP is subsequently exchanged for a higher affinity antigenic peptide; a process that is controlled by two chaperones – DM (HLA-DM in humans) and DO (HLA-DO in humans) (237). The peptide-loaded MHC II molecules move to the plasma membrane either via vesicular transport or in the form of tubules. Antigenic peptide-loaded MHC II molecules on dendritic cells present antigen to naïve $CD4^+$ T cells and later, the

same MHC II-peptide complexes can participate in interaction of B cells and APCs with these peptide-specific $CD4^+$ effector T cells (261). Thus, the MHC II – antigenic peptide interaction is a tightly regulated process that results primarily in activation of $CD4^+$ T cells. Most of these $CD4^+$ T cells are considered to be 'helpers' that, once activated, promote B cell differentiation and antibody production, as well as $CD8^+$ T cell responses. In addition, activated $CD4^+$ T cells secrete a wide variety of cytokines and chemokines, depending on their T helper phenotype, which vary widely in physiologic actions; from differentiation and activation to suppression of other immune cells (225,262,263).

1.2.2.1.3.3. Mechanisms of MHC I-restricted antigen presentation

MHC class I molecules are found on the surface of all nucleated cells. They are heterodimers that consist of two non-covalently linked polypeptides, the α chain and β2-microglobulin. The α chain has three domains, α1, α2, and α3. The first two constitute the peptide-binding groove, whereas the α3 domain mediates the interaction with β2-microglobulin (264). The primary function of peptide-loaded MHC I is priming and activation of antigen-specific $CD8^+$ T cells that monitor all cells of the body, ready to destroy any that constitute a threat to the integrity of the host. Thus, cytotoxic T cells (CTL) kill infected cells, preventing them from supporting viral replication. These CTL also eliminate spontaneous tumors as a result of their ability to detect quantitative and qualitative antigenic differences in transformed cells (265,266). In this respect, the MHC I-associated peptides can originate either from degradation of endogenous/host proteins or from newly-synthesized virus-derived proteins/peptides that have exploited the host cells translation machinery. This process is termed 'classic', or 'direct' presentation (Fig. 1.6). Another source of the MHC I-associated peptides is degradation of internalized exogenous proteins; a process called cross-presentation (144,260,267).

1.2.2.1.3.4. Cross-presentation of exogenous antigens

Antigen cross-presentation occurs primarily in specialized APCs and mostly by DCs (264). However, with appropriate stimulation, macrophages are also able to cross-present endocytosed antigens (268–270). The two major pathways of the cross-presentation are endosomal and cytosolic (Fig. 1.7) (264). Endosomal cross-presentation involves the uptake of protein that is directly degraded in endosomal compartment in a manner independent of

proteasomal degradation and transporter associated with antigen processing (TAP)-mediated transport (220). Antigen delivery and retention in non-acidified endosomal compartments facilitates its cleavage by proteases that work best at neutral pH (e.g. Cathepsin S) and trimming by endosomal insulin-regulated aminopeptidase (IRAP). These processes generate high affinity peptides for MHC I loading (271,272). These peptides are typically 8-11 AA due to closed configuration of the MHC I peptide binding groove (218); under some circumstances however, longer peptides can also bind to MHC I with high affinity (273,274). In general, endosomal processing produces longer peptides compared to the cytosolic mechanism (275). The peptide – MHC I interaction is a dynamic process in which peptides reversibly bind to and dissociate from MHC I and are further trimmed by IRAP until a high affinity peptide – MHC I interaction is achieved (260). Indeed, optimal binding of antigenic peptides on MHC I is an elaborate process that requires the coordinated function of several proteins forming the peptide-loading complex: TAP, tapasin, calreticulin, protein disulfide isomerase Erp57 and the empty MHC I molecules awaiting peptides (264). The peptide-loading complex can be delivered to endosomes by vesicular traffic from the ER-Golgi intermediate compartment through the interaction of Sec22b protein with syntaxin-4 presented on endosomes and phagosomes (276). Thus, MHC I loading with antigenic peptides can be fully executed within the endosome. Acidification of the endosomal milieu impairs cross-presentation, probably due to dissociation of the newly formed peptide-MHC I complexes or by shifting the pH away from the optimal for endosomal proteolysis (220). It is interesting that the oxidative burst in phagocytic cells serves as mechanism that helps to prevent endosomal acidification. Reactive oxygen species can trap protons, providing alkalization of the endosomal milieu (277,278).

In the cytosolic cross-presentation pathway, exogenous antigens are released from the endosomes into the cytosol by the endosomal Sec61 transporter (279). Once in the cytosol, they undergo further degradation by proteasomes and cytosolic aminopeptidases, and the resultant peptides are delivered into ER for trimming by endoplasmic reticulum aminopeptidases ERAP1 and ERAP2 and optimal loading onto MHC I (280). Peptide – MHC I interactions in ER are facilitated by the peptide-loading complex, similar to the process that occurs in endosomes (218,225,264). Reactive oxygen species can also induce leakage of antigens from endosomes into the cytosol as a result of the endosomal lipid peroxidation and disruption of endosomal membranes (281).

Sensing of PAMPs by pathogen recognition receptors in APCs facilitates the cross-presentation mechanisms described above. In particular, RIG-I ligands have been shown to stimulate antigen cross-presentation *in vivo* in a MAVS and type I IFN-dependent manner (282). RIG-I signaling interacts with the stimulator of interferon genes (STING) pathway that generally triggers antiviral responses to DNA viruses (283). The STING signaling pathway is strongly linked to cytosolic cross-presentation mechanisms, and STING ligands are considered to be promising candidate adjuvants for antiviral and cancer vaccines (284). Importantly, STING signaling can also be activated in epithelial cells, macrophages and DCs by fusion of enveloped viruses with either cytoplasmic or endosomal membranes leading to the triggering of a strong type I IFN response (285,286). Stimulation of TLR4 causes spatial re-distribution of lysosomes into a dense perinuclear cluster, delaying their fusion with phagosomes. In the absence of lysosomal proteases in phagosomal milieu, excessive degradation of internalized antigen is prevented, favoring its cross-presentation (287). TLR4 stimulation also leads to routing of $Rab11a^{+}$ recycling endosomes, which are the major intracellular reserve of MHC I. Subsequent phagosome fusion with recycling endosomes brings the MHC I molecules for loading with phagocytosed antigen-derived peptides (288). TLR4- and MyD88–dependent relocation of TAP to early endosomes also supports endosomal loading of antigenic peptides on MHC I (289). Finally, recruitment of the Sec61 translocon to endosomes depends on TLR signaling via TIR-domain-containing adapter-inducing interferon-β (TRIF) and supports endosome-to-cytosol release of an antigen and favors its proteasomal degradation and cross-presentation via the cytosolic pathway (279). Thus, many different innate sensors have been shown to support both the endosomal and cytosolic cross-presentation pathways.

1.2.2.1.3.5. Endosomal trafficking of influenza viruses

Endosomal trafficking of influenza viruses has been well-studied in epithelial cell models. For example, Lakadamyali and colleagues labeled influenza virions with the lyophilic fluorescent dye 1,1-dioctadecyl-3,3,3,3-tetramethylindodicarbocyanine (DiD) which allowed visualization of the virus-bearing endosomal compartment of CHO cells (290). Endosomes containing the fluorescent particles first moved slowly in the cell periphery, then adopted a rapid and unidirectional movement towards the nucleus, followed by intermittent, often bidirectional movement in the perinuclear region. DiD fluorescence dequenching suggested that endosomal

acidification was followed by fusion with the viral envelope in the perinuclear area (290). Sieczkarski *et al.* showed that the influenza virus infectious process required functional Rab5 and Rab7 proteins expressed in HeLa cells and that viral NP colocalized with the early endosome marker EEA1 in the cell periphery approximately 5-15 min post-infection and with the late endosomal marker CD63/LAMP3 in the perinuclear region 35-45 min post-infection (291). These observations suggest that influenza viruses move through the early-to-late endosomal maturation and acidification pathway; exploiting it for release of the viral genome into the cytosol.

Endosomal acidification is essential for influenza genome release into the cytosol and productive viral replication (292). Influenza HA mediates fusion of the virion's lipid envelope with endosomal membrane. The merging of two membranes is a thermodynamically favored process but has a high kinetic barrier. The energy to overcome this barrier is provided by the 'spring-loaded' mechanism of HA conformational change (193). In brief, HA on the surface of influenza virions is presented in a non-cleaved HA0 form. Upon internalization and endosomal handling, HA0 undergoes cleavage by the cellular proteases, yielding HA1 (the receptor-binding subunit) and HA2 (the fusion subunit) that remain disulfide-linked. Endosome acidification to pH between 5.0 and 6.0 triggers conformational change in HA resulting in the insertion of HA2 subunit's fusion peptide into the target membrane and envelope-membrane fusion. In addition, the proton flux driving acidification also enter the virion core via the M2 ion channel where they cause detachment of the M1 layer from the nucleocapsid, making the envelope more malleable and easy to fuse. Membrane fusion results in formation of a fusion pore and release and transport of the viral genome into the nucleus, leading to the viral RNA replication and subsequent assembly of new progeny viruses (53,293,294).

Macrophages and DCs generally support the influenza virus replication, although special conditions may be required for this to occur (138,295,296). Endosomal trafficking of influenza virions has been characterized in human monocyte-derived DCs. The virus particles visualized by NP immunostaining are associated with early endosomes expressing EEA1 at 5 min post infection. Peak association with the late endosomal marker LAMP1 occurs at 15 min post infection, and at 30 min of infection most of the NP signal was observed in the nucleus (297). Thus, in this APC model, the influenza viruses moved from early to late endosomes, and

endosomal maturation facilitated viral RNA release into the cytosol and transportation into the nucleus.

In summary, influenza viruses remain major human pathogens. Understanding the infectious process, and particularly virus interactions with the immune cells, is critically important for disease prevention and treatment. Although a good deal is known, the nature of influenza receptors, mechanisms of cell entry in APCs, as well as the viral antigens processing and presentation still require further research in order to develop more effective vaccines and novel therapeutics that will help to reduce the influenza burden.

1.2.2.2. Effector mechanisms of adaptive immunity against influenza

Efficient viral clearance requires the activation, rapid proliferation, recruitment, and expression of effector activities by multiple cellular elements of the adaptive immune system. Humoral immunity is mediated by production of antibodies against different influenza antigens, among which the HA-specific antibodies play a major role in virus neutralization and prevention of the illness. Cell-mediated immunity, including $CD4^+$ helper T cells and $CD8^+$ cytotoxic T cells, are the other arms of adaptive immunity induced upon influenza virus infection (85,98,298).

1.2.2.2.1. Cytotoxic $CD8^+$ T cell-mediated immunity against influenza

Cytotoxicity mediated by influenza-specific $CD8^+$ T cells is the primary mechanism for elimination of infected cells. Although pre-existing $CD8^+$ T cell-mediated immunity cannot itself prevent infection (i.e. no 'sterile immunity'), this cell population is nonetheless a major contributor to influenza virus elimination and host recovery, leading to a milder disease (299). Among individuals found to have low or absent neutralizing antibodies against the pdmH1N1 strain in 2009-10, those with pre-existing T cells that recognized conserved CD8 influenza epitopes developed less severe illness. The total symptom scores in these individuals were most the strongly (inversely) correlated with the frequency of IFN-γ^+ IL-2^- $CD8^+$ T cells (300). The importance of $CD8^+$ T-cells for protection against severe influenza caused by emerging strains has also been demonstrated with the avian A/H7N9 influenza virus that causes high hospital admission rates (>99%) and mortality (>30%) (301). Patients who are discharged from hospital within 2-3 weeks have early and prominent H7N9-specific $CD8^+$ T cells producing IFN-γ, while

individuals with prolonged hospital stays (recovery by week 4) had slower $CD8^+$ T cell responses. Those who succumbed had minimal influenza-specific immunity and little evidence of T-cell activation. In contrast, the anti-H7N9 antibody titers did not differ between groups (301).

The longevity of $CD8^+$ T cell immunological memory is another important aspect to consider (302). Most adults have been exposed to several influenza viruses by the age of 15 (303). Healthy human lung tissue contains a population of $CD8^+$ resident memory T cells that are highly proliferative and whose progeny are polyfunctional. These cells maintain the diversity of T cell receptors over time with no indication of clonal skewing or receptor repertoire narrowing. The size of the influenza-specific $CD8^+$ T cell population persisting in the lung directly correlates with the efficiency of differentiation into resident memory T cells (304). However, not all individuals are able to rapidly elicit an influenza-specific cytotoxic T cell response and control the disease following subsequent re-infection (299). It has been estimated that more than 100 IFN-γ-secreting cells/10^6 peripheral blood mononuclear cells are needed to provide protection against clinical influenza in children (305). This threshold means that the maintenance of a 'deep' T cell memory pool is necessary to achieve its rapid expansion and protection against the disease. In mice, influenza-specific $CD8^+$ T cells can persist for life-time when the animals are primed as early as at 6 weeks of age (306). The persistence of influenza-specific memory $CD8^+$ T cells can be detected for at least 13 years in humans; however sub-clinical influenza infections are likely to contribute to the maintenance of the memory pool (307). These observations suggest that periodic boosting through vaccination has the potential to reinforce the influenza-specific $CD8^+$ T cell memory pool. A vaccine that can do this might be of particular benefit in the elderly (299).

The $CD8^+$ T cell response against influenza viruses is largely directed towards the internal proteins that are highly conserved across strains. As a result, these CTL have the potential to be cross-protective, possibly even providing benefit against pandemic strains. Eliciting such a response is an attractive strategy in the development of a universal influenza vaccine (299,308,309). According to the Immune Epitope Database (IEDB) (310), most of the human $CD8^+$ T cell epitopes originate from the influenza NP, PB1 and M1 proteins (311). However, contributions of the surface proteins HA, NA and extracellular domain of M2 (eM2) to the cell-mediated protection should not be underestimated. Human monocyte-derived DCs

pulsed *ex vivo* with the virus-like particles (VLPs) containing HA, NA and M1 proteins and co-cultured with autologous $CD8^+$ T cells stimulated proliferation and cytokine production by these T cells in dose-dependent manner (312). In a murine challenge model, intranasal vaccination with VLPs containing HA and M1 proteins led to an increase in HA-specific $CD8^+$ T cells in the lungs and protection from subsequent homologous infection. $CD8^+$ T cell depletion resulted in a substantial reduction of the VLP-induced protection. Moreover, the HA/M1-VLP immunization provided partial protection from a high-dose, heterosubtypic challenge that was attributable to the anti-HA $CD8^+$ T cells (313). Mice immunized with ovalbumin adjuvanted with a STING agonist that induced antigen cross-presentation were protected from a challenge with a recombinant H1N1 influenza PR8 strain expressing the MHC I-restricted SIINFEKL ovalbumin peptide integrated into HA (284). This elegant experiment not only demonstrated the importance of antigen cross-presentation and cell-mediated immunity in the protection against influenza but also revealed the potential contribution of the MHC I-restricted sequences within the HA protein. Among the total of 272 human MHC I-restricted $CD8^+$ T cell influenza A epitopes listed in the IEDB to date (310), 17 peptides (6.25%) are HA-derived, suggesting that HA has the potential to elicit at least some degree of CTL immunity in humans. Importantly, the average length of these peptides is 12.6 amino acids, and 6 of them (35%) are longer than 11 AA that are typically successfully accommodated by MHC I (218).

Although there is considerable interest in developing a $CD8^+$ T cell influenza vaccine, a great deal remains to be learned about the human influenza-specific $CD8^+$ T cell response. Further studies are needed to identify and characterize the novel immunogenic $CD8^+$ T cell epitopes across a range of influenza antigens, and to understand the $CD8^+$ T cell longevity and functionality in order to rationally design the vaccination strategies that optimally balance the $CD8^+$ T cell response with other T cell populations and antibody production.

1.2.2.2.2. The role of $CD4^+$ T cells in providing protection against influenza

$CD4^+$ T cells play a central role in immune responses to viral infections through the multiple effector mechanisms, as well as acting in a regulatory role to maintain homeostasis. For example, a subset of $CD4^+$ T cells can act as cytotoxic, CTL-like effectors in influenza infection (314). These cells require type I IFNs and IL-2 as well as STAT5 phosphorylation and homodimerization to upregulate the expression of perforin and granzyme B in response to

influenza virus infection (315,316). The Homolog of Blimp-1 in T cells (Hobit) transcriptional factor characterises cytotoxic $CD4^+$ T cells that display constitutive expression of granzyme B and perforin at the protein level and mediate MHC class II-dependent killing of target cells (317). Live cytotoxic $CD4^+$ T cells can be sorted based on the surface expression of CRTAM (class I-restricted T cell-associated molecule) and the NK cell marker NKG2C/E (318,319). Cytolytic $CD4^+$ T cells are abundantly present in the lungs during influenza infection (314,318), and have been proposed as a correlate of protection based on human challenge studies (320).

$CD4^+$ T cells also play an indirect cytotoxic role by providing support for $CD8^+$ T cells (321). $CD4^+$ T cells activated in response to the influenza A virus infection are the major source of CD154 (CD40 ligand) signaling, and therefore ensure efficient programming of robust effector and memory virus-specific $CD8^+$ cytotoxic T cell responses (322). In addition, $CD4^+$ T cells from influenza infected mice provide a licensing signal to DCs that results in a greater recall capacity of influenza-specific $CD4^+$ and $CD8^+$ T memory responses after heterologous influenza A virus challenge (323).

The ability of $CD4^+$ T cells to facilitate antibody responses is generally acknowledged (324). The interactions between $CD4^+$ T cells and B cells promote both rapid extrafollicular antibody production as well as the later-evolving germinal center response that drives immunoglobulin affinity maturation and long-lived B cell immunity against influenza (325). Follicular helper T cells efficiently induce memory B cells, but not naïve B cells, to differentiate into plasma cells that produce influenza-specific antibodies *ex vivo* (326). The number of follicular helper T cells in peripheral blood rapidly increases after vaccination, and correlates strongly with the increase in the avidity of anti-influenza antibodies, particularly in subjects who do not have high affinity antibodies at baseline (327).

Finally, influenza-specific $CD4^+$ T cells have regulatory and repair function (85,328). Influenza A virus infection triggers a robust $Foxp3^+CD4^+$ regulatory T cell (Treg) response that paradoxically precedes other effector T cell responses in lungs. The suppressive function of Tregs against antigen-specific $CD4^+$ and $CD8^+$ T cell proliferation and cytokine production correlates with their ability to respond to influenza virus antigens, suggesting that virus-induced Tregs are capable of attenuating the effector immune responses in antigen-dependent manner (329). The precise role of this early $CD4^+$ Treg response is not yet fully understood but it may help to diminish the inflammatory lung damage that can occur during influenza infection.

1.2.2.2.3. Humoral immune response against influenza

The humoral immune response results in production of antibodies targeting different influenza antigens. These antibodies can be classified into two broad groups: neutralizing and non-neutralizing. Non-neutralizing antibodies comprise the greatest part of the antibody pool generated after the disease or vaccination, but only a small fraction of these antibodies have clearly defined functional attributes (330). Neutralizing antibodies against the HA globular head interfere with the sialic acid-dependent binding of the virus to the surface of target cells. At high titres, these antibodies alone can prevent the illness (i.e. provide 'sterile' immunity). However, the host's humoral response exerts strong selective pressure on the HA, focused principally on the highly exposed globular head, giving rise to the antigenic diversity of this protein. Thus, influenza HA is both immunodominant and highly variable. Mutations in the HA gene are largely responsible for escape of influenza viruses from the pre-existing immunity mediated by neutralizing antibodies (157,331).

In contrast to the HA globular head, the stalk domain displays a much higher level of conservation across influenza strains and therefore has the potential to confer broad protection against different influenza strains (332–334). Antibodies against the HA stalk region restrict the pH-dependent conformational changes required for the viral fusion. Thus, anti-stalk antibodies are also functional, and can prevent viral genome release into the cytoplasm of the host cell.

Influenza NA is another target for humoral immunity. Although antibodies against NA are not neutralizing, they can slow virus replication and reduce the viral load in tissues, leading to fewer days of the illness, less severe symptoms, and reduced viral shedding (335). Natural influenza infection also elicits a wide range of non-neutralizing antibodies directed against M1, M2, and NP proteins. Such antibodies can promote Fc-mediated viral clearance with the help of Fc receptors on phagocytic cells and natural killer cells. These antibodies can also drive antibody-dependent cell-mediated cytotoxicity (ADCC) (336). Finally, the complement system can also use these antibodies to clear virus in a process called complement-dependent cytotoxicity (337).

The primary point of entrance for influenza is the respiratory mucosa. Although far less is known about the role of mucosal antibody production in influenza, local production of IgA and, to some extent, IgM may act in respiratory tissues and fluids to neutralize influenza viruses as they first enter the body (157).

Only pre-existing neutralizing antibodies can confer sterile immunity by blocking influenza virus binding and entry into the host cells. Scientists are evaluating a number of strategies to develop an antibody-based universal influenza vaccine that will elicit broadly neutralizing antibodies against influenza HA globular head or antibodies targeting conserved regions of HA stalk, as well as other influenza proteins. The overall aim of this research effort is to provide cross-reactive and durable protection, and avoid the complexities and inevitable errors associated with the current strategy of annual vaccination with ever-changing vaccine formulations (330,331,333).

1.3. INFLUENZA VACCINES

Vaccines are the best tools available for preventing influenza (1). However, the protection provided by the currently marketed seasonal influenza vaccines is far from perfect. Vaccine effectiveness is highly variable, with an average of 50–60% estimated protection when the vaccine is well-matched to circulating viruses, but with substantially reduced effectiveness when there is a mis-match between the vaccine and circulating strains. Furthermore, these vaccines work less well in populations that are at highest risk from influenza such as immunocompromised patients, elderly, and unprimed young children (338–341). To maintain even this moderate effectiveness, the composition of seasonal influenza vaccines must be reviewed and updated regularly to include the HA and NA antigens expressed by circulating influenza viruses (340,342,343). Current vaccines depend almost exclusively on the presence of HA for efficacy (342). The primary mechanism of action of seasonal influenza vaccines is the production of anti-HA antibodies that (as outlined above) can inhibit virus attachment to target cell receptors or fusion of viral envelope with endosomal membrane and thereby limit virus infectivity (331,344,345). At present, commercially available influenza vaccines are either trivalent or quadrivalent formulations that target an H1N1 strain, an H3N2 strain and either one or two influenza B strains belonging to evolutionarily diverging the Yamagata and Victoria lineages (344,346,347).

1.3.1. Overview of the current influenza vaccine landscape

Currently, the most widely used products are either inactivated influenza vaccines (IIV) or live attenuated influenza vaccines (LAIV) (348–350). Different formulations of IIV are used

for parenteral administration: whole virion, split virion and subunit vaccines. The inactivated whole virion vaccines were the first ones introduced but they caused high levels of local and systemic adverse reactions and were abandoned when less-reactogenic split vaccines entered the market (351,352). Split vaccines are created by disrupting influenza virus particles with diethyl ether or detergent treatments. While split vaccines still theoretically contain all the viral components, the original viral particulate organization and the viral RNA are lost, as is some of the inherent immunogenicity of the virus. The only viral protein that is quantified in these vaccines is the HA. Subunit vaccines are generated by purifying HA and NA proteins from solution after diethyl ether or detergent splitting (353,354). Although these formulations are better purified they tend to be less immunogenic, and the addition of an adjuvant is sometimes required to reach an adequate anti-HA response, particularly in the elderly (355–357). The primary mechanism of action for IIVs is production of anti-HA antibodies, whereas cell-mediated immune responses are typically weak or undetectable (358–360).

An alternative to inactivated formulations is the LAIV produced by 'inserting' gene segments encoding the desired HA and NA glycoproteins into an otherwise cold adapted (attenuated) strain (342,354,361). Cold-adaptation is a process of developing live attenuated (weakened) virus that grows best at temperatures well below those of the human lower respiratory tract (37°C). The cold-adapted viruses are grown in eggs incubated at 25°C (362–364). These mutant viruses grow quite well in the nasopharynx of humans but will not grow lower down in the respiratory tract. The LAIV induces both antibodies and cell-mediated immunity (as measured by an IFNγ ELISpot assay). Intranasal delivery of LAIV mimics the natural route of influenza infection, resulting in both systemic and localized mucosal immune response at the site of administration (360,365,366). In addition, LAIV is easy to administer and has better acceptance in the pediatric population (367,368). However, because the LAIV vaccine viruses needs to replicate in the host to elicit an immune response, this vaccine does not work in older people with pre-existing immunity (369).

The first recombinant protein vaccine (Flublok™ manufactured by Protein Sciences Corporation) was approved in the United States in 2013 (370). Flublok is based exclusively on the HA proteins of the targeted virus strains but is not yet available in Canada (371).

1.3.2. Serological tests used for evaluation of the influenza vaccine efficacy

Although vaccine efficacy is generally expressed as a proportionate reduction in disease attack rate between the unvaccinated and vaccinated groups in clinical trial settings (372), regulatory assessment of influenza vaccines is often based on a serologic correlate of protection from a limited number of vaccinated individuals (373–375). For decades, the primary goal of vaccination against influenza was the induction of functional antibodies (330).

The hemagglutination inhibition assay (HAI) is the most widely used test for detection of functional antibodies to influenza viruses that can prevent the interactions between influenza viruses and target cells (374). This assay relies on the ability of HA on the surface of influenza virion to bind to sialic acids on the surface of red blood cells (RBCs), causing their agglutination. If a serum sample contains antibodies that block viral attachment, the virus – RBC interaction is inhibited. To perform the HAI assay, a standardized quantity of viral antigen – usually inactivated influenza virions – is mixed with serial dilutions of test serum. Then, RBCs are added, and if the anti-HA antibodies interact with the virions and prevent their binding to RBCs (i.e. hemagglutination), the inhibition of hemagglutination occurs. The highest dilution of serum that prevents hemagglutination is considered to be the HAI titer (376–378). An HAI titer of ≥1:40 is thought to be associated with a 50% reduction in the risk of illness (379).

Microneutralization (MN) is the second 'classic' assay used for detecting strain-specific functional antibodies that inhibit virus entry or otherwise block virus replication in infection-permissive cells (373,374,376). Live viruses are used in MN assay. Serially diluted sera are preincubated with a standardized viral inoculum prior to adding the serum-virus mixture to a Madin-Darby canine kidney (MDCK) cell monolayer. The presence of infectious virus is usually detected by cytopathic effect on the monolayers on days 3 to 7. The absence of cytopathic effect constitutes a positive neutralization reaction and indicates the presence of virus-specific neutralizing antibodies in the serum sample. The assay read-out is typically the reciprocal of the highest serum dilution that reduces the number of input viral plaques by 50% (377,378).

The single radial haemolysis (SRH) assay is based on immunodiffusion of antibodies in agarose gel containing complement and influenza virus bound to RBCs. This method quantifies antibodies that can drive complement-mediated lysis of the RBC and the readout is the area of hemolysis. The SRH area of 25 mm^2 or greater is considered as a 50% protective titer (374,376,380).

Although HAI, MN and SRH assays are widely used both for licensure of vaccines and in epidemiological studies, they all have limitations. Reproducibility of the assays between laboratories is often poor. The titers reported for identical specimens by different laboratories can vary as much as 80-fold for HAI and 128-fold for MN (381). This variability most probably results from differences in the biological reagents needed, as well as the assay protocols, personnel training and other factors that are hard to identify and address (375,382). Some individuals with documented high HAI titers are not protected from influenza, suggesting that the HAI titer should not be used as a stand-alone correlate of protection; at least not for individuals (383). Finally, conventional serological assays are not suitable for evaluation of protection mechanisms such as mucosal immunity, ADCC or complement-dependent cellular cytotoxicity, and T cell immunity that all likely play important roles in recovery from infection and long-term memory (373,375).

1.3.3. Limitations of the current influenza vaccine production platforms

Both IIV and LAIV vaccines typically require propagation of infectious influenza virus in hens' eggs as part of the production cycle. These production methods are labor intensive and time-consuming and depend upon the availability of embryonated eggs (309,384,385). Although yields can be very low for some strains (385,386), each egg typically yields enough antigen for 8-10 doses (per strain) so 4-5 eggs are required to produce ~10 dose of a quadrivalent vaccine (385,387). The production cycle can take 6-9 months from selection of the vaccine components through delivery of vaccine to the population, due to the many steps in this process (345,385). The IIVs are slightly more complicated to produce than LAIV since they must be inactivated prior to vaccination (353,354).

Influenza wild-type strains need to be optimized for growth in eggs, which involves recombination with high-yield laboratory strains. Mutations in the egg-adapted reassortant strain can contribute to a mismatch between the vaccine strain and the circulating influenza strain (388,389).

Decreasing dependence on egg-based influenza propagation is a crucial step towards increasing global influenza vaccine production capacity (309,384,385). Flucelvax, an inactivated trivalent vaccine produced in cell culture by Novartis Vaccines and Diagnostics, Inc. was

approved in the United States in 2012 (390). Flucelvax is not available in Canada up to now (371).

1.3.4. Approaches to overcome the limitations of currently available influenza vaccines

The limitations of influenza vaccines have recently been addressed with a number of strategies. Poor effectiveness can theoretically be improved by broadening their antigenic spectrum by adding an additional B strain to produce a quadrivalent vaccine (QIV) (347,391,392). The introduction of QIVs (including LAIV) resulted in substantial health benefits; reducing the number of influenza cases, their complications and mortality (393,394).

Another approach to increase the vaccine immunogenicity, especially in the vulnerable populations, is increasing the antigen dose. The available high-dose vaccines have four times the amount of HA included in standard influenza vaccines (e.g. Fluzone High-Dose with 60 µg per antigen strain vs. standard IIV with 15 µg per strain) (395). The high dose vaccines provide improved protection against laboratory-confirmed influenza illness among adults 65 years of age or older, irrespective of age, presence of comorbidities, or frailty-associated conditions (396,397). Also, administration of the high dose vaccines lead to significant reduction in influenza-related hospital admissions compared to the standard-dose vaccine recipients (339).

The immunogenicity of influenza vaccines can be increased by adding adjuvants to the formulation. Potential benefits of adjuvanted vaccines include the induction of higher levels of antibodies, stimulation of immune sensors to boost the cell-mediated immune responses, production of cross-reactive antibodies, and longer duration of the immunity (398,399). Adjuvanted vaccines often require less antigen to elicit a similar response (i.e. antigen-sparing). This allows production of more vaccine doses and more rapid vaccine distribution in case of a public health emergency (400,401).

Although a steadily increasing number of adjuvants have been licensed for use in humans, only two have been used for influenza vaccines to date: MF59 and AS03. MF59 is an oil-in-water, squalene-based emulsion that promotes production of cross-reactive antibodies, and has an established safety record (402). Vaccination of elderly individuals with MF59-adjuvanted trivalent vaccine results in significantly higher antibody titers post-vaccination and seroconversion rates compared to the recipients of non-adjuvanted vaccine (355). Compared to a

non-adjuvanted comparator, an MF59-adjuvanted quadrivalent vaccine also has superior efficacy in young children (6-23 months) and in vaccine-naive children up to 5 years of age (403).

AS03 is another squalene-based, oil-in-water adjuvant used in various vaccine products by GlaxoSmithKline (404). McElhaney and colleagues have shown that an AS03-adjuvanted TIV has slightly better efficacy for some subtypes of influenza than a non-adjuvanted vaccine (356), possibly as a result of induction of antigen-specific $CD4^+$ T cells compared to non-adjuvanted group (405). An AS03-adjuvanted pdmH1N1 vaccine containing one-fourth to one-eighth of the standard dose of HA demonstrated a clinically significant improvement in efficacy compared to a non-adjuvanted vaccine in children (401). An increased risk of narcolepsy associated with AS03-adjuvanted pdmH1N1vaccination was reported and led to concerns about this adjuvant (406,407). However, it is still unclear what role (if any) the adjuvant played in this adverse event, and other factors such as genetic susceptibility, exposure to the pandemic virus *per se*, manufacturing impurities need to be considered (330,408,409).

1.3.5. Virus-like particle-based influenza vaccine candidates

Virus-like particles (VLPs) are nanoparticles bearing viral antigens that resemble native virions in size and sometimes structure. VLPs are often highly immunogenic, but are non-infectious due to lack of the viral genetic material (410–412). Several very successful VLP vaccines based on recombinant antigens are in current use including those targeting hepatitis B virus and human papillomaviruses (411,413). VLPs offer many advantages over vaccines based on inactivated or live viruses. As noted above, VLPs have no RNA/DNA so are safer than live virus vaccines. Since no live virus is needed, the manufacturing processes for VLPs are also safer for production staff and health care providers. VLPs can display a number of antigens and adjuvant molecules, and therefore elicit broad immune responses (411). VLPs retain the native antigenic conformation of the immunogenic proteins; they are organized in an ordered array and in a particulate form, all of which promote strong immune responses (411,414). Due to highly repetitive epitopes on the surface, VLPs are able to stimulate APCs and facilitate the internalization of antigenic material, resulting in strong induction of antibodies as well as stimulation of virus-specific $CD4^+$ and $CD8^+$ T cells (415–417). A number of vaccine candidates expressing influenza HA with or without NA (418,419) and other viral proteins (420–422), are

under development, some of which have demonstrated excellent immunogenicity and safety profiles (423–425).

VLPs can be produced in bacteria (*Escherichia coli*) (426), yeast (427), insect cells (428), mammalian cells (429), and *in vitro* cell-free systems (430). Plants are among the most promising VLP-based vaccine production platforms (431). Plants can produce large quantities of VLPs expressing recombinant protein at low cost, their eukaryotic processing machinery supports the post-translational modifications and proper assembly of antigenic proteins, and the plant-derived VLPs lack human pathogen contaminants (432–434). Plant-derived influenza vaccine candidate VLPs have been successfully produced by a number or academic and industrial groups (435–437).

1.3.5.1. Medicago plant-derived influenza HA-bearing VLPs

Medicago Inc. is a Canadian clinical-stage biotechnology company that uses plants to rapidly develop and produce novel vaccines and antibodies (438). The plant-based manufacturing process developed by Medicago relies on transient expression of influenza HA in *Nicotiana benthamiana* upon the transfer of the viral gene to plant cells by the bacterial vector *Agrobacterium tumefaciens* – a process called agroinfiltration (439). Influenza HA-bearing VLPs self-assemble and bud from the plant cells, and do not require any accessory proteins (435). These plant-derived VLPs present HA in the form of homotrimers inserted into a lipid bilayer envelope, that closely resembles the structure of native influenza virions (439). The plant-based transient expression system allows rapid and large-scale production of influenza HA-based vaccine at relatively low cost, meeting several of the principle challenges for vaccine production in a pandemic (i.e. speed & scalability) and representing an excellent alternative to the currently available manufacturing platforms for seasonal vaccines (435).

1.3.5.1.1. Structure and composition of the plant-derived VLPs

An electron microscopy study revealed that ~65% of VLPs have an oblate spheroid structure (discoid-shaped) with loosely packed HA trimeric spikes concentrated at the equatorial region. The 30 to 50 HA trimers/particle are well separated, with an average 176 Å and 203 Å between the tails and the globular head domains, respectively. The second most abundant class are spheroid-shaped particles that contain HA trimers distributed over the entire lipid membrane

surface (30% of the particles). On these particles, an average distance between the HA trimers is 144 Å and 182 Å between the tails and globular heads of neighboring trimers, respectively. More than 99.9% of the HA contained in these vaccines is present on the discoid- and spheroid-shaped VLPs. A minor portion of plant-derived VLPs adopt a rosette morphology or have no HA on their surface (i.e. 'empty vesicles') (440). Native influenza A virions have approximately 300 HA spikes that are separated by a distance of 104 to 112 Å on average (441,442). The less dense presentation of HA trimers on the plant-derived VLPs may facilitate interactions of immune cells with HA epitopes, especially those located in the HA stalk region near the VLP envelope (440). The average diameter of plant-derived HA-VLPs varies between 50 and 150 nm, depending on the HA type and the measurement technique applied (435,440).

Influenza HA expressed on the surface of plant-derived VLPs is detected by Western blot as a 72 kDa protein corresponding in size to the uncleaved HA0 form (435). The HA1 and HA2 cleavage bands and the dimers of HA0 can also be detected with low intensities (443). Mass spectrometric analysis reveals that the extracellular domain of HA on VLPs has the expected post-translational modifications including six N-glycosylation sites in the HA1 globular head or the HA2 stalk regions. These sites carry complex or hybrid glycans containing core α(1,3)-fucose or β(1,2)-xylose epitopes and Lewis^a extensions. Gas chromatographic analysis has revealed the presence of mannose, xylose, galactose and fucose monosaccharides arising from N-linked glycans (443). By far, the most abundant protein identified on VLPs is influenza HA. A number of host cell proteins, many of which were previously identified in *Nicotiana tabacum* lipid rafts, are detected on VLPs in tiny quantities. These include plasma membrane ATPase, ribulose bisphosphate carboxylase/oxygenase, heat-shock protein 70–3, molecular chaperone Hsp90, and others (443,444). Among the plant-derived lipids identified on VLPs were sphingolipids (glucosylceramide), phosphatidylethanolamines, phosphatidylcholines and phosphatidylserines with alkyl chains of different length (16 or 18 carbons) and a number (0-3) of unsaturated double bonds. Identification of the lipid raft markers suggested that the mechanism of VLP formation in plants is similar to the natural process of influenza virus assembly in the mammalian host cells, including recruitment of the viral protein to plasma membrane at lipid rafts followed by VLP budding from the host cell when the appropriate amount of HA has accumulated. Host proteins are mostly excluded from the lipid rafts during the process of VLP formation, similarly to the budding of influenza viruses (439,443).

1.3.5.1.2. Plant-derived VLP interactions with mammalian immune cells

To explore the mechanisms of plant-derived VLPs' immunogenicity, the interactions between these particles and immune cells have been studied *in vitro* and *in vivo*. Short exposure of human PBMCs to H1-VLPs bearing HA from A/California/7/09 (H1N1) resulted in a massive binding of these particles to B cells, monocytes and, to lesser extend, $CD4^+$ and $CD8^+$ T cells. H5-VLPs bearing influenza HA from A/Indonesia/5/05 (H5N1) showed less prominent binding to PBMCs in general, preferentially interacting with monocytes. The patterns of VLP interactions with monocytes *ex vivo* were also different: H1-VLPs appeared to be present in distinct foci at the interfaces between monocytes and adjacent lymphocytes, whereas H5-VLPs rapidly coated the surface of monocytes, and many of these cells bound substantially more H5- than H1-VLPs (445). The H1- but not H5-VLPs caused rapid formation of PBMC clusters with a great contribution of B cells. H1-VLP-stimulated B cells up-regulated expression of the activation marker CD69. Both H1- and H5-VLPs induced proinflammatory cytokines production by human monocytes; however, the effect of H5-VLPs was only seen at higher concentrations of particles. Studies are underway to determine the influence that these early interactions have on the adaptive immune responses to different types of HA delivered in the form of plant-derived VLPs (445).

Footpad injection of a 'trackable' H5-VLP labeled with enhanced green fluorescent protein (eGFP) in mice resulted in a bright green fluorescence in the draining popliteal lymph nodes as early as at 10 min after administration, showing that VLPs rapidly reach the local lymphoid organs by free-drainage. The fluorescent signal disappeared almost completely by 3 hours after the administration, and no fluorescence was seen at any time in the more proximal lymphoid structures, suggesting that the VLPs were likely internalized and the eGFP degraded in the draining lymph node cells (446).

1.3.5.1.3. Plant-derived VLPs' immunogenicity in animal models

In response to the avian influenza pandemic threat, Medicago first developed and tested VLPs bearing HA from the avian A/Indonesia/5/05 (H5N1) strain. Mice immunized with two doses of aluminium hydroxide (alum)-adjuvanted H5-VLPs mounted readily detectable HAI responses. When these mice were challenged with a heterologous strain (A/Vietnam/1194/04

(H5N1), 100% protection was achieved at all tested HA doses (0.5 to 7.5 μg). These results suggested that HA-VLPs could elicit cross-clade protection against potential influenza pandemic strains (435). Another study with H5-VLPs in ferrets showed detectable HAI titers with homologous A/Indonesia/5/05 (H5N1) strain even after a single administration at the highest dose used (11.0 μg). After two doses, all immunized animals had high HAI titers against the A/Indonesia/5/05 strain. The HAI titers measured with three heterologous influenza strains were lower than those directed against A/Indonesia/5/05 virus but challenge with A/Vietnam/1203/04 revealed complete protection from clinical illness in the vaccinated ferrets regardless of low HAI titers. These observations suggested that immune mechanisms other than HAI antibodies may contribute to the protection against both homologous and heterologous challenge (447).

A VLP-based vaccine bearing the HA of another potentially pandemic avian strain A/Hangzhou/1/2013 (H7N9) has also been tested in mice and ferrets (448). A single dose of the vaccine adjuvanted with alum or GLA-SE induced a strong HAI response in both animal species. The second immunization significantly increased the humoral immune response in both adjuvanted and unadjuvanted animal groups. All the mice immunized with one dose of the adjuvanted formulations survived challenge with heterologous A/Anhui/1/2013 (H7N9) influenza strain while five out of eight mice (62%) that received the non-adjuvanted vaccine survived. Two doses of unadjuvanted vaccine significantly increased the humoral response and resulted in 100% protection with significant reduction of the clinical signs leading to nearly asymptomatic infections. In ferrets, a single immunization with the alum-adjuvanted H7-VLP vaccine induced strong humoral response, and a second dose led to a further increase of the HAI titers. The *ex vivo* stimulation of PBMCs obtained from immunized fetters revealed an increase in cell proliferation as well as IFN-γ production by $CD3^+$ T cells. Ferrets immunized with even a single dose of the alum-adjuvanted H7-VLP vaccine were protected from heterologous A/Anhui/1/2013 challenge (448).

The immunogenicity of VLPs bearing the HA from the human A/California/07/2009 (H1N1) influenza strain has been compared to a licensed monovalent split-virion vaccine in young (5- to 8-week-old) and aged (16- to 20-month-old) mice upon single intramuscular or intranasal administration (449). Both VLP and split vaccines given intramuscularly protected 100% of the young animals; however, the antibody titers measured by HAI and NM assays, as well as the HA-specific IgG measured by ELISA, were higher in mice immunized with H1-VLPs

compared to the split vaccine group. Also, the H1-VLP vaccine elicited stronger antigen-specific cytokine/chemokine and lymphoproliferative responses *ex vivo* that were generally more robust in young mice than in aged mice. Aged mice vaccinated with VLPs were more likely to survive homologous challenge compared to split vaccine recipients. Mice immunized with H1-VLPs given intranasally had little detectable humoral or cellular immune response, but survival was still significantly increased. Thus, this study demonstrated that a single dose of H1-VLP-based vaccine delivered intramuscularly was superior to the standard split virion vaccine for almost all parameters at both ages (449).

1.3.5.1.4. Plant-derived VLPs' immunogenicity in clinical trials

Excellent immunogenicity and efficacy of the HA-bearing VLPs in the absence of safety concerns from pre-clinical studies prompted Medicago to launch its clinical development program of the plant-derived VLP vaccine candidates (Table 1.2). An early phase I clinical trial with H5-VLPs (HA sequence from H5N1 A/Indonesia/5/05 influenza strain) demonstrated good tolerability and safety in humans (447). The H5-VLPs were immunogenic, as measured by HAI, MN and SRH titers, with a clear dose-response. Cross-reactive antibodies against H5N1 A/Anhui//1/05 and A/turkey/Turkey/1/05 strains were detected, whereas antibodies against A/Vietnam/1203/04 virus were barely detectable in any assays (447). Two phase II clinical trials confirmed the immunogenicity of the H5-VLPs when administered with adjuvants such as alum or the synthetic TLR4 agonist GLA-SE (450,451). After the second dose, more than 50% of the subjects who received the alum-adjuvanted H5-VLP vaccine achieved a so-called 'seroprotective' HAI titer >1:40. A significant increase of poly-functional and, to a lesser extent, single positive $CD4^+$ T cells stimulated *ex vivo* with either H5-VLPs or an H5 peptide pool was observed in the alum-adjuvanted H5-VLP vaccine groups 6 months after vaccination. Moreover, recipients of the adjuvanted H5-VLP vaccine mounted cross-reactive $CD4^+$ T cell responses to either heterologous H1-VLP or an H1-based peptide pool (450). The GLA-SE-adjuvanted H5-VLPs antibody response met all Center for Biologics Evaluation & Research (CBER) licensure criteria (451). The GLA-SE-adjuvanted H5-VLP also induced a sustained (up to 6 months) polyfunctional and cross-reactive HA-specific $CD4^+$ T cell response. However, the 6-month samples revealed that alum promoted higher frequencies of H5-specific $CD4^+$ effector memory T cells compared to GLA-SE. The ability of the low dose GLA-SE-adjuvanted H5-VLPs to elicit

both a robust humoral response and a sustained cross-reactive cell-mediated immunity supports the potential of H5-VLPs for dose sparing in case of a serious pandemic threat (451).

Humoral and cell-mediated immune responses in humans following H1-VLP (monovalent) vaccination based on HA sequence from A/California/7/09 (H1N1) strain have also been tested in phase I clinical trial (450). Single administration of H1-VLPs resulted in a robust humoral response, and more that 90% of the study participant were seroprotected at day 21 after vaccination based on the HAI titres. Six months after vaccination, 80% of the H1-VLP vaccine recipients still had seroprotective HAI titers (>1:40). The *ex vivo* stimulation of PBMCs with either H1-VLPs or an H1 peptide pool revealed poly-functional and cross-reactive $CD4^+$ T cell responses. $CD8^+$ T cell responses were also clearly detectable but the differences did not reach statistical significance compared to the placebo group (450).

The safety, tolerability and immunogenicity of a seasonal quadrivalent VLP-based influenza vaccine has been studied recently (452). The vaccine was well-tolerated at each dose level. Robust antibody responses were detected at day 21 after immunization for the four homologous strains and all vaccine doses. The HAI titers met the European licensure criteria for the type A influenza strains at the 3 μg/strain dose and for all four strains at higher doses. High HAI titers were maintained for most of the strains 6 months after vaccination. Also, cross-reactive HAI responses were detectable against heterologous A/H3N2 Uru and B/Mass influenza strains at day 21 after the vaccination. At 6 months, strong heterologous responses against A/H3N2 Uru and, at lower magnitude, against A/H1N1 Bris and B/Mal were still present. The vaccine recipients demonstrated polyfunctional and cross-reactive $CD4^+$ T cell responses upon the *ex vivo* stimulation of PBMCs with VLPs or peptide pools at day 21 and 6 months after immunization. Thus, the quadrivalent plant-derived VLP-based vaccine appears to be well-tolerated while eliciting strong and cross-reactive humoral and cellular immune responses that persist for at least 6 months (452).

Currently, Medicago is conducting a phase III efficacy, safety, and immunogenicity study of the plant-derived VLP-based seasonal quadrivalent influenza vaccine with approximately 10,000 adult participants. The estimated study completion date is April 30, 2018 (453).

1.4. RATIONALE AND RESEARCH OBJECTIVES

Influenza is a vaccine-preventable disease. The World Health Organization considers broad-coverage vaccination against influenza the best approach that allows reducing the pathogen spread and the disease burden. However, vaccine products available on the market do not provide a complete protection against the disease, especially in elderly people, young unprimed children and immunocompromised individuals. There is an ongoing effort to develop a better influenza vaccine. In response to the seasonal influenza public health challenge as well as the pandemic threat caused by newly emerging influenza strains, Medicago Inc., a Canadian biopharmaceutical company, developed a plant-based platform for the rapid and large-scale manufacturing of influenza vaccines. These vaccines consist of biological nanoparticles that largely recapitulate the structure and the mechanisms of formation of the native influenza virions. The plant-derived VLPs were studied in a number of pre-clinical and clinical trials, and demonstrated a strong and balanced immunogenicity.

The aim of this exploratory research project was therefore to better understand immunological characteristics of the plant-derived VLPs bearing influenza HA. The first objective of this thesis was to study the key steps of the interaction between VLPs and human immune cells such as binding to the cell membrane, internalization, endosomal handling, and antigen processing and presentation. We found that VLPs rapidly accumulated in an intracellular compartment that preserved undegraded antigen for a prolonged time. This observation prompted us to define VLPs' endosomal trafficking as the second research objective. In the model of human MDMs that are capable of both rapid degradation of the internalized antigen and its processing, presentation and cross-presentation, we studied the mechanisms of uptake and the colocalization of the influenza HA with a panel of endosomal markers over time. HA-VLPs demonstrated bidirectional mode of endosomal handling: while a substantial portion of HA was losing ability to bind a monoclonal antibody, suggesting that these particles have been delivered to rapidly maturing degradative endosomes, another portion of HA was preserved from degradation and colocalized with the markers of early and recycling endosomes, and the immunostained MHC I molecules. Since these conditions are known to favor the cross-presentation of exogenous antigens, we attempted to further explore the HA-VLPs' endosomal fate. The third research objective was to find out whether or not influenza HA delivered in the form of VLPs may undergo cross-presentation by human MDMs. Finally, we attempted to apply

the phenomenon of a fluorescent dye dequenching to characterization of the influenza virions binding to target cells and the viral envelope fusion with cell membranes in the presence of anti-influenza antibodies. Thus, the fourth objective of this thesis was developing a novel serological method for quantitative measurement of the functional antibodies that interfere with key steps of the influenza virus life cycle.

1.5. REFERENCES

1. World Health Organization. Influenza (Seasonal). 2018. Available from: http://www.who.int/news-room/fact-sheets/detail/influenza-(seasonal)
2. Matias G, Taylor R, Haguinet F, Schuck-Paim C, Lustig R, Shinde V. Estimates of mortality attributable to influenza and RSV in the United States during 1997-2009 by influenza type or subtype, age, cause of death, and risk status. Influenza Other Resp Viruses. 2014;8(5):507–15.
3. Nair H, Brooks WA, Katz M, Roca A, Berkley JA, Madhi SA, et al. Global burden of respiratory infections due to seasonal influenza in young children: A systematic review and meta-analysis. Lancet. 2011;378(9807):1917–30.
4. Centers for Disease Control and Prevention. Estimated Influenza Illnesses, Medical visits, and Hospitalizations Averted by Vaccination in the United States. 2018. Available from: https://www.cdc.gov/flu/about/disease/2016-17.htm#table1
5. Gerke AK, Tang F, Yang M, Foster ED, Cavanaugh JE, Polgreen PM. Predicting chronic obstructive pulmonary disease hospitalizations based on concurrent influenza activity. COPD J Chronic Obstr Pulm Dis. 2013;10(5):573–80.
6. Giakoumelou S, Wheelhouse N, Cuschieri K, Entrican G, Howie SEM, Horne AW. The role of infection in miscarriage. Hum Reprod Update. 2016;22(1):116–33.
7. Gordon A, Reingold A. The Burden of Influenza: a Complex Problem. Curr Epidemiol Reports. 2018;5(1):1–9.
8. Warren-Gash C, Blackburn R, Whitaker H, McMenamin J, Hayward AC. Laboratory-confirmed respiratory infections as triggers for acute myocardial infarction and stroke: a self-controlled case series analysis of national linked datasets from Scotland. Eur Respir J. 2018;51(3):1701794.
9. Peasah SK, Azziz-Baumgartner E, Breese J, Meltzer MI, Widdowson MA. Influenza cost and cost-effectiveness studies globally - A review. Vaccine. 2013;31:5339–48.
10. Cassini A, Colzani E, Pini A, Mangen M-JJ, Plass D, McDonald SA, et al. Impact of infectious diseases on population health using incidence-based disability-adjusted life years (DALYs): results from the Burden of Communicable Diseases in Europe study, European Union and European Economic , on behalf of the BCoDE consortium. Eurosurveillance. 2018;23(16).

11. Chaiyakunapruk N, Kotirum S, Newall AT, Lambach P, Hutubessy RCW. Rationale and opportunities in estimating the economic burden of seasonal influenza across countries using a standardized WHO tool and manual. Influenza Other Respi Viruses. 2018;12(1):13–21.
12. de Francisco Shapovalova N, Donadel M, Jit M, Hutubessy R. A systematic review of the social and economic burden of influenza in low- and middle-income countries. Vaccine. 2015;33:6537–44.
13. Holloway R, Rasmussen SA, Zaza S, Cox NJ, Jernigan DB. Updated preparedness and response framework for influenza pandemics. MMWR Recomm Rep. 2014;63:1–9.
14. Taubenberger JK, Kash JC. Influenza virus evolution, host adaptation, and pandemic formation . Vol. 7, Cell Host and Microbe. 2010:440–51.
15. Taubenberger JK, Morens DM. 1918 Influenza:the Mother of All Pandemics. Emerg Infect Dis . 2006;12(1):12–5.
16. Fineberg H V. Pandemic Preparedness and Response - Lessons from the H1N1 Influenza of 2009. N Engl J Med. 2014;370(14):1335–42.
17. Swerdlow DL, Finelli L, Bridges CB. 2009 H1N1 influenza pandemic: Field and epidemiologic investigations in the united states at the start of the first pandemic of the 21 st century. Clin Infect Dis. 2011;52(SUPPL. 1):S1-3.
18. Simonsen L, Spreeuwenberg P, Lustig R, Taylor RJ, Fleming DM, Kroneman M, et al. Global Mortality Estimates for the 2009 Influenza Pandemic from the GLaMOR Project: A Modeling Study. PLoS Med. 2013;10(11):e1001558.
19. Dawood FS, Iuliano AD, Reed C, Meltzer MI, Shay DK, Cheng PY, et al. Estimated global mortality associated with the first 12 months of 2009 pandemic influenza A H1N1 virus circulation: A modelling study. Lancet Infect Dis. 2012;12(9):687–95.
20. Kapoor S, Dhama K. Insight into Influenza Viruses of Animals and Humans . Cham: Springer International Publishing; 2014. 7-13 p.
21. Flynn O, Gallagher C, Mooney J, Irvine C, Ducatez M, Hause B, et al. Influenza D virus in cattle, Ireland. Emerg Infect Dis. 2018;24(2):389–91.
22. Su S, Fu X, Li G, Kerlin F, Veit M. Novel Influenza D virus: Epidemiology, pathology, evolution and biological characteristics. Virulence. 2017;8(8):1580–91.
23. Byrd-Leotis L, Cummings RD, Steinhauer DA. The interplay between the host receptor

and influenza virus hemagglutinin and neuraminidase. International Journal of Molecular Sciences. 2017;18:1541.

24. Luo M. Influenza virus entry. Adv Exp Med Biol . 2012;726:201–21.
25. A revision of the system of nomenclature for influenza viruses: a WHO memorandum. Bull World Health Organ. 1980;58(4):585–91.
26. Centers for Disease Control and Prevention. Influenza Type A Viruses. 2017. Available from: https://www.cdc.gov/flu/avianflu/influenza-a-virus-subtypes.htm
27. Kanegae Y, Sugita S, Endo A, Ishida M, Senya S, Osako K, et al. Evolutionary pattern of the hemagglutinin gene of influenza B viruses isolated in Japan: cocirculating lineages in the same epidemic season. J Virol. 1990;64(6):2860–5.
28. Tafalla M, Buijssen M, Geets R, Vonk Noordegraaf-Schouten M. A comprehensive review of the epidemiology and disease burden of Influenza B in 9 European countries. Hum Vaccin Immunother. 2016;12(4):993–1002.
29. Tan J, Asthagiri Arunkumar G, Krammer F. Universal influenza virus vaccines and therapeutics: where do we stand with influenza B virus? Current Opinion in Immunology. 2018;53:45–50.
30. Badham MD, Rossman JS. Filamentous Influenza Viruses. Curr Clin Microbiol reports . 2016;3(3):155–61.
31. Dadonaite B, Vijayakrishnan S, Fodor E, Bhella D, Hutchinson EC. Filamentous influenza viruses. J Gen Virol. 2016;97(8):1755–64.
32. Taubenberger JK, Morens DM. The Pathology of Influenza Virus Infections. Annu Rev Pathol Mech Dis. 2008;3(1):499–522.
33. Nishimura H, Hara M, Sugawara K, Kitame F, Takiguchi K, Umetsu Y, et al. Characterization of the cord-like structures emerging from the surface of influenza C virus-infected cells. Virology. 1990;179(1):179–88.
34. Air GM, Laver WG. The neuraminidase of influenza virus. Proteins Struct Funct Bioinforma. 1989;6(4):341–56.
35. Copeland C. Assembly of Influenza Haemagglutinin Trimers and Its Role in Intracellular Transport. J Cell Biol. 1986;103:1179–91.
36. Manzoor R, Igarashi M, Takada A. Influenza A virus M2 protein: Roles from ingress to egress. Int J Mol Sci. 2017;18(12):1–16.

37. Ye ZP, Pal R, Fox JW, Wagner RR. Functional and antigenic domains of the matrix (M1) protein of influenza A virus. J Virol . 1987;61(2):239–46.
38. Sugita Y, Sagara H, Noda T, Kawaoka Y. Configuration of Viral Ribonucleoprotein Complexes within the Influenza A Virion. J Virol. 2013;87(23):12879–84.
39. Dundon WG, Capua I. A closer look at the NS1 of influenza virus. Viruses. 2009;1:1057–72.
40. Shimizu T, Takizawa N, Watanabe K, Nagata K, Kobayashi N. Crucial role of the influenza virus NS2 (NEP) C-terminal domain in M1 binding and nuclear export of vRNP. FEBS Lett. 2011;585(1):41–6.
41. Das K, Aramini JM, Ma LC, Krug RM, Arnold E. Structures of influenza A proteins and insights into antiviral drug targets. Nat Struct Mol Biol. 2010;17(5):530–8.
42. Dubois J, Terrier O, Rosa-Calatrava M. Influenza viruses and mRNA splicing: Doing more with less. mBio. 2014;5:e00070-14.
43. Dawson WK, Lazniewski M, Plewczynski D. RNA structure interactions and ribonucleoprotein processes of the influenza A virus. Brief Funct Genomics. 2017;(May):1–13.
44. Mould JA, Paterson RG, Takeda M, Ohigashi Y, Venkataraman P, Lamb RA, et al. Influenza B virus BM2 protein has ion channel activity that conducts protons across membranes. Dev Cell. 2003;5(1):175–84.
45. Sunstrom NA, Premkumar LS, Premkumar A, Ewart G, Cox GB, Gage PW. Ion channels formed by NB, an influenza B virus protein. J Membr Biol. 1996;150(2):127–32.
46. Furukawa T, Muraki Y, Noda T, Takashita E, Sho R, Sugawara K, et al. Role of the CM2 Protein in the Influenza C Virus Replication Cycle. J Virol. 2011;85(3):1322–9.
47. Wang M, Veit M. Hemagglutinin-esterase-fusion (HEF) protein of influenza C virus. Protein Cell. 2016;7(1):28–45.
48. Bouvier NM, Palese P. The biology of influenza viruses. Vaccine. 2008;26(SUPPL. 4):D49-53.
49. Rossman JS, Leser GP, Lamb RA. Filamentous Influenza Virus Enters Cells via Macropinocytosis. J Virol. 2012;86(20):10950–60.
50. Sieczkarski SB, Whittaker GR. Influenza Virus Can Enter and Infect Cells in the Absence of Clathrin-Mediated Endocytosis Influenza Virus Can Enter and Infect Cells in the

Absence of Clathrin-Mediated Endocytosis. J Virol. 2002;76(20):10455–64.

51. Zhang Y, Whittaker GR. Influenza entry pathways in polarized MDCK cells. Biochem Biophys Res Commun. 2014;450(1):234–9.
52. Chakraborty H, Lentz BR, Kombrabail M, Krishnamoorthy G, Chattopadhyay A. Depth-Dependent Membrane Ordering by Hemagglutinin Fusion Peptide Promotes Fusion. J Phys Chem B. 2017;121(7):1640–8.
53. Fontana J, Steven AC. Influenza virus-mediated membrane fusion: Structural insights from electron microscopy. Archives of Biochemistry and Biophysics. 2015;581;86–97.
54. Li S, Sieben C, Ludwig K, Höfer CT, Chiantia S, Herrmann A, et al. PH-ontrolled two-step uncoating of influenza virus. Biophys J. 2014;106(7):1447–56.
55. Moeller A, Kirchdoerfer RN, Potter CS, Carragher B, Wilson IA. Organization of the influenza virus replication machinery. Science. 2012;338(6114):1631–4.
56. Rossman J, Lamb R. Influenza virus assembly and budding. Virology. 2011;411(2):229–36.
57. Palese P, Tobita K, Ueda M, Compans RW. Characterization of temperature sensitive influenza virus mutants defective in neuraminidase. Virology. 1974;61(2):397–410.
58. Treanor J. Influenza Vaccine - Outmaneuvering Antigenic Shift and Drift. N Engl J Med. 2004;350(3):218–20.
59. Koelle K, Cobey S, Grenfell B, Pascual M. Epochal evolution shapes the phylodynamics of interpandemic influenza a (H3N2) in humans. Science. 2006;314(5807):1898–903.
60. Plotkin JB, Dushoff J, Levin SA. Hemagglutinin sequence clusters and the antigenic evolution of influenza A virus. Proc Natl Acad Sci. 2002;99(9):6263–8.
61. Kim H, Webster RG, Webby RJ. Influenza Virus: Dealing with a Drifting and Shifting Pathogen. Viral Immunol. 2018;31(2): 174-183.
62. World Health Organization. Global Influenza Surveillance and Response System (GISRS). 2018. Available from: http://www.who.int/influenza/gisrs_laboratory/en/
63. Carrat F, Flahault A. Influenza vaccine: The challenge of antigenic drift. Vaccine. 2007;25(39–40):6852–62.
64. Potter CW. A history of influenza. J Appl Microbiol. 2001;91(4):572–9.
65. Buckland BC. The development and manufacture of influenza vaccines. Hum Vaccines Immunother . 2015;11(6):1357–60.

66. Weir JP, Gruber MF. An overview of the regulation of influenza vaccines in the United States. Influenza Other Respi Viruses. 2016;10(5):354–60.
67. Paules C, Subbarao K. Influenza. Lancet. 2017;390:697–708.
68. Blyth CC, Webb SAR, Kok J, Dwyer DE, van Hal SJ, Foo H, et al. The impact of bacterial and viral co-infection in severe influenza. Influenza Other Respi Viruses. 2013;7(2):168–76.
69. Joseph C, Togawa Y, Shindo N. Bacterial and viral infections associated with influenza. Influenza Other Respi Viruses. 2013;7(SUPPL.2):105–13.
70. Robinson KM, Kolls JK, Alcorn JF. The immunology of influenza virus-associated bacterial pneumonia. Current Opinion in Immunology. 2015;34:59–67.
71. Dawood FS, Chaves SS, Pérez A, Reingold A, Meek J, Farley MM, et al. Complications and associated bacterial coinfections among children hospitalized with seasonal or pandemic influenza, United States, 2003-2010. J Infect Dis. 2014;209(5):686–94.
72. Pop-Vicas A, Gravenstein S. Influenza in the elderly - A mini-review. Gerontology. 2011;57(5):397–404.
73. Lemaitre M, Carrat F. Comparative age distribution of influenza morbidity and mortality during seasonal influenza epidemics and the 2009 H1N1 pandemic. BMC Infect Dis. 2010;10:162.
74. Worobey M, Han G-Z, Rambaut A. Genesis and pathogenesis of the 1918 pandemic H1N1 influenza A virus. Proc Natl Acad Sci. 2014;111(22):8107–12.
75. Cocoros NM, Lash TL, Demaria A, Klompas M. Obesity as a risk factor for severe influenza-like illness. Influenza Other Respi Viruses. 2014;8(1):25–32.
76. Rodríguez-Baño J, Paño-Pardo JR, Múñez Rubio E, Segura Porta F. Pregnancy, obesity and other risk factors for complications in influenza A(H1N1) pdm09 infection. Enferm Infecc Microbiol Clin. 2012;30(SUPPL. 4):32–7.
77. Watanabe T. Renal complications of seasonal and pandemic influenza A virus infections. Eur J Pediatr. 2013;172(1):15–22.
78. Warren-Gash C. Influenza and ischaemic heart disease: Research challenges and future directions. Heart. 2013;99(24):1795–6.
79. Meijer WJ, Van Noortwijk AGA, Bruinse HW, Wensing AMJ. Influenza virus infection in pregnancy: A review. Acta Obstet Gynecol Scand. 2015;94(8):797–819.

80. Raj RS, Bonney EA, Phillippe M. Influenza, immune system, and pregnancy. Reprod Sci. 2014;21(12):1434–51.
81. Ribeiro AF, Pellini ACG, Kitagawa BY, Marques D, Madalosso G, Fred J, et al. Severe influenza A(H1N1)pdm09 in pregnant women and neonatal outcomes, State of Sao Paulo, Brazil, 2009. PLoS One. 2018;13(3):e0194392.
82. Goraya MU, Wang S, Munir M, Chen JL. Induction of innate immunity and its perturbation by influenza viruses. Protein Cell. 2015;6(10):712–21.
83. Tripathi S, White MR, Hartshorn KL. The amazing innate immune response to influenza A virus infection. Innate Immun. 2015;21(1):73–98.
84. Iwasaki A, Pillai PS. Innate immunity to influenza virus infection. Nat Rev Immunol. 2014;14(5):315–28.
85. Nüssing S, Sant S, Koutsakos M, Subbarao K, Nguyen THO, Kedzierska K. Innate and adaptive T cells in influenza disease . Frontiers of Medicine. 2018;12:34–47.
86. Andersen O, Vilsgaard Ravn K, Juul Sørensen I, Jonson G, Holm Nielsen E, Svehag SE. Serum amyloid P component binds to influenza A virus haemagglutinin and inhibits the virus infection in vitro. Scand J Immunol. 1997;46(4):331–7.
87. McAuley JL, Corcilius L, Tan HX, Payne RJ, McGuckin MA, Brown LE. The cell surface mucin MUC1 limits the severity of influenza A virus infection. Mucosal Immunol. 2017;10(6):1581–93.
88. Hillaire MLB, van Eijk M, Vogelzang-van Trierum SE, Nieuwkoop NJ, van Riel D, Fouchier RAM, et al. Assessment of the antiviral properties of recombinant surfactant protein D against influenza B virus in vitro. Virus Res. 2015;195:43–6.
89. White MR, Tripathi S, Verma A, Kingma P, Takahashi K, Jensenius J, et al. Collectins, H-ficolin and LL-37 reduce influence viral replication in human monocytes and modulate virus-induced cytokine production. Innate Immun. 2017;23(1):77–88.
90. Park MS, Kim J Il, Lee I, Park S, Bae J-Y, Park M-S. Towards the Application of Human Defensins as Antivirals. Biomol Ther (Seoul). 2018;26(3):242–54.
91. Tripathi S, Wang G, White M, Qi L, Taubenberger J, Hartshorn KL. Antiviral activity of the human cathelicidin, LL-37, and derived peptides on seasonal and pandemic influenza A viruses. PLoS One. 2015;10(4):1–17.
92. Verma A, White M, Vathipadiekal V, Tripathi S, Mbianda J, Ieong M, et al. Human H-

Ficolin Inhibits Replication of Seasonal and Pandemic Influenza A Viruses. J Immunol. 2012;189(5):2478–87.

93. Nosaka N, Hatayama K, Yamada M, Fujii Y, Yashiro M, Wake H, et al. Anti-high mobility group box-1 monoclonal antibody treatment of brain edema induced by influenza infection and lipopolysaccharide. J Med Virol. 2018;90(7):1192–8.
94. Patel MC, Shirey A, Boukhvalova MS, Vogel SN, Blanco CG. Serum High-Mobility-Group Box 1 as a Biomarker and a Therapeutic Target during Respiratory Virus Infections. MBio. 2018;9(2):1–13.
95. Andreakos E, Salagianni M, Galani IE, Koltsida O. Interferon-λs: Front-line guardians of immunity and homeostasis in the respiratory tract. Front Immunol. 2017;8:1–7.
96. Thube MM, Shil P, Kasbe R, Patil AA, Pawar SD, Mullick J. Differences in Type I interferon response in human lung epithelial cells infected by highly pathogenic H5N1 and low pathogenic H11N1 avian influenza viruses. Virus Genes. 2018;1–10.
97. Pizzolla A, Smith JM, Brooks AG, Reading PC. Pattern recognition receptor immunomodulation of innate immunity as a strategy to limit the impact of influenza virus. J Leukoc Biol. 2017;101(4):851–61.
98. Chen X, Liu S, Goraya MU, Maarouf M, Huang S, Chen JL. Host immune response to influenza A virus infection. Front Immunol. 2018;9:1–13.
99. Diebold SS, Kaisho T, Hemmi H, Akira S, Reis e Sousa C. Innate antiviral responses by means of TLR7-mediated recognition of single- stranded RNA. Science. 2004;303:1529–31.
100. Lee NL, Wong CK, Hui DS, Chan PK. Role of toll-like receptors in naturally occurring influenza virus infection. Hong Kong Med J. 2014;20 Suppl 6:11–5.
101. Ablasser A, Poeck H, Anz D, Berger M, Schlee M, Kim S, et al. Selection of Molecular Structure and Delivery of RNA Oligonucleotides to Activate TLR7 versus TLR8 and to Induce High Amounts of IL-12p70 in Primary Human Monocytes. J Immunol. 2009;182(11):6824–33.
102. Han Y, Bo ZJ, Xu MY, Sun N, Liu DH. The protective role of TLR3 and TLR9 ligands in human pharyngeal epithelial cells infected with influenza A virus. Korean J Physiol Pharmacol. 2014;18(3):225–31.
103. Chattopadhyay S, Sen GC. dsRNA-Activation of TLR3 and RLR Signaling: Gene

Induction-Dependent and Independent Effects. J Interf Cytokine Res. 2014;34(6):427–36.
104. Weber F, Wagner V, Rasmussen SB, Hartmann R, Paludan SR. Double-Stranded RNA Is Produced by Positive-Strand RNA Viruses and DNA Viruses but Not in Detectable Amounts by Negative-Strand RNA Viruses. J Virol. 2006;80(10):5059–64.
105. Wisskirchen C, Ludersdorfer TH, Muller DA, Moritz E, Pavlovic J. The Cellular RNA Helicase UAP56 Is Required for Prevention of Double-Stranded RNA Formation during Influenza A Virus Infection. J Virol. 2011;85(17):8646–55.
106. Lee SMY, Kok K-H, Jaume M, Cheung TKW, Yip T-F, Lai JCC, et al. Toll-like receptor 10 is involved in induction of innate immune responses to influenza virus infection. Proc Natl Acad Sci. 2014;111(10):3793–8.
107. Coviello S, Wimmenauer V, Polack FP, Irusta PM. Bacterial lysates improve the protective antibody response against respiratory viruses through Toll-like receptor 4. Hum Vaccines Immunother. 2014;10(10):2896–902.
108. Perkins DJ, Polumuri SK, Pennini ME, Lai W, Xie P, Vogel SN. Reprogramming of Murine Macrophages through TLR2 Confers Viral Resistance via TRAF3-Mediated, Enhanced Interferon Production. PLoS Pathog. 2013;9(7):e1003479.
109. Kell AM, Gale M. RIG-I in RNA virus recognition. Virology. 2015;479-480:110–21.
110. Killip MJ, Fodor E, Randall RE. Influenza virus activation of the interferon system. Virus Res. 2015;209:11–22.
111. Rehwinkel J, Tan CP, Goubau D, Schulz O, Pichlmair A, Bier K, et al. RIG-I Detects Viral Genomic RNA during Negative-Strand RNA Virus Infection. Cell. 2010;140(3):397–408.
112. Brubaker SW, Bonham KS, Zanoni I, Kagan JC. Innate Immune Pattern Recognition: A Cell Biological Perspective. Annu Rev Immunol. 2015;33(1):257–90.
113. Chen IY, Ichinohe T. Response of host inflammasomes to viral infection . Trends in Microbiology. 2015;23:55–63.
114. Motta V, Soares F, Sun T, Philpott DJ. NOD-Like Receptors: Versatile Cytosolic Sentinels. Physiol Rev. 2015;95(1):149–78.
115. Vanaja SK, Rathinam VAK, Fitzgerald KA. Mechanisms of inflammasome activation: Recent advances and novel insights. Trends in Cell Biology. 2015;25:308–15.
116. Dash P, Thomas PG. Host detection and the stealthy phenotype in influenza virus

infection. Curr Top Microbiol Immunol. 2015;386:121–47.

117. Ioannidis I, McNally B, Willette M, Peeples ME, Chaussabel D, Durbin JE, et al. Plasticity and Virus Specificity of the Airway Epithelial Cell Immune Response during Respiratory Virus Infection. J Virol. 2012;86(10):5422–36.

118. Shim J, Kim J, Tenson T, Min J-Y, Kainov D. Influenza Virus Infection, Interferon Response, Viral Counter-Response, and Apoptosis. Viruses. 2017;9(8):223.

119. Desai TM, Marin M, Chin CR, Savidis G, Brass AL, Melikyan GB. IFITM3 Restricts Influenza A Virus Entry by Blocking the Formation of Fusion Pores following Virus-Endosome Hemifusion. PLoS Pathog. 2014;10(4).

120. Blanc M, Hsieh WY, Robertson KA, Kropp KA, Forster T, Shui G, et al. The Transcription Factor STAT-1 Couples Macrophage Synthesis of 25-Hydroxycholesterol to the Interferon Antiviral Response. Immunity. 2013;38(1):106–18.

121. Liu SY, Aliyari R, Chikere K, Li G, Marsden MD, Smith JK, et al. Interferon-Inducible Cholesterol-25-Hydroxylase Broadly Inhibits Viral Entry by Production of 25-Hydroxycholesterol. Immunity. 2013;38(1):92–105.

122. Di Pietro A, Kajaste-Rudnitski A, Oteiza A, Nicora L, Towers GJ, Mechti N, et al. TRIM22 Inhibits Influenza A Virus Infection by Targeting the Viral Nucleoprotein for Degradation. J Virol. 2013;87(8):4523–33.

123. Fu B, Wang L, Ding H, Schwamborn JC, Li S, Dorf ME. TRIM32 Senses and Restricts Influenza A Virus by Ubiquitination of PB1 Polymerase. PLoS Pathog. 2015;11(6):1–23.

124. Zhao C, Hsiang T-Y, Kuo R-L, Krug RM. ISG15 conjugation system targets the viral NS1 protein in influenza A virus-infected cells. Proc Natl Acad Sci. 2010;107(5):2253–8.

125. Turan K, Mibayashi M, Sugiyama K, Saito S, Numajiri A, Nagata K. Nuclear MxA proteins form a complex with influenza virus NP and inhibit the transcription of the engineered influenza virus genome. Nucleic Acids Res. 2004;32(2):643–52.

126. Xiao H, Killip MJ, Staeheli P, Randall RE, Jackson D. The Human Interferon-Induced MxA Protein Inhibits Early Stages of Influenza A Virus Infection by Retaining the Incoming Viral Genome in the Cytoplasm. J Virol. 2013;87(23):13053–8.

127. Gerlach RL, Camp J V., Chu YK, Jonsson CB. Early host responses of seasonal and pandemic influenza a viruses in primary well-differentiated human lung epithelial cells. PLoS One. 2013;8(11):e78912.

128. Oslund KL, Zhou X, Lee B, Zhu L, Duong T, Shih R, et al. Synergistic up-regulation of CXCL10 by virus and IFN γ in human airway epithelial cells. PLoS One. 2014;9(7):e100978.
129. Ito Y, Correll K, Zemans RL, Leslie CC, Murphy RC, Mason RJ. Influenza induces IL-8 and GM-CSF secretion by human alveolar epithelial cells through HGF/c-Met and TGF-α/EGFR signaling. Am J Physiol - Lung Cell Mol Physiol. 2015;308(11):L1178–88.
130. Peiró T, Patel DF, Akthar S, Gregory LG, Pyle CJ, Harker JA, et al. Neutrophils drive alveolar macrophage IL-1β release during respiratory viral infection. Thorax. 2017;73(6): 546-556.
131. Nainu F, Shiratsuchi A, Nakanishi Y. Induction of apoptosis and subsequent phagocytosis of virus-infected cells as an antiviral mechanism. Front Immunol. 2017;8:1–11.
132. Wang J, Nikrad MP, Travanty EA, Zhou B, Phang T, Gao B, et al. Innate immune response of human alveolar macrophages during influenza a infection. PLoS One. 2012;7(3).
133. Ho JW, Hershkovitz O, Peiris M, Zilka A, Bar-Ilan A, Nal B, et al. H5-Type Influenza Virus Hemagglutinin Is Functionally Recognized by the Natural Killer-Activating Receptor NKp44. J Virol. 2008;82(4):2028–32.
134. Shemer-Avni Y, Kundu K, Shemesh A, Brusilovsky M, Yossef R, Meshesha M, et al. Expression of NKp46 splice variants in nasal lavage following respiratory viral infection: Domain 1-negative isoforms predominate and manifest higher activity. Front Immunol. 2017;8:1–10.
135. Downey J, Pernet E, Coulombe F, Divangahi M. Dissecting host cell death programs in the pathogenesis of influenza. Microbes Infect . 2018; doi: 10.1016/j.micinf.2018.03.005.
136. Sarvestani ST, McAuley JL. The role of the NLRP3 inflammasome in regulation of antiviral responses to influenza A virus infection. Antiviral Res. 2017;148:32–42.
137. Yatim N, Cullen S, Albert ML. Dying cells actively regulate adaptive immune responses. Nat Rev Immunol. 2017;17(4):262–75.
138. Chang P, Kuchipudi S V., Mellits KH, Sebastian S, James J, Liu J, et al. Early apoptosis of porcine alveolar macrophages limits avian influenza virus replication and pro-inflammatory dysregulation. Sci Rep. 2015;5:1–11.
139. Tran AT, Cortens JP, Du Q, Wilkins JA, Coombs KM. Influenza Virus Induces Apoptosis

via BAD-Mediated Mitochondrial Dysregulation. J Virol. 2013;87(2):1049–60.
140. Brydon EWA, Morris SJ, Sweet C. Role of apoptosis and cytokines in influenza virus morbidity. FEMS Microbiol Rev. 2005;29(4):837–50.
141. Stray SJ, Air GM. Apoptosis by influenza viruses correlates with efficiency of viral mRNA synthesis. Virus Res. 2001;77(1):3–17.
142. Fujimoto I, Takizawa T, Ohba Y, Nakanishi Y. Co-expression of Fas and Fas-ligand on the surface of influenza virus-infected cells. Cell Death Differ. 1998;5(5):426–31.
143. Blachère NE, Darnell RB, Albert ML. Apoptotic cells deliver processed antigen to dendritic cells for cross-presentation. PLoS Biol. 2005;3(6):1070–8.
144. van Montfoort N, van der Aa E, Woltman AM. Understanding MHC class I presentation of viral antigens by human dendritic cells as a basis for rational design of therapeutic vaccines . Frontiers in Immunology. 2014;5:182.
145. Hoeffel G, Ripoche AC, Matheoud D, Nascimbeni M, Escriou N, Lebon P, et al. Antigen Crosspresentation by Human Plasmacytoid Dendritic Cells. Immunity. 2007;27(3):481–92.
146. Albert ML, Sauter B, Bhardwaj N. Dendritic cells acquire antigen from apoptotic cells and induce class I-restricted CTLs. Nature. 1998;392(6671):86–9.
147. Uhl M, Kepp O, Jusforgues-Saklani H, Vicencio JM, Kroemer G, Albert ML. Autophagy within the antigen donor cell facilitates efficient antigen cross-priming of virus-specific CD8+T cells. Cell Death Differ. 2009;16(7):991–1005.
148. Zhou W, Yuan J. Necroptosis in health and diseases. Semin Cell Dev Biol. 2014;35:14–23.
149. Cai Z, Jitkaew S, Zhao J, Chiang HC, Choksi S, Liu J, et al. Plasma membrane translocation of trimerized MLKL protein is required for TNF-induced necroptosis. Nat Cell Biol. 2014;16(1):55–65.
150. Hartmann BM, Albrecht RA, Zaslavsky E, Nudelman G, Pincas H, Marjanovic N, et al. Pandemic H1N1 influenza A viruses suppress immunogenic RIPK3-driven dendritic cell death. Nat Commun. 2017;8(1):1931.
151. Thapa RJ, Ingram JP, Ragan KB, Nogusa S, Boyd DF, Benitez AA, et al. DAI Senses Influenza A Virus Genomic RNA and Activates RIPK3-Dependent Cell Death. Cell Host Microbe. 2016;20(5):674–81.

152. Nogusa S, Thapa RJ, Dillon CP, Liedmann S, Oguin TH, Ingram JP, et al. RIPK3 Activates Parallel Pathways of MLKL-Driven Necroptosis and FADD-Mediated Apoptosis to Protect against Influenza A Virus. Cell Host Microbe. 2016;20(1):13–24.
153. Nogusa S, Slifker MJ, Ingram JP, Thapa RJ, Balachandran S. Ripk3 is largely dispensable for rig-i-like receptor- and type i interferon-driven transcriptional responses to influenza a virus in murine fibroblasts. PLoS One. 2016;11(7):e0158774.
154. Ward AE, Rosenthal BM. Evolutionary responses of innate immunity to adaptive immunity. Infection, Genetics and Evolution. 2014;21:492–6.
155. La Gruta NL, Turner SJ. T cell mediated immunity to influenza: Mechanisms of viral control. Trends in Immunology. 2014;35:396–402.
156. Kai McKinstry K, Dutton RW, Swain SL, Strutt TM. Memory CD4 T cell-mediated immunity against influenza a virus: More than a little helpful. Archivum Immunologiae et Therapiae Experimentalis. 2013;61:341–53.
157. Bahadoran A, Lee SH, Wang SM, Manikam R, Rajarajeswaran J, Raju CS, et al. Immune responses to influenza virus and its correlation to age and inherited factors. Front Microbiol. 2016;7:1–11.
158. Simon AK, Hollander GA, McMichael A. Evolution of the immune system in humans from infancy to old age. Proceedings of the Royal Society B: Biological Sciences. 2015;282:20143085.
159. Iwasaki A, Medzhitov R. Control of adaptive immunity by the innate immune system. Nature Immunology. 2015;16:343–53.
160. Twigg HL. Macrophages in Innate and Acquired Immunity. Seminars in Respiratory and Critical Care Medicine. 2004;25:21–31.
161. Bhardwaj N, Bender A, Gonzalez N, Bui LK, Garrett MC, Steinman RM. Influenza virus-infected dendritic cells stimulate strong proliferative and cytolytic responses from human CD8+ T cells. J Clin Invest. 1994;94(2):797–807.
162. Campbell GM, Nicol MQ, Dransfield I, Shaw DJ, Nash AA, Dutia BM. Susceptibility of bone marrow-derived macrophages to influenza virus infection is dependent on macrophage phenotype. J Gen Virol. 2015;96(10):2951–60.
163. Smed-Sörensen A, Chalouni C, Chatterjee B, Cohn L, Blattmann P, Nakamura N, et al. Influenza a virus infection of human primary dendritic cells impairs their ability to cross-

present antigen to CD8 T cells. PLoS Pathog. 2012;8(3).

164. Hashimoto Y, Moki T, Takizawa T, Shiratsuchi A, Nakanishi Y. Evidence for Phagocytosis of Influenza Virus-Infected, Apoptotic Cells by Neutrophils and Macrophages in Mice. J Immunol. 2007;178(4):2448–57.

165. Abdel-Motal UM, Guay HM, Wigglesworth K, Welsh RM, Galili U. Immunogenicity of Influenza Virus Vaccine Is Increased by Anti-Gal-Mediated Targeting to Antigen-Presenting Cells. J Virol. 2007;81(17):9131–41.

166. Budimir N, Huckriede A, Meijerhof T, Boon L, Gostick E, Price DA, et al. Induction of heterosubtypic cross-protection against influenza by a whole inactivated virus vaccine: The role of viral membrane fusion activity. PLoS One. 2012;7(1).

167. Di Pucchio T, Chatterjee B, Smed-Sörensen A, Clayton S, Palazzo A, Montes M, et al. Direct proteasome-independent cross-presentation of viral antigen by plasmacytoid dendritic cells on major histocompatibility complex class I. Nat Immunol. 2008;9(5):551–7.

168. O E, Lee Y-T, Ko E-J, Kim K-H, Lee Y-N, Song J-M, et al. Roles of Major Histocompatibility Complex Class II in Inducing Protective Immune Responses to Influenza Vaccination. J Virol. 2014;88(14):7764–75.

169. Traub LM, Bonifacino JS. Cargo recognition in clathrin-mediated endocytosis. Cold Spring Harb Perspect Biol. 2013;5(11):a016790–a016790.

170. Burgdorf S, Kurts C. Endocytosis mechanisms and the cell biology of antigen presentation. Current Opinion in Immunology. 2008;20:89–95.

171. Platt CD, Ma JK, Chalouni C, Ebersold M, Bou-Reslan H, Carano RAD, et al. Mature dendritic cells use endocytic receptors to capture and present antigens. Proc Natl Acad Sci. 2010;107(9):4287–92.

172. Burgdorf S, Lukacs-Kornek V, Kurts C. The Mannose Receptor Mediates Uptake of Soluble but Not of Cell-Associated Antigen for Cross-Presentation. J Immunol. 2006;176(11):6770–6.

173. Burgdorf S, Kautz A, Böhnert V, Knolle P a, Kurts C. Distinct Pathways of Antigen Uptake. Science. 2007;612(316):612–6.

174. Bozzacco L, Trumpfheller C, Siegal FP, Mehandru S, Markowitz M, Carrington M, et al. DEC-205 receptor on dendritic cells mediates presentation of HIV gag protein to CD8+ T

cells in a spectrum of human MHC I haplotypes. Proc Natl Acad Sci. 2007;104(4):1289–94.

175. Idoyaga J, Lubkin A, Fiorese C, Lahoud MH, Caminschi I, Huang Y, et al. Comparable T helper 1 (Th1) and CD8 T-cell immunity by targeting HIV gag p24 to CD8 dendritic cells within antibodies to Langerin, DEC205, and Clec9A. Proc Natl Acad Sci. 2011;108(6):2384–9.
176. Singh SK, Streng-Ouwehand I, Litjens M, Kalay H, Saeland E, Van Kooyk Y. Tumour-associated glycan modifications of antigen enhance MGL2 dependent uptake and MHC class i restricted CD8 T cell responses. Int J Cancer. 2011;128(6):1371–83.
177. Xie J, Zhu H, Guo L, Ruan Y, Wang L, Sun L, et al. Lectin-Like Oxidized Low-Density Lipoprotein Receptor-1 Delivers Heat Shock Protein 60-Fused Antigen into the MHC Class I Presentation Pathway. J Immunol. 2010;185(4):2306–13.
178. Hutten TJA, Thordardottir S, Fredrix H, Janssen L, Woestenenk R, Tel J, et al. CLEC12A-Mediated Antigen Uptake and Cross-Presentation by Human Dendritic Cell Subsets Efficiently Boost Tumor-Reactive T Cell Responses. J Immunol. 2016;197(7):2715–25.
179. Weck MM, Appel S, Werth D, Sinzger C, Bringmann A, Grünebach F, et al. HDectin-1 is involved in uptake and cross-presentation of cellular antigens. Blood. 2008;111(8):4264–72.
180. Klechevsky E, Flamar A-L, Cao Y, Blanck J-P, Liu M, O'Bar A, et al. Cross-priming CD8+ T cells by targeting antigens to human dendritic cells through DCIR. Blood. 2010;116(10):1685–97.
181. Cohn L, Chatterjee B, Esselborn F, Smed-Sörensen A, Nakamura N, Chalouni C, et al. Antigen delivery to early endosomes eliminates the superiority of human blood BDCA3 $^{+}$ dendritic cells at cross presentation. J Exp Med. 2013;210(5):1049–63.
182. Yin W, Gorvel L, Zurawski S, Li D, Ni L, Duluc D, et al. Functional Specialty of CD40 and Dendritic Cell Surface Lectins for Exogenous Antigen Presentation to CD8+ and CD4+ T Cells. EBioMedicine. 2016;5:46–58.
183. Letran SE, Lee SJ, Atif SM, Uematsu S, Akira S, McSorley SJ. TLR5 functions as an endocytic receptor to enhance flagellin-specific adaptive immunity. Eur J Immunol. 2011;41(1):29–38.

184. Leone DA, Peschel A, Brown M, Schachner H, Ball MJ, Gyuraszova M, et al. Surface LAMP-2 Is an Endocytic Receptor That Diverts Antigen Internalized by Human Dendritic Cells into Highly Immunogenic Exosomes. J Immunol. 2017;199(2):531–46.
185. Singh SK, Stephani J, Schaefer M, Kalay H, García-Vallejo JJ, den Haan J, et al. Targeting glycan modified OVA to murine DC-SIGN transgenic dendritic cells enhances MHC class I and II presentation. Mol Immunol. 2009;47(2–3):164–74.
186. Schetters STT, Kruijssen LJW, Crommentuijn MHW, Kalay H, Ochando J, den Haan JMM, et al. Mouse DC-SIGN/CD209a as target for antigen delivery and adaptive immunity. Front Immunol. 2018;9:990.
187. Tacken PJ, Ginter W, Berod L, Cruz LJ, Joosten B, Sparwasser T, et al. Targeting DC-SIGN via its neck region leads to prolonged antigen residence in early endosomes, delayed lysosomal degradation, and cross-presentation. Blood. 2011;118(15):4111–9.
188. Varki A, Schnaar RL, Schauer R. Sialic Acids and Other Nonulosonic Acids. Essentials Glycobiol 3rd Ed. 2017;Chapter 15.
189. Thompson CI, Barclay WS, Zambon MC, Pickles RJ. Infection of Human Airway Epithelium by Human and Avian Strains of Influenza A Virus. J Virol. 2006;80(16):8060–8.
190. Kumlin U, Olofsson S, Dimock K, Arnberg N. Sialic acid tissue distribution and influenza virus tropism. Influenza and other Respiratory Viruses. 2008;2:147–54.
191. Neumann G, Kawaoka Y. Host range restriction and pathogenicity in the context of influenza pandemic. Emerging Infectious Diseases. 2006;12:881–6.
192. de Graaf M, Fouchier RAM. Role of receptor binding specificity in influenza A virus transmission and pathogenesis. EMBO J. 2014;33(8):823–41.
193. Mair CM, Ludwig K, Herrmann A, Sieben C. Receptor binding and pH stability - How influenza A virus hemagglutinin affects host-specific virus infection. Biochim Biophys Acta - Biomembr. 2014;1838(4):1153–68.
194. Cabral MG, Silva Z, Ligeiro D, Seixas E, Crespo H, Carrascal MA, et al. The phagocytic capacity and immunological potency of human dendritic cells is improved by α2,6-sialic acid deficiency. Immunology. 2013;138(3):235–45.
195. Videira PA, Amado IF, Crespo HJ, Algueró MC, Dall'Olio F, Cabral MG, et al. Surface α2-3- and α2-6-sialylation of human monocytes and derived dendritic cells and its

influence on endocytosis. Glycoconj J. 2008;25(3):259–68.

196. Yu WCL, Chan RWY, Wang J, Travanty EA, Nicholls JM, Peiris JSM, et al. Viral Replication and Innate Host Responses in Primary Human Alveolar Epithelial Cells and Alveolar Macrophages Infected with Influenza H5N1 and H1N1 Viruses. J Virol. 2011;85(14):6844–55.
197. Alymova I V., York IA, Air GM, Cipollo JF, Gulati S, Baranovich T, et al. Glycosylation changes in the globular head of H3N2 influenza hemagglutinin modulate receptor binding without affecting virus virulence. Sci Rep. 2016;6:1–15.
198. Bateman AC, Karamanska R, Busch MG, Dell A, Olsen CW, Haslam SM. Glycan analysis and influenza A virus infection of primary swine respiratory epithelial cells: The importance of NeuAcα2-6 glycans. J Biol Chem. 2010;285(44):34016–26.
199. Chu VC, Whittaker GR. Influenza virus entry and infection require host cell N-linked glycoprotein. Proc Natl Acad Sci U S A. 2004;101(52):18153–8.
200. Hillaire MLB, Nieuwkoop NJ, Boon ACM, de Mutsert G, Vogelzang-van Trierum SE, Fouchier RAM, et al. Binding of DC-SIGN to the Hemagglutinin of Influenza A Viruses Supports Virus Replication in DC-SIGN Expressing Cells. PLoS One. 2013;8(2):1–10.
201. Tate MD, Brooks AG, Reading PC. Correlation between sialic acid expression and infection of murine macrophages by different strains of influenza virus. Microbes Infect. 2011;13(2):202–7.
202. Connaris H, Govorkova EA, Ligertwood Y, Dutia BM, Yang L, Tauber S, et al. Prevention of influenza by targeting host receptors using engineered proteins. Proc Natl Acad Sci. 2014;111(17):6401–6.
203. Stray SJ, Cummings RD, Air GM. Influenza virus infection of desialylated cells. Glycobiology. 2000;10(7):649–58.
204. Dimitrov DS. Virus entry: Molecular mechanisms and biomedical applications. Nat Rev Microbiol. 2004;2(2):109–22.
205. Londrigan SL, Tate MD, Brooks AG, Reading PC. Cell-surface receptors on macrophages and dendritic cells for attachment and entry of influenza virus. J Leukoc Biol. 2012;92(1):97–106.
206. Leung HSY, Li OTW, Chan RWY, Chan MCW, Nicholls JM, Poon LLM. Entry of Influenza A Virus with a 2,6-Linked Sialic Acid Binding Preference Requires Host

Fibronectin. J Virol. 2012;86(19):10704–13.
207. Reading PC, Miller JL, Anders EM. Involvement of the mannose receptor in infection of macrophages by influenza virus. J Virol. 2000;74(11):5190–7.
208. Upham JP, Pickett D, Irimura T, Anders EM, Reading PC. Macrophage Receptors for Influenza A Virus: Role of the Macrophage Galactose-Type Lectin and Mannose Receptor in Viral Entry. J Virol. 2010;84(8):3730–7.
209. Ng WC, Liong S, Tate MD, Irimura T, Denda-Nagai K, Brooks AG, et al. The Macrophage Galactose-Type Lectin Can Function as an Attachment and Entry Receptor for Influenza Virus. J Virol. 2014;88(3):1659–72.
210. Ng WC, Londrigan SL, Nasr N, Cunningham AL, Turville S, Brooks AG, et al. The C-type lectin langerin functions as a receptor for attachment and infectious entry of influenza A virus. J Virol. 2016;90(1):206-21.
211. Londrigan SL, Turville SG, Tate MD, Deng Y-M, Brooks AG, Reading PC. N-Linked Glycosylation Facilitates Sialic Acid-Independent Attachment and Entry of Influenza A Viruses into Cells Expressing DC-SIGN or L-SIGN. J Virol. 2011;85(6):2990–3000.
212. Wang SF, Huang JC, Lee YM, Liu SJ, Chan YJ, Chau YP, et al. DC-SIGN mediates avian H5N1 influenza virus infection in cis and in trans. Biochem Biophys Res Commun. 2008;373(4):561–6.
213. Mercer J, Greber UF. Virus interactions with endocytic pathways in macrophages and dendritic cells. Trends Microbiol. 2013;21(8):380–8.
214. Chou LYT, Ming K, Chan WCW. Strategies for the intracellular delivery of nanoparticles. Chem Soc Rev. 2011;40(1):233–45.
215. Blum JS, Wearsch PA, Cresswell P. IY31CH16-Cresswell Pathways of Antigen Processing. Annu. Rev. Immunol. 2013;31:443-73.
216. Burgdorf S, Kurts C. Endocytosis mechanisms and the cell biology of antigen presentation. Curr Opin Immunol. 2008;20(1):89–95.
217. Mantegazza AR, Magalhaes JG, Amigorena S, Marks MS. Presentation of Phagocytosed Antigens by MHC Class I and II. Traffic. 2013;14(2):135–52.
218. Cruz FM, Colbert JD, Merino E, Kriegsman BA, Rock KL. The Biology and Underlying Mechanisms of Cross-Presentation of Exogenous Antigens on MHC-I Molecules. Annu Rev Immunol. 2017;35(1):149–76.

219. van Endert P. Intracellular recycling and cross-presentation by MHC class I molecules. Immunol Rev. 2016;272(1):80–96.
220. Schuette V, Burgdorf S. The ins-and-outs of endosomal antigens for cross-presentation. Curr Opin Immunol. 2014;26(1):63–8.
221. Kiss AL. Caveolae and the regulation of endocytosis. Adv Exp Med Biol. 2012;729:14–28.
222. McCullough KC, Sharma R. Dendritic Cell Endocytosis Essential for Viruses and Vaccines. In: Ghosh A, editor. Biology of Myelomonocytic Cells. InTech; 2017. p. 99–128.
223. Mintern JD, Macri C, Villadangos JA. Modulation of antigen presentation by intracellular trafficking. Curr Opin Immunol. 2015;34:16–21.
224. Lakadamyali M, Rust MJ, Zhuang X. Ligands for clathrin-mediated endocytosis are differentially sorted into distinct populations of early endosomes. Cell. 2006;124(5):997–1009.
225. Wieczorek M, Abualrous ET, Sticht J, Álvaro-Benito M, Stolzenberg S, Noé F, et al. Major histocompatibility complex (MHC) class I and MHC class II proteins: Conformational plasticity in antigen presentation. Front Immunol. 2017;8(MAR):1–16.
226. Roche PA, Furuta K. The ins and outs of MHC class II-mediated antigen processing and presentation. Nature Reviews Immunology. 2015;15:203–16.
227. Ugiyadi M, Tan MI, Giri-Rachman EA, Zuhairi FR, Sumarsono SH. The expression of essential components for human influenza virus internalisation in Vero and MDCK cells. Cytotechnology. 2014;66(3):515–23.
228. Sun EZ, Liu AA, Zhang ZL, Liu SL, Tian ZQ, Pang DW. Real-Time Dissection of Distinct Dynamin-Dependent Endocytic Routes of Influenza A Virus by Quantum Dot-Based Single-Virus Tracking. ACS Nano. 2017;11(5):4395–406.
229. Wang H, Jiang C. Influenza A virus H5N1 entry into host cells is through clathrin-dependent endocytosis. Sci China, Ser C Life Sci. 2009;52(5):464–9.
230. De Conto F, Covan S, Arcangeletti MC, Orlandini G, Gatti R, Dettori G, et al. Differential infectious entry of human influenza A/NWS/33 virus (H1N1) in mammalian kidney cells. Virus Res. 2011;155(1):221–30.
231. Fujioka Y, Tsuda M, Nanbo A, Hattori T, Sasaki J, Sasaki T, et al. A Ca2+-dependent

signalling circuit regulates influenza A virus internalization and infection. Nat Commun. 2013;4:1–13.

232. de Vries E, Tscherne DM, Wienholts MJ, Cobos-Jiménez V, Scholte F, García-Sastre A, et al. Dissection of the influenza a virus endocytic routes reveals macropinocytosis as an alternative entry pathway. PLoS Pathog. 2011;7(3).
233. Itano MS, Neumann AK, Liu P, Zhang F, Gratton E, Parak WJ, et al. DC-SIGN and influenza hemagglutinin dynamics in plasma membrane microdomains are markedly different. Biophys J. 2011;100(11):2662–70.
234. Lejal N, Truchet S, Bechor E, Bouguyon E, Khedkar V, Bertho N, et al. Turning off NADPH oxidase-2 by impeding p67phoxactivation in infected mouse macrophages reduced viral entry and inflammation. Biochim Biophys Acta - Gen Subj. 2018;1862(6):1263–75.
235. Scott CC, Vacca F, Gruenberg J. Endosome maturation, transport and functions. Semin Cell Dev Biol. 2014;31:2–10.
236. Compeer EB, Flinsenberg TWH, van der Grein SG, Boes M. Antigen processing and remodeling of the endosomal pathway: Requirements for antigen cross-presentation. Front Immunol. 2012;3:1–11.
237. ten Broeke T, Wubbolts R, Stoorvogel W. MHC class II antigen presentation by dendritic cells regulated through endosomal sorting. Cold Spring Harb Perspect Biol. 2013;5(12):1–21.
238. Mellman I. Endocytosis and Molecular Sorting. Annu Rev Cell Dev Biol . 1996;12(1):575–625.
239. Scita G, Di Fiore PP. The endocytic matrix. Nature. 2010;463:464–73.
240. Jovic M, Sharma M, Rahajeng J, Caplan S. The early endosome: A busy sorting station for proteins at the crossroads. Histology and Histopathology. 2010;25:99–112.
241. Girard E, Chmiest D, Fournier N, Johannes L, Paul JL, Vedie B, et al. Rab7 is functionally required for selective cargo sorting at the early endosome. Traffic. 2014;15(3):309–26.
242. Scott CC, Vacca F, Gruenberg J. Endosome maturation, transport and functions. Seminars in Cell and Developmental Biology. 2014;31:2–10.
243. Foret L, Dawson JE, Villaseñor R, Collinet C, Deutsch A, Brusch L, et al. A general

theoretical framework to infer endosomal network dynamics from quantitative image analysis. Curr Biol. 2012;22(15):1381–90.
244. Goldenring JR. Recycling endosomes. Current Opinion in Cell Biology. 2015;35:117–22.
245. Huotari J, Helenius A. Endosome maturation. EMBO J. 2011;30(17):3481–500.
246. Bright NA, Davis LJ, Luzio JP. Endolysosomes Are the Principal Intracellular Sites of Acid Hydrolase Activity. Curr Biol. 2016;26(17):2233–45.
247. Wong CO, Gregory S, Hu H, Chao Y, Sepúlveda VE, He Y, et al. Lysosomal Degradation Is Required for Sustained Phagocytosis of Bacteria by Macrophages. Cell Host Microbe. 2017;21(6):719–730.e6.
248. Hanson PI, Cashikar A. Multivesicular Body Morphogenesis. Annu Rev Cell Dev Biol. 2012;28(1):337–62.
249. Kanemoto S, Nitani R, Murakami T, Kaneko M, Asada R, Matsuhisa K, et al. Multivesicular body formation enhancement and exosome release during endoplasmic reticulum stress. Biochem Biophys Res Commun. 2016;480(2):166–72.
250. Robbins PD, Morelli AE. Regulation of immune responses by extracellular vesicles. Nature Reviews Immunology. 2014;14:195–208.
251. Egami Y. Molecular imaging analysis of Rab GTPases in the regulation of phagocytosis and macropinocytosis. Anat Sci Int. 2016;91(1):35–42.
252. Wandinger-Ness A, Zerial M. Rab Proteins and the Compatmentalization of the Endosomal System. Cold Spring Harb Perspect Biol. 2014;6(11):a022616.
253. Mishra A, Eathiraj S, Corvera S, Lambright DG. Structural basis for Rab GTPase recognition and endosome tethering by the C2H2 zinc finger of Early Endosomal Autoantigen 1 (EEA1). Proc Natl Acad Sci. 2010;107(24):10866–71.
254. Rink J, Ghigo E, Kalaidzidis Y, Zerial M. Rab conversion as a mechanism of progression from early to late endosomes. Cell. 2005;122(5):735–49.
255. Cook NR, Row PE, Davidson HW. Lysosome associated membrane protein 1 (Lamp1) traffics directly from the TGN to early endosomes. Traffic. 2004;5(9):685–99.
256. Kobayashi H, Fukuda M. Arf6, Rab11 and transferrin receptor define distinct populations of recycling endosomes. Commun Integr Biol. 2013;6(5):10–3.
257. Adiko AC, Babdor J, Gutiérrez-Martínez E, Guermonprez P, Saveanu L. Intracellular transport routes for MHC I and their relevance for antigen cross-presentation. Front

Immunol. 2015;6:1–11.

258. Zou L, Zhou J, Zhang J, Li J, Liu N, Chai L, et al. The GTPase Rab3b/3c-positive recycling vesicles are involved in cross-presentation in dendritic cells. Proc Natl Acad Sci U S A. 2009;106(37):15801–6.
259. Shishido T, Hachisuka M, Ryuzaki K, Miura Y, Tanabe A, Tamura Y, et al. EpsinR, a target for pyrenocine B, role in endogenous MHC-II-restricted antigen presentation. Eur J Immunol. 2014;44(11):3220–31.
260. Rock KL, Reits E, Neefjes J. Present Yourself! By MHC Class I and MHC Class II Molecules. Trends Immunol. 2016;37(11):724–37.
261. Unanue ER, Turk V, Neefjes J. Variations in MHC Class II Antigen Processing and Presentation in Health and Disease. Annu Rev Immunol. 2016;34(1):265–97.
262. Walker JA, McKenzie ANJ. TH2 cell development and function. Nat Rev Immunol. 2017;18(2):121–33.
263. Ivanova EA, Orekhov AN. T Helper lymphocyte subsets and plasticity in autoimmunity and cancer: An overview. BioMed Research International. 2015;2015:327470.
264. Blander JM. Regulation of the Cell Biology of Antigen Cross Presentation. Annu Rev Immunol. 2018;36:717-753.
265. Cox MA, Kahan SM, Zajac AJ. Anti-viral CD8 T cells and the cytokines that they love. Virology. 2013;435:157–69.
266. Leone P, Shin EC, Perosa F, Vacca A, Dammacco F, Racanelli V. MHC class i antigen processing and presenting machinery: Organization, function, and defects in tumor cells. J Natl Cancer Inst. 2013;105(16):1172–87.
267. Rock KL, Farfán-Arribas DJ, Shen L. Proteases in MHC Class I Presentation and Cross-Presentation. J Immunol. 2010;184(1):9–15.
268. Bernhard CA, Ried C, Kochanek S, Brocker T. CD169 + macrophages are sufficient for priming of CTLs with specificities left out by cross-priming dendritic cells. Proc Natl Acad Sci. 2015;112(17):5461–6.
269. Brayer J, Cheng F, Wang H, Horna P, Vicente-Suarez I, Pinilla-Ibarz J, et al. Enhanced CD8 T cell cross-presentation by macrophages with targeted disruption of STAT3. Immunol Lett. 2010;131(2):126–30.
270. Dinter J, Duong E, Lai NY, Berberich MJ, Kourjian G, Bracho-Sanchez E, et al. Variable

Processing and Cross-presentation of HIV by Dendritic Cells and Macrophages Shapes CTL Immunodominance and Immune Escape. PLoS Pathog. 2015;11(3):1–22.

271. Saveanu L, Carroll O, Weimershaus M, Guermonprez P, Firat E, Lindo V, et al. IRAP identifies an endosomal compartment required for MHC class i cross-presentation. Science. 2009;325(5937):213–7.
272. Shen L, Sigal LJ, Boes M, Rock KL. Important role of cathepsin S in generating peptides for TAP-independent MHC class I crosspresentation in vivo. Immunity. 2004;21(2):155–65.
273. Hassan C, Chabrol E, Jahn L, Kester MGD, De Ru AH, Drijfhout JW, et al. Naturally processed non-canonical HLA-A*02:01 presented peptides. J Biol Chem. 2015;290(5):2593–603.
274. Remesh SG, Andreatta M, Ying G, Kaever T, Nielsen M, McMurtrey C, et al. Unconventional peptide presentation by major histocompatibility complex (MHC) class i allele HLA-A∗02:01: Breaking confinement. J Biol Chem. 2017;292(13):5262–70.
275. Suri A, Walters JJ, Levisetti MG, Gross ML, Unanue ER. Identification of naturally processed peptides bound to the class I MHC molecule H-2Kd of normal and TAP-deficient cells. Eur J Immunol. 2006;36(3):544–57.
276. Cebrian I, Visentin G, Blanchard N, Jouve M, Bobard A, Moita C, et al. Sec22b regulates phagosomal maturation and antigen crosspresentation by dendritic cells. Cell. 2011;147(6):1355–68.
277. Savina A, Jancic C, Hugues S, Guermonprez P, Vargas P, Moura IC, et al. NOX2 Controls Phagosomal pH to Regulate Antigen Processing during Crosspresentation by Dendritic Cells. Cell. 2006;126(1):205–18.
278. Mantegazza AR, Savina A, Vermeulen M, Pérez L, Geffner J, Hermine O, et al. NADPH oxidase controls phagosomal pH and antigen cross-presentation in human dendritic cells. Blood. 2008;112(12):4712–22.
279. Zehner M, Marschall AL, Bos E, Schloetel JG, Kreer C, Fehrenschild D, et al. The Translocon Protein Sec61 Mediates Antigen Transport from Endosomes in the Cytosol for Cross-Presentation to $CD8^+$ T Cells. Immunity. 2015;42(5):850–63.
280. Chen H, Li L, Weimershaus M, Evnouchidou I, van Endert P, Bouvier M. ERAP1-ERAP2 dimers trim MHC I-bound precursor peptides; implications for understanding peptide

editing. Sci Rep. 2016;6(1):28902.

281. Dingjan I, Verboogen DRJ, Paardekooper LM, Revelo NH, Sittig SP, Visser LJ, et al. Lipid peroxidation causes endosomal antigen release for cross-presentation. Sci Rep. 2016;6:1–12.

282. Hochheiser K, Klein M, Gottschalk C, Hoss F, Scheu S, Coch C, et al. Cutting Edge: The RIG-I Ligand 3pRNA Potently Improves CTL Cross-Priming and Facilitates Antiviral Vaccination. J Immunol. 2016;196(6):2439–43.

283. Zevini A, Olagnier D, Hiscott J. Crosstalk between Cytoplasmic RIG-I and STING Sensing Pathways. Trends Immunol. 2017;38(3):194–205.

284. Lirussi D, Ebensen T, Schulze K, Trittel S, Duran V, Liebich I, et al. Type I IFN and not TNF, is Essential for Cyclic Di-nucleotide-elicited CTL by a Cytosolic Cross-presentation Pathway. EBioMedicine. 2017;22:100–11.

285. Holm CK, Jensen SB, Jakobsen MR, Cheshenko N, Horan KA, Moeller HB, et al. Virus-cell fusion as a trigger of innate immunity dependent on the adaptor STING. Nat Immunol. 2012;13(8):737–43.

286. Holm CK, Rahbek SH, Gad HH, Bak RO, Jakobsen MR, Jiang Z, et al. Influenza A virus targets a cGAS-independent STING pathway that controls enveloped RNA viruses. Nat Commun. 2016;7:1–9.

287. Alloatti A, Kotsias F, Pauwels AM, Carpier JM, Jouve M, Timmerman E, et al. Toll-like Receptor 4 Engagement on Dendritic Cells Restrains Phago-Lysosome Fusion and Promotes Cross-Presentation of Antigens. Immunity. 2015;43(6):1087–100.

288. Nair-Gupta P, Baccarini A, Tung N, Seyffer F, Florey O, Huang Y, et al. TLR signals induce phagosomal MHC-I delivery from the endosomal recycling compartment to allow cross-presentation. Cell. 2014;158(3):506–21.

289. Burgdorf S, Schölz C, Kautz A, Tampé R, Kurts C. Spatial and mechanistic separation of cross-presentation and endogenous antigen presentation. Nat Immunol. 2008;9(5):558–66.

290. Lakadamyali M, Rust MJ, Babcock HP, Zhuang X. Visualizing infection of individual influenza viruses. Proc Natl Acad Sci. 2003;100(16):9280–5.

291. Sieczkarski SB, Whittaker GR. Differential Requirements of Rab5 and Rab7 for Endocytosis of Influenza and Other Enveloped Viruses. Traffic. 2003;4(5):333–43.

292. Hamilton BS, Whittaker GR, Daniel S. Influenza virus-mediated membrane fusion:

Determinants of hemagglutinin fusogenic activity and experimental approaches for assessing virus fusion. Viruses. 2012;4(7):1144–68.

293. Edinger TO, Pohl MO, Stertz S. Entry of influenza A virus: Host factors and antiviral targets. J Gen Virol. 2014;95(PART 2):263–77.
294. Skehel JJ, Wiley DC. Receptor Binding and Membrane Fusion in Virus Entry: The Influenza Hemagglutinin. Annu Rev Biochem. 2000;69(1):531–69.
295. Ettensohn DB, Frampton MW, Nichols JE, Roberts NJ. Human alveolar macrophages may not be susceptible to direct infection by a human influenza virus. J Infect Dis. 2016;214(11):1658–65.
296. Ioannidis LJ, Verity EE, Crawford S, Rockman SP, Brown LE. Abortive Replication of Influenza Virus in Mouse Dendritic Cells. J Virol. 2012;86(10):5922–5.
297. Baharom F, Thomas O, Lepzien R, Mellman I, Chalouni C, Smed-Sorensen A. Visualization of early influenza A virus trafficking in human dendritic cells using STED microscopy. PLoS One. 2017;12(6):e0177920.
298. Hufford MM, Kim TS, Sun J, Braciale TJ. The effector t cell response to influenza infection. Curr Top Microbiol Immunol. 2015;386:423–55.
299. Grant EJ, Quinõnes-Parra SM, Clemens EB, Kedzierska K. Human influenza viruses and CD8+T cell responses. Curr Opin Virol. 2016;16:132–42.
300. Sridhar S, Begom S, Bermingham A, Hoschler K, Adamson W, Carman W, et al. Cellular immune correlates of protection against symptomatic pandemic influenza. Nat Med. 2013;19(10):1305–12.
301. Wang Z, Wan Y, Qiu C, Quiñones-Parra S, Zhu Z, Loh L, et al. Recovery from severe H7N9 disease is associated with diverse response mechanisms dominated by CD8+ T cells. Nat Commun. 2015;6:6833.
302. Van Braeckel-Budimir N, Harty JT. Influenza-induced lung T rm: Not all memories last forever. Immunol Cell Biol. 2017;95(8):651–5.
303. Lofgren E, Fefferman NH, Naumov YN, Gorski J, Naumova EN. Influenza Seasonality: Underlying Causes and Modeling Theories. J Virol. 2007;81(11):5429–36.
304. Pizzolla A, Nguyen THO, Sant S, Jaffar J, Loudovaris T, Mannering SI, et al. Influenza-specific lung-resident memory t cells are proliferative and polyfunctional and maintain diverse TCR profiles. J Clin Invest. 2018;128(2):721–33.

305. Forrest BD, Pride MW, Dunning AJ, Capeding MRZ, Chotpitayasunondh T, Tam JS, et al. Correlation of cellular immune responses with protection against culture-confirmed influenza virus in young children. Clin Vaccine Immunol. 2008;15(7):1042–53.
306. Valkenburg SA, Venturi V, Dang THY, Bird NL, Doherty PC, Turner SJ, et al. Early priming minimizes the age-related immune compromise of CD8+ T cell diversity and function. PLoS Pathog. 2012;8(2).
307. van de Sandt CE, Hillaire MLB, Geelhoed-Mieras MM, Osterhaus ADME, Fouchier RAM, Rimmelzwaan GF. Human Influenza A Virus-Specific CD8+ T-Cell Response Is Long-lived. J Infect Dis. 2015;212(1):81–5.
308. Berlanda Scorza F, Tsvetnitsky V, Donnelly JJ. Universal influenza vaccines: Shifting to better vaccines. Vaccine. 2016;34(26):2926–33.
309. Houser K, Subbarao K. Influenza vaccines: Challenges and solutions. Cell Host Microbe. 2015;17(3):295–300.
310. National Institute of Allergy and Infectious Diseases. Free epitope database and prediction resource. 2018. Available from: http://www.iedb.org
311. Grant EJ, Chen L, Quinones-Parra S, Pang K, Kedzierska K, Chen W. T-Cell Immunity to Influenza A Viruses. Crit Rev Immunol. 2014;34(1):15–39.
312. Song H, Wittman V, Byers A, Tapia T, Zhou B, Warren W, et al. In vitro stimulation of human influenza-specific CD8+T cells by dendritic cells pulsed with an influenza virus-like particle (VLP) vaccine. Vaccine. 2010;28(34):5524–32.
313. Hemann EA, Kang S-M, Legge KL. Protective CD8 T Cell-Mediated Immunity against Influenza A Virus Infection following Influenza Virus-like Particle Vaccination. J Immunol. 2013;191(5):2486–94.
314. Brown DM, Lampe AT, Workman AM. The differentiation and protective function of cytolytic CD4 T cells in influenza infection. Front Immunol. 2016;7:1–8.
315. Hua L, Yao S, Pham D, Jiang L, Wright J, Sawant D, et al. Cytokine-Dependent Induction of CD4+ T cells with Cytotoxic Potential during Influenza Virus Infection. J Virol. 2013;87(21):11884–93.
316. Workman AM, Jacobs AK, Vogel AJ, Condon S, Brown DM. Inflammation enhances IL-2 driven differentiation of cytolytic CD4 T cells. PLoS One. 2014;9(2):1–12.
317. Oja AE, Vieira Braga FA, Remmerswaal EBM, Kragten NAM, Hertoghs KML, Zuo J, et

al. The transcription factor hobit identifies human cytotoxic CD4+T cells. Front Immunol. 2017;8:1–11.

318. Marshall NB, Vong AM, Devarajan P, Brauner MD, Kuang Y, Nayar R, et al. NKG2C/E Marks the Unique Cytotoxic CD4 T Cell Subset, ThCTL, Generated by Influenza Infection. J Immunol. 2017;198(3):1142–55.
319. Takeuchi A, Badr MESG, Miyauchi K, Ishihara C, Onishi R, Guo Z, et al. CRTAM determines the CD4 $^{+}$ cytotoxic T lymphocyte lineage. J Exp Med. 2016;213(1):123–38.
320. Wilkinson TM, Li CKF, Chui CSC, Huang AKY, Perkins M, Liebner JC, et al. Preexisting influenza-specific CD4+T cells correlate with disease protection against influenza challenge in humans. Nat Med. 2012;18(2):274–80.
321. Ahrends T, Spanjaard A, Pilzecker B, Bąbała N, Bovens A, Xiao Y, et al. CD4+T Cell Help Confers a Cytotoxic T Cell Effector Program Including Coinhibitory Receptor Downregulation and Increased Tissue Invasiveness. Immunity. 2017;47(5):848–861.e5.
322. Olson MR, Seah SGK, Edenborough K, Doherty PC, Lew AM, Turner SJ. CD154+ CD4+ T-cell dependence for effective memory influenza virus-specific CD8+ T-cell responses. Immunol Cell Biol. 2014;92(7):605–11.
323. Olson MR, Seah SGK, Cullen J, Greyer M, Edenborough K, Doherty PC, et al. Helping Themselves: Optimal Virus-Specific CD4 T Cell Responses Require Help via CD4 T Cell Licensing of Dendritic Cells. J Immunol. 2014;193(11):5420–33.
324. Nayak JL, Fitzgerald TF, Richards KA, Yang H, Treanor JJ, Sant AJ. CD4+ T-cell expansion predicts neutralizing antibody responses to monovalent, inactivated 2009 pandemic influenza A(H1N1) virus subtype H1N1 vaccine. J Infect Dis. 2013;207(2):297–305.
325. Victora GD, Wilson PC. Germinal Center Selection and the Antibody Response to Influenza. Cell. 2015;163:545–8.
326. Bentebibel S-E, Lopez S, Obermoser G, Schmitt N, Mueller C, Harrod C, et al. Induction of ICOS+CXCR3+CXCR5+ T H cells correlates with antibody responses to influenza vaccination. Sci Transl Med. 2013;5(176):1–11.
327. Bentebibel S-E, Khurana S, Schmitt N, Kurup P, Mueller C, Obermoser G, et al. ICOS+PD-1+CXCR3+ T follicular helper cells contribute to the generation of high-avidity antibodies following influenza vaccination. Sci Rep. 2016;6(1):26494.

328. Sant AJ, Richards KA, Nayak J. Distinct and complementary roles of CD4 T cells in protective immunity to influenza virus. Curr Opin Immunol. 2018;53:13–21.
329. Betts RJ, Prabhu N, Ho AWS, Lew FC, Hutchinson PE, Rotzschke O, et al. Influenza A Virus Infection Results in a Robust, Antigen-Responsive, and Widely Disseminated Foxp3+ Regulatory T Cell Response. J Virol. 2012;86(5):2817–25.
330. Lofano G, Kumar A, Finco O, Del Giudice G, Bertholet S. B cells and functional antibody responses to combat influenza. Front Immunol. 2015;6:336.
331. Sautto GA, Kirchenbaum GA, Ross TM. Towards a universal influenza vaccine: Different approaches for one goal. Virol J. 2018;15(1):1–12.
332. Ekiert DC, Bhabha G, Elsliger M, Friesen RHE, Jongeneelen M, Throsby M, et al. Antibody recognition of a highly conserved influenza virus epitope : implications for universal prevention and therapy. Science. 2009;324(5924):246–51.
333. Neu KE, Henry Dunand CJ, Wilson PC. Heads, stalks and everything else: how can antibodies eradicate influenza as a human disease? Curr Opin Immunol. 2016;42:48–55.
334. Sui J, Hwang WC, Perez S, Wei G, Aird D, Chen LM, et al. Structural and functional bases for broad-spectrum neutralization of avian and human influenza A viruses. Nat Struct Mol Biol. 2009;16(3):265–73.
335. Wohlbold TJ, Krammer F. In the shadow of hemagglutinin: A growing interest in influenza viral neuraminidase and its role as a vaccine antigen. Viruses. 2014;6(6):2465–94.
336. Jegaskanda S, Vandenberg K, Laurie KL, Loh L, Kramski M, Winnall WR, et al. Cross-reactive influenza-specific antibody-dependent cellular cytotoxicity in intravenous immunoglobulin as a potential therapeutic against emerging influenza viruses. J Infect Dis. 2014;210(11):1811–22.
337. Co MDT, Terajima M, Thomas SJ, Jarman RG, Rungrojcharoenkit K, Fernandez S, et al. Relationship of Preexisting Influenza Hemagglutination Inhibition, Complement-Dependent Lytic, and Antibody-Dependent Cellular Cytotoxicity Antibodies to the Development of Clinical Illness in a Prospective Study of A(H1N1)pdm09 Influenza in Children. Viral Immunol. 2014;27(8):375–82.
338. Banzhoff A, Stoddard JJ. Effective influenza vaccines for children: a critical unmet medical need and a public health priority. Hum Vaccin Immunother. 2012;8(3):398–402.

339. Izurieta HS, Thadani N, Shay DK, Lu Y, Maurer A, Foppa IM, et al. Comparative effectiveness of high-dose versus standard-dose influenza vaccines in US residents aged 65 years and older from 2012 to 2013 using Medicare data: A retrospective cohort analysis. Lancet Infect Dis. 2015;15(3):293–300.
340. Monto AS. Seasonal influenza and vaccination coverage. Vaccine. 2010;28(SUPPL. 4):33–44.
341. Zbinden D, Manuel O. Influenza vaccination in immunocompromised patients: efficacy and safety. Immunotherapy. 2014;6(2):131–9.
342. Nafziger AN, Pratt DS. Seasonal influenza vaccination and technologies. J Clin Pharmacol. 2014;54(7):719–31.
343. Weir JP, Gruber MF. An overview of the regulation of influenza vaccines in the United States. Influenza Other Respi Viruses. 2016;10(5):354–60.
344. Ellebedy AH, Webby RJ. Influenza vaccines. Vaccine. 2009;27(SUPPL. 4):D65–8.
345. Huber VC. Influenza vaccines: From whole virus preparations to recombinant protein technology. Expert Rev Vaccines. 2014;13(1):31–42.
346. Beran J, Peeters M, Dewé W, Raupachová J, Hobzová L, Devaster JM. Immunogenicity and safety of quadrivalent versus trivalent inactivated influenza vaccine: A randomized, controlled trial in adults. BMC Infect Dis. 2013;13(1).
347. Ambrose CS, Levin MJ. The rationale for quadrivalent influenza vaccines. Human Vaccines and Immunotherapeutics. 2012;8:81–8.
348. Chung JR, Flannery B, Thompson MG, Gaglani M, Jackson ML, Monto AS, et al. Seasonal Effectiveness of Live Attenuated and Inactivated Influenza Vaccine. Pediatrics. 2016;137(2):e20153279.
349. Ilyushina NA, Haynes BC, Hoen AG, Khalenkov AM, Housman ML, Brown EP, et al. Live attenuated and inactivated influenza vaccines in children. J Infect Dis. 2015;211(3):352–60.
350. Woolpert T, Phillips CJ, Sevick C, Crum-Cianflone NF, Blair PJ, Faix D. Health-related behaviors and effectiveness of trivalent inactivated versus live attenuated influenza vaccine in preventing influenza-like illness among young adults. PLoS One. 2014;9(7).
351. Beyer WEP, Nauta JJP, Palache AM, Giezeman KM, Osterhaus ADME. Immunogenicity and safety of inactivated influenza vaccines in primed populations: A systematic literature

review and meta-analysis. Vaccine. 2011;29(34):5785–92.
352. Dormitzer PR, Tsai TF, Giudice G Del. New technologies for influenza vaccines. Hum Vaccin Immunother. 2012;8(1):45–58.
353. Kon TC, Onu A, Berbecila L, Lupulescu E, Ghiorgisor A, Kersten GF, et al. Influenza vaccine manufacturing: Effect of inactivation, splitting and site of manufacturing. Comparison of influenza vaccine production processes. PLoS One. 2016;11(3):1–19.
354. Wong S-S, Webby RJ. Traditional and New Influenza Vaccines. Clin Microbiol Rev. 2013;26(3):476–92.
355. Frey SE, Reyes MRADL, Reynales H, Bermal NN, Nicolay U, Narasimhan V, et al. Comparison of the safety and immunogenicity of an MF59®-adjuvanted with a non-adjuvanted seasonal influenza vaccine in elderly subjects. Vaccine. 2014;32(39):5027–34.
356. McElhaney JE, Beran J, Devaster JM, Esen M, Launay O, Leroux-Roels G, et al. AS03-adjuvanted versus non-adjuvanted inactivated trivalent influenza vaccine against seasonal influenza in elderly people: A phase 3 randomised trial. Lancet Infect Dis. 2013;13(6):485–96.
357. Seo Y Bin, Choi WS, Lee J, Song JY, Cheong HJ, Kim WJ. Comparison of the immunogenicity and safety of the conventional subunit, MF59-adjuvanted, and intradermal influenza vaccines in the elderly. Clin Vaccine Immunol. 2014;21(7):989–96.
358. Chotpitayasunondh T, Thisyakorn U, Pancharoen C, Pepin S, Nougarede N. Safety, humoral and cell mediated immune responses to two formulations of an inactivated, split-virion influenza A/H5N1 vaccine in children. PLoS One. 2008;3(12):e4028.
359. Christensen D, Christensen JP, Korsholm KS, Isling LK, Erneholm K, Thomsen AR, et al. Seasonal influenza split vaccines confer partial cross-protection against heterologous influenza virus in ferrets when combined with the CAF01 adjuvant. Front Immunol. 2018;8:1928.
360. He X-S, Holmes TH, Zhang C, Mahmood K, Kemble GW, Lewis DB, et al. Cellular Immune Responses in Children and Adults Receiving Inactivated or Live Attenuated Influenza Vaccines. J Virol. 2006;80(23):11756–66.
361. Soema PC, Kompier R, Amorij JP, Kersten GFA. Current and next generation influenza vaccines: Formulation and production strategies. Eur J Pharm Biopharm. 2015;94:251–63.
362. Jin H, Chen Z, Liu J, Kemble G. Genetic Engineering of Live Attenuated Influenza

Viruses. 2012:163–74.
363. Jin H, Chen Z. Production of live attenuated influenza vaccines against seasonal and potential pandemic influenza viruses. Curr Opin Virol. 2014;6(1):34–9.
364. Toback SL, Levin MJ, Block SL, Belshe RB, Ambrose CS, Falloon J. Quadrivalent Ann Arbor strain live-attenuated influenza vaccine. Expert Rev Vaccines. 2012;11(11):1293–303.
365. Barría MI, Garrido JL, Stein C, Scher E, Ge Y, Engel SM, et al. Localized mucosal response to intranasal live attenuated influenza vaccine in adults. J Infect Dis. 2013;207(1):115–24.
366. Jang YH, Seong BL. Cross-protective immune responses elicited by live attenuated influenza vaccines. Yonsei Med J. 2013;54(2):271–82.
367. Kwong JC, Pereira JA, Quach S, Pellizzari R, Dusome E, Russell ML, et al. Randomized evaluation of live attenuated vs. inactivated influenza vaccines in schools (RELATIVES) pilot study: A cluster randomized trial. Vaccine. 2015;33(4):535–41.
368. Rodgers L, Pabst LJ, Chaves SS. Increasing uptake of live attenuated influenza vaccine among children in the United States, 2008-2014. Vaccine. 2015;33(1):22–4.
369. Powers DC, Fries LF, Murphy BR, Thumar B, Clements ML. In elderly persons live attenuated influenza A virus vaccines do not offer an advantage over inactivated virus vaccine in inducing serum or secretory antibodies or local immunologic memory. J Clin Microbiol. 1991;29(3):498–505.
370. Traynor K. First recombinant flu vaccine approved. Am J Health Syst Pharm. 2013;70(5):382.
371. National Advisory Commitee on Immunization. Canadian immunization guide: Chapter on influenza and statement on Seasonal influenza vaccine for 2017-2018. 2017. 76 p.
372. Weinberg GA, Szilagyi PG. Vaccine Epidemiology: Efficacy, Effectiveness, and the Translational Research Roadmap. J Infect Dis. 2010;201(11):1607–10.
373. McCullers JA, Huber VC. Correlates of vaccine protection from influenza and its complications. Hum Vaccines Immunother. 2012;8(1):34–44.
374. Reber A, Katz J. Immunological assessment of influenza vaccines and immune correlates of protection. Expert Review of Vaccines. 2013;12:519–36.
375. Ward BJ, Pillet S, Charland N, Trepanier S, Couillard J, Landry N. The establishment of

surrogates and correlates of protection: Useful tools for the licensure of effective influenza vaccines? Hum Vaccines Immunother. 2018;14(3):647–56.

376. Katz JM, Hancock K, Xu X. Serologic assays for influenza surveillance, diagnosis and vaccine evaluation. Expert Rev Anti Infect Ther. 2011;9(6):669–83.
377. Klimov A, Balish A, Veguilla V, Sun H, Schiffer J, Lu X, et al. Influenza virus titration, antigenic characterization, and serological Mmethods for antibody detection. Methods Mol Biol. 2012;865:25–51.
378. WHO Global Influenza Surveillance Network. Manual for the laboratory diagnosis and virological surveillance of influenza. World Health Organization. 2011. 153 p.
379. Coudeville L, Bailleux F, Riche B, Megas F, Andre P, Ecochard R. Relationship between haemagglutination-inhibiting antibody titres and clinical protection against influenza: Development and application of a bayesian random-effects model. BMC Med Res Methodol. 2010;10:18.
380. Trombetta C, Perini D, Mather S, Temperton N, Montomoli E. Overview of Serological Techniques for Influenza Vaccine Evaluation: Past, Present and Future. Vaccines. 2014;2(4):707–34.
381. Wood JM, Major D, Heath A, Newman RW, Höschler K, Stephenson I, et al. Reproducibility of serology assays for pandemic influenza H1N1: Collaborative study to evaluate a candidate WHO International Standard. Vaccine. 2012;30(2):210–7.
382. Zacour M, Ward BJ, Brewer A, Tang P, Boivin G, Li Y, et al. Standardization of Hemagglutination Inhibition Assay for Influenza Serology Allows for High Reproducibility between Laboratories. Clin Vaccine Immunol. 2016;23(3):236–42.
383. Ohmit SE, Petrie JG, Cross RT, Johnson E, Monto AS. Influenza hemagglutination-inhibition antibody titer as a correlate of vaccine-induced protection. J Infect Dis. 2011;204(12):1879–85.
384. Lambert LC, Fauci AS. Influenza Vaccines for the Future. N Engl J Med. 2010;363(21):2036–44.
385. Milián E, Kamen AA. Current and emerging cell culture manufacturing technologies for influenza vaccines. Biomed Res Int. 2015;2015: 504831.
386. Manini I, Trombetta C, Lazzeri G, Pozzi T, Rossi S, Montomoli E. Egg-Independent Influenza Vaccines and Vaccine Candidates. Vaccines. 2017;5(3):18.

387. Kistner O, Barrett PN, Mundt W, Reiter M, Schober-Bendixen S, Dorner F. Development of a mammalian cell (Vero) derived candidate influenza virus vaccine. Vaccine. 1998;16(9–10):960–8.
388. Skowronski DM, Janjua NZ, De Serres G, Sabaiduc S, Eshaghi A, Dickinson JA, et al. Low 2012-13 influenza vaccine effectiveness associated with mutation in the egg-adapted H3N2 vaccine strain not antigenic drift in circulating viruses. PLoS One. 2014;9(3).
389. Tricco AC, Chit A, Soobiah C, Hallett D, Meier G, Chen MH, et al. Comparing influenza vaccine efficacy against mismatched and matched strains: A systematic review and meta-analysis. BMC Med. 2013;11(1):1.
390. Moro PL, Winiecki S, Lewis P, Shimabukuro TT, Cano M. Surveillance of adverse events after the first trivalent inactivated influenza vaccine produced in mammalian cell culture (Flucelvax®) reported to the Vaccine Adverse Event Reporting System (VAERS), United States, 2013-2015. Vaccine. 2015;33(48):6684–8.
391. Haber P, Moro PL, Cano M, Lewis P, Stewart B, Shimabukuro TT. Post-licensure surveillance of quadrivalent live attenuated influenza vaccine United States, Vaccine Adverse Event Reporting System (VAERS), July 2013-June 2014. Vaccine. 2015;33(16):1987–92.
392. Suryadevara M, Domachowske JB. Quadrivalent influenza vaccine in the United States. Hum Vaccines Immunother. 2014;10(3):596–9.
393. Jamotte A, Chong CF, Manton A, Macabeo B, Toumi M. Impact of quadrivalent influenza vaccine on public health and influenza-related costs in Australia. BMC Public Health. 2016;16(1):1–12.
394. Tisa V, Barberis I, Faccio V, Paganino C, Trucchi C, Martini M, et al. Quadrivalent influenza vaccine: A new opportunity to reduce the influenza burden. J Prev Med Hyg. 2016;57(1):E28–33.
395. Wang JM, Vardeny O, Zorek JA. High-dose influenza vaccine in older adults. J Am Pharm Assoc. 2016;56(1):95–7.
396. DiazGranados CA, Dunning AJ, Robertson CA, Talbot HK, Landolfi V, Greenberg DP. Efficacy and immunogenicity of high-dose influenza vaccine in older adults by age, comorbidities, and frailty. Vaccine. 2015;33(36):4565–71.
397. DiazGranados CA, Dunning AJ, Kimmel M, Kirby D, Treanor J, Collins A, et al. Efficacy

of High-Dose versus Standard-Dose Influenza Vaccine in Older Adults. N Engl J Med. 2014;371(7):635–45.

398. Principi N, Esposito S. Adjuvanted influenza vaccines. Hum Vaccin Immunother. 2012;8(1):59–66.
399. Tregoning JS, Russell RF, Kinnear E. Adjuvanted influenza vaccines . Vol. 14, Human Vaccines and Immunotherapeutics. 2018:550–64.
400. Launay O, Duval X, Fitoussi S, Jilg W, Kerdpanich A, Montellano M, et al. Extended antigen sparing potential of AS03-adjuvanted pandemic H1N1 vaccines in children, and immunological equivalence of two formulations of AS03-adjuvanted H1N1 vaccines: Results from two randomised trials. BMC Infect Dis. 2013;13(1).
401. Nolan T, Roy-Ghanta S, Montellano M, Weckx L, Ulloa-Gutierrez R, Lazcano-Ponce E, et al. Relative efficacy of AS03-adjuvanted pandemic influenza A(H1N1) vaccine in children: Results of a controlled, randomized efficacy trial. J Infect Dis. 2014;210(4):545–57.
402. Black S. Safety and effectiveness of MF-59 adjuvanted influenza vaccines in children and adults. Vaccine. 2015;33:B3–5.
403. Vesikari T, Kirstein J, Devota Go G, Leav B, Ruzycky ME, Isakov L, et al. Efficacy, immunogenicity, and safety evaluation of an MF59-adjuvanted quadrivalent influenza virus vaccine compared with non-adjuvanted influenza vaccine in children: a multicentre, randomised controlled, observer-blinded, phase 3 trial. Lancet Respir Med. 2018;6(5):345–56.
404. Garçon N, Vaughn DW, Didierlaurent AM. Development and evaluation of AS03, an Adjuvant System containing α-tocopherol and squalene in an oil-in-water emulsion. Expert Rev Vaccines. 2012;11(3):349–66.
405. Couch RB, Bayas JM, Caso C, Mbawuike IN, López CN, Claeys C, et al. Superior antigen-specific CD4+T-cell response with AS03-adjuvantation of a trivalent influenza vaccine in a randomised trial of adults aged 65 and older. BMC Infect Dis. 2014;14(1):425.
406. Nohynek H, Jokinen J, Partinen M, Vaarala O, Kirjavainen T, Sundman J, et al. AS03 adjuvanted AH1N1 vaccine associated with an abrupt increase in the incidence of childhood narcolepsy in Finland. PLoS One. 2012;7(3).

407. Stowe J, Andrews N, Kosky C, Dennis G, Eriksson S, Hall A, et al. Risk of Narcolepsy after AS03 Adjuvanted Pandemic A/H1N1 2009 Influenza Vaccine in Adults: A Case-Coverage Study in England. Sleep. 2016;39(5):1051–7.
408. Sturkenboom MCJM. The narcolepsy-pandemic influenza story: Can the truth ever be unraveled? Vaccine. 2015;33(S2):B6–13.
409. Verstraeten T, Cohet C, Dos Santos G, Ferreira GL, Bollaerts K, Bauchau V, et al. Pandemrix™ and narcolepsy: A critical appraisal of the observational studies. Hum Vaccin Immunother. 2016;12(1):187–93.
410. Chroboczek J, Szurgot I, Szolajska E. Virus-like particles as vaccine. Acta Biochimica Polonica. 2014;61:531–9.
411. Liu J, Dai S, Wang M, Hu Z, Wang H, Deng F. Virus like particle-based vaccines against emerging infectious disease viruses. Virologica Sinica. 2016;31:279–87.
412. Rynda-Apple A, Patterson DP, Douglas T. Virus-like particles as antigenic nanomaterials for inducing protective immune responses in the lung. Nanomedicine (Lond). 2014;9(12):1857–68.
413. Yan D, Wei YQ, Guo HC, Sun SQ. The application of virus-like particles as vaccines and biological vehicles. Applied Microbiology and Biotechnology. 2015;99:10415–32.
414. Kang S-M, Kim M-C, Compans RW. Virus-like particles as universal influenza vaccines. Expert Rev Vaccines. 2012;11(8):995–1007.
415. Andreasson K, Eriksson M, Tegerstedt K, Ramqvist T, Dalianis T. CD4+ and CD8+ T cells can act separately in tumour rejection after immunization with murine pneumotropic virus chimeric Her2/neu virus-like particles. PLoS One. 2010;5(7):e11580.
416. Moffat JM, Cheong WS, Villadangos JA, Mintern JD, Netter HJ. Hepatitis B virus-like particles access major histocompatibility class I and II antigen presentation pathways in primary dendritic cells. Vaccine. 2013;31(18):2310–6.
417. Ponterio E, Petrizzo A, Di Bartolo I, Buonaguro FM, Buonaguro L, Ruggeri FM. Pattern of activation of human antigen presenting cells by genotype GII.4 norovirus virus-like particles. J Transl Med. 2013;11(1):127.
418. Chen S, Zheng D, Li C, Zhang W, Xu W, Liu X, et al. Protection against multiple subtypes of influenza viruses by virus-like particle vaccines based on a hemagglutinin conserved epitope. Biomed Res Int. 2015;2015:901817.

419. Schmeisser F, Adamo JE, Blumberg B, Friedman R, Muller J, Soto J, et al. Production and characterization of mammalian virus-like particles from modified vaccinia virus Ankara vectors expressing influenza H5N1 hemagglutinin and neuraminidase. Vaccine. 2012;30(23):3413–22.
420. Gao X, Wang WJ, Li YF, Zhang SG, Duan YQ, Xing L, et al. Enhanced Influenza VLP vaccines comprising matrix-2 ectodomain and nucleoprotein epitopes protects mice from lethal challenge. Antiviral Res. 2013;98(1):4–11.
421. Ren Z, Zhao Y, Liu J, Ji X, Meng L, Wang T, et al. Intramuscular and intranasal immunization with an H7N9 influenza virus-like particle vaccine protects mice against lethal influenza virus challenge. Int Immunopharmacol. 2018;58:109–16.
422. Xue C, Tian G, Chen X, Liu Q, Ma J, Xu S, et al. Incorporation of conserved nucleoprotein into influenza virus-like particles could provoke a broad protective immune response in BALB/c mice and chickens. Virus Res. 2015;195:35–42.
423. Chung KY, Coyle EM, Jani D, King LR, Bhardwaj R, Fries L, et al. ISCOMATRIX™ adjuvant promotes epitope spreading and antibody affinity maturation of influenza A H7N9 virus like particle vaccine that correlate with virus neutralization in humans. Vaccine. 2015;33(32):3953–62.
424. Cummings JF, Guerrero ML, Moon JE, Waterman P, Nielsen RK, Jefferson S, et al. Safety and immunogenicity of a plant-produced recombinant monomer hemagglutinin-based influenza vaccine derived from influenza A (H1N1)pdm09 virus: A Phase 1 dose-escalation study in healthy adults. Vaccine. 2014;32(19):2251–9.
425. Low JGH, Lee LS, Ooi EE, Ethirajulu K, Yeo P, Matter A, et al. Safety and immunogenicity of a virus-like particle pandemic influenza A (H1N1) 2009 vaccine: Results from a double-blinded, randomized Phase I clinical trial in healthy Asian volunteers. Vaccine. 2014;32(39):5041–8.
426. Huang X, Wang X, Zhang J, Xia N, Zhao Q. Escherichia coli-derived virus-like particles in vaccine development. npj Vaccines. 2017;2(1):1–8.
427. Penkert RR, Young NS, Surman SL, Sealy RE, Rosch J, Dormitzer PR, et al. Saccharomyces cerevisiae-derived virus-like particle parvovirus B19 vaccine elicits binding and neutralizing antibodies in a mouse model for sickle cell disease. Vaccine. 2017;35(29):3615–20.

428. Kim HJ, Cho SY, Park MH, Kim HJ. Comparison of the size distributions and immunogenicity of human papillomavirus type 16 L1 virus-like particles produced in insect and yeast cells. Arch Pharm Res. 2018;41(5):1–10.
429. Walpita P, Johns LM, Tandon R, Moore ML. Mammalian cell-derived respiratory syncytial virus-like particles protect the lower as well as the upper respiratory tract. PLoS One. 2015;10(7):1–18.
430. Rodríguez-Limas WA, Sekar K, Tyo KEJ. Virus-like particles: The future of microbial factories and cell-free systems as platforms for vaccine development. Curr Opin Biotechnol. 2013;24(6):1089–93.
431. Scotti N, Rybicki EP. Virus-like particles produced in plants as potential vaccines. Expert Rev Vaccines. 2013;12(2):211–24.
432. Chen Q, Lai H. Plant-derived virus-like particles as vaccines. Hum Vaccines Immunother. 2013;9(1):26–49.
433. Marsian J, Lomonossoff GP. Molecular pharming-VLPs made in plants. Current Opinion in Biotechnology. 2016;37:201–6.
434. Steele JFC, Peyret H, Saunders K, Castells-Graells R, Marsian J, Meshcheriakova Y, et al. Synthetic plant virology for nanobiotechnology and nanomedicine. Wiley Interdiscip Rev Nanomedicine Nanobiotechnology. 2017;9(4):1–18.
435. D'Aoust MA, Lavoie PO, Couture MMJ, Trépanier S, Guay JM, Dargis M, et al. Influenza virus-like particles produced by transient expression in Nicotiana benthamiana induce a protective immune response against a lethal viral challenge in mice. Plant Biotechnol J. 2008;6(9):930–40.
436. Ravin N V., Kotlyarov RY, Mardanova ES, Kuprianov V V., Migunov AI, Stepanova LA, et al. Plant-produced recombinant influenza vaccine based on virus-like HBc particles carrying an extracellular domain of M2 protein. Biochem. 2012;77(1):33–40.
437. Shoji Y, Prokhnevsky A, Leffet B, Vetter N, Tottey S, Satinover S, et al. Immunogenicity of H1N1 influenza virus-like particles produced in Nicotiana benthamiana. Hum Vaccines Immunother. 2015;11(1):118–23.
438. Medicago Inc. 2018. Available from: http://medicago.com/
439. D'Aoust MA, Couture MMJ, Charland N, Trépanier S, Landry N, Ors F, et al. The production of hemagglutinin-based virus-like particles in plants: A rapid, efficient and

safe response to pandemic influenza. Plant Biotechnol J. 2010;8(5):607–19.

440. Lindsay BJ, Bonar MM, Costas-Cancelas IN, Hunt K, Makarkov AI, Chierzi S, et al. Morphological characterization of a plant-made virus-like particle vaccine bearing influenza virus hemagglutinins by electron microscopy. Vaccine. 2018;36(16):2147–54.
441. Harris A, Cardone G, Winkler DC, Heymann JB, Brecher M, White JM, et al. Influenza virus pleiomorphy characterized by cryoelectron tomography. Proc Natl Acad Sci. 2006;103(50):19123–7.
442. Wasilewski S, Calder LJ, Grant T, Rosenthal PB. Distribution of surface glycoproteins on influenza A virus determined by electron cryotomography. Vaccine. 2012;30(51):7368–73.
443. Le Mauff F, Mercier G, Chan P, Burel C, Vaudry D, Bardor M, et al. Biochemical composition of haemagglutinin-based influenza virus-like particle vaccine produced by transient expression in tobacco plants. Plant Biotechnol J. 2015;13(5):717–25.
444. Morel J, Claverol S, Mongrand S, Furt F, Fromentin J, Bessoule J-J, et al. Proteomics of Plant Detergent-resistant Membranes. Mol Cell Proteomics. 2006;5(8):1396–411.
445. Hendin HE, Pillet S, Lara AN, Wu CY, Charland N, Landry N, et al. Plant-made virus-like particle vaccines bearing the hemagglutinin of either seasonal (H1) or avian (H5) influenza have distinct patterns of interaction with human immune cells in vitro. Vaccine. 2017;35(19):2592–9.
446. Young KR, Arthus-Cartier G, Yam KK, Lavoie PO, Landry N, D'Aoust MA, et al. Generation and characterization of a trackable plant-made influenza H5 virus-like particle (VLP) containing enhanced green fluorescent protein (eGFP). FASEB J. 2015;29(9):3817–27.
447. Landry N, Ward BJ, Trépanier S, Montomoli E, Le Dargis M, Lapini G, et al. Preclinical and clinical development of plant-made virus-like particle vaccine against avian H5N1 influenza. Fouchier RAM, editor. PLoS One. 2010;5(12):e15559.
448. Pillet S, Racine T, Nfon C, Di Lenardo TZ, Babiuk S, Ward BJ, et al. Plant-derived H7 VLP vaccine elicits protective immune response against H7N9 influenza virus in mice and ferrets. Vaccine. 2015;33(46):6282–9.
449. Hodgins B, Yam KK, Winter K, Pillet S, Landry N, Ward BJ. A single intramuscular dose of a plant-made virus-like particle vaccine elicits a balanced humoral and cellular response

and protects young and aged mice from influenza H1N1 virus challenge despite a modest/absent humoral response. Clin Vaccine Immunol. 2017;24(12):1–14.

450. Landry N, Pillet S, Favre D, Poulin JF, Trépanier S, Yassine-Diab B, et al. Influenza virus-like particle vaccines made in Nicotiana benthamiana elicit durable, poly-functional and cross-reactive T cell responses to influenza HA antigens. Clin Immunol. 2014;154(2):164–77.

451. Pillet S, Aubin É, Trépanier S, Poulin JF, Yassine-Diab B, Ter Meulen J, et al. Humoral and cell-mediated immune responses to H5N1 plant-made virus-like particle vaccine are differentially impacted by alum and GLA-SE adjuvants in a Phase 2 clinical trial. npj Vaccines. 2018;3(1):3.

452. Pillet S, Aubin É, Trépanier S, Bussière D, Dargis M, Poulin JF, et al. A plant-derived quadrivalent virus like particle influenza vaccine induces cross-reactive antibody and T cell response in healthy adults. Clin Immunol. 2016;168:72–87.

453. National Institutes of Health. ClinicalTrials.gov. 2018. Available from: https://www.clinicaltrials.gov/

1.6. TABLES

Table 1. 1. Influenza A virus RNA segments and the proteins they encode

RNA segment number	Number of nucleotides	Gene product(s)	Number of amino acids	Function
				Viral RNA-dependent RNA polymerase (vRdRP) Binds to the ends of each ssRNA segment and synthesizes new copies of the viral RNP. The subunits combine together after import into the nucleus. The vRdRP consists of three main subunits (PB1, PB2 and PA) and peripherally a matrix of NP.
1	2341	PB2	759	**PB2**: Responsible for cap binding. The globular domain is essential for proper association with importin α3 and to a lesser extent α1 and α7.
		PB2-S1	508	An alternative splicing product of PB2: appears to localize in the mitochondria and inhibit the RIG-I-dependent interferon signaling pathway (humoral immunity).
2	2341	PB1	757	**PB1**: Involved in capturing the cap regions of the host's mRNA and inserting the primer into the viral mRNA. Holds the polymerase active site and harbors endonuclease activity.
		PB1-F2	87–90	From an alternative reading frame. Can induce apoptosis, regulate host interferon response and modulate susceptibility to bacterial superinfection. May influence intracellular localization of PB1.
		PB1-N40		N-terminally truncated version of PB1; a product from an in-frame downstream initiation site. The function is unknown, but it might modulate virus-induced pathogenesis.
3	2233	PA	716	**Polymerase acidic**: functions as an RNA-endonuclease. Cleaves capped RNA fragments off of the host's pre-RNA to be used as primers for constructing viral mRNA.
	252	PA-X	61	Frameshifted PA at 191-252 (H7N7), postulated to play an important role in virus replication and shutdown of host innate responses in animal models, but its expression during *in vivo* infection has not been observed.
		PA-N155	561	Ribosomal frameshift to AUG start codon at position 155; possible role in viral replication, but function unknown.
		PA-N182	534	Ribosomal frameshift to AUG start codon at position 182; function unknown.

4	1778	HA	566	**Hemagglutinin**: The outer glycoprotein that binds sialic acid of epithelial cells and plays a central role in the fusion process.
5	1565	NP	498	**Nucleoprotein**: binds the ssRNA into a large ds (NP protein) helix and serves to regulate the export and import of viral RNPs.
6	1413	NA	454	**Neuraminidase**: Helps the virion cut through the mucous coating of epithelial cells. Also thought to be important during the budding process where the newly forming virion breaks away from the host cell.
7				**Matrix proteins**
	1027	M1	252	Full-length structure. Involved in regulating the import and export of the viral RNP. A key regulator for viral assembly, preferentially binding viral RNPs during viral assembly.
		M2	97	Alternative splice produce. Combines in the form of a tetramer in the viral envelope where it regulates the flow of protons into the viral genome after the capsid has entered the cell and before release of the viral RNPs (endocytosis).
		M3	9	Alternative splice product; function unknown.
		M4	54	Alternative splice product; function unknown.
		M42	99	Alternative splice product; function not fully established; however, it can serve in the place of M2.
8				**Nonstructural proteins**
	890	NS1	230	Full-length structure. Inhibits the interferon-mediated antiviral response [38]. The NS1 protein of IAV serves a critical role in suppressing the production of host mRNAs by inhibiting the 3′-end processing of host pre-mRNAs and consequently blocking the production of host mRNAs, including interferon-β mRNAs. Also involved in the import of the viral RNPs, tends to help hijack the import mechanism using importin alpha.
		NEP (formerly NS2)	98	Important both for the import and export of viral RNPs and mRNA copies to and from the nucleus to the cytosol.
		NS3		Function unknown but may be an important protein factor for adaptation to new hosts.

The table is adapted from (43), with modifications.

Table 1. 2. Medicago influenza HA-VLP clinical trials

NCT Number	Title	Phases	Start Date	Completion Date
NCT03301051	Efficacy, Safety, and Immunogenicity of a Plant-Derived Quadrivalent Virus-Like Particles Influenza Vaccine in Adults	Phase 3	August 31, 2017	April 30, 2018
NCT03321968	Lot-to-lot Consistency of a Plant-Derived Quadrivalent Virus-Like Particles Influenza Vaccine in Healthy Adults	Phase 3	September 29, 2017	November 16, 2017
NCT02831751	Immunogenicity, Safety, and Tolerability of a Plant-Derived Quadrivalent VLP Influenza Vaccine in Elderly Adults	Phase 2	April 2016	January 2017
NCT02768805	Immunogenicity of a Quadrivalent Virus-Like Particles (VLP) Influenza Vaccine in Healthy Adults	Phase 2	March 2016	December 2016
NCT02236052	Immunogenicity, Safety and Tolerability of a Plant-Derived Seasonal VLP Quadrivalent Influenza Vaccine in the Elderly Population	Phase 2	August 2014	June 2016
NCT02233816	Immunogenicity, Safety and Tolerability of a Plant-Derived Seasonal Virus-Like-Particle Quadrivalent Influenza Vaccine in Adults	Phase 2	August 2014	May 2016
NCT02022163	Safety, Tolerability and Immunogenicity of a Plant-made H7 Virus-like Particle (VLP) Influenza Vaccine in Adults	Phase 1	December 2013	December 2014
NCT01991587	Safety, Tolerability and Immunogenicity of a Plant-made Seasonal Quadrivalent VLP Influenza Vaccine in Adults	Phase 1 / Phase 2	October 2013	September 2014
NCT01991561	Immunogenicity, Safety, Tolerability of a Plant-made H5 Virus-like-particle (VLP) Influenza Vaccine	Phase 2	June 2013	November 2014
NCT01657929	H5-VLP + GLA-AF Vaccine Trial in Healthy Adult Volunteers	Phase 1	September 2012	January 2014
NCT01302990	Safety, Tolerability and Immunogenicity of a Plant-Made H1 VLP Influenza Vaccine in Adults	Phase 1	February 2011	November 2011
NCT01244867	Immunogenicity, Safety, Tolerability of a Plant-Made H5 VLP Influenza Vaccine	Phase 2	November 2010	September 2011
NCT00984945	Safety Study of a Plant-based H5 Virus-Like Particles (VLP) Vaccine in Healthy Adults	Phase 1	September 2009	July 2010

Retrieved from (453) on June 03, 2018

1.7. FIGURES AND FIGURE LEGENDS

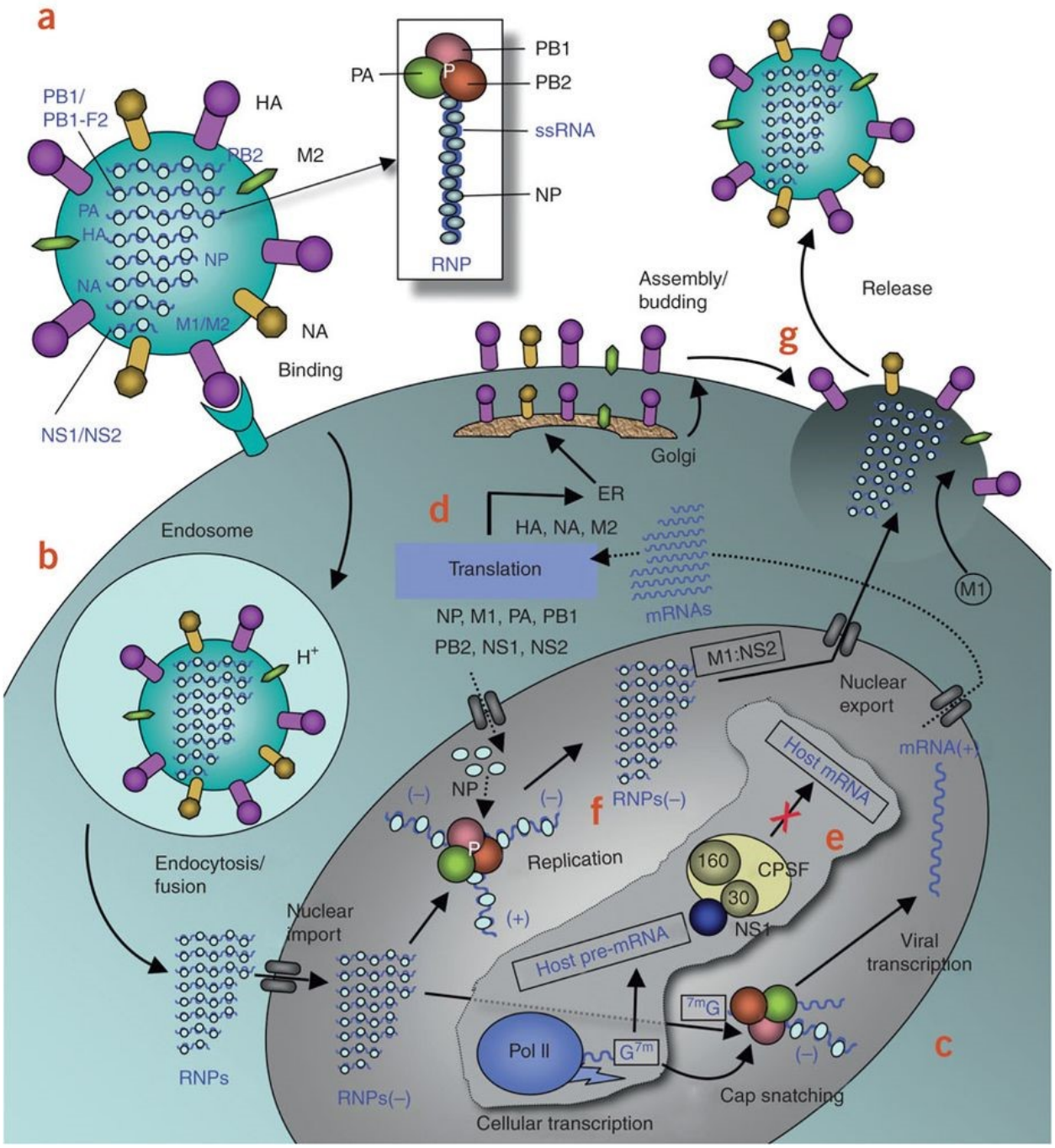

Figure 1. 1. Structure and life cycle of influenza A virus

Influenza A virus has a lipid bilayer envelope, within which are eight RNA genomic segments, each of which is associated with the trimeric viral RNA polymerase (PB1, PB2, PA) and coated with multiple nucleoproteins (NPs) to form the vRNPs. The outer layer of the

(legend continued on next page)

lipid envelope is spiked with multiple copies of HA, NA and a small number of M2, whereas the M1 molecules keep vRNPs attached to the inner layer. (**b**) The viral surface glycoprotein HA binds to the host cell-surface sialic acid receptors, and the virus is transported into the cell in an endocytic vesicle. The low pH in the endosome triggers a conformational change in the HA protein that leads to fusion of the viral and endosomal membranes. The low pH also triggers the flow of protons into the virus via the M2 ion channel, thereby dissociating the vRNPs from M1 matrix proteins. The vRNPs that are released into the cytoplasm are transported into the nucleus by recognition of the nuclear localization sequences (NLSs) on nucleoproteins only when the M1 molecules are dissociated. (**c**) In the nucleus, the viral polymerase initiates viral mRNA synthesis with 5′-capped RNA fragments cleaved from host pre-mRNAs. The PB2 subunit binds the 5′ cap of host pre-mRNAs, and the endonuclease domain in PA subunit cleaves the pre-mRNA 10–13 nucleotides downstream from the cap. Viral mRNA transcription is subsequently initiated from the cleaved 3′ end of the capped RNA segment. This 'cap snatching' occurs on nascent pre-mRNAs. (**d**) Viral mRNAs are transported to the cytoplasm for translation into viral proteins. The surface proteins HA, M2 and NA are processed in the endoplasmic reticulum (ER), glycosylated in the Golgi apparatus and transported to the cell membrane. I The NS1 protein of influenza A virus serves a critical role in suppressing the production of host mRNAs by inhibiting the 3′-end processing of host pre-mRNAs, consequently blocking the production of host mRNAs, including interferon-β mRNAs. Unlike host pre-mRNAs, the viral mRNAs do not require 3′-end processing by the host cell machinery. Therefore, the viral mRNAs are transported to the cytoplasm, whereas the host mRNA synthesis is predominantly blocked. (**f**) The viral polymerase is responsible for not only capped RNA-primed mRNA synthesis but also unprimed replication of vRNAs in steps (−) vRNA → (+) cRNA → (−) vRNA. The nucleoprotein molecules are required for these two steps of replication and are deposited on the cRNA and vRNA during RNA synthesis. The resulting vRNPs are subsequently transported to the cytoplasm, mediated by a M1–NS2 complex that is bound to the vRNPs; NS2 interacts with human CRM1 protein that exports the vRNPs from the nucleus. (**g**) The vRNPs reach the cell membrane to be incorporated into new viruses that are budded out.

(legend continued on next page)

The HA and NA proteins in new viruses contain terminal sialic acids that would cause the viruses to clump together and adhere to the cell surface. The NA of newly formed viruses cleaves these sialic acid residues, thereby releasing the virus from the host cell.

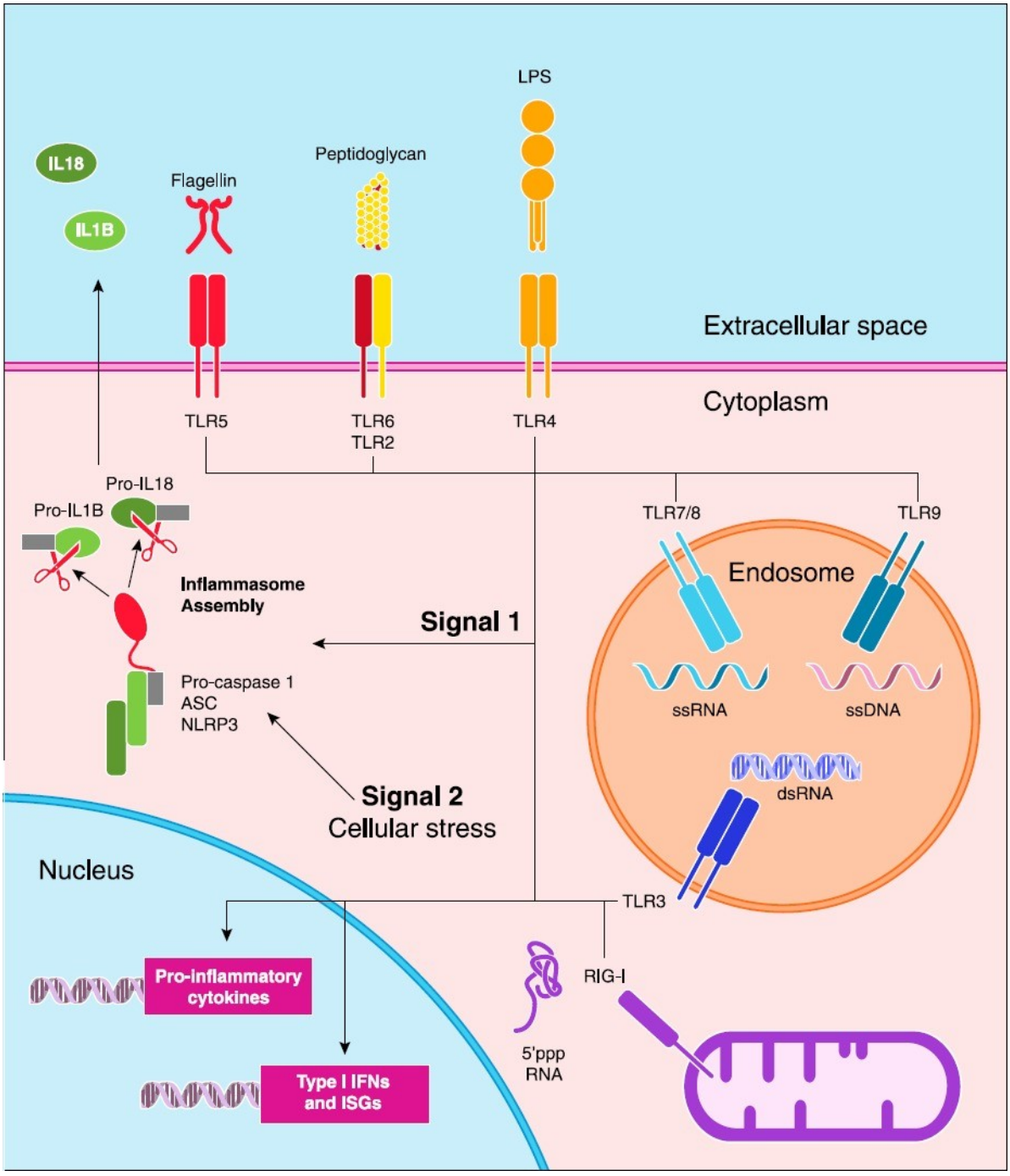

Figure 1. 2. Pattern recognition receptors (PRRs) and influenza virus

The cellular localization, major ligands, and effects of triggering PRRs are illustrated. The extracellular domain of each TLR is involved in recognition of specific microbial ligands to activate downstream signaling pathways that are generally MyD88 dependent (with the exception of TLR3).

(legend continued on next page)

TLR activation results in transcriptional activation and production of proinflammatory cytokines, ISGs, and IFN. RIG-I is a cytosolic helicase that specifically targets 5′-triphosphate-containing viral RNA, thereby, distinguishing viral from host transcripts. Detection triggers a signaling cascade that culminates in the production of IFNs and proinflammatory mediators. The inflammasome NLRP3 (the best characterized inflammasome) comprises the NLR protein NLRP3, the adapter ASC, and procaspase 1. The consensus is that 2 distinct signals are required for inflammasome activation: the first signal leads to synthesis of pro-IL-1β/IL-18 and other components of the inflammasome; the second signal results in the assembly of the NLRP3 inflammasome, caspase 1 activation, and IL-1β/IL-18 secretion.

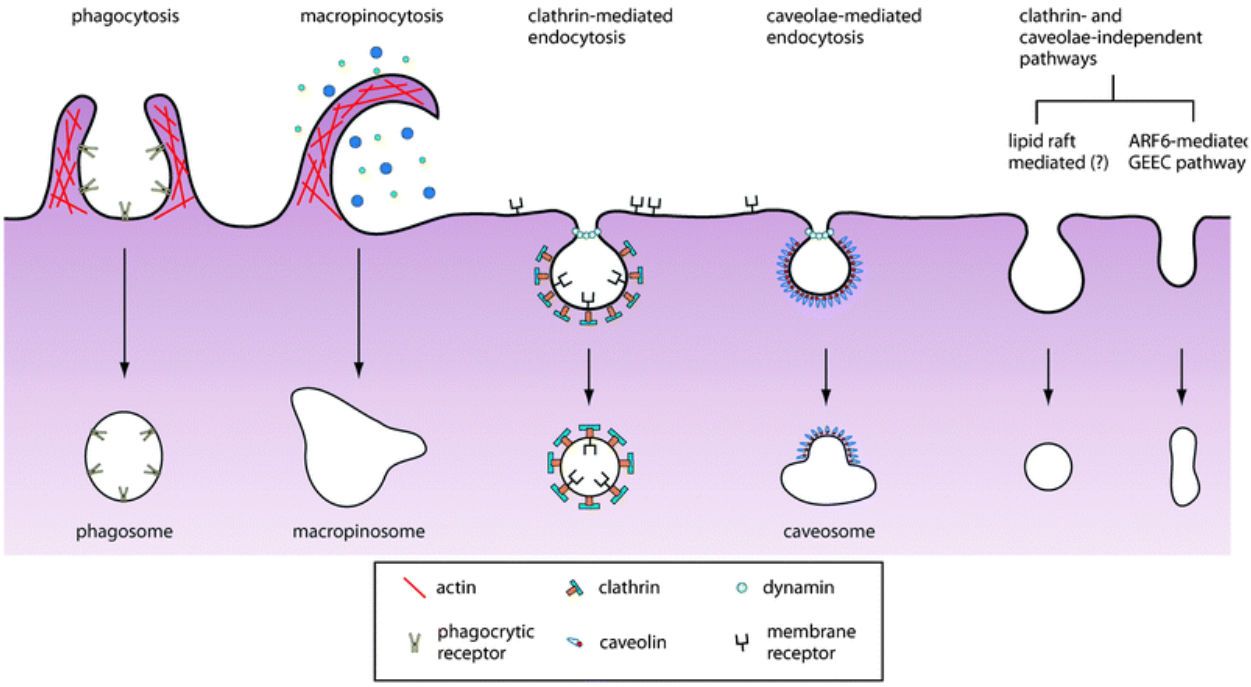

Figure 1. 3. Pathways of entry into the cell

An increasing number of endocytic pathways are being defined, each mechanistically distinct and highly regulated at the molecular level. These pathways facilitate cellular signaling and cargo transport. Controlling the route of nanoparticle uptake is important for both mediating their intracellular fate as well as their biological response.

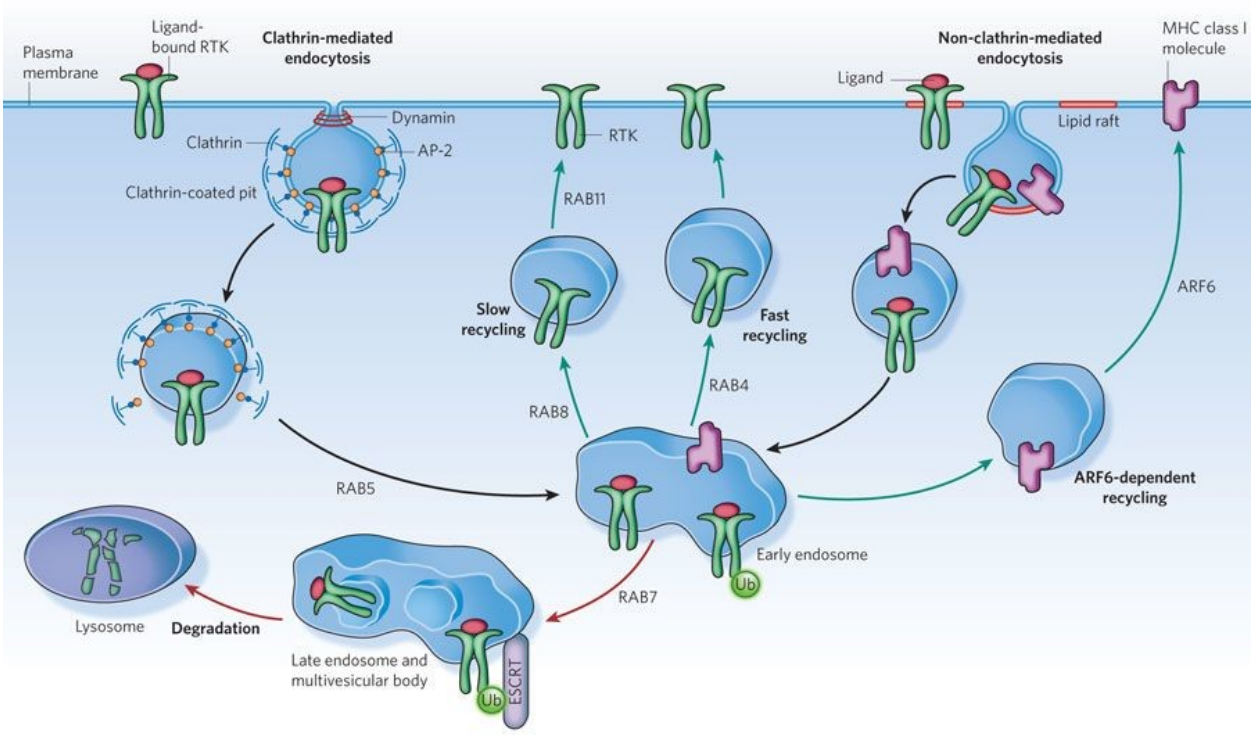

Figure 1. 4. Endosomal trafficking system

Signalling receptors (in this example receptor tyrosine kinases (RTKs)) are mainly internalized through clathrin-mediated endocytosis (left). In this pathway of endocytosis, ligand binding accelerates the recruitment of receptors to clathrin (present in clathrin-coated pits) through adaptors, such as AP-2 or β-arrestins. Clathrin then polymerizes, and this drives the invagination of the pit, which is eventually released into the cytoplasm through the action of the GTPase dynamin. This process seems simple but is clearly highly complex given that more than 50 different proteins can be found in clathrin-coated pits. There are many forms of non-clathrin-mediated endocytosis (right), which, in some cases, depends on plasma-membrane microdomains enriched in particular lipids (known as lipid rafts). Non-clathrin-mediated endocytosis is still poorly understood at the molecular level, and the term encompasses many heterogeneous mechanisms. After internalization, by either clathrin-mediated endocytosis or non-clathrin-mediated endocytosis, receptors are routed to early endosomes. Trafficking in the endosomal compartment is controlled by small GTP-binding proteins of the RAB and ARF (ADP-ribosylation factor) families (some of which are

(legend continued on next page)

indicated). From the early endosome, cargo is either recycled to the plasma membrane (green arrows) or degraded (red arrows). Cargo can be recycled through a fast recycling route (which depends on RAB4) or a slow recycling route (which depends on the combined action of RAB8 and RAB11). In addition, proteins that have been internalized by non-clathrin-mediated endocytosis, such as major histocompatibility complex (MHC) class I molecules, can be recycled to the plasma membrane through ARF6-dependent pathways. Cargo can also be trafficked through a RAB7-dependent, degradative route, through late endosomes and multivesicular bodies, and then lysosomes. A crucial signal in this route is ubiquitylation of the receptors. Ubiquitylated receptors are recognized by a series of ubiquitin-binding protein complexes: HRS–STAM (also known as ESCRT-0), and endosomal sorting complex required for transport I (ESCRT-I), ESCRT-II and ESCRT-III.

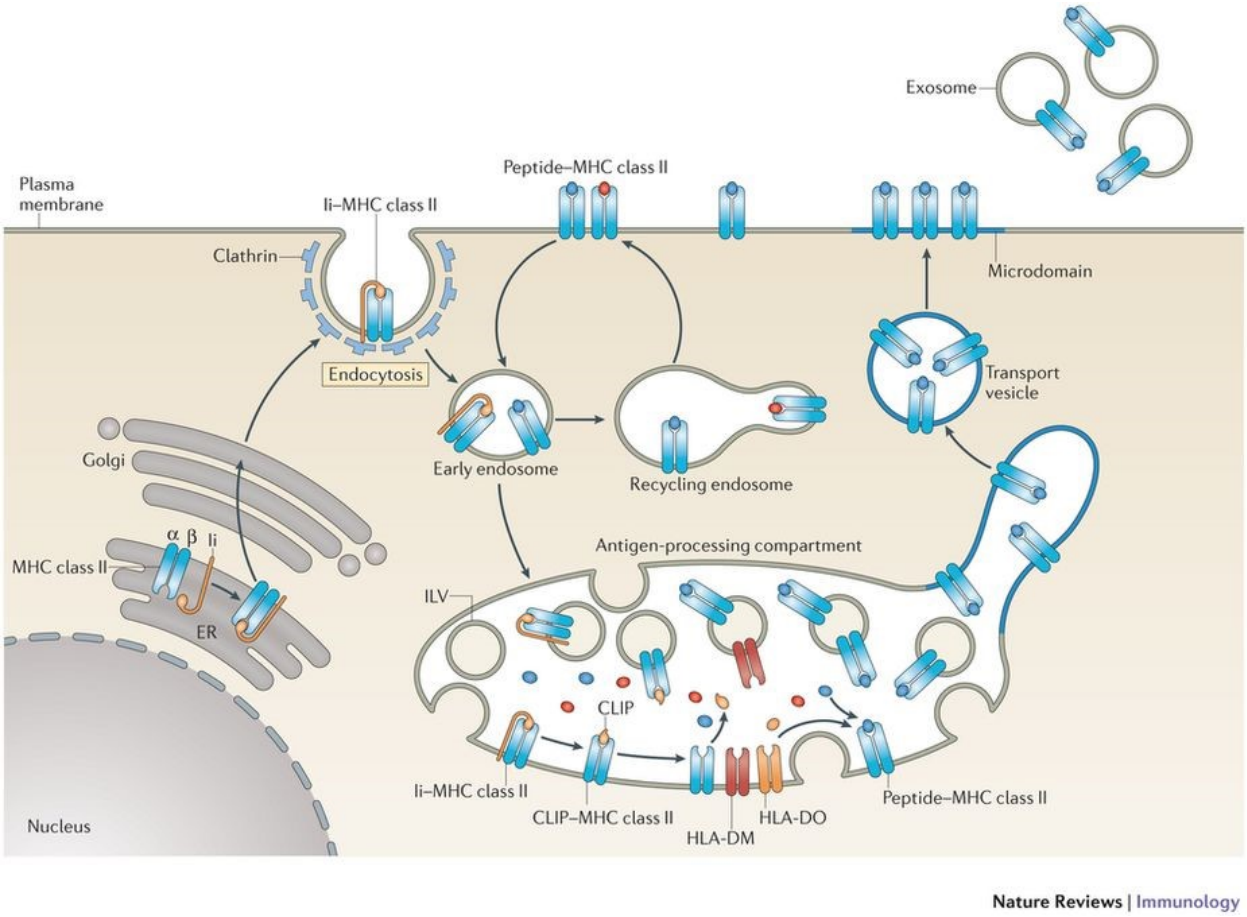

Figure 1. 5. Generation of peptide–MHC class II complexes in antigen-presenting cells

MHC class II αβ dimers associate with the invariant chain (Ii) in the endoplasmic reticulum (ER), traffic through the Golgi apparatus and are delivered to the plasma membrane. Ii–MHC class II complexes are internalized by clathrin-mediated endocytosis and traffic to multivesicular antigen-processing compartments. Some of these complexes are sorted into the intraluminal vesicles (ILVs) of multivesicular bodies (MVBs), in which sequential Ii proteolysis leads to the generation of a fragment of Ii, termed class II-associated invariant chain peptide (CLIP), which remains in the peptide-binding groove of MHC class II. CLIP is removed from CLIP–MHC class II complexes by the enzyme HLA-DM, which is present in the MVB internal and limiting membranes, thereby facilitating peptide binding onto nascent MHC class II. The activity of HLA-DM is regulated by HLA-DO, but the mechanism of regulation remains unknown. ILV-associated peptide–MHC class II somehow associates with the MVB limiting membrane, and endosomal–lysosomal tubules directed towards the plasma membrane either directly fuse or give

(legend continued on next page)

rise to transport vesicles that fuse with the plasma membrane. MVB membranes are rich in the lipids that constitute lipid raft membrane microdomains, and fusion of peptide–MHC class II from MVB-derived membranes with the plasma membrane leads to the deposition of lipid raft-associated peptide–MHC class II directly into the plasma membrane. In circumstances in which an entire MVB fuses with the plasma membrane, the ILVs of MVBs are released from the APC in the form of exosomes. Surface expressed peptide–MHC class II can be internalized through a clathrin-independent endocytosis pathway and can be targeted for lysosomal degradation or can recycle back to the plasma membrane.

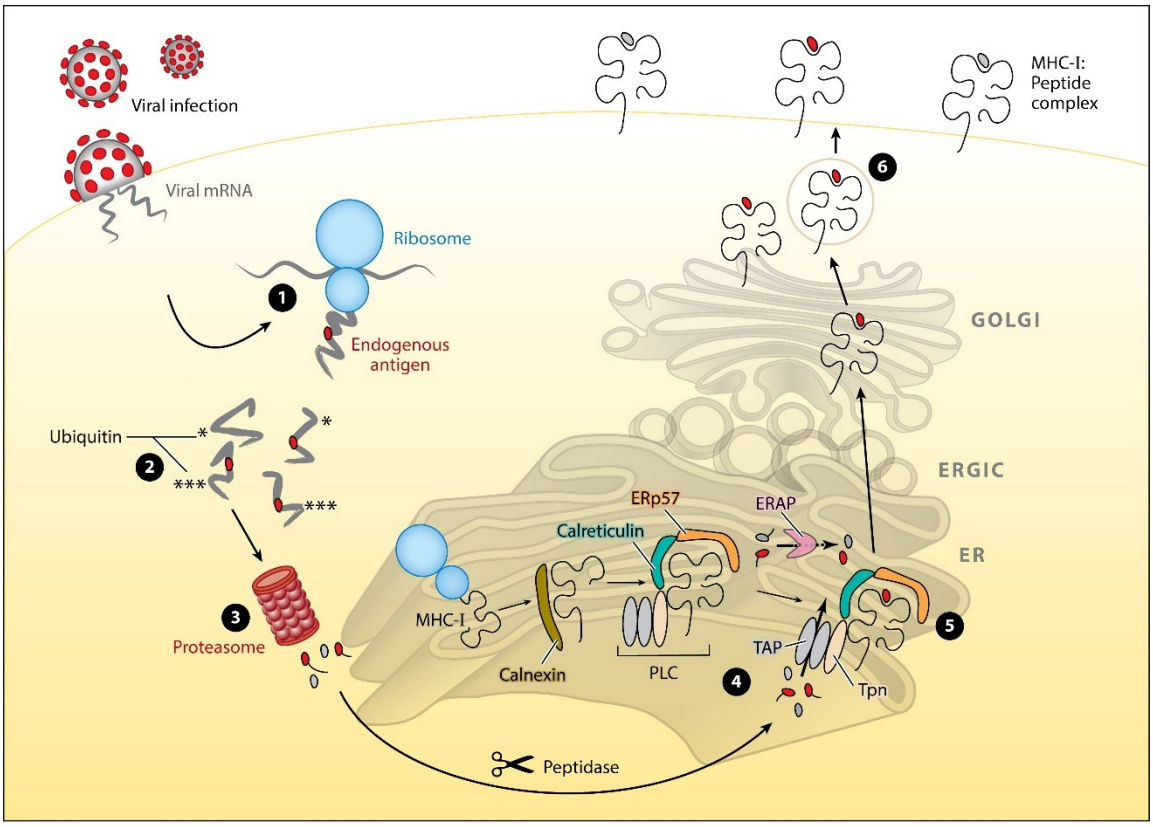

Cruz FM, et al. 2017.
Annu. Rev. Immunol. 35:149–76

Figure 1. 6. Classical class I antigen presentation.

The classical pathway monitors the self-proteins and foreign proteins that are synthesized by cells. Expressed proteins destined for degradation are **(2)** conjugated with ubiquitin and then **(3)** degraded by proteasomes. Long peptides undergo trimming by cytosolic peptidases. **(4)** A fraction of peptides are translocated into the lumen of the ER via TAP. Some long peptides undergo trimming in the ER by ERAP. Newly synthesized MHC-I molecules associate first with the chaperone calnexin and then, via Tpn, with TAP in the PLC. After **(5)** binding TAP-transported peptide, the MHC-I:peptide complexes are **(6)** transported through the secretory pathway to the plasma membrane, where they are presented to CD8+ cytotoxic T cells. Abbreviations: ER, endoplasmic reticulum; ERAP, ER aminopeptidase; ERGIC, ER-Golgi intermediate compartment; PLC, peptide-loading complex; TAP, transporter associated with antigen processing; Tpn, tapasin.

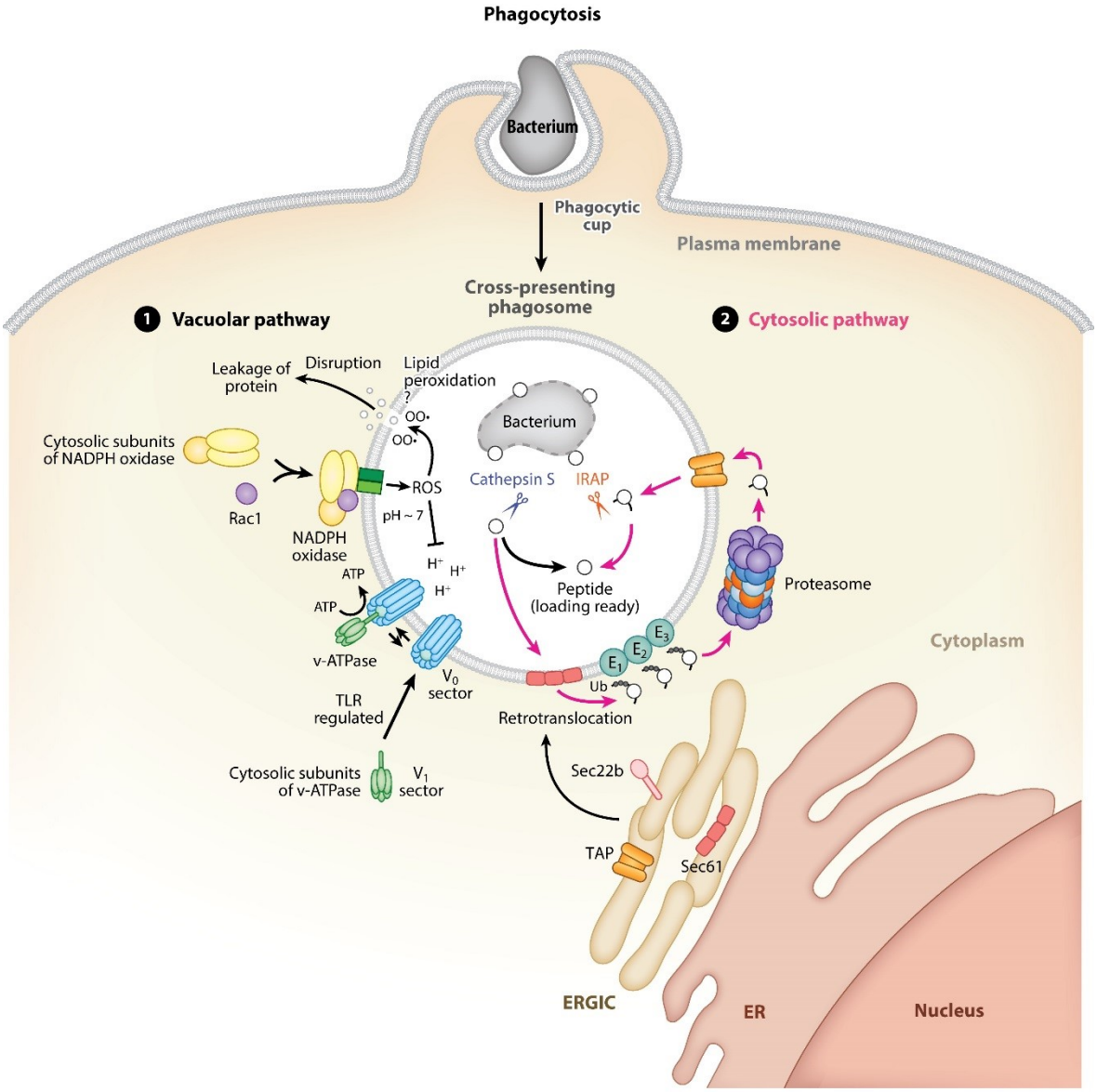

Blander JM. 2018. *Annu. Rev. Immunol.* 36:717–53

Figure 1. 7. The vacuolar and cytosolic pathways of generating peptides for cross-presentation

Shown are subcellular events within the first 1-4 hours following phagocytosis of bacteria by dendritic cells. Experimental evidence also supports the occurrence of similar events around endosomes or parasitophorous vacuoles. The nascent phagosome carrying an internalized bacterium matures into a cross-presentation compartment made possible through the activity of several players within both the vacuolar and the cytosolic pathways. **(1)** The vacuolar pathway of

(legend continued on next page)

cross-presentation contributes to the degradation of proteins, derived from the internalized bacterium in this case, through the activity of vacuolar proteases, most prominent among which is cathepsin S because of its ability to be functional at a pH that is relatively alkaline compared to the pH optima ~4.5-5 for the majority of vacuolar proteases. In dendritic cells, a pH ~7-7.3, most conducive to cross-presentation, is maintained for the first few hours through phagosomal reactive oxygen species (ROS) generated by the activity of the NADPH oxidase. A functional NADPH oxidase involves the assembly of its cytosolic subunits and the small GTPase Rac1 with its phagosome membrane integral subunits. Resultant ROS neutralize the acidic protons (H^+) generated through the activity of the v-ATPase, which in turn is assembled by recruitment of its cytosolic V1 sector subunits to its phagosome membrane integral V0 sector subunits, and in a TLR-regulated manner. Counteraction of the v-ATPase by the NADPH oxidase serves to temporarily maintain a neutral phagosomal pH to preserve proteins from excessive degradation by vacuolar proteases and promote cross-presentation. ROS lead to lipid peroxidation (indicated as OO·) and disruption of endosomal membranes, and they may also have the same effects on phagosomal membranes (*question mark*). **(2)** The cytosolic pathway of cross-presentation relies on recruitment of various players from the endoplasmic reticulum (ER)-Golgi intermediate compartment (ERGIC) to phagosomes through the pairing of the ER soluble *N*-ethylmaleimide-sensitive factor attachment receptor (SNARE) Sec22b with syntaxin 4 (not shown) on phagosomes. In this manner, the retrotranslocon Sec61 and the transporter associated with antigen processing (TAP) present in the ERGIC are recruited to the cross-presenting phagosome and function collaboratively to mediate the exit and reentry, respectively, of polypeptides derived here from the internalized bacterium. Phagosomal Sec61 transports peptides through retrotranslocation to the cytoplasmic side of phagosomes, where they have access to the ubiquitin (E1, E2, E3 ligases) and proteasome complex assembled on the cytoplasmic side of phagosomes. This compartmentalization along the phagosomal membrane presumably facilitates translocation of resultant proteasome-degraded peptides back into phagosomes via TAP that had been recruited to phagosomes from the ERGIC. Inside phagosomes, the insulin-regulated aminopeptidase (IRAP) is a trimming aminopeptidase that preferentially acts on those peptides that have been subjected to cytosolic degradation by the proteasome. The combined results of the

(legend continued on next page)

vacuolar and cytosolic pathways contribute to a diverse repertoire of peptides that are available for binding to MHC-I molecules during cross-presentation. For simplicity, MHC-I molecules are not depicted in this figure.

Chapter 2: Plant-made virus-like particles bearing influenza hemagglutinin (HA) recapitulate early interactions of native influenza virions with human monocytes/macrophages

Alexander I. Makarkov [a,b], Sabrina Chierzi [b,d], Stéphane Pillet [b,c], Keith K. Murai [d], Nathalie Landry [c], Brian J. Ward [b]

[a] Division of Experimental Medicine, Department of Medicine, McGill University, 1001 Décarie Boul., Montréal, Québec H4A 3J1, Canada
[b] Research Institute of McGill University Health Centre, Glen Site, 1001 Décarie Boul., Montréal, Québec H4A 3J1, Canada
[c] Medicago Inc., 1020 Route de l'Église, Bureau 600, Québec, Québec G1V 3V9, Canada
[d] Research Institute of McGill University Health Centre, Montreal General Hospital, 1650 Cedar Avenue, Montréal, Québec H3G 1A4, Canada

Adapted from *Vaccine*, with permission from Elsevier, Copyright © 2017 Elsevier Ltd.
Makarkov AI, Chierzi S, Pillet S, Murai KK, Landry N, Ward BJ. Plant-made virus-like particles bearing influenza hemagglutinin (HA) recapitulate early interactions of native influenza virions with human monocytes/macrophages. Vaccine. 2017;35(35 Pt B):4629-36.

2.1. PREFACE

In Chapter 1 of this thesis, we described the structure, composition, and the mechanisms of formation of the plant-derived VLP. The VLP are biological nanoparticles 50 to 150 nm in diameter, mostly discoid or spheroid-shaped, enveloped, with HA trimers integrated into the lipid bilayer and organized in an ordered array. These VLP bud from the plasma membrane of plant cells at the lipid rafts; host proteins are mostly excluded from the membrane budding area during the process of VLP formation. Thus, except for the lack of genetic material, plant-derived VLP are very similar to the native influenza virions. These similarities prompted us to study the interactions between the hemagglutinin (HA)-bearing plant-derived VLP and human antigen presenting cells (APC) that can potentially shed the light on the immunogenicity of the nanoparticles. The following chapter describes the mechanisms and kinetics of VLP binding to

the surface of monocytoid/macrophage cells, their internalization and trafficking towards acidified endosomal compartments, fusion of VLP envelopes with endosomal membranes of the host cells, and HA processing and presentation to autologous lymphoid cells. We also compare two types of VLP bearing either H1 (based on the HA sequence of A/California/07/2009 (H1N1) virus) or H5 (based on the HA sequence of A/Indonesia/05/2005 (H5N1) proteins.

2.2. ABSTRACT

Introduction: Plant-made virus-like particles (VLP) bearing influenza virus hemagglutinins (HA) are novel vaccine candidates that induce cross-reactive humoral and poly-functional T cell responses. To better understand the mechanisms that underlie this broad immunogenicity we studied early interactions of VLPs bearing either H1 (A/California/07/2009 (H1N1)) or H5 (A/Indonesia/05/2005 (H5N1)) with a human monocytoid cell line (U-937 cells) and human monocyte-derived macrophages (MDMs) as model antigen-presenting cells (APC).

Methods and results: Using *Vibrio cholerae* sialidase and lectins that target α2,6- (*Sambucus nigra* lectin) or α2,3-linked sialic acids (*Maackia amurensis* lectin I), we demonstrated that VLPs bind to these APCs in a sialic acid-dependent manner. Using lysosomal markers and DiD-labelled VLPs, we found that attachment to the cell surface leads to internalization, trafficking to acidic cell compartments and fusion of the VLP lipid envelope with endosomal membranes. Incubation of MDMs with H1- but not H5-VLPs induced proliferation of autologous peripheral blood mononuclear cells suggesting antigen processing and stimulation of a memory T cell response.

Conclusions: Plant-made VLPs bearing influenza HA not only mimic the structure of influenza virions to some degree but also recapitulate key features of the initial virus-APC interaction. These observations may help to explain the balanced humoral and cellular responses to plant-made VLP vaccines.

2.3. INTRODUCTION

Influenza viruses cause significant worldwide morbidity and mortality every year (1,2). Vaccines are the best tools available to prevent the disease burden (3); however, vaccine efficacy (VE) can vary significantly between years, target populations and strains (4,5). A vaccine mismatch in 2014–15 influenza season resulted in a VE of 18% for H3N2-caused diseases, and

the influenza-associated hospitalization rate among people ≥65 years of age was the highest since the beginning of tracking those data in 2005 (6). Novel vaccines are needed that have improved VE in the most vulnerable populations, elicit both humoral and cell-mediated immune responses and provide greater cross-protection (7,8).

Among the most promising new approaches are virus-like particle (VLP) vaccines. VLPs are nanoparticles with one or more viral components that mimic wild-type virus morphology but lack viral genetic material. Antigens on VLPs are typically in their native conformation without either mutations introduced when live viruses are grown in eggs to make vaccine strains or alterations due to inactivating agents or detergents treatment (9). Antigenic proteins on VLPs are presented in an immunologically-relevant array, they can be protected from degradation and are often delivered more efficiently to antigen-presenting cells (APCs) such as macrophages and dendritic cells (10).

Several influenza VLP vaccines produced using different recombinant platforms are in various stages of pre-clinical and clinical development (11). VLPs can be produced efficiently in both insect cells and plants that express only the influenza hemagglutinin (HA) (12,13). Although both platforms have advantages over egg-based production, the approach based on Agrobacterium-mediated transient expression in *Nicotiana benthamiana* is increasingly recognized as a rapid, flexible and cost-effective way to produce highly immunogenic vaccines (14). Indeed, such plant-made VLPs bearing different HAs have recently been shown to elicit strong humoral and cell-mediated immune responses that are cross-reactive in both pre-clinical and clinical studies (12,15–17). The mechanisms that underlie the unusual immunogenicity of these candidate vaccines are not yet fully understood.

In this work, we demonstrate that plant-made VLPs bearing influenza HA rapidly interact with monocyte/macrophage cells in a sialic acid-dependent manner. Attachment of the VLPs to the cell surface leads to their internalization and fusion of VLP lipid components with endosomal membranes. Exposure of human monocyte-derived macrophages (MDMs) to influenza HA delivered by the plant-made H1-VLPs stimulates a lymphoproliferation response in autologous peripheral blood mononuclear cells (PBMCs), suggesting competent antigen processing and presentation in support of a recall response. The absence of a lymphoproliferation following H5-VLP stimulation in vitro is likely attributable to lack of prior exposure of the blood donors to H5 antigens.

2.4. MATERIALS AND METHODS

2.4.1. Plant-made VLPs bearing influenza Hemagglutinins and empty vesicles

The VLPs produced in *N. benthamiana* were kindly provided by Medicago Inc. (Quebec, QC) and were manufactured as previously described (15,18). The influenza HA proteins were based on the sequences of A/California/07/2009 H1N1 for H1-VLPs or A/Indonesia/05/2005 H5N1 for H5-VLPs. Empty vesicles (Evs) were generated from homogenized *N. benthamiana* cell membranes. The Evs have a general structure and lipid profile similar to that of the HA-bearing VLPs (data not shown). For the purpose of confocal microscopy and dequenching experiments, VLPs or Evs were stained with the fluorescent lipophilic carbocyanine dye, DiD (Thermo Fisher Scientific, Eugene, OR) at a concentration of 20 µg/mL for 30 min at room temperature (RT), and then purified from free dye using gel filtration columns (PD MiniTrap G-25, GE Healthcare, Buckinghamshire, UK). Influenza A (H1N1) 2009 monovalent vaccine (Sanofi Pasteur Inc, Swiftwater, PA) and recombinant H1 and H5 proteins produced in human embryonic kidney 293 cells (Immune Technology, New York, NY) were used as comparators in internalization and antigen processing experiments.

2.4.2. Cells and immunostaining

Most experiments were performed using U-937 cells, a human histiocytic lymphoma cell line (ATCC CRL-1593.2), that were maintained in RPMI-1640 Medium supplemented with 10% fetal bovine serum (FBS), 50 IU/mL penicillin, 50 µg/mL streptomycin and 10 mM HEPES (all from Wisent, Saint-Jean-Baptiste, QC). Some key experiments were performed using MDMs differentiated from human PBMCs isolated from healthy donors between the ages of 23–45. All studies with human cells were carried out with approval from the Research Ethics Committee of the McGill University Health Centre. Written informed consent was obtained from all donors prior to blood drawing. PBMCs were separated from whole blood samples by differential density gradient centrifugation. The monocyte $CD14^+$ cell fraction was isolated by negative selection using magnetic microbeads according to the manufacturer's instructions (EasySep Human Monocyte Enrichment Kit, STEMCELL, Vancouver, BC). Monocytes at 10^6 cells/mL were cultured in RPMI-1640 supplemented with 10% FBS and 20 ng/mL recombinant human macrophage colony-stimulating factor (Gibco, Frederick, MD) in a 5% CO_2 incubator at 37°C

for 7 days; at day 3 and day 6, half of the medium was changed. To verify the purity of MDMs, cells were stained for CD68 or Iba-1 markers overnight using mouse monoclonal anti-human CD68 antibody, dilution 1:100 (clone Y1/82 A, BioLegend, San Diego, CA), or polyclonal rabbit anti-human Iba-1 antibody, dilution 1:500 (Thermo Fisher Scientific, Rockford, IL), respectively. HA immunostaining was performed with mouse monoclonal anti-HA antibody (clone IVC102, Meridian Life Science, Memphis, TN), dilution 1:200.

2.4.3. Confocal microscopy

VLPs, influenza A (H1N1) 2009 monovalent vaccine or recombinant HA were added to cultures in serum-free RPMI-1640 at a final concentration of 15.0 µg/mL (by HA content). In time-lapse experiments, VLPs were labelled with DiD and images were acquired at 37°C at one-minute interval up to 60 min. To visualize acidic cell compartments, cells were pre-loaded with LysoSensor Green DND-189 (1 µM, Life Technologies Corporation, Carlsbad, CA). In some experiments, live cells were treated with *Vibrio cholerae* sialidase (Roche, Mannheim, Germany) 250 mU/mL in serum-free RPMI-1640 for two hours, washed and exposed to DiD-labelled VLPs. In parallel experiments, cells were fixed with 3.7% formaldehyde in PBS for 30 min at 4°C, treated with sialidase 250 mU/mL in acetate buffer (pH 5.5) overnight and then exposed to DiD-labelled H5-VLPs. Sialidase-treated live cells were stained with 20 µg/mL fluorescein-labelled *Maackia amurensis* Lectin I (MAL-I: preferentially targets α2,3-linked sialic acids) or *Sambucus nigra* Lectin (SNA: preferentially targets α2,6-linked sialic acids) (both from Vector Laboratories, Burlingame, CA) for 30 min at 4°C. A laser scanning confocal microscope (Zeiss LSM780, RI-MUHC Molecular Imaging Core Facility, Montreal, QC) was used in all imaging experiments. Fluorescence intensity was quantified using ImageJ software.

2.4.4. Fluorescence dequenching fusion assay

Fusion assays were based on fluorescence dequenching of DiD-labelled VLPs upon interaction with unlabelled cell membrane. A volume of 200 µL of VLPs (HA concentration 90.0 µg/mL) was added to 5×10^6 U-937 cells in 1000 µL of serum-free RPMI-1640 (final HA concentration 15.0 µg/mL); sample was kept at 4°C for one hour to permit VLP attachment but not entry into the cells, washed with ice-cold serum-free RPMI-1640 twice and re-suspended in 1000 µL of ice-cold RPMI-1640 supplemented with 10% FBS. Dynasore hydrate (Sigma-

Aldrich) was applied to some wells at a concentration 50 μM to prevent dynamin-dependent endocytosis of VLPs (19). Cells were plated in 96-well black flat-bottom plates (Corning, Kennebunk, ME), 100 μL per well, in triplicate. The plates were placed into a pre-warmed (37°C) spectrophotometer (Infinite 200 PRO, Tecan, Männedorf, Switzerland), and DiD fluorescence was measured at 15-min intervals over two hours. Fusion efficiency, reported as a %, was determined following addition of Triton X-100 to each well (final concentration 1%) to obtain full DiD dequenching.

2.4.5. Autologous PBMCs proliferation

MDMs were detached from the plastic plate surface using Accutase Cell Detachment Solution (BioLegend, Dan Diego, CA) and plated on 96-well black (Corning, Kennebunk, ME) or transparent (Corning, Corning, NY) flat bottom plates, 2×10^4 cells per well. The next day, MDMs in triplicate wells were exposed to H1 or H5 in the form of VLPs (Medicago Inc, Quebec, QC) or as recombinant proteins (Immune Technology, New York, NY) at concentrations 15.0, 5.0, 1.0 or 0.1 μg/mL (based on HA content) for two hours, washed and co-cultured for 5 days with freshly-isolated autologous PBMCs, 2×10^5 cells per well. Proliferation was determined by measuring 5-bromo-2′-deoxyuridine (BrdU) incorporation using chemiluminescent or colorimetric ELISA kits according to the manufacturer's instructions (Roche, Mannheim, Germany).

2.4.6. Statistical analysis

Statistical analysis was performed using PASW Statistics 18 software. All experiments were analysed by Student's t-test for independent or related samples. P values <0.05 were considered statistically significant.

2.5. RESULTS

2.5.1. VLP binding to U-937 cells and human macrophages

Initially we verified that labelling of H1- or H5-VLP preparations (normalized by HA concentration) with DiD resulted in an equal accumulation of the dye in the particles (Suppl. Fig. 2.1). Time-lapse imaging of DiD-labelled VLPs revealed rapid adherence of the particles to U-

937 cells. Although individual DiD-labelled particles were too small to be visualized by confocal microscopy, H5-VLP binding to the cell surface (possibly small clusters of VLPs) was observed during the first minutes of exposure, and increased rapidly to maximum fluorescence between 30 and 45 min. H1-VLPs demonstrated a similar kinetics of association with U-937 cells but the interaction was less intense (Fig. 2.1A). At 30 min, the intensity of DiD fluorescence of the H5-VLP-treated U-937 cells was three-fold higher than cells exposed to H1-VLPs at similar concentrations (Fig. 2.1B). VLPs also rapidly associated with the cell surface of human MDMs, and peak fluorescence signal was two-fold higher with H5-VLPs than H1-VLPs (Fig. 2.1C). Binding of VLPs to the surface of U-937 cells was energy-independent. A one-hour exposure to H5-VLPs at 4°C resulted in prominent adherence of the particles without entry into the cells (Fig. 2.1D). Moreover, formaldehyde fixation of the U-937 cells prior to VLP exposure did not prevent VLP binding (Fig. 2.1F). Sialidase treatment effectively removed both α2,3- and α2,6-linked sialic acids from the surface of living U-937 cells as shown by reduced binding of MAL-I and SNA lectins, respectively (Suppl. Fig. 2.2A and B). H5-VLP binding to sialidase-treated live or fixed U-937 cells was reduced ∼90%, compared to non-treated cells (Fig. 2.1E and F). In parallel experiments, we observed a dramatic reduction of both H1- and H5-VLPs binding to sialidase-treated live MDMs (data not shown). Of note, the fluorescence intensity of MDMs exposed to DiD-labelled Evs (normalized by lipid concentration) was ∼5-fold less than H1-VLPs and ∼10-fold less than H5-VLPs (data not shown), suggesting that HA plays a role in the capacity of VLPs to bind to APCs. In summary, the plant-made VLPs bearing either H1 or H5 bind to the surface of both a monocyte cell line and MDMs in an energy-independent manner. This association is mediated by sialic acid residues present on the cell surface.

2.5.2. Internalization of VLPs

Surface binding of VLPs was followed by their internalization at 37°C. Confocal imaging unambiguously demonstrated the intracellular localization of DiD-fluorescent particles after one hour of H5-VLP exposure (Fig. 2.1D). Using a standardized dose of HA, fluorescence intensity after HA immunostaining of MDMs exposed to H1-VLPs was ∼5-fold greater than in those exposed to monovalent split virion H1N1 vaccine and ∼3-fold greater compared to recombinant H1 (data now shown). These observations suggest that HA delivery in a form of VLPs facilitates antigen uptake by APCs. Visualization of the acidic intracellular compartments showed good co-

localization of LysoSensor Green and DiD-labelled H1- or H5-VLPs in U-937 cells and MDMs (Fig. 2.2A–C). We next studied fusion of the plant-made VLPs with cell membranes by monitoring dequenching of DiD. We observed a rapid increase of DiD fluorescence after 10–15 min (Fig. 2.2D) of incubation. Fluorescence rose to a plateau phase at ~90 min that was nearly 60-fold higher than background levels. The kinetics of DiD fluorescence increase suggested that the VLPs were fusing with endosomal rather than cytoplasmic membranes of the target cells (20,21). To verify this observation, we performed dequenching experiments in the presence of Dynasore, an inhibitor of dynamin-dependent endocytosis (22). Dynasore completely blocked DiD dequenching, confirming that VLPs endocytosis preceded their fusion with endosomal membranes. In parallel experiments, exposure of MDMs to either H1- or H5-VLPs resulted in DiD dequenching that was substantially inhibited in the presence of Dynasore (data not shown). In summary, our data suggest that VLPs attach to the surface of monocyte-macrophage cells via sialic acid residues, undergo internalization in an energy-dependent fashion and move, at least in part, to acidic cell compartments such as late endosomes. Internalization of VLPs is then followed by fusion of the particles' lipid envelope with endosomal membranes.

2.5.3. Processing of VLP-delivered HA by MDMs and antigen presentation to PBMCs

To determine the fate of endocytosed VLPs – i.e. protein degradation versus processing and antigen presentation – we exposed human MDMs to plant-made VLPs bearing either H1 or H5. All donors had been vaccinated against and possibly naturally exposed to H1N1 influenza and none had any known exposure to H5N1 antigens. Purity of the obtained MDM populations was verified by staining for CD68 and Iba-1 (Suppl. Fig. 2.3A and B), and exceeded 98%. The duration of MDM exposure to VLPs (2 h) was chosen based on our imaging observations (i.e. kinetics of internalization) and the DiD dequenching dynamics. We found that BrdU incorporation by autologous PBMCs co-cultured with MDMs exposed to either H1-VLPs or recombinant H1 was significantly greater than in the control wells (Fig. 2.3). Lymphoproliferation in response to H1-VLP-exposed MDMs was concentration-dependent, reaching a maximum effect at the highest tested HA concentration (15.0 μg/mL). At all but the lowest HA concentration, lymphoproliferation was greater in the PBMC co-cultured with MDM exposed to H1-VLP compared to recombinant H1 although none of the individual comparisons reached statistical significance. In contrast, there was no increase in BrdU incorporation by

PBMCs co-cultured with MDMs stimulated with H5-VLP or recombinant H5. In conclusion, the MDMs isolated from healthy donors appeared to act as antigen-presenting cells rather than phagocytes. At least some of the internalized HA was processed by MDMs and presented to autologous PBMCs that recognized H1-derived antigenic peptides.

2.6. DISCUSSION

Monocytes migrating into the lungs and lung-resident macrophages are major contributors to the first-line defence against influenza virus infection (23). These cells are key innate immune effectors and play an important role in antigen processing and presentation for adaptive responses (24,25), particularly for recall antigens (26). The plant-made VLPs used in the current studies are similar in size to native influenza virions (12), they display influenza HA trimers in an immunologically-relevant array (18) and induce pro-inflammatory cytokine production by human monocytes in vitro (27). In a mouse model of footpad immunization, they have recently been shown to traffic rapidly to regional lymph nodes where they preferentially interact with B cells and $CD11c^+$ APCs (28), unpublished data).

In this work, we studied VLP binding to the cell surface, internalization and intracellular localization, as well as antigen presentation; all key steps in the interaction of APCs with influenza viruses and vaccines. These studies took advantage of the convenience of U-937 cells and verified key observations in human MDMs differentiated from primary monocytes.

The initial interactions of influenza virions with target cells are mediated by HA binding to sialic acid residues on the cell surface. After binding to the plasma membrane, influenza virions are thought to enter the cell by endocytosis. In the endosome pathway, low pH triggers conformational changes in the HA molecules that facilitate fusion of the viral envelope and cellular membranes, and release of the viral genome and viral proteins into the cytosol. Both infection of APCs as well as endocytosis of viral antigenic material likely contribute to influenza antigen processing and presentation leading to stimulation of the adaptive immune responses (29).

Highly pathogenic avian strains such as H5N1 (A/Indonesia/05/2005) preferentially bind to sialic acids attached to galactose via α2,3 linkage that are found on epithelial cells in the human lower respiratory tract. In contrast, seasonal strains like H1N1 (A/California/07/2009) preferentially bind to sialic acids attached to galactose by α2,6 linkage that predominate on upper

respiratory tract epithelial cells (30). Unlike respiratory epithelial cells, human peripheral blood monocytes (31), MDMs and alveolar macrophages (32) have both α2,3- and α2,6-linked sialic acids, and sialylation patterns can change with cell activation or differentiation (31). Based upon staining with MAL-I and SNA lectins respectively, we found both α2,3- and α2,6-linked sialic acids on the surface of U-937 cells. Cleavage of sialic acid residues with V. cholerae sialidase markedly reduced MAL-I and SNA staining so it was no surprise that both the H1- and H5-VLPs bound to the surface of U-937 cells and human MDMs. MAL lectins also interact with glycans containing the SO4-3-Galβ group which are more resistant to sialidases. This characteristic may explain the lesser effect of sialidase treatment on MAL-I binding compared to SNA (33).

It is more difficult to understand the apparently greater binding and internalization of H5-VLPs compared to the H1-VLPs (Fig. 2.1A –C) or to reconcile these observations with the prior demonstration of greater activation of human monocytes by H1-VLPs compared to H5-VLPs (27) and the generally stronger humoral and cellular responses elicited by the former in both animal models and human trials (12,15,16). Based on cryo-electron microscopy, plant-made H1- and H5-VLPs have similar numbers of HA trimers per particle (Dr. Isabelle Rouiller, personal communication). However, immunofluorescence is only semi-quantitative, and it is possible that surface expression of α2,3-linked sialic acids is greater than α2,6 on these monocytic cells (31). It is also possible that α2,3-linked sialic acids cooperate with other surface molecules that facilitate binding and internalization (34,35) but that lead to different intracellular handling. Studies to better understand the nature of H1- and H5-VLP binding to human monocytes and MDMs and the implications of this first interaction for VLP internalization and subsequent processing are currently underway.

To what degree monocyte/macrophages participate in supporting adaptive immune responses against influenza virus antigens during infection or following vaccination is currently unknown. However, recent evidence suggests that these cells may play a much larger role than previously thought (36). In our experiments, a two-hour exposure of MDMs from young adults to the H1- but not the H5-VLPs led to active proliferation (BrdU incorporation) of autologous lymphocytes in vitro. Since this work was conducted between 2015 and 2016, it is virtually certain that most of the young adults from whom PBMCs were isolated had ‘seen’ H1N1 (A/California/07/2009) antigens through infection, vaccination or both but had not had previous exposure to H5 antigens. This difference in prior antigen exposure likely explains the in vitro

autologous lymphoproliferative response to H1- but not H5-VLP despite similar handling by the MDMs. Visualization of acidic cell compartments with LysoSensor Green demonstrated co-localization with DiD-labelled VLPs, suggesting that both H1- and H5-VLPs moved, at least in part, into late endosomes where the HA was processed for presentation (37).

Fusion of influenza viruses with cell membranes can be studied using dequenching assays. Many fluorophores, including lipophilic dyes like R18, DiD, DiO or DiI are self-quenching (38). When VLPs are stained with DiD, the concentration of the probe is high enough that efficient auto-quenching occurs. When the VLPs fuse with non-labelled cell membranes, the probe is diluted, leading to a rise in DiD fluorescence that is proportional to the degree of fusion, allowing both kinetic and quantitative measurements (38). The lag phase of the dequenching curve suggests that the lipid component of the VLPs fused with the endosomal rather than cytoplasmic cell membrane. The inhibitory effect of Dynasore on the H5-VLPs uptake by U-937 cells in dequenching experiments suggests that these particles are internalized through the dynamin-dependent endocytosis (22), and the absence of VLP internalization at 4°C argues for energy-dependent mechanisms. In this context, it is interesting that influenza-infected macrophages appear to be particularly good at promoting poly-functional $CD8^+$ T cell responses (39). $CD4^+$ T cell response to HA epitopes has been demonstrated following plant-made VLP vaccination (15,16). In future experiments, it will be of particular interest to include live influenza virus and split virion preparations to determine to what extent the plant-made VLPs are capable of activating defined pathogen-recognition pathways (26,40,41).

In summary, using imaging and functional immunological approaches, we have demonstrated that plant-made VLPs bearing influenza HA trimers not only mimic the structure of influenza virions (12,18), but also recapitulate key aspects of their early interactions with human monocyte/macrophages. Specifically, both H1- and H5-VLPs attach to sialic acid residues on the surface of these cells followed by internalization into the endosomal compartment where acidification and some degree of fusion of VLP and endosomal membranes occurs. We further demonstrated that the H1-VLPs stimulate a vigorous lymphoproliferative response in vitro suggesting that macrophage processing of the plant-made VLPs can support an adaptive recall response. Our findings show that, at least initially, monocytes/macrophages handle the plant-made VLPs bearing influenza HA proteins in a fashion similar to their handling

of living virions, suggesting a mechanism for the balanced humoral and cellular responses elicited by these new vaccines.

2.7. ACKNOWLEDGEMENTS

We thank members of collaborating laboratories (Aldridge and Rouiller groups at McGill University) for helpful discussions during planning of experiments and manuscript preparation. We thank the Molecular Imaging Platform of the Research Institute of the McGill University Health Centre and staff for services provided. Data included in this article were previously presented in part at the 1st Annual Immune Imaging Symposium, Rochester, New York, USA, November 2015, the 2016 Canadian Immunization Research Network Annual General Meeting, Toronto, Canada, May 2016, and the 6th Influenza Vaccines for the World conference, Lausanne, Switzerland, April 2017.

2.8. REFERENCES

1. Fischer WA, Gong M, Bhagwanjee S, Sevransky J. Global burden of influenza as a cause of cardiopulmonary morbidity and mortality. Global Heart. 2014;9:325–36.
2. Peasah SK, Azziz-Baumgartner E, Breese J, Meltzer MI, Widdowson MA. Influenza cost and cost-effectiveness studies globally - A review. Vaccine. 2013;31:5339–48.
3. World Health Organization. Fact sheet N 211, Influenza (Seasonal). March 2014. Available from: http://www.who.int/mediacentre/factsheets/fs211/en/
4. Ortiz JR, Neuzil KM, Rue TC, Zhou H, Shay DK, Cheng PY, et al. Population-based incidence estimates of influenza-associated respiratory failure hospitalizations, 2003 to 2009. American Journal of Respiratory and Critical Care Medicine. 2013;188:710–5.
5. Thompson WW, Shay DK, Weintraub E, Brammer L, Cox N, Anderson LJ, et al. Mortality Associated with Influenza and Respiratory Syncytial Virus in the United States. JAMA. 2003;289(2):179–86.
6. Berlanda Scorza F, Tsvetnitsky V, Donnelly JJ. Universal influenza vaccines: Shifting to better vaccines. Vaccine. 2016;34(26):2926–33.
7. Houser K, Subbarao K. Influenza vaccines: Challenges and solutions. Cell Host Microbe. 2015;17(3):295–300.
8. Subbarao K, Matsuoka Y. The prospects and challenges of universal vaccines for influenza. Trends in Microbiology. 2013;21:350–8.
9. Song J-M. Advances in novel influenza vaccines: a patent review. J Microbiol. 2016;54(6):403–12.
10. Kushnir N, Streatfield SJ, Yusibov V. Virus-like particles as a highly efficient vaccine platform: Diversity of targets and production systems and advances in clinical development. Vaccine. 2012;31:58–83.
11. Quan F-S, Lee Y-T, Kim K-H, Kim M-C, Kang S-M. Progress in developing virus-like particle influenza vaccines. Expert Rev Vaccines. 2016;15(10):1281–93.
12. D'Aoust MA, Lavoie PO, Couture MMJ, Trépanier S, Guay JM, Dargis M, et al. Influenza virus-like particles produced by transient expression in Nicotiana benthamiana induce a protective immune response against a lethal viral challenge in mice. Plant Biotechnol J. 2008;6(9):930–40.
13. Nerome K, Sugita S, Kuroda K, Hirose T, Matsuda S, Majima K, et al. The large-scale

production of an artificial influenza virus-like particle vaccine in silkworm pupae. Vaccine. 2015;33(1):117–25.

14. Marsian J, Lomonossoff GP. Molecular pharming-VLPs made in plants. Current Opinion in Biotechnology. 2016;37:201–6.
15. Landry N, Pillet S, Favre D, Poulin JF, Trépanier S, Yassine-Diab B, et al. Influenza virus-like particle vaccines made in Nicotiana benthamiana elicit durable, poly-functional and cross-reactive T cell responses to influenza HA antigens. Clin Immunol. 2014;154(2):164–77.
16. Pillet S, Aubin É, Trépanier S, Bussière D, Dargis M, Poulin JF, et al. A plant-derived quadrivalent virus like particle influenza vaccine induces cross-reactive antibody and T cell response in healthy adults. Clin Immunol. 2016;168:72–87.
17. Pillet S, Racine T, Nfon C, Di Lenardo TZ, Babiuk S, Ward BJ, et al. Plant-derived H7 VLP vaccine elicits protective immune response against H7N9 influenza virus in mice and ferrets. Vaccine. 2015;33(46):6282–9.
18. D'Aoust MA, Couture MMJ, Charland N, Trépanier S, Landry N, Ors F, et al. The production of hemagglutinin-based virus-like particles in plants: A rapid, efficient and safe response to pandemic influenza. Plant Biotechnology Journal. 2010;8:607–19.
19. Gillespie L, Roosendahl P, Ng WC, Brooks AG, Reading PC, Londrigan SL. Endocytic function is critical for influenza A virus infection via DC-SIGN and L-SIGN. Sci Rep. 2016;6:1–11.
20. Chu VC, McElroy LJ, Chu V, Bauman BE, Whittaker GR. The avian coronavirus infectious bronchitis virus undergoes direct low-pH-dependent fusion activation during entry into host cells. J Virol. 2006;80(7):3180–8.
21. Cox RG, Mainou BA, Johnson M, Hastings AK, Schuster JE, Dermody TS, et al. Human Metapneumovirus Is Capable of Entering Cells by Fusion with Endosomal Membranes. PLoS Pathog. 2015;11(12):e1005303.
22. Preta G, Cronin JG, Sheldon IM. Dynasore - Not just a dynamin inhibitor. Cell Communication and Signaling. 2015;13:24.
23. Duan M, Hibbs ML, Chen W. The contributions of lung macrophage and monocyte heterogeneity to influenza pathogenesis. Immunology and Cell Biology. 2017;95:225–35.
24. Hume DA. Macrophages as APC and the Dendritic Cell Myth. J Immunol.

2008;181(9):5829–35.

25. O'Keeffe M, Mok WH, Radford KJ. Human dendritic cell subsets and function in health and disease. Cellular and Molecular Life Sciences. 2015;72:4309–25.
26. Guilliams M, Lambrecht BN, Hammad H. Division of labor between lung dendritic cells and macrophages in the defense against pulmonary infections. Mucosal Immunology. 2013;6:464–73.
27. Hendin HE, Pillet S, Lara AN, Wu CY, Charland N, Landry N, et al. Plant-made virus-like particle vaccines bearing the hemagglutinin of either seasonal (H1) or avian (H5) influenza have distinct patterns of interaction with human immune cells in vitro. Vaccine. 2017;35(19):2592–9.
28. Young KR, Arthus-Cartier G, Yam KK, Lavoie PO, Landry N, D'Aoust MA, et al. Generation and characterization of a trackable plant-made influenza H5 virus-like particle (VLP) containing enhanced green fluorescent protein (eGFP). FASEB J. 2015;29(9):3817–27.
29. Fontana J, Steven AC. Influenza virus-mediated membrane fusion: Structural insights from electron microscopy. Archives of Biochemistry and Biophysics. 2015;581:86–97.
30. Mair CM, Ludwig K, Herrmann A, Sieben C. Receptor binding and pH stability - How influenza A virus hemagglutinin affects host-specific virus infection. Biochim Biophys Acta - Biomembr. 2014;1838(4):1153–68.
31. Videira PA, Amado IF, Crespo HJ, Algueró MC, Dall'Olio F, Cabral MG, et al. Surface α2-3- and α2-6-sialylation of human monocytes and derived dendritic cells and its influence on endocytosis. Glycoconj J. 2008;25(3):259–68.
32. Yu WCL, Chan RWY, Wang J, Travanty EA, Nicholls JM, Peiris JSM, et al. Viral Replication and Innate Host Responses in Primary Human Alveolar Epithelial Cells and Alveolar Macrophages Infected with Influenza H5N1 and H1N1 Viruses. J Virol. 2011;85(14):6844–55.
33. Geisler C, Jarvis DL. Letter to the glyco-forum: Effective glycoanalysis with Maackia amurensis lectins requires a clear understanding of their binding specificities. Glycobiology. 2011;21(8):988–93.
34. Ng WC, Londrigan SL, Nasr N, Cunningham AL, Turville S, Brooks AG, et al. The C-type lectin langerin functions as a receptor for attachment and infectious entry of influenza

A virus. J Virol. 2016;90(1):206-21.

35. Reading PC, Miller JL, Anders EM. Involvement of the mannose receptor in infection of macrophages by influenza virus. J Virol. 2000;74(11):5190–7.
36. Chatziandreou N, Farsakoglu Y, Palomino-Segura M, D'Antuono R, Pizzagalli DU, Sallusto F, et al. Macrophage Death following Influenza Vaccination Initiates the Inflammatory Response that Promotes Dendritic Cell Function in the Draining Lymph Node. Cell Rep. 2017;18(10):2427–40.
37. Roche PA, Furuta K. The ins and outs of MHC class II-mediated antigen processing and presentation. Nature Reviews Immunology. 2015;15:203–16.
38. Chu VC, McElroy LJ, Bauman BE, Whittaker GR. Fluorescence dequenching assays of coronavirus fusion. Advances in Experimental Medicine and Biology. 2006;581:241–6.
39. Short KR, Grant EJ, Vissers M, Reading PC, Diavatopoulos DA, Kedzierska K. A novel method linking antigen presentation by human monocyte-derived macrophages to CD8+ T cell polyfunctionality. Front Immunol. 2013;4:389.
40. Oslund KL, Baumgarth N. Influenza-induced innate immunity: Regulators of viral replication, respiratory tract pathology & adaptive immunity. Future Virology. 2011;6:951–62.
41. Tripathi S, White MR, Hartshorn KL. The amazing innate immune response to influenza A virus infection. Innate Immun. 2015;21(1):73–98.

2.9. FIGURES AND LEGENDS

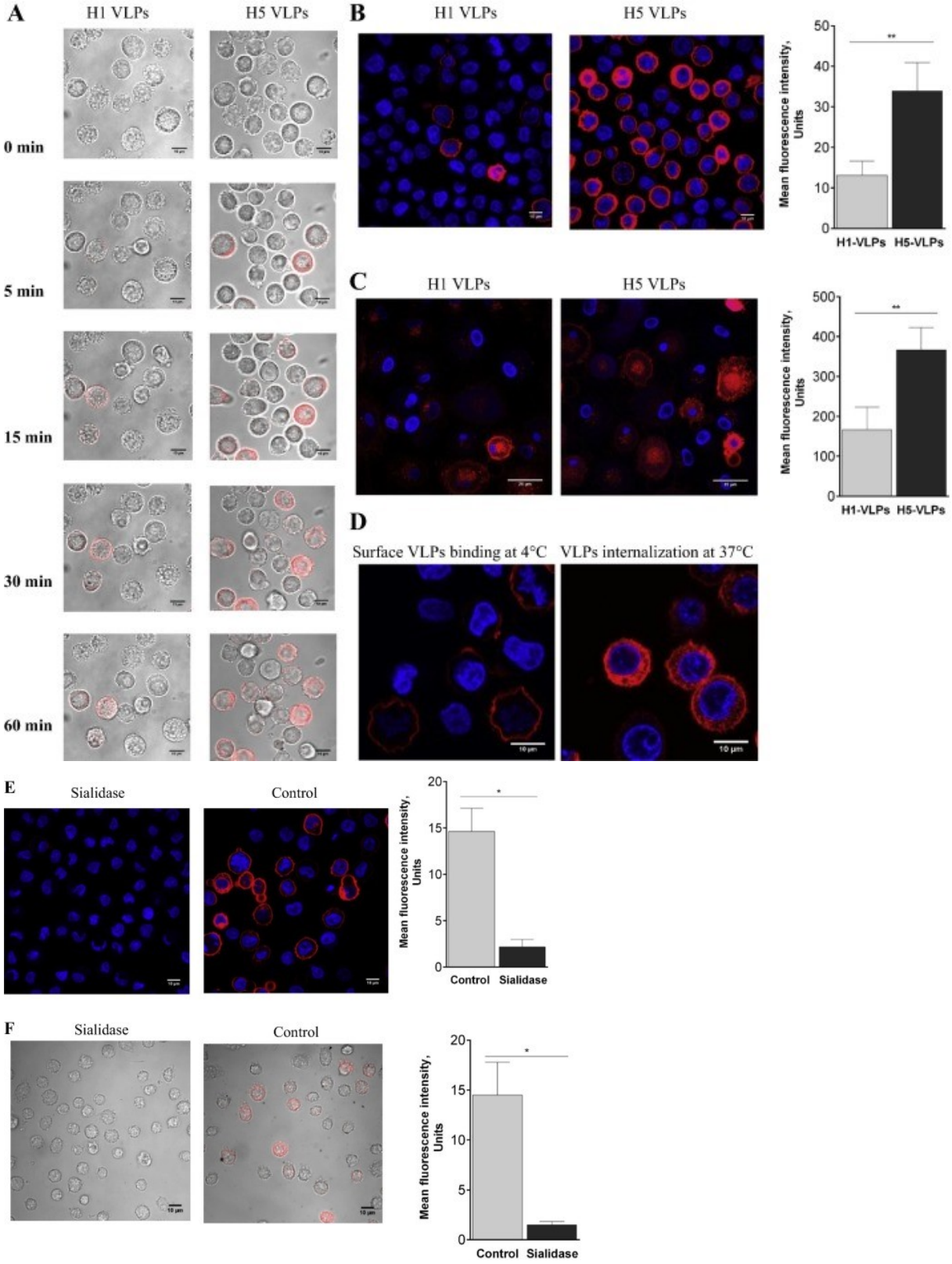

(legend on next page)

Figure 2. 1. VLPs binding to U-937 cells and macrophages

DiD-labelled H1- or H5-VLPs were added to U-937 cells in serum-free RPMI-1640 (media), and time-lapse images were acquired at 37°C. Representative images at 0 (prior to adding VLPs), 5, 15, 30 and 60 min are presented. Scale bar indicates 10 μm. (B) U-937 cells exposed to H1- (left) or H5-VLPs (middle) for 30 min. DiD fluorescence, mean ± s. e. m., presented (right, n = 6). Scale bar indicates 10 μm. (C) Human MDMs exposed to H1- (left) or H5-VLPs (middle) for 30 min. DiD fluorescence, mean ± s. e. m., presented (right, n = 7). Scale bar indicates 25 μm. (D) U-937 cells exposed to H5-VLPs for 60 min at 4°C (left) or at 37°C (right). Scale bar indicates 10 μm. I *V. cholerae* sialidase-treated (250 mU/mL in media for two hrs) live U-937 were exposed to DiD-labelled H5-VLPs for 30 min (left). Control sample was kept in media for two hrs and exposed to DiD-labelled H5-VLPs for 30 min (middle). DiD fluorescence, mean ± s. e. m. presented (right, n = 3). Scale bar indicates 10 μm. (F) Formaldehyde-fixed and *V. cholerae* sialidase-treated (250 mU/mL in acetate buffer, pH 5.5 overnight) U-937 were exposed to DiD-labelled H5-VLPs for 60 min (left). Control sample was kept in acetate buffer overnight and exposed to DiD-labelled H5-VLPs for 60 min (middle). DiD fluorescence, mean ± s. e. m. presented (right, n = 5). Scale bar indicates 10 μm. DiD shown in red. Cell nuclei stained with 4′,6-diamidino-2-phenylindole (DAPI), blue. * - $p < 0.05$, ** - $p < 0.01$.

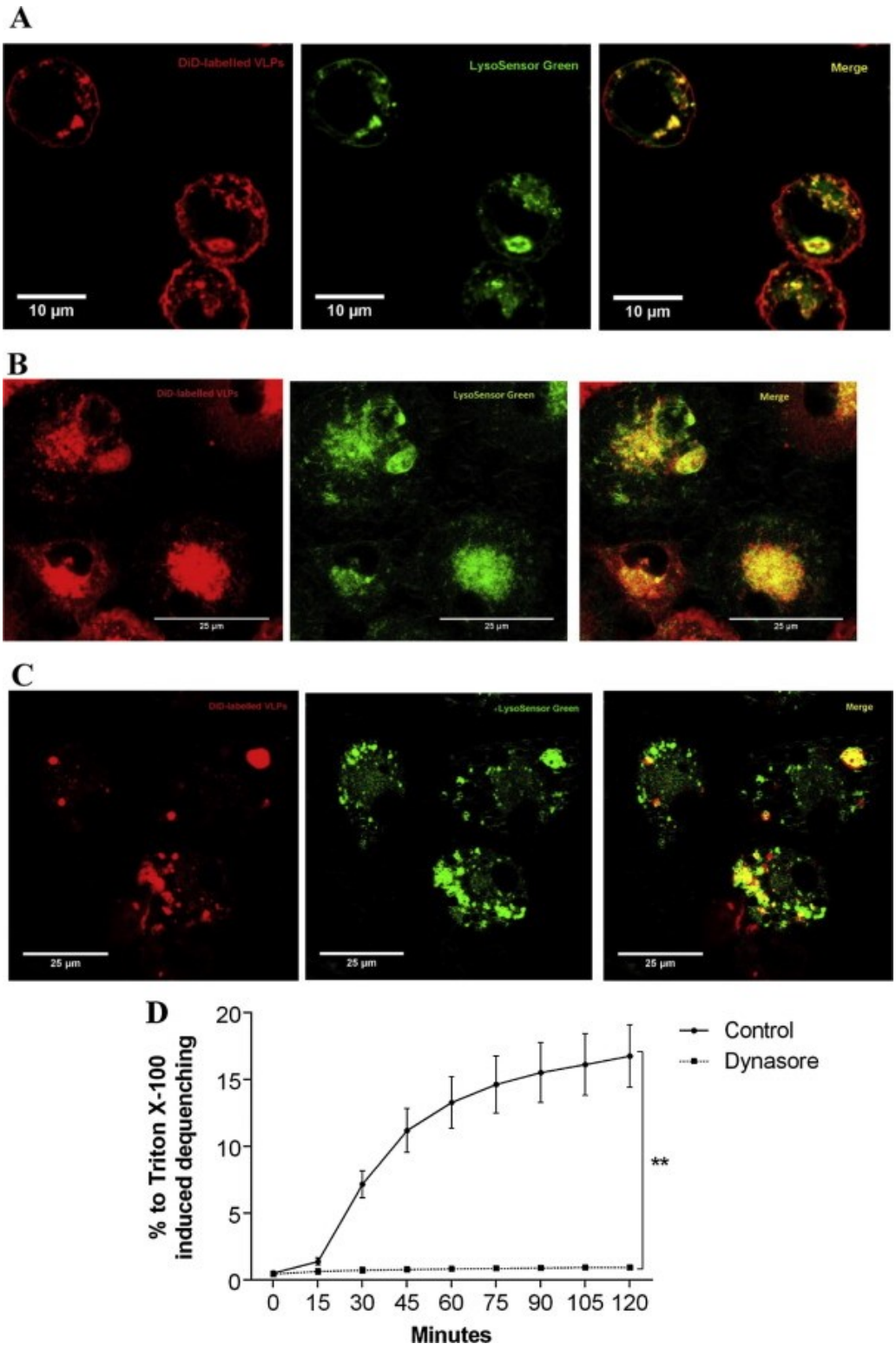

Figure 2. 2. Internalization of VLPs adhered to cell surface

U-937 cells were pre-loaded with LysoSensor Green DND-189 and exposed to DiD-labelled

(legend continued on next page)

H5-VLPs for 45 min. Images are DiD fluorescence (red – left), LysoSensor Green DND-189 fluorescence (green-middle) and merged (right). Scale bar indicates 10 μm. (B) Human MDMs were pre-loaded with LysoSensor Green DND-189 and exposed to DiD-labelled H1-VLPs for 45 min. Images are DiD fluorescence (red-left), LysoSensor Green DND-189 fluorescence (green-middle) and merged (right). Scale bar indicates 25 μm. (C) Human MDMs were pre-loaded with LysoSensor Green DND-189 and exposed to DiD-labelled H5-VLPs for 45 min. Images are DiD fluorescence (red-left), LysoSensor Green DND-189 fluorescence (green-middle) and merged (right). Scale bar indicates 25 μm. (D) U-937 cells exposed to H5-VLPs at 4°C for one hr to permit VLP attachment but not entry into the cells, washed, re-suspended in ice-cold media supplemented with 10% FBS and plated in 96-well plastic flat bottom plates. Dynasore hydrate applied to some wells at a concentration 50 μM. The plates were placed into a pre-warmed (37°C) spectrophotometer, and DiD fluorescence was measures at 15-min intervals over two hours. Fusion efficiency, reported as %, was determined following addition of Triton X-100 to each well (final concentration 1%) to obtain full DiD dequenching. Mean ± s. e. m. presented (n = 9). ** - $p < 0.01$.

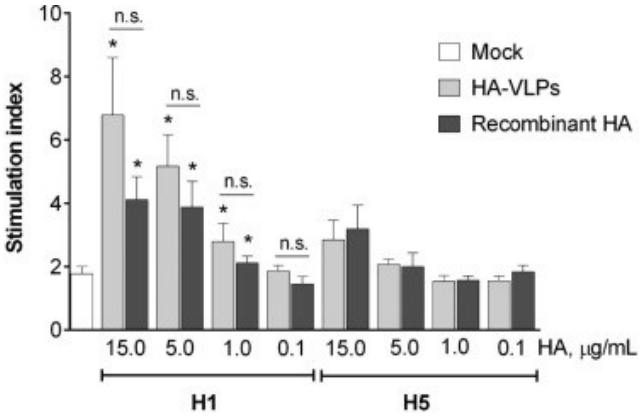

Figure 2. 3. Proliferation of autologous PBMCs co-cultured with MDMs exposed to H1 or H5 in a form of VLPs or recombinant proteins

MDMs differentiated from primary human monocytes, detached with Accutase Cell Detachment Solution and plated on 96-well black or transparent plastic flat bottom plates (2×10^4 cells/well). The next day, MDMs were exposed to H1 or H5 as VLPs or soluble recombinant proteins at 15.0, 5.0, 1.0 or 0.1 μg/mL for two hours, washed and co-cultured for 5 days with freshly-isolated autologous PBMCs, 2×10^5 cells/well (MDMs to PBMCs ratio 1:10). BrdU incorporation (cell proliferation) was measured by either colorimetric (optical density) or chemiluminescence. Stimulation indices (SI) were calculated: SI = proliferation with PBMCs + MDMs + antigen / proliferation with PBMCs alone. Mean ± s. e. m. presented (n = 5). * - $p < 0.05$ compared to mock-treated MDMs + PBMCs; n.s. – difference not significant.

2.10. SUPPLEMENTARY MATERIAL

Plant-made virus-like particles bearing influenza hemagglutinin (HA) recapitulate early interactions of native influenza virions with human monocytes/macrophages

Alexander I. Makarkov, Sabrina Chierzi, Stéphane Pillet, Keith K. Murai, Nathalie Landry, Brian J. Ward

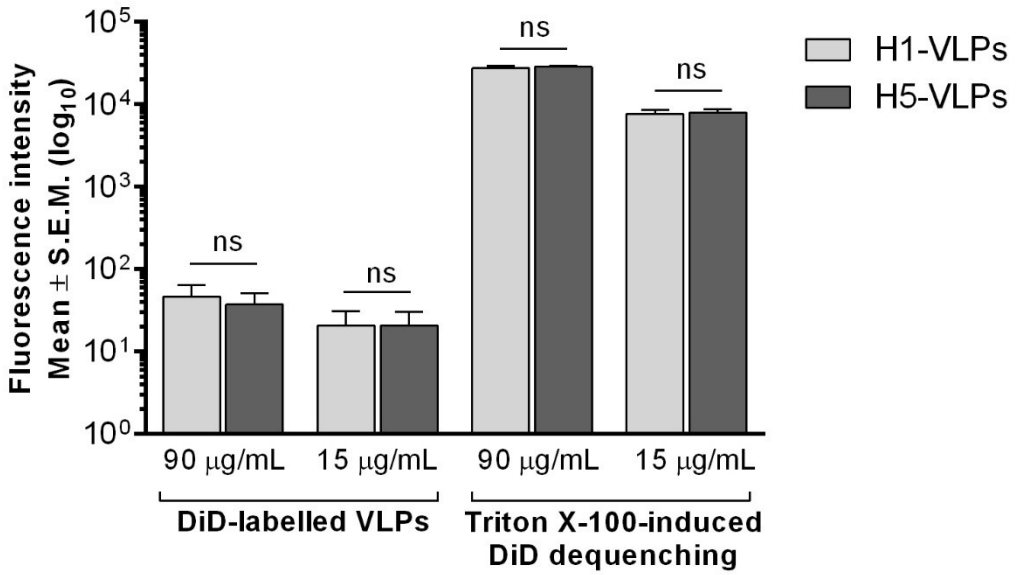

Supplemental Figure 2. 1. H1- and H5-VLPs staining with DiD

VLP samples diluted in PBS to make the same HA concentration were stained with DiD at a concentration of 20μg/mL for 30 minutes, and then purified from free dye by gel filtration. DiD fluorescence was measured prior to and following addition of Triton X-100 (final concentration 1%) to obtain full DiD dequenching. Mean ± s. e. m. presented (n=3). Ns – difference not significant.

A

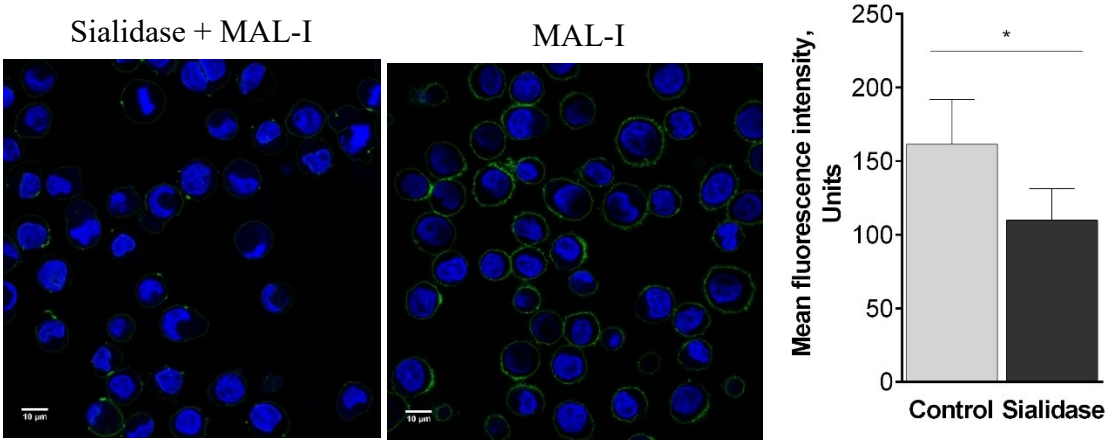

B

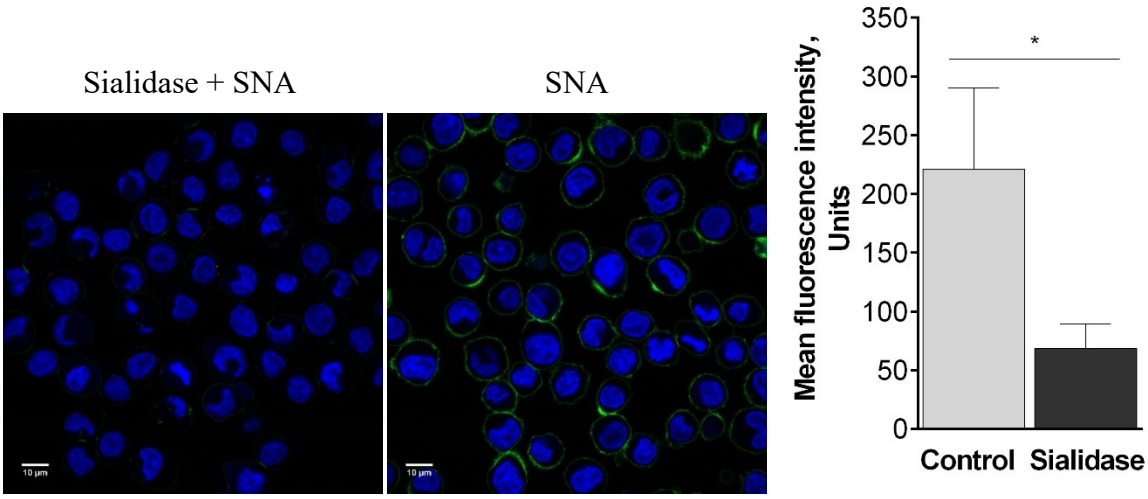

Supplemental Figure 2. 2. Effect of sialidase treatment on MAL-I (A) and SNA (B) lectin binding to live U-937 cells

V. Cholerae sialidase-treated live U-937 cells were stained with fluorescein-labeled *Maackia Amurensis* Lectin I (MAL-I, green) for 30 minutes at 4°C and then fixed with formaldehyde (left). Control sample was stained with fluorescein-labeled MAL-I and then fixed (middle).

(legend continued on next page)

Fluorescein fluorescence, mean ± s. e. m., presented (right, n=6). (B) *V. Cholerae* sialidase-treated live U-937 cells were stained with fluorescein-labeled *Sambucus Nigra* Lectin (SNA, green) for 30 minutes at 4°C and then fixed with formaldehyde (left). Control sample was stained with fluorescein-labeled SNA and then fixed (middle). Fluorescein fluorescence, mean ± s. e. m., presented (right, n=5). Cell nuclei stained with DAPI, blue. Scale bar indicates 10 μm. * - $p<0.05$.

A **B**

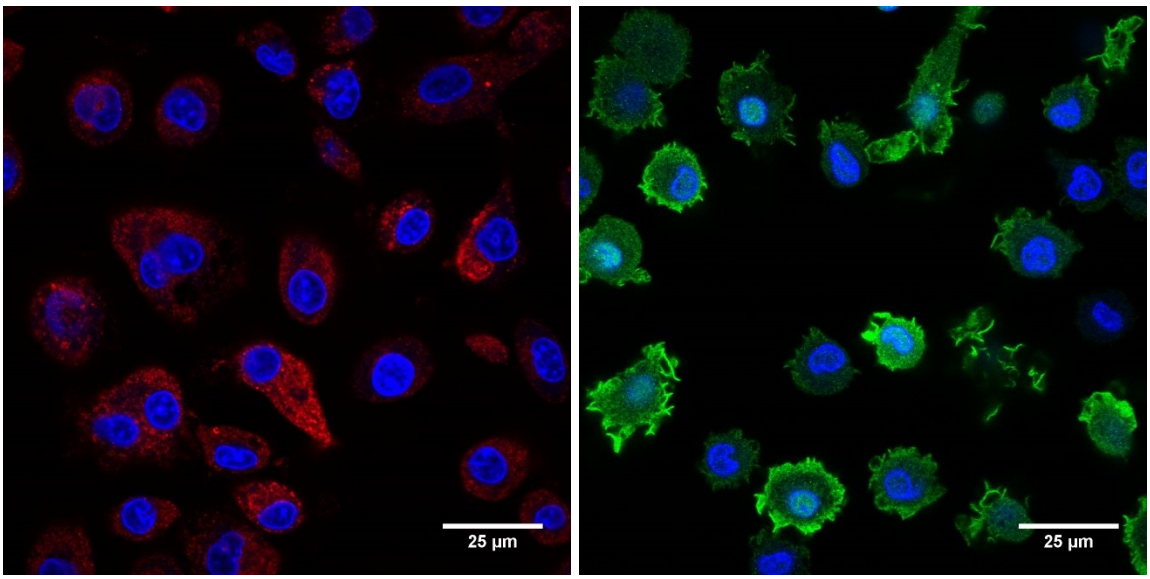

Supplemental Figure 2. 3. Phenotype of MDMs differentiated from CD14^{+} enriched population of PBMCs

MDMs stained for CD68 marker (red). (B) MDMs stained for Iba-1 marker (green). Cell nuclei stained with DAPI, blue. Scale bar indicates 25 µm.

Chapter 3: Plant-derived virus-like particle vaccines drive cross-presentation of influenza A hemagglutinin peptides by human monocyte-derived macrophages

Alexander I. Makarkov[1,2], Makan Golizeh[2], Angelica A. Gopal[3,4], Ian N. Costas-Cancelas[5], Sabrina Chierzi[6], Stephane Pillet[2,7], Nathalie Charland[7], Nathalie Landry[7], Isabelle Rouiller[5,8], Paul W. Wiseman[3,9], Momar Ndao[2,10], Brian J. Ward[2]

[1] Division of Experimental Medicine, Department of Medicine, McGill University, 1001 Décarie Street, Montréal, Québec, H4A 3J1, Canada
[2] Infectious Diseases and Immunity in Global Health Program, Research Institute of McGill University Health Centre, Glen Site, 1001 Décarie Street, Montréal, Québec, H4A 3J1, Canada
[3] Department of Chemistry, McGill University, 801 Sherbrooke St, W, Montreal, Québec, H3A 0B8, Canada
[4] Department of Physiology, McGill University, 3655 Promenade Sir William Osler, Montreal, Quebec, H3G 1Y6, Canada
[5] Department of Anatomy & Cell Biology; Faculty of Medicine; McGill University; Groupe de Recherche Axe sur la Structure des Protéines (GRASP); Groupe d'Étude des Protéines Membranaires (GEPROM), 3640 University Street, Montreal, Québec, H3A 2B2, Canada
[6] Research Institute of McGill University Health Centre, Montreal General Hospital, 1650 Cedar Av, Montréal, Québec, H3G 1A4, Canada
[7] Medicago Inc., 1020 Route de l'Église, Bureau 600, Québec, Québec, G1V 3V9, Canada
[8] Department of Biochemistry and Molecular Biology and Bio21 Molecular Science and Biotechnology Institute; The University of Melbourne, Parkville, VIC, 3010, Australia
[9] Department of Physics, McGill University, 3600 University St, Montreal, Québec, H3A 2T8, Canada
[10] Department of Medicine, Division of Infectious Diseases, Faculty of Medicine, McGill University, Montreal, Québec, H4A 3J1, Canada

This article has been submitted to *npj Vaccines.*

3.1. PREFACE

In chapter 2 of this thesis, we described robust surface binding and internalization of plant-derived VLPs by human MDM and U-937 cells. As demonstrated by confocal microscopy and DiD fluorescence dequenching, DiD-labelled VLPs were partially delivered into acidified endosomal compartments where they underwent fusion with endosomal membranes. In this chapter, we continued this work by further characterization of the specific mechanisms of VLP uptake by human MDM and compare them with the internalization of soluble HA. We study the intracellular handling and fate of influenza HA delivered in a form of plant-derived VLP vs. soluble protein with the specific focus on endosomal trafficking of HA towards the compartments favoring either MHC II-restricted antigen presentation or MHC I-restricted cross-presentation. We show that MDM exposure to H1-VLP results in a massive cross-presentation of influenza HA.

3.2. ABSTRACT

A growing body of evidence supports the importance of T cell responses to protect against severe influenza, promote viral clearance and ensure long-term immunity. Plant-derived virus-like particle (VLP) vaccines bearing influenza hemagglutinin (HA) have been shown to elicit strong humoral and $CD4^+$ T cell responses in both pre-clinical and clinical studies. To better understand the immunogenicity of theses vaccines, we tracked the intracellular fate of a model HA (A/California/07/2009 H1N1) in human monocyte-derived macrophages (MDMs) following delivery either as VLPs (H1-VLP) or in soluble form. Compared to exposure to soluble HA, pulsing with VLPs resulted in ~3-fold greater intracellular accumulation of HA at 15 minutes that was driven by clathrin-dependent and -independent endocytosis as well as macropinocytosis/phagocytosis. At 45 minutes, soluble HA had largely disappeared suggesting its handling primarily by high-degradative endosomal pathways. Although the overall fluorescence intensity/cell had declined 25% at 45 min after H1-VLP exposure, the endosomal distribution pattern and degree of aggregation suggested that HA delivered by VLP had entered both high-degradative late and low-degradative static early and/or recycling endosomal pathways. At 45 minutes in the cells pulsed with VLPs, HA was strongly co-localized with Rab5, Rab7, Rab11, MHC II and MHC I. High-resolution tandem mass spectrometry identified 115 HA-derived peptides associated with MHC I in the H1-VLP-treated MDMs. These data suggest

that HA delivery to antigen-presenting cells on plant-derived VLPs facilitates antigen uptake, endosomal processing and cross-presentation. These observations may help to explain the broad and cross-reactive immune responses generated by these vaccines.

3.3. INTRODUCTION

The cellular arm of the adaptive immune response is increasingly recognized as important for both recovery and long-term protection from influenza viruses. $CD4^+$ T cells provide support for antibody production and maturation as well as the induction of cytotoxic $CD8^+$ T cells (CTL) that target infected cells for elimination (1). In adults, pre-existing poly-functional $CD4^+$ T cells have been proposed as a better correlate of protection than antibody titers (2). Although influenza-specific CTLs cannot prevent disease, they can reduce both the severity and duration of infection (3). T cell responses may be particularly important for vulnerable populations such as young children and the elderly (4,5). The most commonly used influenza vaccines based on detergent-split virions typically elicit a strong antibody response but are weak inducers of cellular immunity (6). Although live attenuated vaccines elicit T cell responses, systemic humoral responses are often weak and interference from pre-existing immunity makes these vaccines less effective after early childhood (7). A vaccine that elicits both strong antibody and cell-mediated responses might have significant advantages over current split virion products.

Plant-derived VLP vaccines bearing the influenza virus HA protein appear to have this capability (8,9). Produced by *Agrobacterium*-mediated transient expression of influenza HA proteins in *Nicotiana benthamiana*, these vaccines recapitulate the structure and key features of native influenza virions such as sialic acid-mediated adherence and internalization by target cells, fusion of the VLP envelope with endosomal membranes, and rapid induction of an innate immune response (10–12). These vaccines have been shown to elicit strong and cross-reactive antibody responses against both seasonal and pandemic influenza strains in animal models and human trials (13–15). They also induce polyfunctional and cross-reactive HA-specific $CD4^+$ T cell responses (8,13,14). Simultaneous administration of a plant-derived H5-VLP vaccine with ovalbumin (OVA) was recently shown to elicit an OVA-specific $CD8^+$ T cell response in C57Bl/6 mice (16). The subcellular mechanisms that account for the unusual immunogenicity of the plant-derived VLP-based vaccines are not yet well understood.

In the current work, we demonstrated that human monocyte-derived macrophages (MDMs) internalize H1-VLPs using both clathrin-mediated and clathrin-independent endocytosis (CME and CIE respectively) as well as macropinocytosis and, probably, phagocytosis. Soluble H1 was internalized almost exclusively by CME and was trafficked predominantly to the high-degradative late endosome/endolysosome compartment. In contrast, a substantial portion of H1 delivered by VLP was retained in low-degradative static early and/or recycling endosomes where the HA co-localized with major histocompatibility complex class I (MHC I). Immunoprecipitation of MHC I and high-resolution mass spectrometry revealed a large number of HA-derived peptides in MDMs exposed to H1-VLP but not soluble H1. These findings demonstrate that intracellular processing of influenza HA by human MDMs is very different when the protein is delivered by VLP or in a soluble form. These observations help to explain the dual humoral and $CD4^+$ responses seen in humans with the plant-derived VLP vaccines and raise the possibility that cross-presentation of HA peptides to $CD8^+$ T cells may also occur.

3.4. RESULTS

3.4.1. H1-VLPs are efficiently internalized by human MDMs

Classical electron microscopy (EM) was used to document early endocytotic events such as formation of endocytic vesicles that are too small to be well-visualized with confocal microscopy (17). Exposure of MDMs to H1-VLPs led to a rapid activation of the endocytosis machinery. The number of endocytic vesicles doubled during the first 5 minutes of exposure to H1-VLPs while soluble H1 had no significant effect (Fig. 3.1a). Intracellular HA immunofluorescence was apparent at 5 min of exposure to H1-VLPs and reached a plateau at 10 min. Further incubation did not change the fluorescence signal (Suppl. Fig. 3.1a). To eliminate continuous internalization, MDMs were pulsed with either H1-VLPs or soluble H1 for 15 min followed by a 30 min incubation. At 15 min, the fluorescence was 3-fold higher in H1-VLP-treated MDMs compared to soluble H1 (Fig. 3.1b). Next, we used a 1,1'-dioctadecyl-3,3,3',3'-tetramethylindodicarbocyanine perchlorate (DiD) dequenching assay (12) and a panel of endocytosis inhibitors (Suppl. Table 3.1; Suppl. Fig. 3.1b – d) to demonstrate that H1-VLPs were internalized primarily through CME and CIE with smaller contributions from macropinocytosis

and, probably, phagocytosis (Fig. 3.1c). The prominent role of CME was further demonstrated by direct HA immunofluorescence in the presence of CME inhibitor chlorpromazine (Fig. 3.1d) and by co-localization of HA with fluorescently-labeled transferrin that is exclusively taken up by CME (Fig. 3.1e). Immunolabelling of clathrin and caveolin-1 in EM images of MDMs exposed to H1-VLPs confirmed that the total endocytic vesicle pool included both clathrin-coated and caveolin-coated structures (Fig. 3.1f). Soluble H1 endocytosis was largely unaffected by the CIE inhibitor genistein but was greatly reduced by chlorpromazine (Fig. 3.1d). Internalized soluble HA was almost perfectly co-localized with transferrin (Fig. 3.1e).

In summary, MDMs exposed to H1-VLPs internalized much more HA compared to those pulsed with soluble H1. H1-VLP internalization occurred through multiple endocytic pathways including CME, CIE, macropinocytosis and, probably, phagocytosis while soluble H1 was internalized almost exclusively by CME. The diversity of H1-VLPs internalization mechanisms raised the possibility that antigen delivered in this form might experience different acidification and degradative environments, leading to a broader range of antigen processing and presentation pathways (18). It was therefore of interest to study endosomal trafficking and the intracellular fate of the two forms of HA.

3.4.2. H1-VLPs are handled in two distinct endosomal pools: high- and low-degradative

Both the amount of internalized HA and the degree of degradation over time varied with delivery form (Fig. 3.2a, Suppl. Fig. 3.2a). We used the intensity of HA fluorescence as a surrogate for protein degradation, assuming that the monoclonal antibody-binding epitope would be preserved in a low-degradative intracellular compartment (early-static or recycling endosomes). Conversely, disappearance of the fluorescent signal would suggest trafficking to late endosomes/endolysosomes. Using confocal microscopy, the intensity of HA fluorescence in MDMs pulsed with soluble H1 dropped dramatically over 45 minutes (>90%) while the cells pulsed with H1-VLP retained ~75% of the HA signal, suggesting that a substantial portion of the internalized protein delivered by VLP had found its way into low-degradative cellular compartments. To more precisely define the fate of the internalized HA, we analyzed the confocal data using the fluorescence fluctuation method image cross-correlation spectroscopy (ICCS) with segmentation (19,20). We based the segmentation on HA-positive endosomes (Suppl. Fig. 3.2b) via automatic thresholding based on the fluorescence intensity. The intensity

of HA fluorescence in the endosomes of VLP-pulsed cells increased more than two-fold between 15 and 45 min. The cluster density (number of HA particles per μm^2) and the degree of HA aggregation also increased (Fig. 3.2b). In contrast, HA fluorescence intensity fell ~97% in the endosomes of MDMs pulsed with soluble H1 during this same time period. The cluster density and the degree of HA aggregation in these samples was greatly reduced as well, suggesting that the internalized soluble protein was almost completely degraded by 45 min.

Thus, exposure of MDMs to H1-VLPs resulted in rapid and substantial endocytosis. A large proportion of HA remained intact for at least 45 min after the VLP pulse. Moreover, increases in HA fluorescence intensity, cluster density and degree of aggregation all suggested homotypic fusion of the HA-positive endosomes (21). The simultaneous reduction in overall HA fluorescence intensity per cell area argued for movement of some of the protein to high-degradative late endosomes, supporting a bidirectional trafficking model for the HA delivered by the VLPs. In contrast, the uptake of soluble H1 was less important at the outset (15 min) and the HA fluorescence had almost completely disappeared at 45 min. These observations prompted us to further characterize the endosomal compartments contributing to the complex handling of HA delivered on VLPs or as soluble protein.

3.4.3. H1-VLPs move towards static early and/or recycling endosomes in human MDMs

Conventional colocalization analysis based on 'per cell' image segmentation suggested that H1-VLPs preferentially track from early, Rab5-positive endosomes to low-degradative Rab11-positive recycling endosomes rather than to late Rab7-positive endosomes/endolysosomes (Suppl. Fig. 3.3a) (22). Of note, in a significant minority of H1-VLP-exposed cells (~15%), we observed peripheral re-distribution (recycling) of undegraded HA towards the plasma membrane at 45 min (Suppl. Fig. 3.3b). Soluble H1 was partially co-localized with all three endosomal markers at 15 min but was undetectable in any endosomal compartment by 45 min suggesting that the HA had been almost fully degraded (data not shown). When the HA-positive endosomal compartment was characterized by segmentation ICCS analysis, there was a substantial increase in the HA colocalized cluster density (number of colocalized particles per μm^2) with Rab5 and Rab11 markers at 45 min suggesting protein retention in static early and/or recycling endosomes (Fig. 3.3a). Unexpectedly, we also observed an increase of HA – Rab7 colocalized cluster density, which may possibly be explained by Rab conversion of the slowly-maturing endosomes

(23). The HA – MHC II colocalized cluster density was ~4-fold higher in the H1-VLP-pulsed MDMs compared to those treated with soluble H1 at 15 min, and did not change by 45 min (Fig. 3.3b) suggesting that VLPs facilitate HA delivery, at least partially, in high-degradative $Rab7^+$ compartments that favor MHC II-restricted antigen presentation (18,24). The fraction of HA particles interacting with endosomal proteins remained unchanged between 15 and 45 min in the MDMs exposed to H1-VLPs (Fig. 3.3), suggesting that HA-enriched endosomes retained association with Rab proteins that regulate endosomal trafficking, cargo sorting and organelle maturation (25).

In summary, a large portion of the HA delivered on VLPs is retained in low-degradative endosomal compartments (static early and/or recycling endosomes) for at least 45 min, while the remainder follows the 'classic' endosomal degradation pathway. In contrast, soluble H1 is mostly trafficked towards high-degradative intracellular compartments. These striking differences in the intracellular handling of HA raised questions about the possible immunological consequences of the two forms of antigen delivery.

3.4.4. HA delivery in the form of VLPs favors antigen cross-presentation by human MDMs

A large portion of intracellular MHC I pool resides in recycling Rab11a-postive endosomes that can support cross-presentation of phagocytosed antigens (26). It was therefore of interest to explore HA delivery into the MHC I-positive endosomal compartments following pulsing of MDMs with the different forms of HA. ICCS colocalization revealed strong association between HA and MHC class I molecules in MDMs pulsed with either H1-VLPs or soluble H1 at 15 min (Fig. 3.4a). By 45 min however, HA – MHC I colocalized cluster density had greatly increased in H1-VLP-exposed cells (213%) but fell by 63% in the MDMs pulsed with soluble HA. The fraction of interacting HA particles remained unchanged by 45 min in H1-VLP-exposed MDMs. Based on the assumption that prolonged retention of antigen in low-degradative (MHC-I^+, $Rab11^+$) compartments favors cross-presentation (27), we immunoprecipitated MHC I – peptide complexes from lysates of MDMs that had been pulsed overnight with H1-VLPs or soluble H1 and analyzed the eluted peptides using high-resolution tandem mass spectrometry (MS). No confident HA-derived peptides were detected in the lysate of MDMs exposed to soluble H1. In contrast, 115 HA-derived MHC I-associated peptides were

identified in MDMs exposed to the H1-VLPs (posterior error probability (PEP) score ≤0.01), contributing to an HA sequence coverage of 12-89% (Table 3.1; Suppl. Table 3.2). Eight peptides were detected in more than one donor and the HA protein scores varied from 32 to 323. Average protein quantity in cell lysates did not differ between HA treatment groups (2773.8 ± 595.2 µg/mL in VLP group and 2440.4 ± 468.1 µg/mL in soluble HA group; p=0.70). The HA-derived peptides averaged 18 amino acids (AA) and only ~10% had an 'optimal' length for MHC I loading (8-10 AA: Fig 3.4b) (27). This observation suggested that the lysates contained a mixture of optimally-trimmed peptides and immature peptides from the endoplasmic reticulum (ER)/endosome compartments still being processed and sorted for either presentation or degradation (28).

3.5. DISCUSSION

As bridges between innate and adaptive immune responses, 'professional' phagocytes such as macrophages are first-line defenders against invading pathogens (29). Among other activities, antigen uptake, processing and display by these cells contribute to both the strength and the pattern of the immune response. In this *in vitro* work, we focused on human MDMs that phenotypically and functionally resemble the inflammatory-type macrophages (30) implicated in orchestrating early responses to both influenza virus infection (31) and live-attenuated vaccine (32). Our goal was to better understand how these cells handle influenza HA proteins when delivered either as a soluble protein (i.e. the form found in most commercial influenza vaccines) or decorating the surface of 80-100 nm plant-derived VLPs. We have previously shown that these VLPs rapidly interact with human immune cells including B cells, monocytes and dendritic cells (10,11,16) and that early interactions with human MDMs (i.e. binding, internalization, entry into endosomes and fusion with endosomal membranes) are similar to what happens with wild-type influenza virions (12). In the current work, we tracked intracellular handling by MDMs at much higher resolution and demonstrated that a large proportion of the HA delivered on these VLPs enter static and recycling endosomal pathways leading to MHC class I cross-presentation.

Many factors contribute to how antigen-presenting cells (APCs) handle any given antigen including the dose and form of the antigen itself, the nature and activation state of the APCs as well as the microenvironment in which these processes occur. How the antigen first enters the cell can also strongly influence the outcome and APCs have many choices from 'bulk' processes

like phagocytosis and macropinocytosis or more controlled processes like CME or CIE. Antigens internalized through CME are usually delivered rapidly to maturing degradative endosomes that undergo quick acidification and fusion with lysosomes (33). The cleavage products of lysosomal proteases and peptidases are typically longer peptides (13-25 AA) appropriate for MHC II loading that leads to priming of $CD4^+$ T cells and support of strong humoral responses (24). In our studies, H1-VLP-pulsed MDMs demonstrated substantially greater HA – MHC II colocalization that soluble H1-treated cells, suggested that the VLPs may favor, at least in part, MHC II-restricted presentation of HA-derived peptides. We also observed nearly complete disappearance of soluble H1 immunofluorescence at 45 minutes of pulsing the human MDMs, suggested predominant trafficking towards the highly degradative endolysosomal compartment. Such handling is certainly consistent with the observation that split virion influenza vaccines typically elicit strong antibody responses but little-to-no priming of $CD8^+$ T cells and only limited cell-mediated immunity against influenza (6).

In contrast, CIE often leads to homotypic fusion of caveolin-coated endocytic vesicles and formation of large caveosomes that can retain non-degraded antigenic material for long periods of time (34). Although the mechanisms are not yet fully understood, both static early endosomes (35) and non-acidified endosomes in the vacuolar pathway (27) have been reported to support cross-presentation. Phagocytosis and macropinocytosis typically result in internalization of large quantities of an antigenic material that may also favor cross-presentation and priming of $CD8^+$ T cells (27,36). Although some of the HA-specific immunofluorescence was lost shortly after pulsing human MDMs with H1-VLPs, a substantial portion of the initial fluorescence was still detectable at 45 min and the ICCS analysis revealed striking increases in HA fluorescence intensity, cluster density and aggregation in the endosomes. The trafficking of the HA delivered on the plant-derived VLPs therefore appeared to be bidirectional: with a small portion moving rapidly into the high-degradative late endosome/endolysosome pathway (similar to soluble HA) while a substantial amount was retained in low-degradative compartments. At 45 min, both immunostaining and ICCS analysis demonstrated increasing colocalization of the VLP-HA with both $Rab5^+$ (early static) and $Rab11^+$ (recycling) low-degradative endosomes.(23,35) Nair-Gupta *et al.* have reported that recycling $Rab11a^+$ endosomes represent a major intracellular pool for MHC I molecules (26), and colocalization of the VLP-delivered HA with MHC I in these low-

degradative compartments increased almost 3-fold between 15 and 45 minutes after the MDMs were pulsed.

Although our imaging studies provided good evidence for HA-VLP delivery into endosomal compartments that favor antigen cross-presentation, direct proof of HA processing by the human MDMs leading to the generation of MHC I-associated peptides was missing. MS-based immunopeptidome studies have historically required billions of cells to obtain sufficient numbers of MHC molecules for efficient detection of MHC-associated peptides (37). One consequence of this technical limitation is that most MS-based immunopeptidome work has focused on immortalized cell lines or animal cells (38,39). Recent improvements in MS technology combined with nano-flow chromatography now offer better sensitivity for the detection of MHC-associated peptides from relatively small numbers of cells. In our study, the use of a recently developed nanospray ion source with a constant flow of dopant gas permitted enhanced ionization and more efficient detection of MHC I peptides from only 3–10 million MDMs. The Maxis II mass spectrometer used in this study also has a unique hardware configuration that allows very high transmission of peptides into the collision cell enabling the detection of a wide range of peptides of various lengths (40). Our data unambiguously show that cross-presentation of HA peptides by human macrophages is possible when the HA is delivered by plant-derived VLPs. So far, MHC I-restricted presentation of influenza virus-derived peptides was thought to require infection or administration of the live attenuated vaccine, involving viral replication (3,4).

Internal (structural) proteins of influenza viruses (i.e. NP, PB1, M1) are thought the principle targets of the human $CD8^+$ T cell response (3) and only a limited number of influenza HA-derived MHC I-restricted peptides have been reported to date (41,42). We were therefore surprised to find 115 HA-derived peptides from the VLP-pulsed MDMs, 8 of which were identified in more than one donor (Suppl. Table 3.2). Among previously described 17 HA-derived human MHC I-restricted epitopes (43), 4 peptides (23%) were fully overlapping with up to three unique AA sequences identified in our study. Since we used unfractionated cell lysates containing MHC I molecules from the cell surface as well as those present in endosomes and the ER-Golgi compartment, it was not unexpected that many of the HA-derived peptides identified were longer than the 8-10 AA thought to be optimal for MHC I loading (27). It is likely that the longer peptides immunoprecipitated with MHC I were destined either for further trimming to

achieve a better fit in the MHC I peptide binging groove or for degradation (28,44). Together, the imaging and MS results presented herein collectively suggest that influenza HA delivery to human MDMs in the form of VLPs can result in cross-presentation.

These plant-derived influenza vaccines have moved rapidly through clinical trials, demonstrating strong antibody responses as well as poly-functional $CD4^+$ T cell responses to both homotypic and heterotypic viruses (8,14,15). The potential for these vaccines to induce $CD8^+$ T cells has been demonstrated in mice (16) and studies are on-going to determine whether or not similar responses can be elicited in humans. Although conserved T cell epitopes from influenza core proteins have attracted the most attention to date (3,42), several human $CD8^+$ epitopes have been identified in the HA proteins of both seasonal and avian influenza strains (45,46) and our data suggest that many more may exist. A non-living vaccine that can induce strong antibody production as well as both $CD4^+$ and $CD8^+$ T cell responses might have significant advantages over currently licensed products (47).

3.6. MATERIALS AND METHODS

3.6.1. Plant-made VLP bearing influenza hemagglutinin

The VLPs produced in *N. benthamiana* were kindly provided by Medicago Inc. (Quebec, QC) and were manufactured as previously described (8,9). The influenza HA protein was based on the sequence of A/California/07/2009 H1N1 virus. Recombinant soluble H1 protein (Immune Technology, New York, NY) was used as a control.

3.6.2. Monocyte-derived macrophages (MDMs)

MDMs were differentiated from human peripheral blood mononuclear cells (PBMCs) isolated from healthy donors between the ages of 23-47. All studies with human cells were carried out with approval from the Research Ethics Committee of the McGill University Health Centre. Written informed consent was obtained from all donors prior to blood drawing. PBMCs were separated from whole blood by centrifugation using SepMate-50 tubes (STEMCELL, Vancouver, BC). Monocytes were isolated by negative selection using magnetic microbeads according to the manufacturer's instructions (EasySep Human Monocyte Enrichment Kit, STEMCELL). Monocytes were cultured in RPMI-1640 with 50 IU/mL penicillin, 50 μg/mL

streptomycin and 10 mM HEPES (medium) supplemented with 10% fetal bovine serum (FBS, all from Wisent, Saint-Jean-Baptiste, QC) and 20 ng/mL recombinant human macrophage colony-stimulating factor (Gibco, Frederick, MD) for 7 days.

3.6.3. VLPs endocytosis assessment based on fluorescence dequenching

VLPs were stained with DiD (Thermo Fisher Scientific, Eugene, OR) at 20μg/mL for 30 minutes at room temperature (RT), and then purified from free dye using gel filtration columns (PD MiniTrap G-25, GE Healthcare, Buckinghamshire, UK). MDMs were detached from plastic plate surface using Accutase Cell Detachment Solution (BioLegend, San Diego, CA) and plated on 96-well Nunclon Delta black flat-bottom plates (Thermo Fisher Scientific, Roskilde, Denmark) at 5 x 10^4 cells/well. The following day, MDMs were exposed to DiD-labelled VLPs (HA concentration 15.0 μg/mL) at 4°C for one hour. Endocytosis inhibitors were applied in ice-cold medium supplemented with 10% FBS: dynasore hydrate 50 μM, genistein 200 μM, amiloride hydrochloride 1 mM, cytochalasin D 4 μM (all from Sigma-Aldrich, St. Louis, MO). DiD fluorescence was measured with pre-heated (37°C) spectrophotometer (Infinite 200 PRO, Tecan, Männedorf, Switzerland) at 15-min intervals over two hours. Fusion efficiency was determined following the addition of Triton X-100 (Sigma-Aldrich) to each well (final concentration 1%) to obtain full DiD dequenching.

3.6.4. Immunostaining and confocal microscopy

MDMs were exposed to H1-VLPs or soluble H1 at concentration 15 μg/mL (by HA content) in 5% CO_2 incubator at 37°C for 5, 10, 15 or 45 min. Endocytosis inhibitor chlorpromazine hydrochloride (10 μg/mL, Sigma-Aldrich) or genistein (200 μM) were applied 30 min prior to adding H1-VLPs or soluble H1, and the duration of HA exposure was 15 min. Transferrin (human) CF568 conjugate (Biotium, Fremont, CA) was mixed with either H1-VLPs or soluble H1 (both transferrin and HA concentrations 15 μg/mL), and the mixture was applied to the MDMs for 15 min (5% CO_2, 37°C). In the pulse-exposure experiments, MDMs were exposed to H1-VLPs or soluble H1 for 15 min, and then the supernatant was replaced by medium and kept for another 30 min at 5% CO_2 and 37°C. MDMs were fixed with 4% methanol-free formaldehyde (Thermo Fisher Scientific, Rockford, IL), blocked and permeabilized with 5% goat and 5% donkey serum (both from EMD Millipore Corporation,

Darmstadt, Germany) in 0.3% Triton X-100. HA immunostaining was performed using mouse anti-H1 antibody (clone IVC102, Meridian Life Science, Memphis, TN). Endosomal proteins were visualized with rabbit anti-Rab5 (clone C8B1), anti-Rab7 (clone D95F2), anti-Rab11 (clone D4F5) antibodies (all from Cell Signaling Technology, Danvers, MA), anti-HLA-DPB1 (clone EPR11226) from Abcam (Cambridge, MA) or anti-HLA-A antibody (clone EP1395Y) from GeneTex (Irvine, CA). Secondary donkey anti-mouse Alexa Fluor 488 and goat anti-rabbit Alexa Fluor 647 antibodies (both from Thermo Fisher Scientific) were applied for one hour at RT. NucBlue Live ReadyProbes Reagent – 4',6-diamidino-2-phenylindole (DAPI, Thermo Fisher Scientific) used to stain cell nuclei. A laser scanning confocal microscope (Zeiss LSM780, RI-MUHC Molecular Imaging Core Facility, Montreal, QC) was used in all imaging experiments. Fluorescence intensity after cell-based segmentation of the images was quantified using ImageJ software (48).

3.6.5. Quantitative image analysis

The fluorescence fluctuation analysis method image cross-correlation spectroscopy (ICCS) was applied to evaluate the HA endosomal distribution and the degree of HA colocalization with endosomal proteins as previously described (19,20). In brief, ICCS measures molecular concentrations and interaction fractions based on correlation analysis of fluorescence fluctuations detected from imaged biomolecules as a function of space across an image. Automatic thresholding of fluorescence intensity via Otsu's method was applied to identify the high intensity HA-positive endosomal area in images. The number of HA particles per μm^2, the HA fluorescence intensity and the aggregation state of HA particles in the HA-positive endosomal area per cell can be calculated from the spatial autocorrelation function of the fluorescence intensity fluctuations in an image from a single detection channel. Particles formed by endosomal proteins of interest (Rab5, Rab7, Rab11 and MHC I) were also identified.

To evaluate the colocalization between HA and specific endosomal proteins, we calculated the spatial cross-correlation function from the fluorescence intensity fluctuations between images recorded in two different wavelength detections channels (expressed as (i) number of colocalized HA particles per μm^2 and (ii) fraction of interacting HA particles) in two-color images.

3.6.6. Electron microscopy (EM)

MDMs were exposed to H1-VLPs or soluble H1 at concentration 15 µg/mL (by HA content) in 5% CO_2 incubator at 37°C for 5 min before fixation with 2.5% glutaraldehyde (EMS Inc., Hatfield, PA). Samples for nanogold immuno-labeling were initially fixed with 2% methanol-free formaldehyde (15 min at RT) and permeabilized/blocked with 0.2% Triton X-100 plus 1% goat serum for 5 min on ice. Primary rabbit anti-clathrin (clone D3C6) or anti-caveolin-1 (clone D46G3) antibodies (both from Cell Signaling Technology) were applied overnight at 4°C. Secondary nanogold-conjugated goat anti-rabbit antibody (Nanoprobes, Yaphank, NY) was applied in 1% non-fat dried milk, and then cells were fixed with 2.5% glutaraldehyde. Samples were washed with 0.1 M sodium cacodylate (EMS Inc.). Cells were silver-enhanced for 30 s using HQ Silver enhancement kit (Nanoprobes). Post-fixation was done in 1% osmium tetroxide (EMS Inc.) containing potassium ferrocyanide (Fisher Scientific, Pittsburgh, PA). Cells were dehydrated with 0-100% ethanol and progressively embedded in EPON resin (EMS Inc.). The samples were sectioned and imaged with a Tecnai T12 microscope (FEI Inc., Hillsboro, OR).

3.6.7. Mass spectrometry analysis

MDMs were exposed to either H1-VLPs or soluble H1 at HA concentration 15 µg/mL in 5% CO_2 incubator at 37°C for 16 h. Cells were lysed (1 h, 4°C) with a buffer containing 4% NP-40 Surfact-Amps™ (Thermo Fisher Scientific), 50 mM Tris-HCl (pH 7.0), 150 mM NaCl and protease inhibitors (Pierce™ Protease Inhibitor Mini Tablets, Thermo Fisher Scientific). Lysate total protein concentration was determined using Pierce™ BCA Protein Assay (Thermo Fisher Scientific). MHC I–peptide complexes were immunoprecipitated using Dynabeads™ protein G immunoprecipitation kit (Thermo Fisher Scientific) and anti-human HLA-A,B,C antibody (clone W6/32, BioLegend, 10 µg per 500 µL lysate, 45 min, 4°C). Dynabeads™-antibody-antigen complexes were washed three times, transferred into clean tubes, and the peptides were eluted with 10% acetic acid (70°C, 15 min). The immunoprecipitation eluate was cleaned on a C18 solid-phase extraction Macro Spin column (Harvard Apparatus, Holliston, MA) using water and methanol following manufacturer's instructions, and evaporated to dryness under vacuum (37°C, 120 min). Samples were reconstituted in 0.1% formic acid (60 µL) and injected (20 µL) onto a Maxis II (Bruker, Billerica, MA) high-resolution quadrupole-time of flight tandem mass spectrometer equipped with a Dionex UltiMate 3000 (Thermo Fisher Scientific, Waltham, MA)

ultra-high-performance liquid chromatography (UHPLC) system using an Acclaim PepMap 300 RSLC C18 2 µm 100 Å 150 x 0.075 mm UHPLC column (Thermo Fisher Scientific) with water (A) and acetonitrile (B) both containing 0.1% formic acid at a flow rate of 0.3 µL/min (50°C). Elution gradient started at 5% B, was held for 3 min, then increased to 35% at 73 min, 55% at 90 min, and 80% at 95 min. MS spectra were acquired at *m/z* 400–2200 and MS/MS spectra were recorded at *m/z* 150–2200 using collision-induced dissociation (CID) activation in Auto MS/MS mode with a collision energy of 21–55 eV depending on precursor ion *m/z* value and charge state (*z*). Ions with *z* = 2–5 were preferred whereas singly charged ions were excluded. Redundant ions were also excluded for 2 min. Acquisition time was 0.5 s for MS and 0.06–0.25 s for each MS/MS scan depending on precursor ion signal intensity, with a total cycle time of 3.0 s. CaptiveSpray (Bruker) nanospray ionization source operated in positive mode with a capillary voltage of 1.8 kV. To enhance ionization, a continuous flow of nitrogen and vaporized acetonitrile (as dopant) was injected into the ion source during the analysis using a nanoBooster module (Bruker). Nitrogen (99.5% pure) was used as dry gas (150°C) at a flow rate of 3.0 L/min. Samples were analyzed in duplicate.

3.6.8. Analysis of proteomics data

Mass spectra were imported into the MaxQuant software (49) and searched against an in-house influenza A virus (A/California/07/2009(H1N1)) hemagglutinin FASTA file including six UniProt-TrEMBL identifiers: C3W627, C3W5X2, I6T4Z8, R9RVT8, U3M8B4, U3M8F8. An unspecific search was conducted for peptides with a length of 5–20 residues at 0.01 false-discovery rate (FDR). Methionine oxidation and N-terminal acetylation were defined as variable modifications. A posterior error probability (PEP) threshold of 0.01 was set for all MaxQuant searches. To account for LC retention shifts, the 'match between runs' option was enabled with a match time window of 0.7 min and an alignment time window of 20 min. Only hits with a protein score > 30 were accepted.

3.6.9. Statistical analysis

Statistical analysis was performed using GraphPad Prism 6.0 software. One-way analysis of variance (ANOVA) followed by Tukey's multiple comparisons post-test were used to examine the differences between samples. P values < 0.05 were considered statistically significant.

3.6.10. Availability of data

The datasets generated during and/or analyzed during the current study are available from the corresponding author on reasonable request. The mass spectrometry proteomics data have been deposited to the ProteomeXchange Consortium via the PRIDE partner repository (50) with the dataset identifier PXD010519.

3.7. ACKNOWLEDGEMENTS

We thank Dr. John Presley at McGill University for helpful discussions during planning of experiments and manuscript preparation. We thank the Molecular Imaging Platform of Research Institute of the McGill University Health Centre and its staff for the kind services provided.

3.8. REFERENCES

1. Sridhar S. Heterosubtypic T-cell immunity to influenza in humans: Challenges for universal T-cell influenza vaccines. Frontiers in Immunology. 2016;7:195.
2. Wilkinson TM, Li CKF, Chui CSC, Huang AKY, Perkins M, Liebner JC, et al. Preexisting influenza-specific CD4+T cells correlate with disease protection against influenza challenge in humans. Nat Med. 2012;18(2):274–80.
3. Grant EJ, Quinõnes-Parra SM, Clemens EB, Kedzierska K. Human influenza viruses and CD8+T cell responses. Curr Opin Virol. 2016;16:132–42.
4. Mohn KG-I, Smith I, Sjursen H, Cox R. Immune responses after live attenuated influenza vaccination. Hum Vaccin Immunother. 2018;14(3):571–8.
5. Nguyen THO, Sant S, Bird NL, Grant EJ, Clemens EB, Koutsakos M, et al. Perturbed CD8 + T cell immunity across universal influenza epitopes in the elderly. J Leukoc Biol. 2017;103(2):321-339.
6. Bonduelle O, Yahia N, Siberil S, Benhabiles N, Carrat F, Krivine A, et al. Longitudinal and Integrative Biomodeling of Effector and Memory Immune Compartments after Inactivated Influenza Vaccination. J Immunol. 2013;191(2):623–31.
7. Hoft DF, Lottenbach KR, Blazevic A, Turan A, Blevins TP, Pacatte TP, et al. Comparisons of the humoral and cellular immune responses induced by live attenuated influenza vaccine and inactivated influenza vaccine in adults. Clin Vaccine Immunol. 2017;24(1):e00414-16.
8. Landry N, Pillet S, Favre D, Poulin JF, Trépanier S, Yassine-Diab B, et al. Influenza virus-like particle vaccines made in Nicotiana benthamiana elicit durable, poly-functional and cross-reactive T cell responses to influenza HA antigens. Clin Immunol. 2014;154(2):164–77.
9. D'Aoust MA, Couture MMJ, Charland N, Trépanier S, Landry N, Ors F, et al. The production of hemagglutinin-based virus-like particles in plants: A rapid, efficient and safe response to pandemic influenza. Plant Biotechnol J. 2010;8(5):607–19.
10. Hendin HE, Pillet S, Lara AN, Wu CY, Charland N, Landry N, et al. Plant-made virus-like particle vaccines bearing the hemagglutinin of either seasonal (H1) or avian (H5) influenza have distinct patterns of interaction with human immune cells in vitro. Vaccine. 2017;35(19):2592–9.

11. Lindsay BJ, Bonar MM, Costas-Cancelas IN, Hunt K, Makarkov AI, Chierzi S, et al. Morphological characterization of a plant-made virus-like particle vaccine bearing influenza virus hemagglutinins by electron microscopy. Vaccine. 2018;36(16):2147–54.
12. Makarkov AI, Chierzi S, Pillet S, Murai KK, Landry N, Ward BJ. Plant-made virus-like particles bearing influenza hemagglutinin (HA) recapitulate early interactions of native influenza virions with human monocytes/macrophages. Vaccine. 2017;35(35):4629–36.
13. Hodgins B, Yam KK, Winter K, Pillet S, Landry N, Ward BJ. A single intramuscular dose of a plant-made virus-like particle vaccine elicits a balanced humoral and cellular response and protects young and aged mice from influenza H1N1 virus challenge despite a modest/absent humoral response. Clin Vaccine Immunol. 2017;24(12):1–14.
14. Pillet S, Aubin É, Trépanier S, Bussière D, Dargis M, Poulin JF, et al. A plant-derived quadrivalent virus like particle influenza vaccine induces cross-reactive antibody and T cell response in healthy adults. Clin Immunol. 2016;168:72–87.
15. Pillet S, Aubin É, Trépanier S, Poulin JF, Yassine-Diab B, Ter Meulen J, et al. Humoral and cell-mediated immune responses to H5N1 plant-made virus-like particle vaccine are differentially impacted by alum and GLA-SE adjuvants in a Phase 2 clinical trial. npj Vaccines. 2018;3:3.
16. Hunt K. Plant-made influenza virus-like-particles (VLPs) activate dendritic cells and promote Type 1 immune responses. McGill University; 2016.
17. Klumperman J, Raposo G. The complex ultrastructure of the endolysosomal system. Cold Spring Harb Perspect Biol. 2014;6(10):a016857–a016857.
18. Burgdorf S, Kurts C. Endocytosis mechanisms and the cell biology of antigen presentation. Current Opinion in Immunology. 2008;20:89–95.
19. Kolin DL, Wiseman PW. Advances in image correlation spectroscopy: Measuring number densities, aggregation states, and dynamics of fluorescently labeled macromolecules in cells. Cell Biochemistry and Biophysics. 2007;49:141–64.
20. Gopal AA, Ricoult SG, Harris SN, Juncker D, Kennedy TE, Wiseman PW. Spatially Selective Dissection of Signal Transduction in Neurons Grown on Netrin-1 Printed Nanoarrays via Segmented Fluorescence Fluctuation Analysis. ACS Nano. 2017;11(8):8131–43.
21. Gautreau A, Oguievetskaia K, Ungermann C. Function and regulation of the endosomal

fusion and fission machineries. Cold Spring Harb Perspect Biol. 2014;6(3):a016832–a016832.

22. Jovic M, Sharma M, Rahajeng J, Caplan S. The early endosome: A busy sorting station for proteins at the crossroads. Histology and Histopathology. 2010;25:99–112.
23. Lakadamyali M, Rust MJ, Zhuang X. Ligands for clathrin-mediated endocytosis are differentially sorted into distinct populations of early endosomes. Cell. 2006;124(5):997–1009.
24. ten Broeke T, Wubbolts R, Stoorvogel W. MHC class II antigen presentation by dendritic cells regulated through endosomal sorting. Cold Spring Harb Perspect Biol. 2013;5(12):a016873.
25. Donaldson JG, Johnson DL, Dutta D. Rab and Arf G proteins in endosomal trafficking and cell surface homeostasis. Small GTPases. 2016;7:247–51.
26. Nair-Gupta P, Baccarini A, Tung N, Seyffer F, Florey O, Huang Y, et al. TLR signals induce phagosomal MHC-I delivery from the endosomal recycling compartment to allow cross-presentation. Cell. 2014;158(3):506–21.
27. Blander JM. Regulation of the Cell Biology of Antigen Cross Presentation. Annu Rev Immunol. 2018;36:717-753.
28. Saveanu L, Carroll O, Lindo V, Del Val M, Lopez D, Lepelletier Y, et al. Concerted peptide trimming by human ERAP1 and ERAP2 aminopeptidase complexes in the endoplasmic reticulum. Nat Immunol. 2005;6(7):689–97.
29. Duan M, Hibbs ML, Chen W. The contributions of lung macrophage and monocyte heterogeneity to influenza pathogenesis. Immunology and Cell Biology. 2017;95:225–35.
30. Sander J, Schmidt S V, Cirovic B, McGovern N, Papantonopoulou O, Hardt AL, et al. Cellular Differentiation of Human Monocytes Is Regulated by Time-Dependent Interleukin-4 Signaling and the Transcriptional Regulator NCOR2. Immunity. 2017;47(6):1051–1066.e12.
31. He W, Chen CJ, Mullarkey CE, Hamilton JR, Wong CK, Leon PE, et al. Alveolar macrophages are critical for broadly-reactive antibody-mediated protection against influenza A virus in mice. Nat Commun. 2017;8(1):846.
32. Chatziandreou N, Farsakoglu Y, Palomino-Segura M, D'Antuono R, Pizzagalli DU, Sallusto F, et al. Macrophage Death following Influenza Vaccination Initiates the

Inflammatory Response that Promotes Dendritic Cell Function in the Draining Lymph Node. Cell Rep. 2017;18(10):2427–40.

33. Scott CC, Vacca F, Gruenberg J. Endosome maturation, transport and functions. Semin Cell Dev Biol. 2014;31:2–10.
34. Yan M, Peng J, Jabbar IA, Liu X, Filgueira L, Frazer IH, et al. Despite differences between dendritic cells and Langerhans cells in the mechanism of papillomavirus-like particle antigen uptake, both cells cross-prime T cells. Virology. 2004;324(2):297–310.
35. Tanaka T, Okuya K, Kutomi G, Takaya A, Kajiwara T, Kanaseki T, et al. Heat shock protein 90 targets a chaperoned peptide to the static early endosome for efficient cross-presentation by human dendritic cells. Cancer Sci. 2015;106(1):18–24.
36. Hari A, Ganguly A, Mu L, Davis SP, Stenner MD, Lam R, et al. Redirecting soluble antigen for MHC class I cross-presentation during phagocytosis. Eur J Immunol. 2015;45(2):383–95.
37. Caron E, Kowalewski DJ, Chiek Koh C, Sturm T, Schuster H, Aebersold R. Analysis of Major Histocompatibility Complex (MHC) Immunopeptidomes Using Mass Spectrometry. Mol Cell Proteomics. 2015;14(12):3105–17.
38. Karunakaran KP, Yu H, Jiang X, Chan Q, Goldberg MF, Jenkins MK, et al. Identification of MHC-Bound Peptides from Dendritic Cells Infected with Salmonella enterica Strain SL1344: Implications for a Nontyphoidal Salmonella Vaccine. J Proteome Res. 2017;16(1):298–306.
39. Mobbs JI, Illing PT, Dudek NL, Brooks AG, Baker DG, Purcell AW, et al. The molecular basis for peptide repertoire selection in the human leucocyte antigen (HLA) C∗06:02 molecule. J Biol Chem. 2017;292(42):17203–15.
40. Beck S, Michalski A, Raether O, Lubeck M, Kaspar S, Goedecke N, et al. The Impact II, a Very High-Resolution Quadrupole Time-of-Flight Instrument (QTOF) for Deep Shotgun Proteomics. Mol Cell Proteomics. 2015;14(7):2014–29.
41. Keskin DB, Reinhold BB, Zhang GL, Ivanov AR, Karger BL, Reinherz EL. Physical detection of influenza A epitopes identifies a stealth subset on human lung epithelium evading natural CD8 immunity. Proc Natl Acad Sci. 2015;112(7):2151–6.
42. Wahl A, Schafer F, Bardet W, Buchli R, Air GM, Hildebrand WH. HLA class I molecules consistently present internal influenza epitopes. Proc Natl Acad Sci. 2009;106(2):540–5.

43. National Institute of Allergy and Infectious Diseases. Free epitope database and prediction resource. 2018. Available from: http://www.iedb.org
44. Saveanu L, Carroll O, Weimershaus M, Guermonprez P, Firat E, Lindo V, et al. IRAP identifies an endosomal compartment required for MHC class i cross-presentation. Science. 2009;325(5937):213–7.
45. Qiu X, Duvvuri VR, Gubbay JB, Webby RJ, Kayali G, Bahl J. Lineage-specific epitope profiles for HPAI H5 pre-pandemic vaccine selection and evaluation. Influenza Other Respi Viruses. 2017;11(5):445–56.
46. Muralidharan A, Gravel C, Duran A, Larocque L, Li C, Zetner A, et al. Identification of immunodominant CD8 epitope in the stalk domain of influenza B viral hemagglutinin. Biochemical and Biophysical Research Communications. 2018;502(2):226-231.
47. Schmidt ME, Varga SM. The CD8 T cell response to respiratory virus infections. Frontiers in Immunology. 2018;9:678.
48. Schneider CA, Rasband WS, Eliceiri KW. NIH Image to ImageJ: 25 years of image analysis. Nat Methods. 2012;9(7):671–5.
49. Cox J, Mann M. MaxQuant enables high peptide identification rates, individualized p.p.b.-range mass accuracies and proteome-wide protein quantification. Nat Biotechnol. 2008;26(12):1367–72.
50. Vizcaíno JA, Deutsch EW, Wang R, Csordas A, Reisinger F, Ríos D, et al. ProteomeXchange provides globally coordinated proteomics data submission and dissemination. Nature Biotechnology. 2014;32:223–6.

3.9. TABLE

Table 3. 1. Mass spectrometry analysis of HA-derived peptides from H1-VLP or soluble H1-treated MDMs obtained from four donors

Parameters	**Donor A**	**Donor B**	**Donor C**	**Donor D**
HA treatment	**soluble H1**	**-**	**soluble H1**	**soluble H1**
Total protein amount, µg	2397	-	1652	3272
Sequence coverage (%)	0	-	0	0
Protein score	0	-	0	0
# MS/MS spectra	0	-	0	0
# peptides	0	-	0	0
HA treatment	**H1-VLPs**	**H1-VLPs**	**H1-VLPs**	**H1-VLPs**
Total protein amount, µg	2653	1444	2658	4340
Sequence coverage (%)	61	12	30	89
Protein score	32	75	152	323
# MS/MS spectra	29	11	16	84
# peptides	25	10	14	66

3.10. FIGURES AND FIGURE LEGENDS

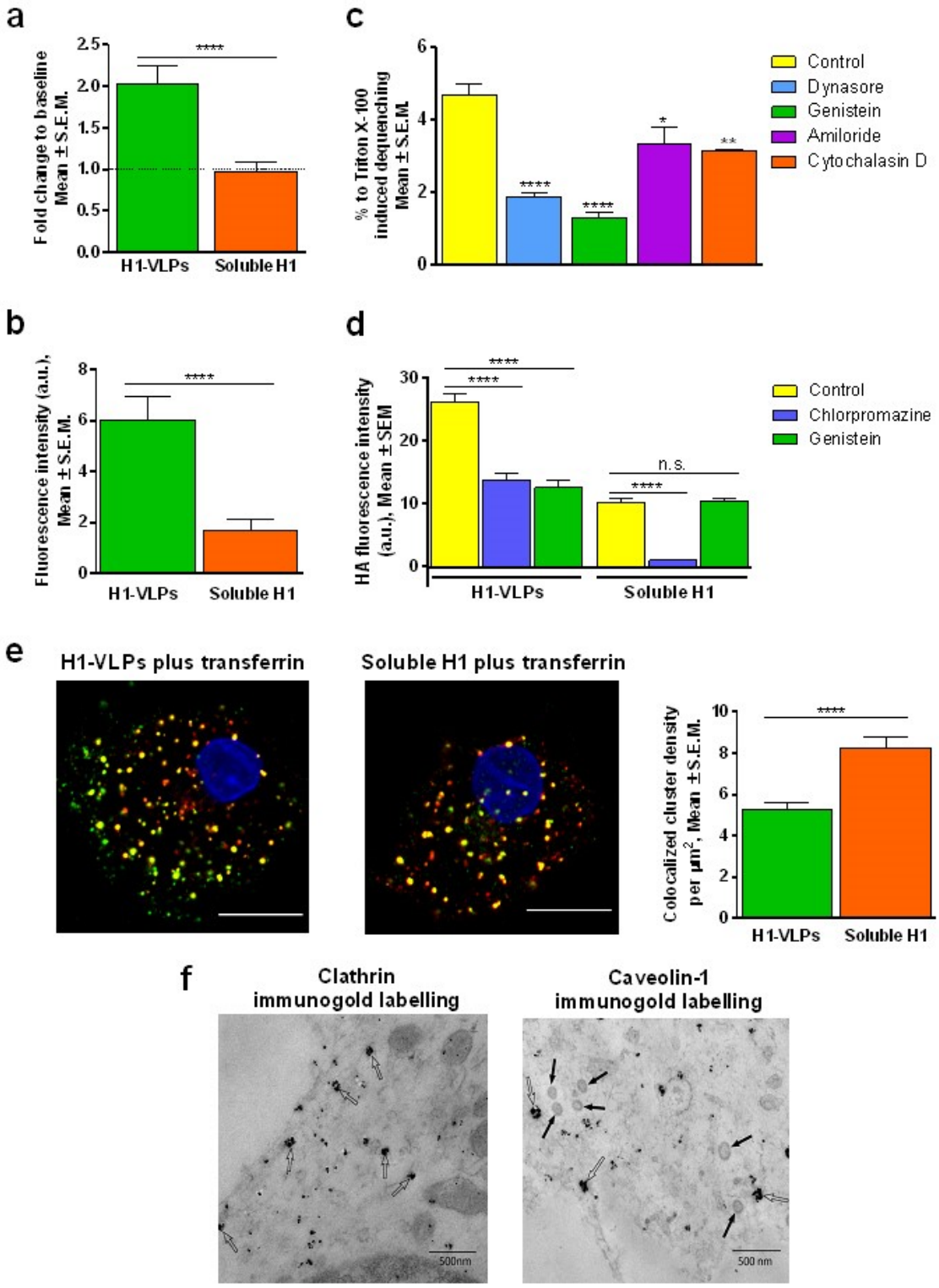

(legend on next page)

Figure 3. 1. Mechanisms of H1-VLPs and soluble H1 internalization by human MDMs
(a) Number of endocytic vesicles in MDMs exposed to H1-VLPs or soluble H1 for 5 min, normalized against the baseline count (taken as 1, dotted line). Data from two experiments were analyzed. **(b)** HA internalization by MDMs exposed to either H1-VLPs or soluble H1 for 15 min. The amount of internalized protein was evaluated by the intensity of HA immunofluorescence per cell area on confocal microscopy images. Based on 4 experiments. **(c)** Effect of endocytosis inhibitors on DiD dequenching by MDMs loaded with DiD-labelled H1-VLPs (at 2 hours). Data from 3 experiments were analyzed. **(d)** Effect of chlorpromazine and genistein on H1-VLPs or soluble H1 internalization by MDMs upon 15 min of exposure. The amount of internalized protein evaluated by the intensity of HA immunofluorescence per cell area on confocal microscopy images. Based on 6 experiments. **(e)** Colocalization of HA and transferrin in MDMs exposed to H1-VLPs and transferrin (left) or soluble H1 and transferrin (center), and segmentation ICCS colocalization (number of colocalized particles per μm^2 - right). Representative images from 3 experiments shown. Scale bar – 10 μm. Green: fluorescently labeled HA, red: transferrin conjugated with CF568 fluorophore (yellow shows colocalization of two proteins), blue: nuclei stained with DAPI. **(f)** Representative EM image with nanogold immunolabelled clathrin (left). Open arrows indicate clathrin-coated endocytic vesicles. Representative EM image with nanogold immunolabelled caveolin-1 (right). Open arrows indicate caveolin-coated endocytic vesicles. Solid arrows indicate unlabeled clathrin-coated endocytic vesicles with typical clathrin spikes. Scale bar – 500 nm. * $p<0.05$, ** $p<0.01$, **** $p<0.0001$. n.s.: nonsignificant.

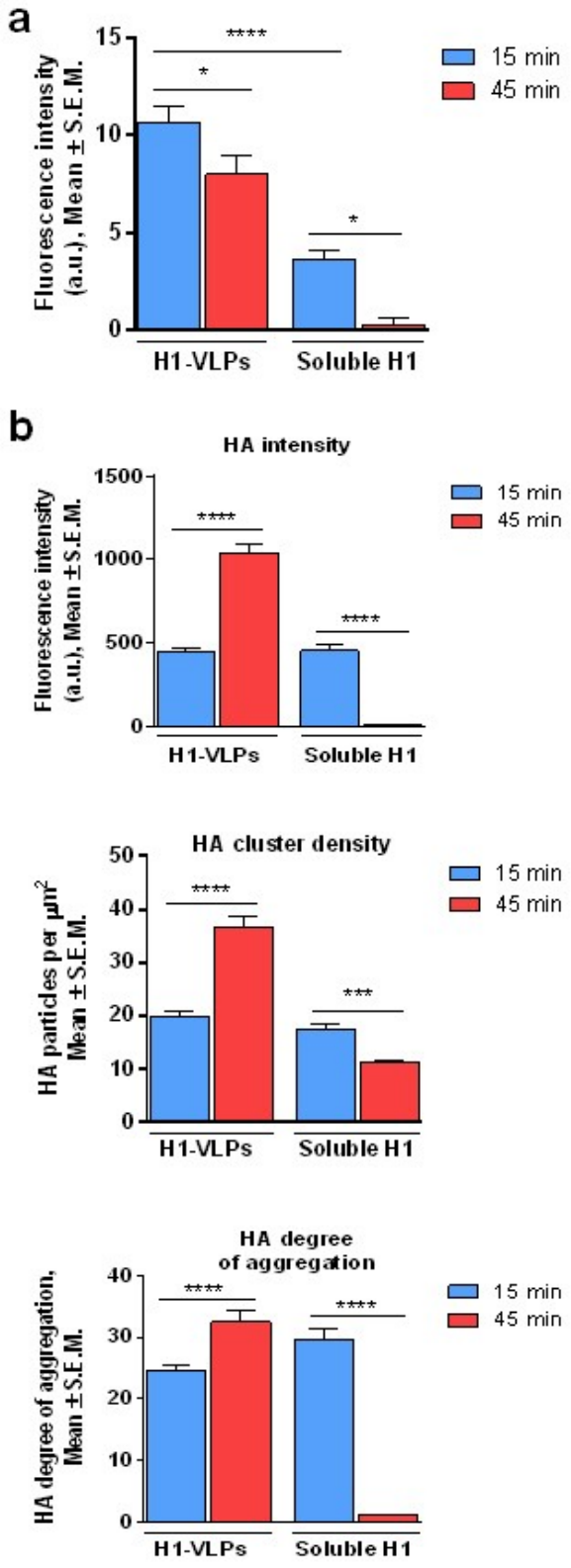

(legend on next page)

Figure 3. 2. Intracellular HA distribution in human MDMs exposed to H1-VLPs or soluble H1

(a) HA internalization and degradation by MDMs pulsed with either H1-VLPs or soluble H1. The amount of internalized protein evaluated by the intensity of HA immunofluorescence per cell area on confocal microscopy images. Data from 9 experiments were analyzed. **(b)** Segmentation ICCS analysis of the HA endosomal distribution in MDMs pulsed (15 min) with either H1-VLPs or soluble H1 shows HA fluorescence intensity (top), cluster density (number of fluorescent particles per μm^2 - middle) and degree of HA aggregation (bottom). Based on 7 experiments. * $p<0.05$, *** $p<0.001$, **** $p<0.0001$.

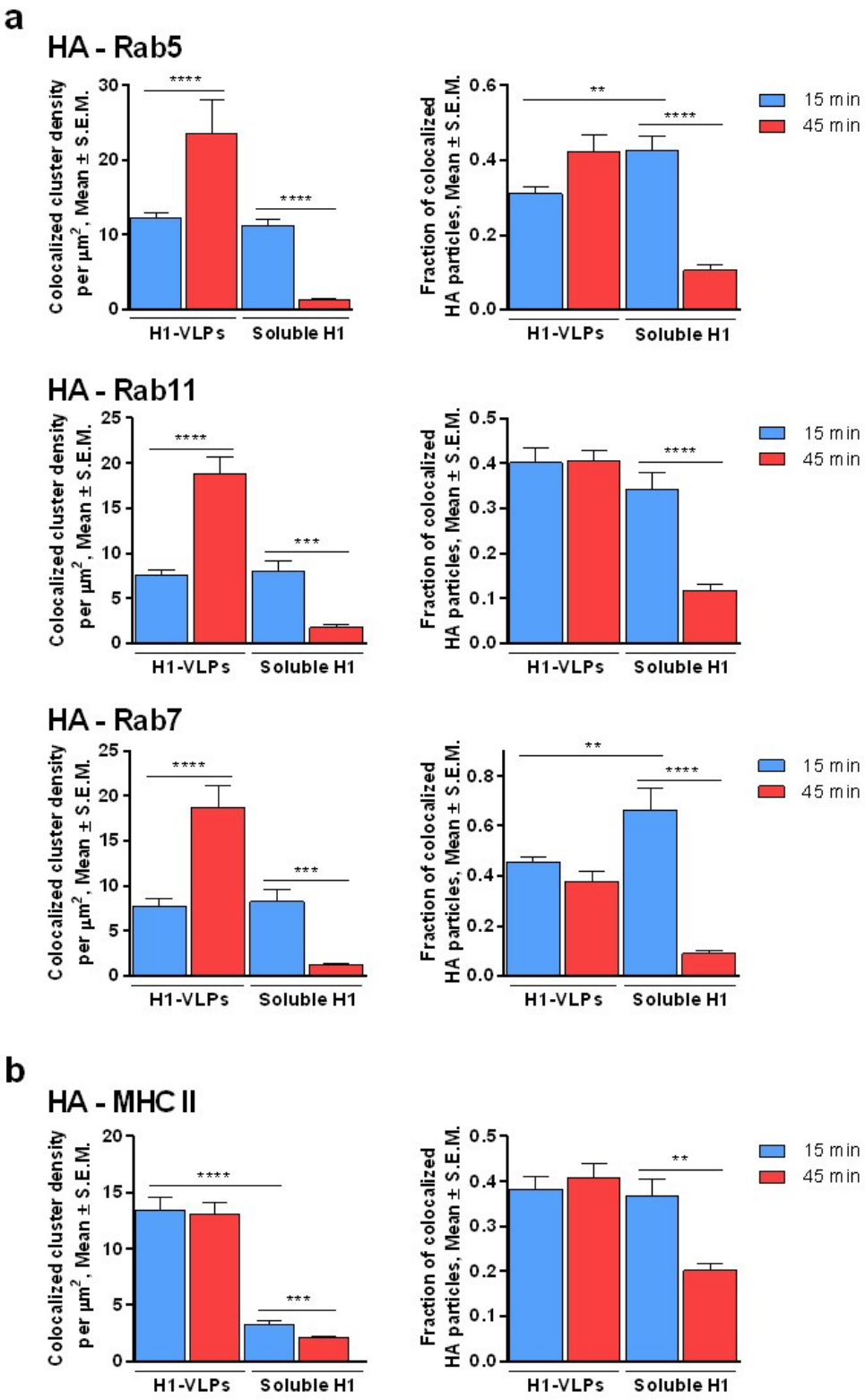

(legend on next page)

Figure 3. 3. Segmentation ICCS analysis of HA colocalization with Rab proteins and MHC II

(a) HA colocalization (number of colocalized particles per μm^2 - left) and colocalized fraction of HA (right) with Rab5 (top), Rab11 (middle) and Rab7 (bottom) are presented. Based on 3 or more experiments for each condition. **(b)** HA colocalization (number of colocalized particles per μm^2 - left) and colocalized fraction of HA (right) with MHC II are presented. Based on two experiments. ** $p<0.01$, *** $p<0.001$, **** $p<0.0001$.

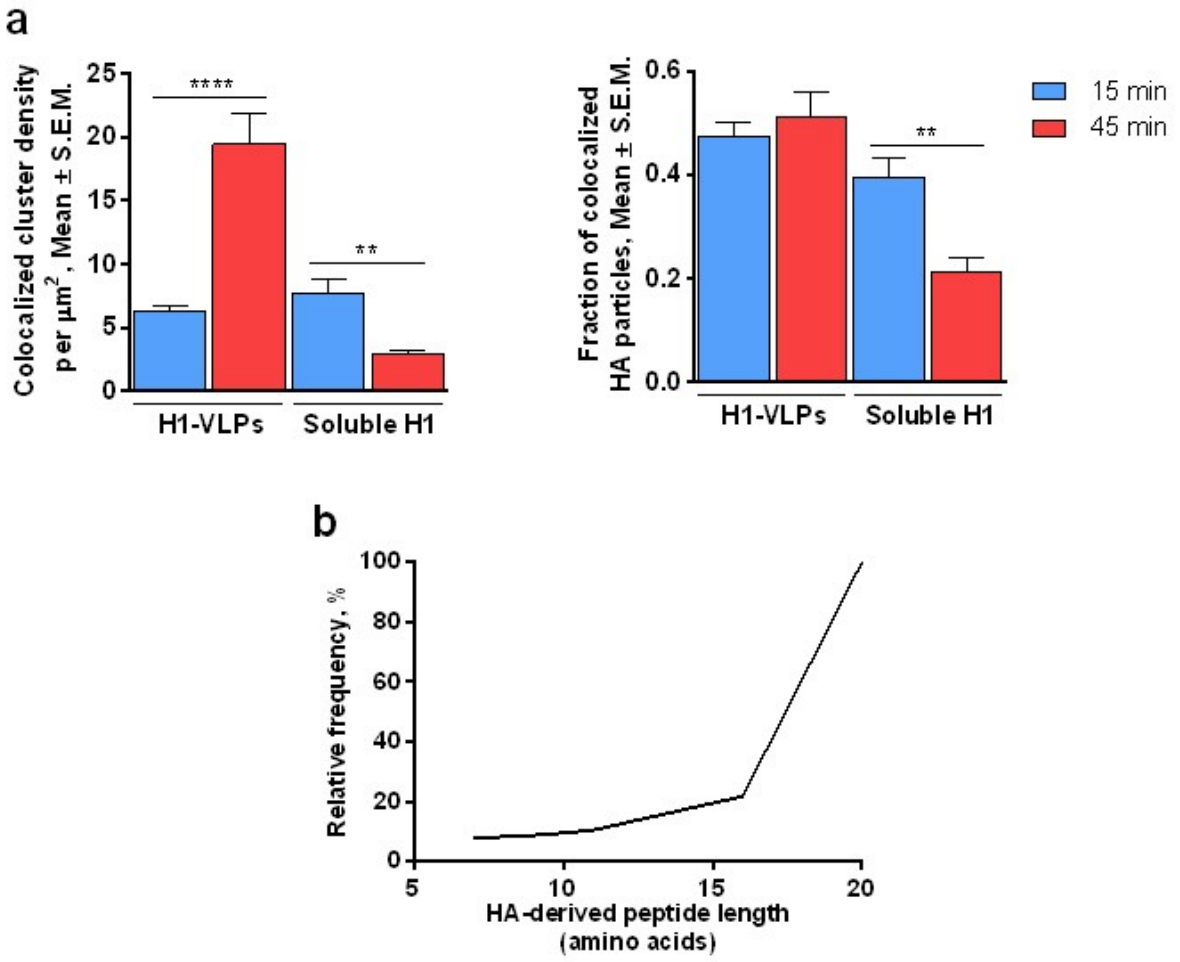

Figure 3. 4. HA cross-presentation by human MDMs exposed to H1-VLPs

(a) Segmentation ICCS analysis of HA colocalization with MHC I. The colocalization (number of colocalized particles per μm^2 - left) and colocalized fraction of HA (right) with MHC I presented. Based on 3 experiments. ** $p<0.01$, **** $p<0.0001$. **(b)** Cumulative curve shows the distribution by length (number of amino acids) of the HA-derived peptides detected from H1-VLP-treated MDMs.

3.11. SUPPLEMENTAL INFORMATION

Plant-derived virus-like particle vaccines drive cross-presentation of influenza A hemagglutinin peptides by human monocyte-derived macrophages

Alexander I. Makarkov, Makan Golizeh, Angelica A. Gopal, Ian N. Costas-Cancelas, Sabrina Chierzi, Stephane Pillet, Nathalie Charland, Nathalie Landry, Isabelle Rouiller, Paul W. Wiseman, Momar Ndao, Brian J. Ward

Supplemental Materials and Methods

Endocytosis inhibitors screening

A number of endocytosis inhibitors were screened based on their effect on virus-like particles (VLPs) internalization measured by 1,1'-dioctadecyl-3,3,3',3'-tetramethylindodicarbocyanine perchlorate (DiD - Thermo Fisher Scientific, Eugene, OR) fluorescence dequenching upon VLP fusion with cell membranes. H1-VLPs (influenza hemagglutinin (HA) protein based on the sequence of A/California/07/2009 H1N1 virus, Medicago Inc., Quebec, QC) were labelled with DiD (see Materials and methods section of the manuscript). B10R cell culture (an immortalized murine bone marrow-derived macrophage cell line) was maintained in RPMI-1640 with 50 IU/mL penicillin, 50 µg/mL streptomycin and 10 mM HEPES (medium) supplemented with 10% fetal bovine serum (FBS, all from Wisent, Saint-Jean-Baptiste, QC) until reaching cell confluency. B10R cells were detached from plastic flask surface using 0.25% trypsin/2.21 mM EDTA in HBSS (Wisent) and plated on 96-well Nunclon Delta black flat-bottom plates (Thermo Fisher Scientific, Roskilde, Denmark) at 5 x 10^4 cells per well. The following day, B10R cells in triplicate wells were exposed to DiD-labelled VLPs in the medium (HA concentration 15.0 µg/mL); plates were kept at 4°C for one hour and then washed with ice-cold medium twice. Endocytosis inhibitors were applied in ice-cold medium supplemented with 10% FBS (100 µL/well): dynasore hydrate (50 µM), chlorpromazine hydrochloride (10 µg/mL), sucrose (0.45 M), pitstop 2 (25 µM), genistein (200 µM), filipin III from *Streptomyces filipinensis* (5 µg/mL), amiloride hydrochloride (1 mM), cytochalasin D (4 µM) (all from Sigma-Aldrich, St. Louis, MO). Pitstop 2 was also tested at the same concentration in serum-free medium. The plates were placed into a pre-heated (37°C) spectrophotometer (Infinite 200 PRO, Tecan, Männedorf, Switzerland), and DiD fluorescence was measured at 15-min intervals over 2 h. Fusion efficiency (%) was determined following addition of Triton X-100 (Sigma-Aldrich) to each well (final concentration 1%) to obtain full DiD dequenching.

Toxicity assessment of endocytosis inhibitors

B10R cell culture was maintained in the medium supplemented with 10% FBS until reaching cell confluency. B10R cells were detached from plastic flask surface using 0.25%

trypsin/2.21 mM EDTA in HBSS and plated on 96-well Nunclon Delta black flat-bottom plates at 5 x 10^4 cells per well. The following day, endocytosis inhibitors (see the endocytosis inhibitors screening section and the Supplemental Table 3.1) in the medium supplemented with 10% FBS were applied to B10R cells in triplicate wells in a volume 100 µL/well (5% CO_2, 37°C for 2 h). Pitstop 2 was also tested in serum-free medium. 0.01% solution of Triton X-100 served as a positive control. The effects of endocytosis inhibitors on B10R cells viability were evaluated in parallel experiments with the CytoTox-ONE™ homogeneous membrane integrity assay and the CellTiter-Glo® 2.0 assay (both from Promega, Madison, WI). Cell membrane integrity was assessed by lactate dehydrogenase (LDH) release. CytoTox-ONE™ reagent (100 µL/well) was applied for 10 min at RT. Stop solution (50µl) was then added to each well, and the fluorescence was measured on Infinite 200 PRO spectrophotometer at excitation and emission wavelengths 560 and 600 nm, respectively. The results were reported as a % of the maximum LDH release caused by adding lysis solution to the control wells. The effects of endocytosis inhibitors on metabolically active cells were quantitated by the amount of ATP with CellTiter-Glo® luminescent cell viability assay. CellTiter-Glo® 2.0 reagent (100 µl/well) was applied for 10 min at RT. Luciferase luminescence was measured on Infinite 200 PRO spectrophotometer. The results were reported as a % of ATP level reduction compared to control wells unexposed to any endocytosis inhibitor.

Conventional image analysis

Confocal microscopy images were analyzed with ImageJ software (1) for the purpose of evaluation the fluorescence intensity of immunolabelled HA or fluorophore-conjugated transferrin, or for the assessment of colocalization of HA with endosomal markers Rab5, Rab7 and Rab11 as described elsewhere (2). In brief, to analyze the HA or transferrin fluorescence intensity per cell area we identified cellular boundaries on the brightfield channel, and used them to establish the regions of interest (ROIs) on the fluorescent channel(s). Then we determined the background fluorescence intensity in each experiment by averaging the values obtained from cells in the control sample (for HA: monocyte-derived macrophages (MDMs) unexposed to HA but stained with anti-HA primary and fluorescent secondary antibody; for transferrin: MDMs unexposed to transferrin). The average background fluorescence intensity was subtracted from the fluorescence values measured from HA or transferrin-exposed cells. For ‘cell-based’

colocalization analysis, both ‘green’ and ‘red’ channels were denoised with ImageJ PureDenoise plugin (3), then image background was subtracted with the ‘rolling ball’ algorithm (4). HA colocalization with endosomal markers was determined within cell boundaries-defined ROIs (see above) using Colocalization Threshold plugin (5); Costes thresholding approach was applied (6). Pearson correlation coefficient R, Pearson coefficient for pixels whose intensity falls above a threshold value R (>t), and Manders above threshold colocalization coefficients tM1 and tM2 were analyzed (2,7,8).

Supplemental Table 3. 1. Endocytosis inhibitors used in screening experiments and their suggested mechanism of action

Inhibitor of endocytosis	Tested concentration / condition	Suggested mechanism of action	Toxicity
Dynamin-dependent endocytosis			
Dynasore	50 µM	Non-competitive and reversible inhibitor of GTPase activity of dynamin.(9) Dynasore suppresses both CME and CIE (10,11).	Non-toxic
Clathrin-mediated endocytosis (CME)			
Chlorpromazine	10 – 100 µg/mL	Not well understood. It has been suggested that chlorpromazine causes AP-2 and clathrin relocation from plasma membrane to endosomal membranes and therefore depletes AP-2 and clathrin from the plasma membrane and prevents clathrin-coated endocytic vesicles formation (12). Chlorpromazine probably affects dynamin activity (13).	Non-toxic at 10 µg/mL. Toxicity observed at higher concentrations
Hyperosmotic sucrose	0.45 M	Not well understood. It has been suggested that hyperosmolarity leads to trapping clathrin in 'microcages' and depleting it from plasma membrane (14).	Greatly reduced ATP level in cells
Pitstop 2	25 µM (applied in serum-free or 10% FBS supplemented medium)	Not well understood. Pitstop 2 was developed as cell-permeable selective CME inhibitor (15). However, later pitstop 2 has been shown to potently inhibit CIE (16,17).	Toxic in serum-free medium (recommended use due to sequestering by serum albumins)
Clathrin-Independent Endocytosis			
Genistein	200 µM	Tyrosine-kinase inhibitor (18). Phosphorylation of tyrosine at caveolin-1 is the prerequisite for pinching off caveolar vesicles from plasma membrane (19).	Non-toxic
Filipin III	5 µg/mL	Cholesterol depleting and lipid-raft disrupting agent (20).	Moderate cytotoxicity and massive ATP level reduction.
Macropinocytosis			

Amiloride	1 mM	Inhibition of Na^+/H^+ exchange leads to lowering submembranous pH and preventing Rac1 and Cdc42 signaling that is essential for actin remodeling (21).	Non-toxic
Phagocytosis / macropinocytosis			
Cytochalasin D	4 μM	Blocking of actin polymerization, disassembly of actin cytoskeleton (22,23).	Non-toxic

Supplemental Table 3. 2. HA-derived peptides associated with major histocompatibility complex (MHC) I identified in MDM lysates using high-resolution tandem mass spectrometry analysis

##	Sequence *	Length	Mass	Start position	End position	Charge state	PEP	MS/MS Count	Sample
1	AILVVLLYTFATANADTLCI	20	2124.1541	3	22	2	0.01	2	D
2	VVLLYTFATANADTLCIGYH	20	2184.0925	6	25	3	0.01	1	D
3	LYTFATANADTLCIGYHANN	20	2171.9946	9	28	3	0.01	1	D
4	LCIGYHA	7	775.3687	20	26	2	0.01	1	B
5	LCIGYHANNSTDTVDTVLEK	20	2192.0419	20	39	3	0.01	1	D
6	CIGYHAN	7	776.3276	21	27	2	0.01	1	B
7, 8	**GYHANNSTDTVDTVLEKNVT**	**20**	**2177.0237**	**23**	**42**	**3**	**0.01**	**3(A), 2(D)**	**A, D**
9, 10	**DTVLEKNVTVTHSVNLLEDK**	**20**	**2253.1852**	**34**	**53**	**3(A), 2(D)**	**0.01**	**1**	**A, D**
11	LEDKHNGKLCKLRGVAPLHL	20	2240.2576	50	69	3	0.01	1	D
12	GKLCKLRGVAPLHLGK	16	1689.0236	56	71	3	0.01	1	C
13	LRGVAPLHLGKCNIAGWILG	20	2087.1826	61	80	2	0.01	1	A
14	PLHLGKC	7	766.4160	66	72	2	0.01	1	B
15	LGNPECESLSTASSWSYIVE	20	2170.9729	79	98	3	0.01	1	D
16	LSTASSWSY	9	1000.4502	87	95	2	0.00	1	A
17	TASSWSYIVETPSSDNGTCY	20	2166.9052	89	108	3	0.01	1	D
18	SWSYIVETPSSDNGTCYPGD	20	2176.8895	92	111	2	0.01	2	A
19	VETPSSDNGTCYPGDFIDYE	20	2207.8841	97	116	3	0.01	1	D
20	ETPSSDNGTCYPGDFIDYEE	20	2237.8583	98	117	3	0.01	1	A
21	PSSDNGT	7	676.2664	100	106	2	0.01	1	B
22	PSSDNGTCYPGDFIDYEELR	20	2276.9532	100	119	3	0.01	1	D
23	CYPGDFI	7	813.3367	107	113	2	0.01	1	B
24	YEELREQLSSVSSFERFEIF	20	2494.2016	115	134	3	0.01	1	A
25	VSSFERFEIFPKTSSWPNHD	20	2409.1390	125	144	3	0.01	1	D
26	RFEIFPKTSSWPNHDSNKGV	20	2345.1553	130	149	2	0.01	1	D
27	SSWPNHDSNKGVTAACPHAG	20	2034.8966	138	157	3	0.01	2	D

28	SNKGVTAACPHAGAKSFYKN	20	2050.0054	145	164	3	0.01	1	D
29	KGVTAACPHAGAKSFYKNLI	20	2075.0986	147	166	3	0.01	1	D
30	HAGAKSF	7	716.3606	155	161	2	0.01	2	B
31	AKSFYKNLIWLVKKGNSYPK	20	2383.3416	158	177	3	0.01	2	D
32	NLIWLVKKGNSYPKLSKSYI	20	2350.3413	164	183	3	0.01	2	D
33	IWLVKKGNSYPKLSKS	16	1847.0669	166	181	2	0.01	1	C
34	WLVKKGNSYPKLSKSYINDK	20	2367.2951	167	186	3	0.01	1	D
35	VKKGNSYPKLSKSYINDKGK	20	2253.2481	169	188	3	0.01	1	A
36	KLSKSYINDKGKEVLVLWGI	20	2289.3097	177	196	3	0.01	2	D
37	SKSYINDKGKEVLVLWGIHH	20	2322.2485	179	198	3	0.01	1	D
38	NDKGKEVLVLWGIHHPPTSA	20	2197.1644	184	203	3	0.01	1	A
39	DKGKEVLVLWGIHHPSTSAD	20	2188.1277	185	204	3	0.01	1	A
40	EVLVLWGIHHPSTSADQQSL	20	2216.1226	189	208	3	0.01	1	D
41	LWGIHHPSTSADQQSLYQNA	20	2252.0610	193	212	3	0.01	1	D
42	PSTSADQ	7	704.2977	199	205	2	0.01	1	B
43	LYQNADAYVFVGSSRY	16	1851.8792	208	223	3	0.01	1	C
44	YVFVGSSRYSKKFKPEIAIR	20	2374.3161	215	234	3	0.01	2	D
45	VFVGSSRYSKKFKPEIAIRP	20	2308.3056	216	235	3	0.01	3	D
46	SSRYSKKFKPEIAIRPKVRD	20	2404.3703	220	239	3	0.01	1	D
47	SRYSKKFKPEIAIRPKVRDR	20	2473.4394	221	240	3	0.01	1	A
48	RYSKKFKPEIAIRPKVRDRE	20	2515.4499	222	241	3	0.01	1	D
49	SKKFKPEIAIRPKVRD	16	1911.1418	224	239	3	0.01	3	C
50	KFKPEIAIRPKVRDREGRMN	20	2439.3645	226	245	3	0.01	1	D
51	KPEIAIRPKVRDQEGR	16	1891.0752	228	243	3	0.01	1	C
52	IRPKVRDREGRMNYYWTLVE	20	2580.3383	233	252	3	0.01	1	D
53	RDREGRMNYYWTLVEPGDKI	20	2497.2172	238	257	3	0.01	1	D
54	PGDKITFEATG	11	1134.5557	253	263	3	0.00	1	B
55	ATGNLVVPRYAFAMERNAGS	20	2123.0582	261	280	2	0.01	1	A
56, 57	**YAFAMERNAGSGIIISDTPV**	**20**	**2111.0357**	**270**	**289**	**2**	**0.01**	**1**	**A, D**
58	FAMERNAGSGIIISDTPVHD	20	2129.0212	272	291	2	0.01	1	D

59	AGSGIIISDTPVHDCNTTCQ	20	2030.9037	278	297	3	0.01	1	D
60	SGIIISDTPVHDCNTTCQTP	20	2100.9456	280	299	3	0.01	1	A
61, 62	**SDTPVHDCNTTCQTPKGAIN**	**20**	**2100.9205**	**285**	**304**	**2(A), 3(D)**	**0.01**	**1**	**A, D**
63	TPVHDCNTTCQTPKGAINTS	20	2086.9412	287	306	3	0.01	1	A
64	KGAINTSLPFQNIHPI	16	1748.9574	300	315	2	0.01	1	C
65	GAINTSLPFQNIHPITIGKC	20	2123.1197	301	320	3	0.01	1	A
66	PITIGKCPKYVKSTKL	16	1775.0379	314	329	3	0.01	1	C
67	YVKSTKLRLATGLRNI	16	1832.0996	323	338	3	0.01	1	C
68	YVKSTKLRLATGLRNIPSIQ	20	2257.3270	323	342	3	0.01	1	D
69	TKLRLATGLRNIPSIQ	16	1780.0683	327	342	3	0.01	1	C
70	RLATGLRNIP	10	1109.6669	330	339	2	0.00	1	C
71	LATGLRNIPSIQSRGLFGAI	20	2083.1902	331	350	3	0.01	1	D
72	RNIPSIQSRGLFGAIAGFIE	20	2145.1695	336	355	3	0.01	1	D
73	IPSIQSRGLFGAIAGFIEGG	20	1989.0684	338	357	2	0.01	1	D
74	SIQSRGLFGAIAGFIEGGWT	20	2066.0585	340	359	3	0.01	1	D
75, 76	**LFGAIAGFIEGGWTGMVDGW**	**20**	**2082.9873**	**346**	**365**	**3**	**0.01**	**1(A), 6(D)**	**A, D**
77	IAGFIEGGWTGMVDGWYGYH	20	2214.9833	350	369	3	0.01	1	D
78	GFIEGGWTGMVDGWYGYHHQ	20	2295.9796	352	371	3	0.01	1	D
79	GYHHQNEQGSGYAADLKSTQ	20	2189.9726	367	386	3	0.01	1	A
80	STQNAIDEITNKVNSVIEKM	20	2233.1260	384	403	3	0.01	1	D
81	FTAVGKEFNHLEKRIENLNK	20	2386.2757	407	426	3	0.01	1	D
82	EFNHLEKRIENLNKKVDDGF	20	2444.2448	413	432	3	0.01	1	D
83	FNHLEKRIENLNKKVDDGFL	20	2428.2863	414	433	3	0.01	1	D
84	LEKRIEN	7	900.5029	417	423	3	0.01	1	B
85, 86	**NKKVDDGFLDIWTYNAELLV**	**20**	**2352.2002**	**425**	**444**	**3**	**0.01**	**1**	**A, D**
87	VDDGFLDIWTYNAELLVLLE	20	2337.1780	428	447	3	0.01	1	D
88	DDGFLDIWTYNAELLVLLEN	20	2352.1525	429	448	2;3	0.01	2	D
89	DIWTYNAELLVLLENERTLD	20	2419.2271	434	453	3	0.01	1	D
90	LVLLENERTLDYHDSN	16	1929.9432	443	458	3	0.01	1	C
91, 92	**LLENERTLDYHDSNVKNLYE**	**20**	**2464.1870**	**445**	**464**	**2**	**0.01**	**1**	**A, D**

93	LDYHDSNVKNLYEKVRSQLK	20	2448.2761	452	471	3	0.01	1	D
94	SNVKNLYEKVRSQLKNNAKE	20	2361.2765	457	476	2	0.01	1	D
95	VKNLYEKVRSQLKNNA	16	1903.0639	459	474	2	0.01	1	C
96	RSQLKNNAKEIGNGCFEFYH	20	2354.1226	467	486	3	0.01	1	D
97	NNAKEIGNGCFEFYHKCDNT	20	2302.9736	472	491	3	0.01	2	D
98	GNGCFEFYHKCDNTCMESVK	20	2310.9166	478	497	2	0.01	1	D
99	EFYHKCDNTCMESVKNGTYD	20	2382.9555	483	502	2	0.01	1	D
100	CDNTCMESVKNGTYDYPKYS	20	2316.9337	488	507	3	0.01	1	A
101	TCMESVK	7	796.3459	491	497	2	0.01	1	B
102	KNGTYDYPKYSEEAKLNREE	20	2433.1448	497	516	3	0.01	1	D
103	REEIDGVKLESTRIYQILAI	20	2345.2955	514	533	2	0.01	1	D
104	DGVKLESTRIYQILAIYSTV	20	2268.2365	518	537	2	0.01	1	D
105	STRIYQILAIYSTVASSLVL	20	2197.2358	524	543	3	0.01	1	D
106	RIYQILAIYSTVASSL	16	1797.0036	526	541	2	0.01	1	C
107, 108	**QILAIYSTVASSLVLVVSLG**	**20**	**2032.1820**	**529**	**548**	**3**	**0.01**	**3(A), 2(D)**	**A, D**
109	AIYSTVASSLVLVVSLGAIS	20	1949.1085	532	551	3	0.01	1	D
110	IYSTVASSLVLVVSLGAISF	20	2025.1398	533	552	3	0.01	1	D
111	STVASSLVLVVSLGAISFWM	20	2066.1122	535	554	2	0.01	1	D
112	VASSLVLVVSLGAISFWMCS	20	2068.0737	537	556	3	0.01	1	A
113	VASSLVLVVSLGAISF	16	1560.9127	537	552	3	0.01	1	C
114	LVLVVSLGAISFWMCSNGSL	20	2095.0846	541	560	3	0.01	1	A
115	SLGAISFWMCSNGSLQCRIC	20	2174.9734	546	565	3	0.01	2	D

*** sequences found in more than one sample highlighted in bold font**

Supplemental Figures

a

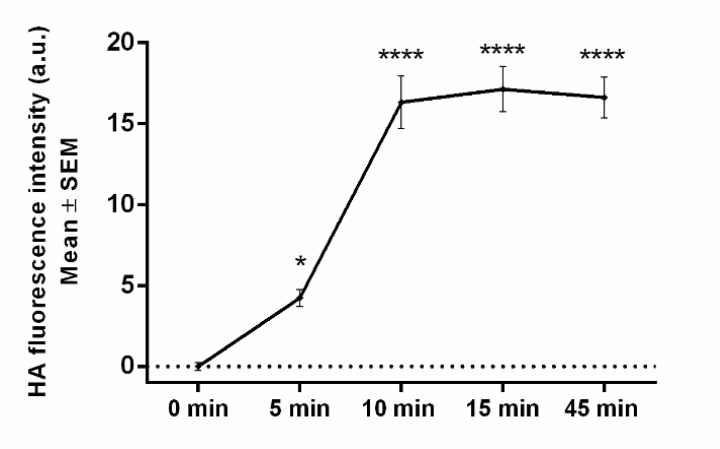

b

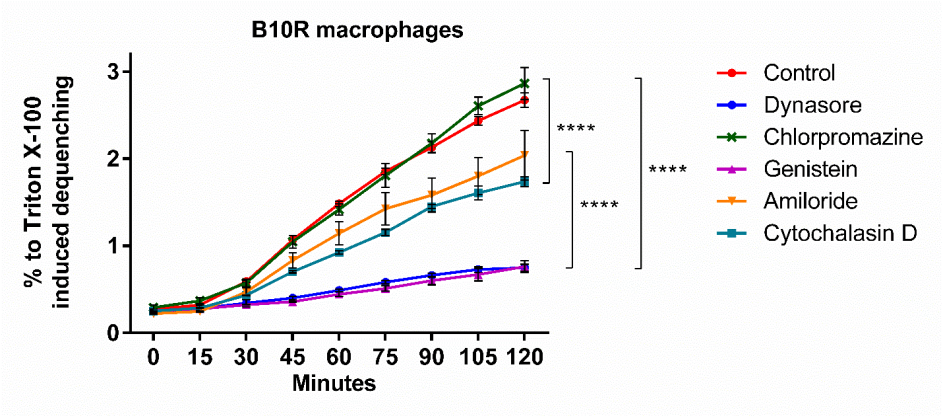

c

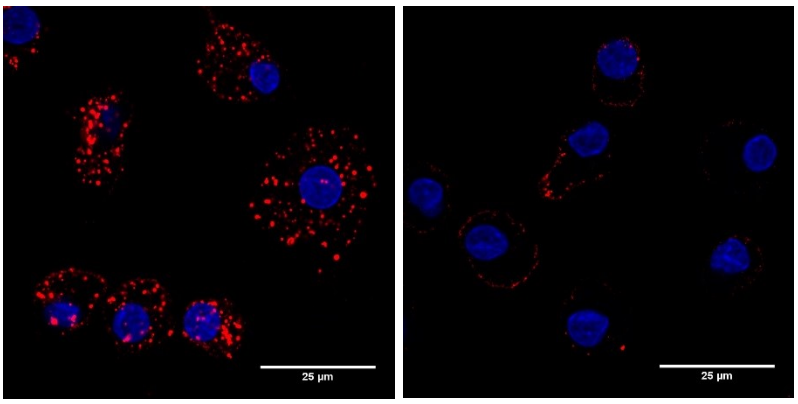

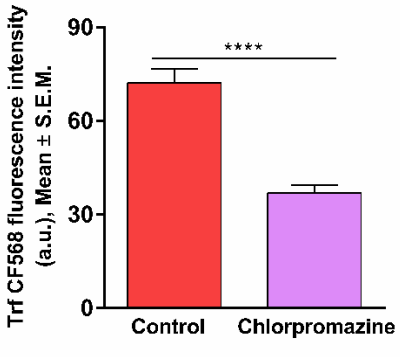

(continued on next page)

d

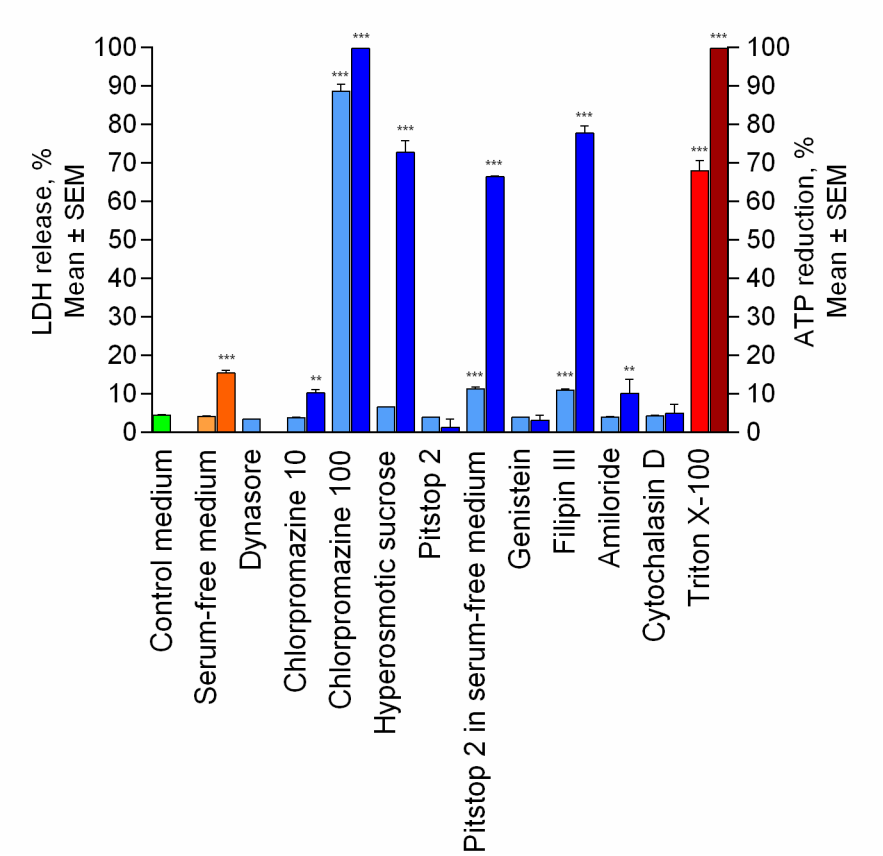

Supplemental Figure 3. 1. Endocytic pathways in human and murine macrophages

(a) Time-course of HA internalization by human MDMs. The amount of internalized protein was evaluated by the intensity of HA immunofluorescence per cell area on confocal microscopy images. The fluorescence intensity increased by 10 min and then remained at the same level up to 45 min. Based on three experiments. **(b)** Effects of selected endocytosis inhibitors on DiD fluorescence dequenching by murine B10R macrophages loaded with DiD-labeled H1-VLPs (n=3). Chlorpromazine (10 µg/mL) did not affect DiD fluorescence. **(c)** Chlorpromazine (10 µg/mL) reduced transferrin (Trf) uptake by human MDMs. Representative images of the control sample treated with fluorescently-labelled transferrin (left), cell exposed to transferrin in the presence of chlorpromazine (middle) and the analysis of transference fluorescence intensities (right) are presented; based on three experiments. Red: transferrin conjugated with CF568

(legend continued on next page)

fluorophore, blue: nuclei stained with DAPI. **(d)** Cytotoxic effects of endocytosis inhibitors on murine B10R macrophages assessed by LDH release (left Y axis) and ATP level reduction (right Y axis) (n=3). * $p<0.05$, ** $p<0.01$, *** $p<0.001$, **** $p<0.0001$.

a

H1-VLPs, 15 min

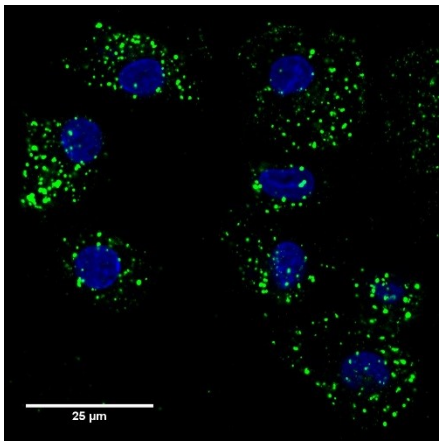

Soluble H1, 15 min

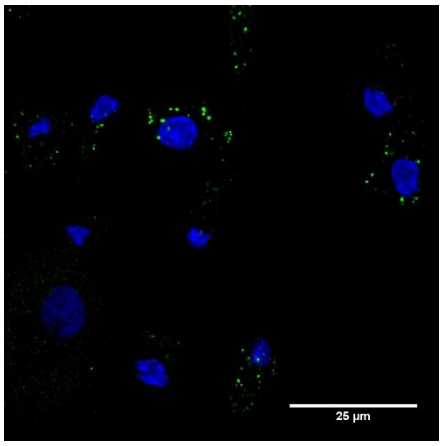

H1-VLPs, 45 min

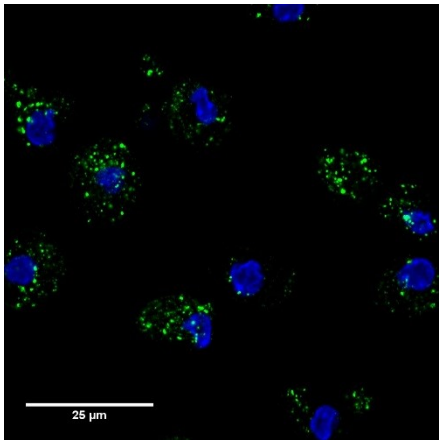

Soluble H1, 45 min

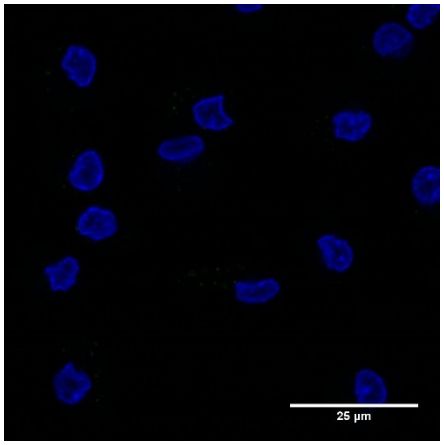

b

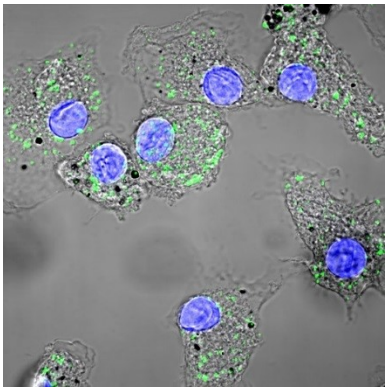

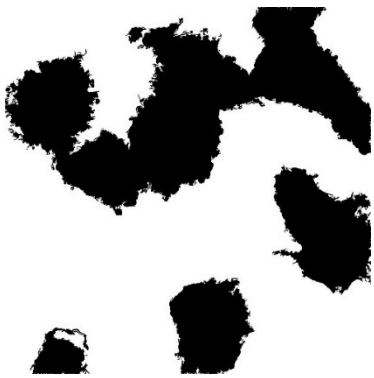

(legend on next page)

Supplemental Figure 3. 2. HA internalization by human MDMs exposed to H1-VLPs or soluble H1

(a) Representative images of MDMs pulsed (15 min) with H1-VLPs or soluble H1 at 15 min and 45 min. Green: fluorescently labeled HA, blue: nuclei stained with DAPI. **(b)** Examples of image segmentation strategies. Left - bright-field image of MDMs with internalized HA (green) and nuclei stained with DAPI (blue). Image segmentation based on identification of cell boundaries – entire cell area (center). Image segmentation based on detecting HA-positive endosomes (right).

a

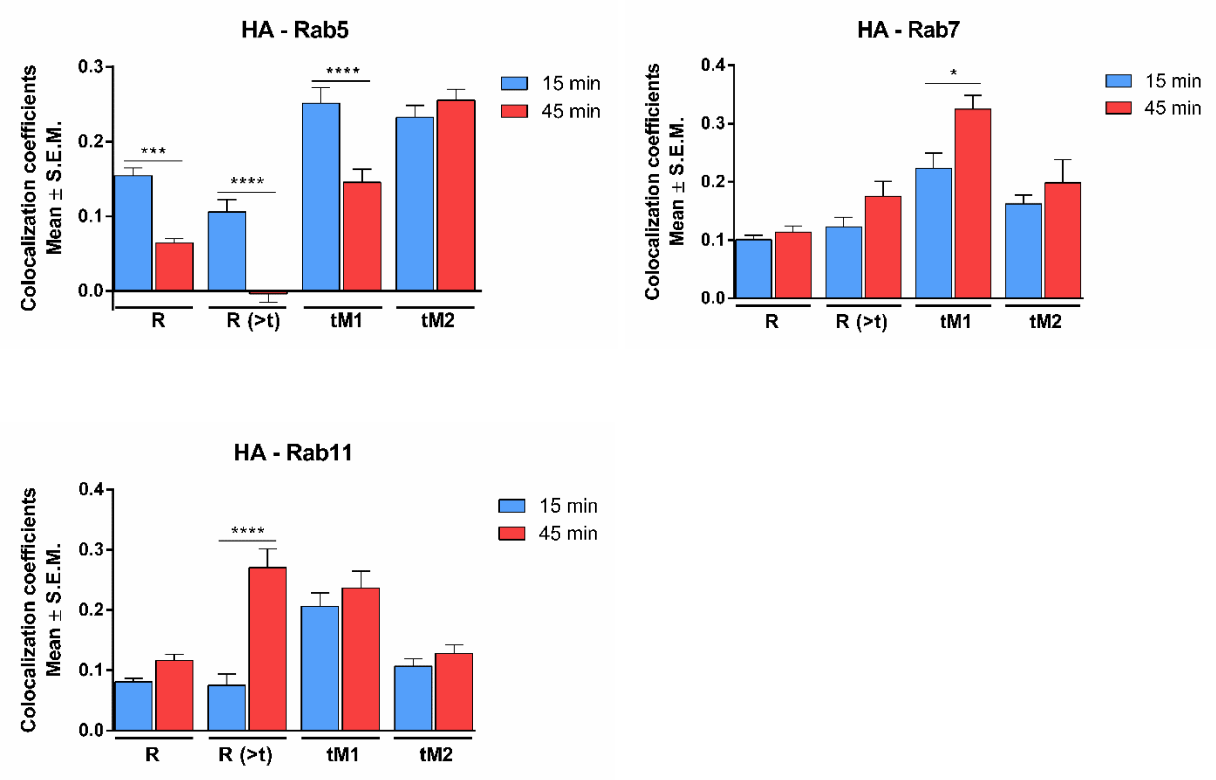

b

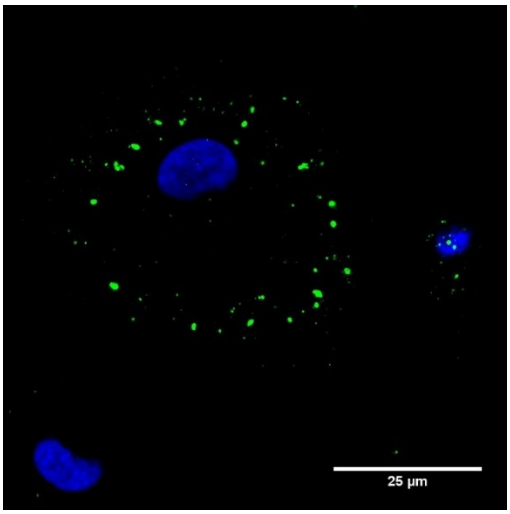

(legend on next page)

Supplemental Figure 3. 3. Endosomal trafficking of HA in MDMs pulsed (15 min) with H1-VLPs or soluble H1

(a) Conventional analysis of HA colocalization with Rab5, Rab7 or Rab11. Based on three or more experiments for each condition. * $p<0.05$, *** $p<0.001$, **** $p<0.0001$. **(b)** Representative image of MDM pulsed with H1-VLPs at 45 min. Peripheral (towards the plasma membrane) re-distribution (recycling) of non-degraded HA can be seen. Green: fluorescently labeled HA, blue: nuclei stained with DAPI.

Supplemental references

1. Schneider CA, Rasband WS, Eliceiri KW. NIH Image to ImageJ: 25 years of image analysis. Nat Methods. 2012;9(7):671–5.
2. Pike JA, Styles IB, Rappoport JZ, Heath JK. Quantifying receptor trafficking and colocalization with confocal microscopy. Methods. 2017;115:42–54.
3. Luisier F. High-quality denoising of multidimensional fluorescence microscopy images (2D+t, 3D or color) . Biomedical Imaging Group (BIG), EPFL, Switzerland. 2014. Available from: http://bigwww.epfl.ch/algorithms/denoise/
4. Castle M, Keller J. Rolling Ball Background Subtraction . Mental Health Research Institute, University of Michigan. 2015. Available from: https://imagej.net/Rolling_Ball_Background_Subtraction
5. Collins T. Colocalization Threshold. 2015. Available from: https://imagej.net/Colocalization_Threshold
6. Costes S V, Daelemans D, Cho EH, Dobbin Z, Pavlakis G, Lockett S. Automatic and quantitative measurement of protein-protein colocalization in live cells. Biophys J. 2004;86(6):3993–4003.
7. Dunn KW, Kamocka MM, McDonald JH. A practical guide to evaluating colocalization in biological microscopy. AJP Cell Physiol. 2011;300(4):C723–42.
8. Bolte S, Cordelières FP. A guided tour into subcellular colocalization analysis in light microscopy. Journal of Microscopy. 2006;224:213–32.
9. Macia E, Ehrlich M, Massol R, Boucrot E, Brunner C, Kirchhausen T. Dynasore, a Cell-Permeable Inhibitor of Dynamin. Dev Cell. 2006;10(6):839–50.
10. Delvendahl I, Vyleta NP, von Gersdorff H, Hallermann S. Fast, Temperature-Sensitive and Clathrin-Independent Endocytosis at Central Synapses. Neuron. 2016;90(3):492–8.
11. Preta G, Cronin JG, Sheldon IM. Dynasore - Not just a dynamin inhibitor. Cell Communication and Signaling. 2015;13:24.
12. Wang LH, Rothberg KG, Anderson RGW. Mis-assembly of clathrin lattices on endosomes reveals a regulatory switch for coated pit formation. J Cell Biol. 1993;123(5):1107–17.
13. Daniel JA, Chau N, Abdel-Hamid MK, Hu L, von Kleist L, Whiting A, et al. Phenothiazine-Derived Antipsychotic Drugs Inhibit Dynamin and Clathrin-Mediated

Endocytosis. Traffic. 2015;16(6):635–54.

14. Heuser JE, Anderson RGW. Hypertonic media inhibit receptor-mediated endocytosis by blocking clathrin-coated pit formation. J Cell Biol. 1989;108(2):389–400.
15. Von Kleist L, Stahlschmidt W, Bulut H, Gromova K, Puchkov D, Robertson MJ, et al. Role of the clathrin terminal domain in regulating coated pit dynamics revealed by small molecule inhibition. Cell. 2011;146(3):471–84.
16. Willox AK, Sahraoui YME, Royle SJ. Non-specificity of Pitstop 2 in clathrin-mediated endocytosis. Biol Open. 2014;3(5):326–31.
17. Dutta D, Williamson CD, Cole NB, Donaldson JG. Pitstop 2 Is a Potent Inhibitor of Clathrin-Independent Endocytosis. PLoS One 2012;7(9):e45799.
18. Akiyama T, Ishida J, Nakagawa S, Ogawara H, Watanabe S, Itoh N, et al. Genistein, a specific inhibitor of tyrosine-specific protein kinases. J Biol Chem. 1987;262(12):5592–5.
19. Tiruppathi C, Song W, Bergenfeldt M, Sass P, Malik AB. Gp60 activation mediates albumin transcytosis in endothelial cells by tyrosine kinase-dependent pathway. J Biol Chem. 1997;272(41):25968–75.
20. Orlandi PA, Fishman PH. Filipin-dependent inhibition of cholera toxin: Evidence for toxin internalization and activation through caveolae-like domains. J Cell Biol. 1998;141(4):905–15.
21. Koivusalo M, Welch C, Hayashi H, Scott CC, Kim M, Alexander T, et al. Amiloride inhibits macropinocytosis by lowering submembranous pH and preventing Rac1 and Cdc42 signaling. J Cell Biol. 2010;188(4):547–63.
22. Elliott JA, Winn WC. Treatment of alveolar macrophages with cytochalasin D inhibits uptake and subsequent growth of Legionella pneumophila. Infect Immun. 1986;51(1):31–6.
23. Kuhn DA, Vanhecke D, Michen B, Blank F, Gehr P, Petri-Fink A, et al. Different endocytotic uptake mechanisms for nanoparticles in epithelial cells and macrophages. Beilstein J Nanotechnol. 2014;5(1):1625–36.

Chapter 4: MHC I-restricted immunopeptidomics analysis of human monocyte-derived macrophages exposed to biological nanoparticles bearing influenza hemagglutinin

Makan Golizeh[1,†], Alexander I. Makarkov[1,†], Nathalie Landry[2], Brian J. Ward[1,2], Momar Ndao[1]

[1] Infectious Diseases and Immunity in Global Health Program, Research Institute of the McGill University Health Centre, 1000 Decarie Street, Montreal, Quebec, H4A 3J1, Canada
[2] Medicago Inc., 1020 route de l'Église, Quebec, Quebec, G1V 2V9, Canada

[†] These authors contributed equally to this work.

This article has been submitted to *Molecular & Cellular Proteomics*.

4.1. PREFACE

In chapter 3 of this thesis, we described the bidirectional model of endosomal trafficking of HA-bearing VLPs. While a portion of internalized HA was handled in high-degradative mature endosomes that facilitate protein cleavage by lysosomal proteases and peptidases, and presentation of antigenic peptides in a context of MHC II molecules, another portion of HA was retained in low-degradative static early and/or recycling endosomes that support antigen cross-presentation. Using nano-flow ultra-high pressure liquid chromatography high-resolution mass spectrometry, we were able to characterize the HA-derived peptide pool associated with MHC I molecules in H1-VLP-treated MDM. In this chapter, we examined the MHC I-restricted peptides derived from host proteins after the exposure of human MDM to either H1-VLP or soluble H1 protein.

4.2. ABSTRACT

Recent advances in mass spectrometry-based proteomics have greatly expanded our knowledge about the peptide repertoire presented by major histocompatibility complex (MHC) molecules that is referred to as immunopeptidome. To date, immunopeptidome studies have focused on discovery of tumor neoantigens and exploring the MHC-restricted peptide landscape

in inflammation and autoimmunity, transplantation and infections. Major changes in the host immunopeptidome are observed in virus-infected cells, suggesting that the host peptide repertoire may provide insight into the mechanisms of cell responses to pathogen invasion as well as infected cell – immune system interactions. In this study, primary human monocyte-derived macrophages were exposed to plant-derived virus-like particles (VLPs) bearing influenza A hemagglutinin (HA) or soluble influenza HA, as control. Immunopurified MHC class I-associated peptides were analysed by nano-flow high pressure liquid chromatography coupled to high-resolution dopant-assisted electrospray ionisation mass spectrometry. A total of 109 host-derived MHC I peptides were identified in the VLP-treated samples, two of which were also detected in controls. The peptides unique to VLP treatment were, on average, ~13 amino acid residues long, more basic and hydrophilic, and were mainly processed via proteolysis by matrix metalloproteinases and cathepsins. The proteins associated with these peptides were primarily involved in cellular, metabolic and regulatory processes and activated several pathways including inflammation stimulation and attenuation, response to stimuli, innate and adaptive immunity, clathrin-mediated endocytosis, protein synthesis and endo-lysosomal degradation. This study is the first report to describe the response of a primary human antigen-presenting cell to nanoparticulate vs. soluble antigen exposure from an immunopeptidomics point of view.

4.3. INTRODUCTION

The repertoire of peptides associated with and presented by major histocompatibility complex (MHC) molecules is referred to as the immunopeptidome (1–3) or the human leukocyte antigen (HLA) ligandome (4,5). These peptides rise either from the host proteins that have undergone degradation through the ubiquitination/proteasomal pathway or from exogenous proteins subjected to endosomal or cytosolic processing and presentation (6,7). The MHC molecules are generally divided into two classes: MHC I that are expressed on all nucleated cells and mediate recognition of the antigenic peptides by $CD8^+$ T cells (8) and MHC II that are normally expressed on the surface of antigen-presenting cells (APCs) such as macrophages, dendritic cells, B lymphocytes and monocytes, delivering antigen-specific stimuli to $CD4^+$ T cells (9). The immunopeptidome is a critical component of the immune recognition and self/non-self discrimination, and immunopeptidome research can theoretically make major contributions

to the development of next-generation vaccines and immunotherapeutics aiming to control autoimmunity, infection and cancer burden (10–12).

Mass spectrometry (MS) is the method of choice for the study of proteins and peptides in biological samples (13). Recent developments in sample processing and enrichment, protein and peptide separation, MS instrumentation and acquisition methods have increased the efficiency of proteomic analyses (14). However, unlike conventional proteomics, immunopeptidomics often requires target-specific enrichment and high-sensitivity MS analysis to increase the sequencing coverage, depth, and confidence of MHC-associated peptides, in a more of a 'sniper' rather than a 'shotgun' fashion (3).

Thus far, immunopeptidomics has focused primarily on the identification of tumor-specific neoantigens expressed on the surface of malignant or transformed tissues and cell lines (4,10,15). The immunological rationale behind these studies is that abnormal proteins associated with tumor transformation and progression give rise to tumor-specific amino acid sequences that are presented on the MHC I molecules. Tumor surveillance performed is thought to be based primarily on the recognition of these tumor-specific peptide–MHC complexes by cytotoxic $CD8^+$ lymphocytes, facilitating the elimination of transformed cells (16). Immunopeptidomic studies usually exploit immortalized malignant cells and cell lines to harvest large amounts of peptides from as many as 10^8–10^{10} cells (2,5,17). However, modern MS-based methodologies have recently made the immunopeptidome of primary cells accessible (18,19), and the spectrum of pathological conditions studied with these new tools has been extended to bacterial (20), viral (11) and parasitic (21) infections, inflammation and autoimmunity (12,22), and transplantation complications (23). Almost all of this work has been published in the last few years, highlighting the growing interest in immunopeptidomics as a valuable approach to address fundamental questions in biomedical research.

To date, only a small number of studies have focused on the identification of pathogen-derived peptides presented by infected cells (11,20,24). Spencer *et al.* demonstrated that viral infection can induce dramatic changes in the host cell immunopeptidome, a phenomenon they called 'self peptidome shift' (25). *Vaccinia* virus-infected HeLa cells results in the presentation of hundreds of MHC I-restricted self peptides that are not found in non-infected cells, and ~40% of these arise from interferon-stimulated genes, consistently with the cell response to a viral infection (25). The infection of B lymphoblastoid cells with measles virus results in changes of

the repertoire of MHC I-restricted self peptides that allow for recognition of unique self epitopes by natural killer cells, suggesting a novel regulatory mechanism for the innate immune response (26). HeLa cells infection with influenza virus leads to the expression of 20 MHC I-restricted host peptides that are not found in non-infected cells, and up-regulates the expression of 347 other host peptides. Proteins associated with these influenza virus-induced peptides are involved in regulation of cellular metabolism, cell cycle, protein synthesis and RNA processing (27). Together, these observations demonstrate that studying host immunopeptidomics can provide important detailed insights into cellular responses to infection and can broaden our understanding of host-pathogen interactions. Given the growing importance of vaccines in maintaining health, it is thus of considerable interest to explore host immunopeptidome changes in response to vaccine antigen exposure in human primary APCs. Such studies may not only help to understand responses to existing vaccines but may also guide the development of novel vaccine candidates that target distinct immunological pathways to achieve more desirable immune responses.

The aim of this work was to identify the MHC I targets derived from host proteins in response to particulate vs. soluble antigenic stimuli delivered to human APCs. Monocyte-derived macrophages (MDMs) from five donors were exposed to plant-derived nanoparticles bearing influenza hemagglutinin (HA) (known as the 'virus-like particles' or VLPs) (28) or soluble influenza HA, as control. MHC I-peptide complexes were immunopurified and analysed by nano-flow liquid chromatography coupled with high-resolution tandem mass spectrometry (LC-HR-MS/MS) using dopant-assisted electrospray ionisation (DA-ESI). Analysis of the proteomics data yielded interesting observations on the physicochemical properties of endogenous MHC I peptides, the nature of MHC I-presented proteins, and the biological pathways stimulated in response to the HA-bearing nanoparticles.

4.4. METHODS

4.4.1. Influenza hemagglutinin-bearing nanoparticles

VLPs produced in *Nicotiana benthamiana* were provided by Medicago Inc. (Quebec, QC) and were manufactured as previously described (28,29) based on the sequence of A/California/07/2009 (H1N1) influenza virus HA. A recombinant soluble HA protein produced

in human embryonic kidney 293 cells (Immune Technology, New York, NY) was used as control.

4.4.2. Monocyte-derived macrophages

Fifty milliliters of whole blood were collected from five healthy human donors 23–47 years of age. Peripheral blood mononuclear cells (PBMCs) were separated by density gradient centrifugation (SepMate-50, STEMCELL Technologies, Vancouver, BC), and $CD14^+$ monocytes were isolated using EasySep human monocyte enrichment kit (STEMCELL Technologies) following the manufacturer's instructions. Monocytes were cultured (10^6 cells/mL) in RPMI-1640, 50 IU/mL penicillin, 50 µg/mL streptomycin, 10 mM HEPES supplemented with 10% fetal bovine serum (Wisent, Saint-Jean-Baptiste, QC) and 20 ng/mL recombinant human macrophage colony-stimulating factor (Gibco, Frederick, MD) under 5% CO_2 (37°C) for 7 days. At days 3 and 6, one half of the media was replaced. All study procedures were approved by the Research Ethics Committee of the McGill University Health Centre and written informed consent was obtained from donors prior to venipuncture.

4.4.3. Cell lysis and immunoprecipitation

MDMs were exposed to either VLPs or soluble HA (15 µg/mL HA in culture medium, 5% CO_2, 37°C, 16 h) and then lysed (4°C, 1 h) with 4% NP-40 Surfact-Amps (Thermo Fisher Scientific, Waltham, MA) in 50 mM Tris.HCl (pH 7.0), 150 mM NaCl and protease inhibitors (Pierce, Thermo Fisher Scientific). Lysate total protein concentration was determined using the Pierce BCA protein assay kit (Thermo Fisher Scientific). MHC I-peptide complexes were immunoprecipitated using Dynabeads protein G immunoprecipitation kit (Thermo Fisher Scientific) with anti-human MHC I antibody (clone W6/32, BioLegend, 10 µg per 500 µL lysate, 45 min, 4°C). Peptides were eluted (10% acetic acid, 70°C, 15 min) from the beads, desalted on a C_{18} solid-phase extraction Macro Spin column (Harvard Apparatus, Holliston, MA) using water and methanol following the manufacturer's instructions, and evaporated to dryness under vacuum (37°C, 120 min).

4.4.4. Mass spectrometry analysis

Samples was reconstituted (60 µL 0.1% formic acid) and injected (20 µL) on to a Maxis II (Bruker, Billerica, MA) quadrupole-time of flight tandem mass spectrometer equipped with a Dionex UltiMate 3000 (Thermo Fisher Scientific) UHPLC system using an Acclaim PepMap 300 RSLC C_{18} 2 µm 100 Å 150 x 0.075 mm UHPLC column (Thermo Fisher Scientific) with water (A) and acetonitrile (B) both containing 0.1% formic acid at a flow rate of 300 nL/min (50°C). Elution gradient started at 5% B, was held for 3 min, then increased to 35% at 73 min, 55% at 90 min, and 80% at 95 min. MS spectra were acquired at *m/z* 400–2200 and MS/MS spectra were recorded at *m/z* 150–2200 using collision-induced dissociation activation and data-dependent acquisition with a collision energy of 21–55 eV depending on precursor ion *m/z* value and charge state (*z*). Ions with *z* = 2–5 were preferred whereas singly charged ions were excluded. Redundant ions were also excluded for 2 min. Acquisition time was 0.5 s for MS and 0.06–0.25 s for each MS/MS scan depending on precursor ion signal intensity, with a total cycle time of 3.0 s. CaptiveSpray (Bruker) nano-spray ionisation source operated in positive mode with a capillary voltage of 1.8 kV. To enhance ionisation, a continuous flow of nitrogen and vaporized acetonitrile (as dopant) was injected into the ion source during the analysis using a nanoBooster module (Bruker). nanoBooster pressure was set to 0.3 bar. Nitrogen (99.5% pure) was used as dry gas (150°C) at a flow rate of 3.0 L/min. Samples were analyzed in duplicate.

4.4.5. Data processing

Mass spectra were imported into the MaxQuant software (30) and searched against the human subset of the UniProt-SwissProt protein database (downloaded on 9/11/2017). An unspecific search was conducted for peptides 5–20 residues long at 0.01 false-discovery rate. Methionine oxidation and N-terminal acetylation were defined as variable modifications. A posterior error probability (PEP) threshold of 0.01 was set for all MaxQuant searches. To account for LC retention shifts, the 'match between runs' option was enabled with a match time window of 0.7 min and an alignment time window of 20 min. The MEROPS database (31) (http://merops.sanger.ac.uk) was used for the analysis of proteolysis sites. Cleavage site sequence logos and specificity matrices were transferred into a scripted Microsoft Excel worksheet to facilitate simultaneous analysis of a list of peptides. PANTHER (32) (http://www.pantherdb.org) was used for gene ontology (GO) analysis. Additional pathway

analysis was done using the Reactome database (https://www.reactome.org). Protein interaction analysis was performed by InnateDB (33) integrated analysis platform (http://www.innatedb.ca) with UniProt identifiers as the cross-reference database and filtered to show only interactions between uploaded proteins. The results were subsequently visualized with the Cerebral plugin (34) of Cytoscape software (http://www.cytoscape.org) to organize the interaction network in the context of subcellular localisation for all of the proteins displayed and visualized by Cerebral. GRAVY-calculator (http://www.gravy-calculator.de) and the ExPASy compute pI/MW tool (https://web.expasy.org/compute_pi) were used to calculate grand average of hydropathy (GRAVY) score and theoretical isoelectric point, respectively. All other calculations were made using Microsoft Excel.

4.4.6. Availability of data

The datasets generated and/or analyzed during this study are available through the corresponding author upon request. The MS proteomics data have been deposited to the ProteomeXchange Consortium via the PRIDE (35) partner repository with the dataset identifier PXD010741.

4.5. RESULTS AND DISCUSSION

4.5.1. Blood donors and sample properties

Five blood donors (A–E) were recruited for this study. To increase proteome coverage and confidence of peptide spectral matches, samples were analyzed on two separate occasions except for Sample 0 that was used primarily for method development. Donors D and C produced the highest and lowest numbers of MHC I peptides, respectively. No significant correlation was found between the number of PBMC isolated and the number of identified MHC I peptides. However, the number of identified peptides inversely correlated with the average peptide score, i.e. the more peptides extracted from and/or detected in a sample, the lower the confidence of the spectral matches; potentially due to increased sample complexity and/or ion suppression. Moreover, samples from the same donors exposed to the same stimulus (i.e. VLP or soluble protein) did not follow a consistent pattern i.e. VLP-treatment did not always result in more or larger MHC I peptides (see sample pairs 5/8, 2/6 or 4/7 in Tab. 4.1). This may be attributable, at

least in part, to the fact that samples were collected at several-week intervals, and the donors could potentially have been naturally exposed to a wide range of environmental stimuli, even wild-type influenza viruses, with resultant triggering of innate and/or adaptive immune responses and accompanying changes in the functional state of their peripheral blood monocytes. Donors' demographic profile and a summary of proteomics analysis results for the VLP-treated and control samples can be found in Tab. 4.1.

4.5.2. Number and characteristics of identified MHC I-associated peptides

A total of 165 MHC I-associated peptides were identified from immunopurified human MDM lysates with 109 and 58 peptides detected in VLP-treated and control samples, respectively. Only two peptides were found with both treatments: VIISSSILLLGTLLI and TMGHW. The former belongs to the [848–863] region of leptin receptor (LEPR), a 132-kDa single-pass type I membrane protein involved in multiple signaling pathways such as JAK2/STAT3 and MAPK cascade/FOS. LEPR is known to play important roles in innate and adaptive immunity (36,37). The [848–863] peptide is located on LEPR's transmembrane region and is in the vicinity of the protein's JAK2 activation site. The second peptide represents the [393–397] region of midasin (MDN1), a 633-kDa nuclear chaperone involved in the assembly of the 60S ribosomal subunit and other protein complexes (38). The peptide lies within one of the six MDN1's AAA-ATPase protomers. LEPR[848–863] was found in samples from all donors exposed to VLPs with a high average peptide score of 61.4, whereas MDN1[393–397] was only detected in two donors (one VLP, one soluble HA; average score 20.1).

Peptides unique to the VLP-treated samples had an average score of 12.4 (*vs.* 20.7 for peptides unique to control) and an average length of 12.7 amino acid residues (*vs.* 7.0 for peptides unique to control). On average, the peptides identified from these samples were 10.8 residues long, which is in agreement with the widely accepted length of 8–11 residues for MHC I-associated peptides (8). However, a large proportion of the identified peptides – both in VLP-treated samples and in controls – were found to be larger than usually expected for MHC I peptides. One possible explanation for this observations is that the cell lysates contained optimally-trimmed peptides for MHC I binding as well as 'immature' peptides from endoplasmic reticulum (ER) or endosomes that were still in the process of proteolysis for the purpose of MHC I presentation or housekeeping/protein degradation (39,40). Moreover, the MS platform used in

this study has been shown to possess hardware features that allow very high transmission of peptides into the collision cell enabling the detection of a wide range of peptides with various lengths (41).

Fig. 4.1 demonstrates the overall distribution of identified MHC I peptides in terms of length, isoelectric point and GRAVY score. The identified peptides were more basic than acidic (60:40 ratio, in both VLP and soluble HA) and had more hydrophilic (GRAVY < 0) backbones (60:40 in VLP, 70:30 in soluble HA).

Since early 2000s, various dopants have been used to enhance ionisation in both desorption and atmospheric-pressure applications. DA-ESI has however been applied to only a limited number of metabolomics studies (42–44). The CaptiveSpray nano-ESI source used for this analysis was coupled to a nanoBooster unit that delivered a constant flow of dopant-enriched inert gas into the ion source. The addition of an appropriate dopant to the ionisation mixture can enhance the charge of peptides that enter the emitter and improve ionisation efficiency resulting in a higher sensitivity than the conventional ESI. To assess the role of the dopant and to maximise the booster's performance, we tested several dopant systems including methanol, acetone, acetonitrile, and their 1:1 (v/v) mixtures ± formic acid (0.1% v/v) with nitrogen as the inert gas. Using pure acetonitrile as dopant led to the most satisfactory results in terms of number of identified peptides, average signal intensity, and average MaxQuant score (Suppl. Table 4.1).

Analysis of the proteolysis sites showed that the overall cleavage patterns changed when cells were exposed to the VLPs.

Fig. 4.2 illustrates the relative abundance of amino acid residues in the vicinity of N- and C-terminal cleavage sites. In general, Trp (11%), Gln (9%), Phe (8%) and Leu (8%) were the preferred cleavage sites (CR_1 and NR_1) in peptides detected from the control samples. For the VLP-treated samples, this changed to Glu (9%), Leu (8%) and Lys (8%). Of note, there was also a shift from aromatic to aliphatic (polar and non-polar) residues in the VLP-treated MDMs suggesting that peptidases with preference for aliphatic residues, such as matrix metalloproteinases (MMPs), were more active in these cells. Also, while basic cleavage sites were generally more frequent than the acidic sites, C-terminal proteolysis at acidic cleavage sites was substantially increased in the VLP-treated cells. This could potentially be due to an increase in the activity of caspases that usually cut at the C-termini of acidic residues. Proteolysis patterns from other peptidases with preferred acidic cleavage sites, such as cytosolic carboxypeptidase 1,

glutamyl aminopeptidase and dipeptidyl peptidase 1, were also found to be more active in the VLP-treated samples.

Using the MEROPS peptidase database, cathepsins and MMPs were found to be the main protease families involved in the generation and processing of the peptides identified in the MDMs. However, while the majority of peptides detected in control samples were produced by cathepsins (42% *vs.* 35% in VLP-treated samples), MMP-cleaved peptides were more abundant in the VLP-treated samples (38% *vs.* 32% in control). Cathepsin K (23%), L (23%) and V (19%) were the major proteases of this family generating MHC I peptides in control and VLP-treated samples. Likewise, MMP-1 (14%), MMP-2 (14%) and MMP-10 (16%) led to the highest number of MMP-cleaved peptides. A previous study using a similar approach for the analysis of MHC class II peptidome from human dendritic cells also highlighted cathepsins and MMPs as the primary proteases in the processing of antigenic peptides (18).

Fig. 4.3A provides an overview of various protease families producing the identified MHC-1 peptides. For more details on proteolysis analysis see Suppl. Table 4.2.

Cleavage site analysis also demonstrated that while most of the identified MHC I-associated peptides were cut from internal regions of the proteins, relative abundance of N- and C-terminal peptides was slightly decreased in the VLP-treated samples (Fig. 4.3.B). Furthermore, N-terminal peptides were generally more abundant than C-terminal peptides. This ratio of N- to C-terminal peptides that we observed was the opposite of what has been reported for MHC II-associated peptides (18); a finding consistent with the very different pathways and processes involved in MHC I versus MHC II peptide loading (7). For this analysis, peptides cleaved within 10% of protein termini were considered N- or C-terminal. A complete list of the MHC I peptides identified in this study can be found in Suppl. Table 4.3.

4.5.3. Proteins associated with the MHC I-restricted peptides identified

A total of 109 and 55 human proteins were represented by at least one peptide from VLP-treated and control samples, respectively. Three proteins were found under both treatment conditions: leptin receptor (LEPR), midasin (MDN1) and GPI ethanolamine phosphate transferase 3 (PIGO). LEPR and MDN1 were described previously. PIGO is a 119-kDa ER multi-pass membrane protein involved in glycosylphosphatidylinositol anchor biosynthesis. This protein was processed in two different peptides in the VLP-treated and control samples. The

smaller non-unique WLPAL peptide found in the control condition is located on the protein's [933–937] cytosolic region whereas the larger GLVGAIAYAGLLG detected in a VLP-treated sample is unique to PIGO, comprises the protein's [490–502] region, and is located in a transmembrane domain. Three other proteins had more than one MHC I peptide associated with them: SCO-spondin, uncharacterized protein KIAA1551 (or niban-like protein 1) and cip1-interacting zinc finger protein (or nuclear receptor coactivator 2). SCO-spondin (SSPO) was identified based on two unique peptides in its [1003–1007] and [4158–4162] regions and is an extracellular peptidase inhibitor and cell adhesion protein. The second peptide is located on one of the protein's thrombospondin type 1 domains. The two other proteins were characterized based on low-score and non-unique peptides, and little information is available about them. These three proteins were only found in the control samples. The average protein quantity in the cell lysates (μg) was not significantly different between the treatment groups (2.8 ± 0.5 in VLP *vs.* 2.4 ± 0.5 in control, $p = 0.64$).

GO analysis of the proteins identified under VLP treatment demonstrated that the majority of MHC I-presented proteins had binding (36%), catalytic (34%) and transporter (10%) activities. Other important molecular functions included signal transducer, receptor, structural molecule and translation regulator activities. Also, these proteins were primarily involved in cellular (29%), metabolic (20%) and biological regulation (10%) processes with response to stimuli (9%), cellular component organisation or biogenesis (9%), localisation (8%) and developmental processes (6%) being among the other classified biological processes. In terms of subcellular localisation, the identified proteins were mainly localized in cell parts (34%), organelles (25%), macromolecular complexes (20%) and membrane (18%). Very few proteins were found in the extracellular region/matrix (2%) suggesting that the large majority of MHC I peptides were processed from internal proteins. Moreover, the most important protein classes identified from the MHC I-associated peptides were nucleic acid binding proteins (20%), enzyme modulators (12%), transcription factors (10%), receptors (10%) and transporters (10%). For more details on GO classification see Suppl. Table 4.4.

The plant-derived VLPs used in this study have been shown to recapitulate the structure and key features of native influenza virions (45) and are the basis of a promising new vaccine for influenza (28,29). They bind to the surface of human PBMCs and MDMs in a sialic acid-dependent manner and undergo rapid internalization through a dynamin-dependent endocytic

pathway, resulting in stimulation of the innate and adaptive immune responses *in vitro* (46,47). These HA-VLP have been shown to induce strong antibody production and sustained poly-functional and cross-reactive HA-specific T cell responses in both animal models and human studies (29,48,49). Our proteomics-based pathway analysis generally supported these observations from immunological and imaging studies, and revealed that the peptides presented on the MHC I in the VLP-treated MDMs were derived from proteins mainly involved in the following six pathways: inflammation mediated by chemokine and cytokine signaling pathway (6%), EGF receptor (EGFR) signaling pathway (6%), angiogenesis (6%), gonadotropin-releasing hormone receptor (GnRHR) pathway (6%), T cell activation (5%) and nicotinic acetylcholine receptor (nAChR) signaling pathway (5%). While up-regulation of chemokine/cytokine-mediated inflammation and T cell activation pathways could be directly linked to the MDM reaction to VLP treatment, it is not clear why or how the four other major pathways have been activated. The EGFR signaling and angiogenesis pathways both involve cell growth, differentiation, migration, adhesion and survival through various interacting signaling pathways. The EGFR signaling pathway also includes several proteins that have been reported to promote clathrin-mediated endocytosis (CME) (50). Up-regulation of this pathway in the VLP-treated MDMs suggests that CME may be a major mechanism for the internalisation of HA-VLPs. The nAChR signaling pathway plays a central role in the vagus nerve-regulated cholinergic anti-inflammatory pathway and has been found to attenuate inflammation in a number of conditions including hepatic steatosis (51,52), brain injury (53) and cancer (54,55) potentially via modulation of certain MMPs and cytokines (56). The GnRHR pathway is critical for normal secretion of gonadotropins, pubertal development and reproduction. Previous studies have shown that some potent pro-inflammatory cytokines such as TNF-α, IL-1β, and IL-6 likely inhibit the GnRHR pathway during severe illnesses (57,58).

Fig. 4.4 presents a complete list of pathways related to the proteins from which the identified MHC I peptides originated.

An interaction analysis identified 41 reported protein-protein interactions between the proteins expressed on the MHC I sites of VLP-treated MDMs including 27 physical associations, 5 phosphorylation and phosphorylation reactions, 5 co-localisations, 3 associations and one self-interaction. Several interactions were found between nucleic proteins and cytoplasmic and extracellular proteins. These interactors were grouped into 4 clusters. **(1)** The UTP20-VSP18-

VSP16 cluster comprises UTP20, a processome component involved in rRNA processing and negative regulation of cell proliferation (59), and two vacuolar protein sorting-associated proteins, which facilitate vesicle-mediated protein trafficking to lysosomal compartments including the endocytic membrane transport and autophagic pathways (60). **(2)** The EIF2S1-POP1 pair is involved in tRNA processing and protein biosynthesis particularly in response to stress. **(3)** The PAK1-MAP3K1 pair includes proteins from the MAP kinase pathway that are also activated in response to stimuli and play role in immune system pathways via C-type lectin, Fc-γ, Fc-ε, toll-like receptor signaling and CD28 co-stimulation (Reactome database). **(4)** The PRKCZ-HIST1H1B-IRAK4 cluster consists of a histone protein and two protein kinases that are crucial for initiating an innate immune response against foreign pathogens. PRKCZ and IRAK4 are both involved in the IL-1 signaling pathway. While the former is believed to positively regulate T-helper 2 cell cytokine production (UniProt database) the latter is involved in neutrophil-mediated immunity (61). Overall, the protein-protein interactions predicted in VLP-treated cells argue for a robust and balanced activation of receptor-mediated endocytosis and antigen processing mechanisms likely contributing to up-regulation of both innate and adaptive immune responses. These findings therefore provide a cell biology background that supports the strong immunogenicity reported for the plant-derived HA-VLPs in clinical trials and animal experiments (28,29,48,49).

Fig. 4.5 illustrates the protein-protein interaction network in the context of subcellular localisation for the proteins partially expressed on the MHC I sites of VLP-treated MDMs. A complete list of interactions as well as their citations can be found in Suppl. Table 4.5.

In summary, upon treatment of human MDMs with plant-derived VLPs bearing an influenza HA, 109 MHC class I-associated human peptides were identified by LC-MS/MS, two of which were also detected in the soluble HA-treated macrophages used as controls. The peptides unique to VLP treatment were, on average, 13 residues long with slightly more basic and hydrophilic properties. These peptides were mainly processed via proteolysis by MMPs and cathepsins with Glu, Leu and Lys being the most prevalent cleavage sites. A total of 109 differentially-expressed proteins were identified by our analysis of the MHC I-associated peptides. The majority of these proteins had binding, catalytic or transporter functions and were involved in cellular, metabolic and regulatory processes. Inflammation stimulation and

attenuation, response to stimuli, innate and adaptive immunity, clathrin-mediated endocytosis, protein synthesis and endo-lysosomal degradation were the pathways found to be primarily up-regulated in VLP-treated MDMs. These results shed new light on the mechanism of action of these HA-VLPs upon their internalisation by macrophages. Additional studies will be required to more fully understand the immunologic implications of the immunopeptidomic response of APCs to these novel, plant-derived VLPs. The analytical approach presented here could also serve as a model for similar experiments to study MHC I-associated peptides under different treatment conditions.

4.6. REFERENCES

1. Alvarez B, Barra C, Nielsen M, Andreatta M. Computational Tools for the Identification and Interpretation of Sequence Motifs in Immunopeptidomes. Proteomics. 2018;e1700252.
2. Caron E, Kowalewski DJ, Chiek Koh C, Sturm T, Schuster H, Aebersold R. Analysis of Major Histocompatibility Complex (MHC) Immunopeptidomes Using Mass Spectrometry. Mol Cell Proteomics. 2015;14(12):3105–17.
3. Faridi P, Wayne Purcell A, Croft NP. In Immunopeptidomics We Need a Sniper Instead of a Shotgun. Proteomics. 2018;e1700464.
4. Freudenmann LK, Marcu A, Stevanović S. Mapping the tumour human leukocyte antigen (HLA) ligandome by mass spectrometry. Immunology. 2018;154(3):331-345.
5. Müller M, Gfeller D, Coukos G, Bassani-Sternberg M. "Hotspots" of antigen presentation revealed by human leukocyte antigen ligandomics for neoantigen prioritization. Front Immunol. 2017;8:1367.
6. Blander JM. Regulation of the Cell Biology of Antigen Cross Presentation. Annu Rev Immunol. 2018;36:717-53.
7. Neefjes J, Jongsma MLM, Paul P, Bakke O. Towards a systems understanding of MHC class I and MHC class II antigen presentation. Nat Rev Immunol. 2011;11(12):823–36.
8. Cruz FM, Colbert JD, Merino E, Kriegsman BA, Rock KL. The Biology and Underlying Mechanisms of Cross-Presentation of Exogenous Antigens on MHC-I Molecules. Annu Rev Immunol. 2017;35(1):149–76.
9. Roche PA, Furuta K. The ins and outs of MHC class II-mediated antigen processing and presentation. Nature Reviews Immunology. 2015;15:203–16.
10. Bassani-Sternberg M, Coukos G. Mass spectrometry-based antigen discovery for cancer immunotherapy. Current Opinion in Immunology. 2016;41:9–17.
11. Blatnik R, Mohan N, Bonsack M, Falkenby LG, Hoppe S, Josef K, et al. A Targeted LC-MS Strategy for Low-Abundant HLA Class-I-Presented Peptide Detection Identifies Novel Human Papillomavirus T-Cell Epitopes. Proteomics. 2018;e1700390.
12. Crèvecoeur I, Vig S, Mathieu C, Overbergh L. Understanding type 1 diabetes through proteomics. Expert Review of Proteomics. 2017;14:571–80.
13. Van Den Broek I, Blokland M, Nessen MA, Sterk S. Current trends in mass spectrometry

of peptides and proteins: Application to veterinary and sports-doping control. Mass Spectrometry Reviews. 2015;34:571–94.

14. Segura V, Garin-Muga A, Guruceaga E, Corrales FJ. Progress and pitfalls in finding the 'missing proteins' from the human proteome map. Expert Review of Proteomics. 2017;14:9–14.
15. Bräunlein E, Krackhardt AM. Identification and Characterization of Neoantigens As Well As Respective Immune Responses in Cancer Patients. Frontiers in Immunology. 2017;8:1702.
16. Ostroumov D, Fekete-Drimusz N, Saborowski M, Kühnel F, Woller N. CD4 and CD8 T lymphocyte interplay in controlling tumor growth. Cellular and Molecular Life Sciences. 2018;75:689–713.
17. Chong C, Marino F, Pak H, Racle J, Daniel RT, Müller M, et al. High-throughput and Sensitive Immunopeptidomics Platform Reveals Profound Interferonγ-Mediated Remodeling of the Human Leukocyte Antigen (HLA) Ligandome. Mol Cell Proteomics. 2018;17(3):533–48.
18. Ciudad MT, Sorvillo N, van Alphen FP, Catalán D, Meijer AB, Voorberg J, et al. Analysis of the HLA-DR peptidome from human dendritic cells reveals high affinity repertoires and nonconventional pathways of peptide generation. J Leukoc Biol. 2017;101(1):15–27.
19. Olsson N, Schultz LM, Zhang L, Khodadoust MS, Narayan R, Czerwinski DK, et al. T-Cell Immunopeptidomes Reveal Cell Subtype Surface Markers Derived From Intracellular Proteins. Proteomics. 2018;e1700410.
20. Karunakaran KP, Yu H, Jiang X, Chan Q, Goldberg MF, Jenkins MK, et al. Identification of MHC-Bound Peptides from Dendritic Cells Infected with Salmonella enterica Strain SL1344: Implications for a Nontyphoidal Salmonella Vaccine. J Proteome Res. 2017;16(1):298–306.
21. Draheim M, Wlodarczyk MF, Crozat K, Saliou J-M, Alayi TD, Tomavo S, et al. Profiling MHC II immunopeptidome of blood-stage malaria reveals that cDC1 control the functionality of parasite-specific CD4 T cells. EMBO Mol Med. 2017;9(11):e201708123.
22. Fugmann T, Sofron A, Ritz D, Bootz F, Neri D. The MHC Class II Immunopeptidome of Lymph Nodes in Health and in Chemically Induced Colitis. J Immunol. 2017;198(3):1357–64.

23. Bijen HM, Hassan C, Kester MGD, Janssen GMC, Hombrink P, de Ru AH, et al. Specific T Cell Responses against Minor Histocompatibility Antigens Cannot Generally Be Explained by Absence of Their Allelic Counterparts on the Cell Surface. Proteomics. 2018;e1700250.
24. Ramarathinam SH, Gras S, Alcantara S, Yeung AWS, Mifsud NA, Sonza S, et al. Identification of Native and Posttranslationally Modified HLA-B*57:01-Restricted HIV Envelope Derived Epitopes Using Immunoproteomics. Proteomics. 2018;e1700253.
25. Spencer CT, Bezbradica JS, Ramos MG, Arico CD, Conant SB, Gilchuk P, et al. Viral infection causes a shift in the self peptide repertoire presented by human MHC class I molecules. Proteomics - Clin Appl. 2015;9(11–12):1035–52.
26. Carrillo-Bustamante P, de Boer RJ, Keşmir C. Specificity of inhibitory KIRs enables NK cells to detect changes in an altered peptide environment. Immunogenetics. 2018;70(2):87–97.
27. Wahl A, Schafer F, Bardet W, Hildebrand WH. HLA class I molecules reflect an altered host proteome after influenza virus infection. Hum Immunol. 2010;71(1):14–22.
28. D'Aoust MA, Couture MMJ, Charland N, Trépanier S, Landry N, Ors F, et al. The production of hemagglutinin-based virus-like particles in plants: A rapid, efficient and safe response to pandemic influenza. Plant Biotechnol J. 2010;8(5):607–19.
29. Landry N, Pillet S, Favre D, Poulin JF, Trépanier S, Yassine-Diab B, et al. Influenza virus-like particle vaccines made in Nicotiana benthamiana elicit durable, poly-functional and cross-reactive T cell responses to influenza HA antigens. Clin Immunol. 2014;154(2):164–77.
30. Cox J, Mann M. MaxQuant enables high peptide identification rates, individualized p.p.b.-range mass accuracies and proteome-wide protein quantification. Nat Biotechnol. 2008;26(12):1367–72.
31. Rawlings ND, Barrett AJ, Bateman A. MEROPS--the peptidase database. Nucleic Acids Res. 2010;38(Database issue):D227–33.
32. Thomas PD, Campbell MJ, Kejariwal A, Mi H, Karlak B, Daverman R, et al. PANTHER: A library of protein families and subfamilies indexed by function. Genome Res. 2003;13(9):2129–41.
33. Breuer K, Foroushani AK, Laird MR, Chen C, Sribnaia A, Lo R, et al. InnateDB: Systems

biology of innate immunity and beyond - Recent updates and continuing curation. Nucleic Acids Res. 2013;41(D1):D1228-33.

34. Barsky A, Gardy JL, Hancock REW, Munzner T. Cerebral: A Cytoscape plugin for layout of and interaction with biological networks using subcellular localization annotation. Bioinformatics. 2007;23(8):1040–2.

35. Vizcaíno JA, Deutsch EW, Wang R, Csordas A, Reisinger F, Ríos D, et al. ProteomeXchange provides globally coordinated proteomics data submission and dissemination. Nature Biotechnology. 2014;32:223–6.

36. Zhao Y, Sun R, You L, Gao C, Tian Z. Expression of leptin receptors and response to leptin stimulation of human natural killer cell lines. Biochem Biophys Res Commun. 2003;300(2):247–52.

37. Cassano S, Pucino V, La Rocca C, Procaccini C, De Rosa V, Marone G, et al. Leptin modulates autophagy in human CD4+CD25-conventional T cells. Metabolism. 2014;63(10):1272–9.

38. Raman N, Weir E, Müller S. The AAA ATPase MDN1 Acts as a SUMO-Targeted Regulator in Mammalian Pre-ribosome Remodeling. Mol Cell. 2016;64(3):607–15.

39. Saveanu L, Carroll O, Weimershaus M, Guermonprez P, Firat E, Lindo V, et al. IRAP identifies an endosomal compartment required for MHC class i cross-presentation. Science. 2009;325(5937):213–7.

40. Saric T, Chang SC, Hattori A, York IA, Markant S, Rock KL, et al. An IFN-γ-induced aminopeptidase in the ER, ERAP I, trims precursors to MHC class I-presented peptides. Nat Immunol. 2002;3(12):1169–76.

41. Beck S, Michalski A, Raether O, Lubeck M, Kaspar S, Goedecke N, et al. The Impact II, a Very High-Resolution Quadrupole Time-of-Flight Instrument (QTOF) for Deep Shotgun Proteomics. Mol Cell Proteomics. 2015;14(7):2014–29.

42. Gu D, Raymundo MM, Kadlubar FF, Turesky RJ. Ultraperformance liquid chromatography-tandem mass spectrometry method for biomonitoring cooked meat carcinogens and their metabolites in human urine. Anal Chem. 2011;83(3):1093–101.

43. Luo X, An M, Cuneo KC, Lubman DM, Li L. High-Performance Chemical Isotope Labeling Liquid Chromatography Mass Spectrometry for Exosome Metabolomics. Anal Chem. 2018;90(14):8314-9.

44. Luo X, Li L. Metabolomics of Small Numbers of Cells: Metabolomic Profiling of 100, 1000 and 10000 Human Breast Cancer Cells. Anal Chem. 2017;89(21):11664-71.
45. Lindsay BJ, Bonar MM, Costas-Cancelas IN, Hunt K, Makarkov AI, Chierzi S, et al. Morphological characterization of a plant-made virus-like particle vaccine bearing influenza virus hemagglutinins by electron microscopy. Vaccine. 2018;36(16):2147–54.
46. Makarkov AI, Chierzi S, Pillet S, Murai KK, Landry N, Ward BJ. Plant-made virus-like particles bearing influenza hemagglutinin (HA) recapitulate early interactions of native influenza virions with human monocytes/macrophages. Vaccine. 2017;35(35 Pt B):4629–36.
47. Hendin HE, Pillet S, Lara AN, Wu CY, Charland N, Landry N, et al. Plant-made virus-like particle vaccines bearing the hemagglutinin of either seasonal (H1) or avian (H5) influenza have distinct patterns of interaction with human immune cells in vitro. Vaccine. 2017;35(19):2592–9.
48. Pillet S, Aubin É, Trépanier S, Bussière D, Dargis M, Poulin JF, et al. A plant-derived quadrivalent virus like particle influenza vaccine induces cross-reactive antibody and T cell response in healthy adults. Clin Immunol. 2016;168:72–87.
49. Pillet S, Racine T, Nfon C, Di Lenardo TZ, Babiuk S, Ward BJ, et al. Plant-derived H7 VLP vaccine elicits protective immune response against H7N9 influenza virus in mice and ferrets. Vaccine. 2015;33(46):6282–9.
50. Kandasamy K, Sujatha Mohan S, Raju R, Keerthikumar S, Sameer Kumar GS, Venugopal AK, et al. NetPath: A public resource of curated signal transduction pathways. Genome Biol. 2010;11(1):R3.
51. Hasan MK, Friedman TC, Sims C, Lee DL, Espinoza-Derout J, Ume A, et al. a7-nicotinic acetylcholine receptor agonist ameliorates nicotine plus high-fat Diet–Induced hepatic steatosis in male mice by inhibiting oxidative stress and stimulating AMPK signaling. Endocrinology. 2018;159(2):931–44.
52. Li DJ, Liu J, Hua X, Fu H, Huang F, Fei YB, et al. Nicotinic acetylcholine receptor α7 subunit improves energy homeostasis and inhibits inflammation in nonalcoholic fatty liver disease. Metabolism. 2018;79:52–63.
53. Sun Y, Song D, Wang M, Chen K, Zhang T. α7 nicotinic acetylcholine receptor agonist attenuates the cerebral injury in a rat model of cardiopulmonary bypass by activating the

Akt/GSK3β pathway. Mol Med Rep. 2017;16(6):7979–86.

54. Fei R, Zhang Y, Wang S, Xiang T, Chen W. α7 nicotinic acetylcholine receptor in tumor-associated macrophages inhibits colorectal cancer metastasis through the JAK2/STAT3 signaling pathway. Oncol Rep. 2017;38(5):2619–28.

55. Zhang C, Yu P, Zhu L, Zhao Q, Lu X, Bo S. Blockade of α7 nicotinic acetylcholine receptors inhibit nicotine-induced tumor growth and vimentin expression in non-small cell lung cancer through MEK/ERK signaling way. Oncol Rep. 2017;38(6):3309–18.

56. Liu L, Wu H, Cao Q, Guo Z, Ren A, Dai Q. Stimulation of Alpha7 Nicotinic Acetylcholine Receptor Attenuates Nicotine-Induced Upregulation of MMP, MCP-1, and RANTES through Modulating ERK1/2/AP-1 Signaling Pathway in RAW264.7 and MOVAS Cells. Mediators Inflamm. 2017;2017:2401027.

57. Igaz P, Salvi R, Rey JP, Glauser M, Pralong FP, Gaillard RC. Effects of cytokines on gonadotropin-releasing hormone (GnRH) gene expression in primary hypothalamic neurons and in GnRH neurons immortalized conditionally. Endocrinology. 2006;147(2):1037–43.

58. Herman AP, Skipor J, Krawczyńska A, Bochenek J, Wojtulewicz K, Antushevich H, et al. Peripheral Inhibitor of AChE, Neostigmine, Prevents the Inflammatory Dependent Suppression of GnRH/LH Secretion during the Follicular Phase of the Estrous Cycle. Biomed Res Int. 2017;2017:6823209.

59. Schwirzke M, Gnirke A, Bork P, Tarin D, Weidle U. Differential gene expression in mammary carcinoma cell lines: identification of DRIM, a new gene down-regulated in metastasis. Anticancer Res. 1998;18(3A):1409–21.

60. Kim BY, Krämer H, Yamamoto A, Kominami E, Kohsaka S, Akazawa C. Molecular Characterization of Mammalian Homologues of Class C Vps Proteins That Interact with Syntaxin-7. J Biol Chem. 2001;276(31):29393–402.

61. Bouma G, Doffinger R, Patel SY, Peskett E, Sinclair JC, Barcenas-Morales G, et al. Impaired neutrophil migration and phagocytosis in IRAK-4 deficiency. British Journal of Haematology. 2009;147:153–6.

4.7. TABLE

Table 4. 1. Demographic profile of blood donors and summary of the proteomics analysis results for VLP-treated and control (soluble HA) samples

Sample	Donor	Age/Sex	Ethnicity	# PBMC	Treatment	# LC-MS replicates	# Peptides identified	Average peptide score	Average peptide length
0	A	47 M	Caucasian	1.5×10^8	VLP	1	9	31.9	11.9
1	B	46 F	Caucasian	9.7×10^7	VLP	2	5	38.7	15.4
2	C	26 M	South Asian	1.4×10^8	VLP	2	1	61.1	15.0
3	D	21 M	East Asian	1.2×10^8	VLP	2	87	8.3	13.0
4	E	24 M	West Asian	1.3×10^8	Soluble HA	2	9	42.7	12.7
5	A	47 M	Caucasian	2.3×10^8	Soluble HA	2	5	49.6	15.2
6	C	26 M	South Asian	2.3×10^8	Soluble HA	2	46	15.6	5.6
7	E	24 M	West Asian	1.5×10^8	VLP	2	4	35.2	14.0
8	A	47 M	Caucasian	1.9×10^8	VLP	2	6	30.8	6.8

PBMC: peripheral blood mononuclear cells; VLP: virus-like particles

4.8. FIGURES AND FIGURE LEGENDS

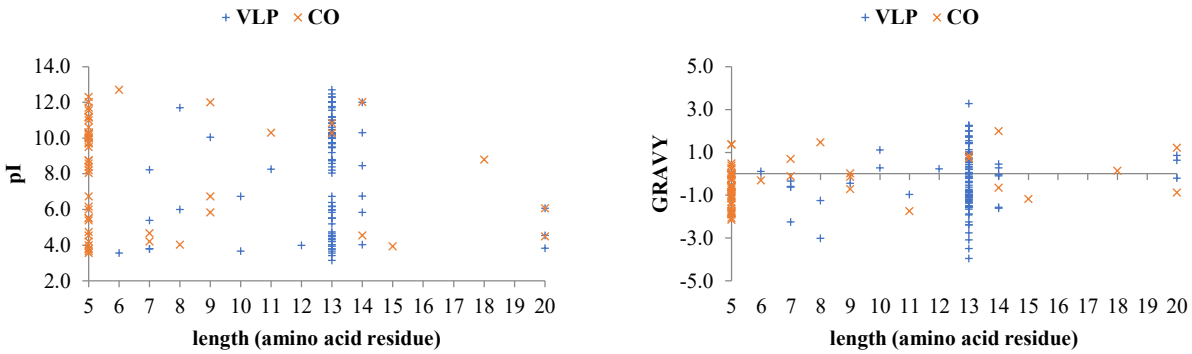

Figure 4. 1. Physicochemical properties of endogenous MHC I-restricted peptides

Length of sequence *vs.* (theoretical) isoelectric point (left) and GRAVY (grand average of hydropathy) score (right) of identified MHC I-associated peptides from monocyte-derived macrophages ± VLPs

VLP: virus-like particles; CO: soluble HA control.

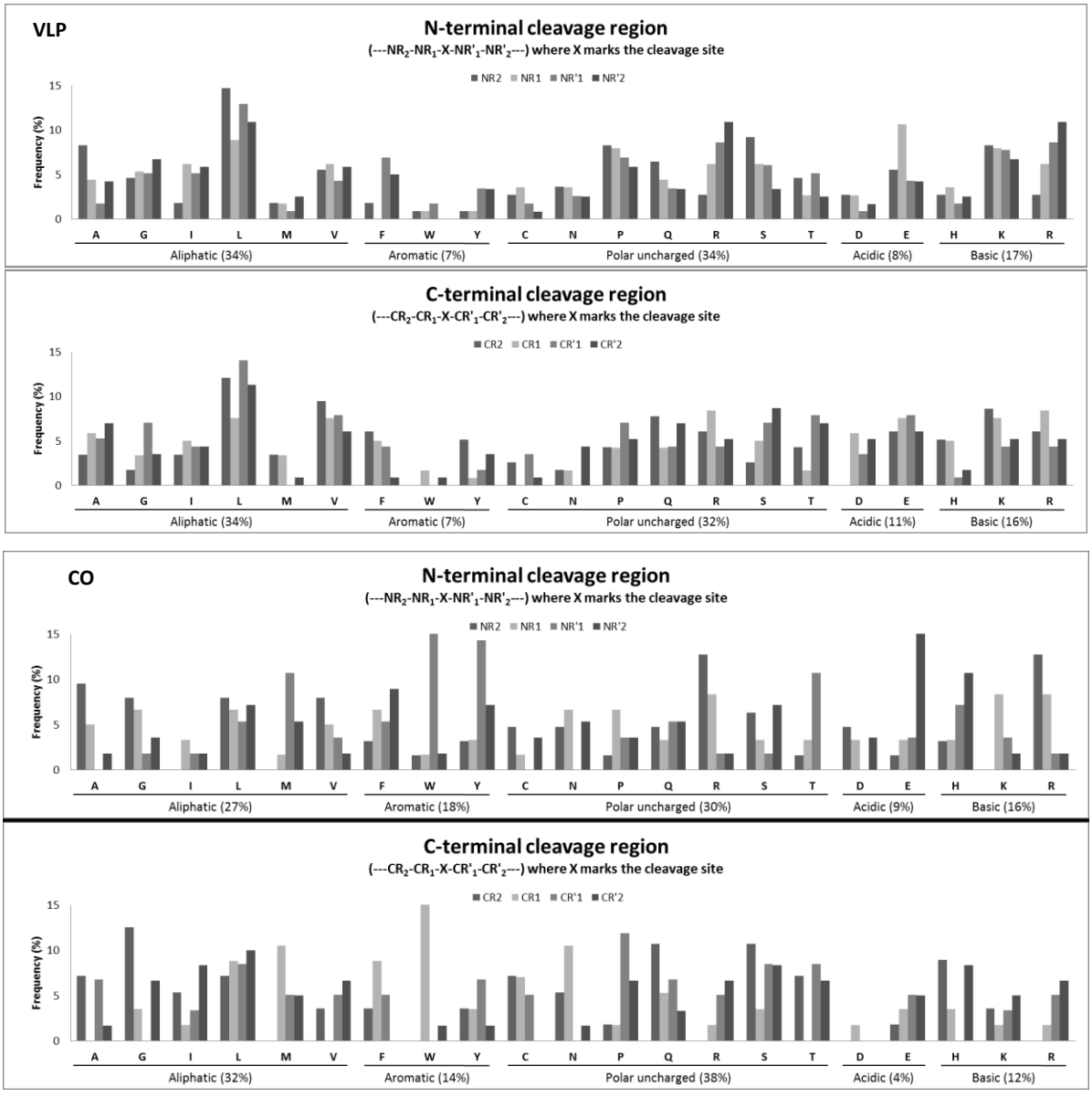

Figure 4. 2. Proteolysis patterns of MHC I-associated peptides identified from monocyte-derived macrophages

VLP-treated (above) and control (below) samples show changes in the preferred cleavage sites. VLP: virus-like particles; CO: soluble HA control.

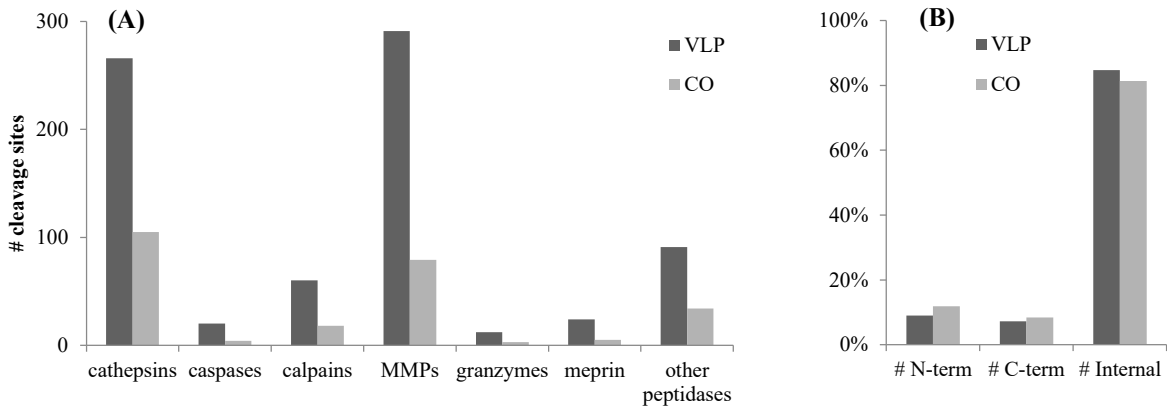

Figure 4. 3. Mechanisms of MHC I-restricted peptides generation

(A) Cellular proteases potentially involved in the processing of MHC I-associated peptides. While matrix metalloproteinases (MMPs) and cathepsins have produced the majority of the identified peptides, there was a shift from cathepsin- to MMP-cleaved peptides in VLP-treated macrophages. **(B)** Relative abundance of N-terminal, C-terminal and internal MHC I peptides in VLP-treated and control samples. Peptides cleaved within 10% of protein termini were considered N- or C-terminal.

VLP: virus-like particles; CO: soluble HA control.

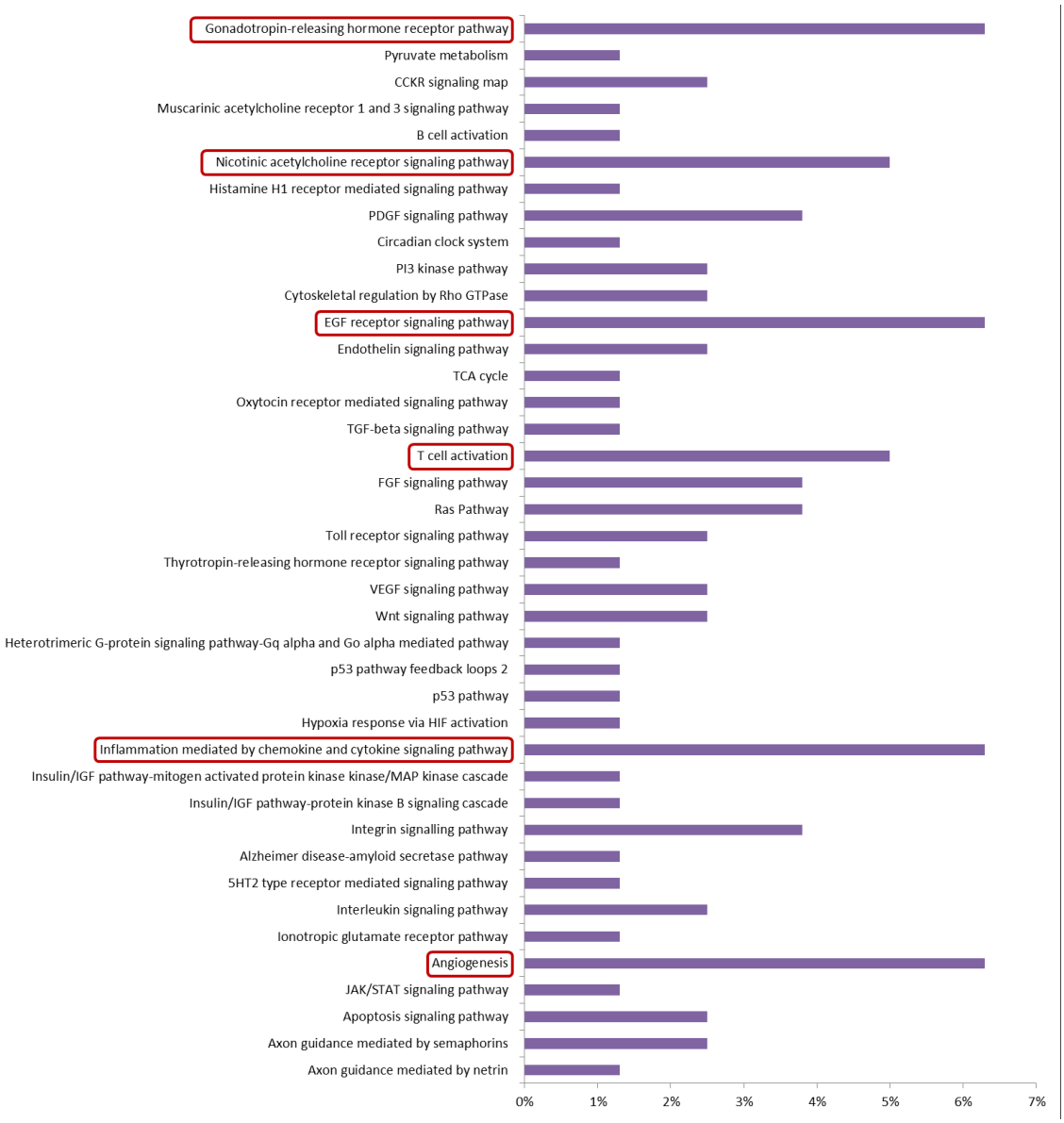

Figure 4. 4. Major pathways governed by the proteins expressed on the MHC I sites of VLP-treated monocyte-derived macrophages

Pathways with over 5% contribution were highlighted.

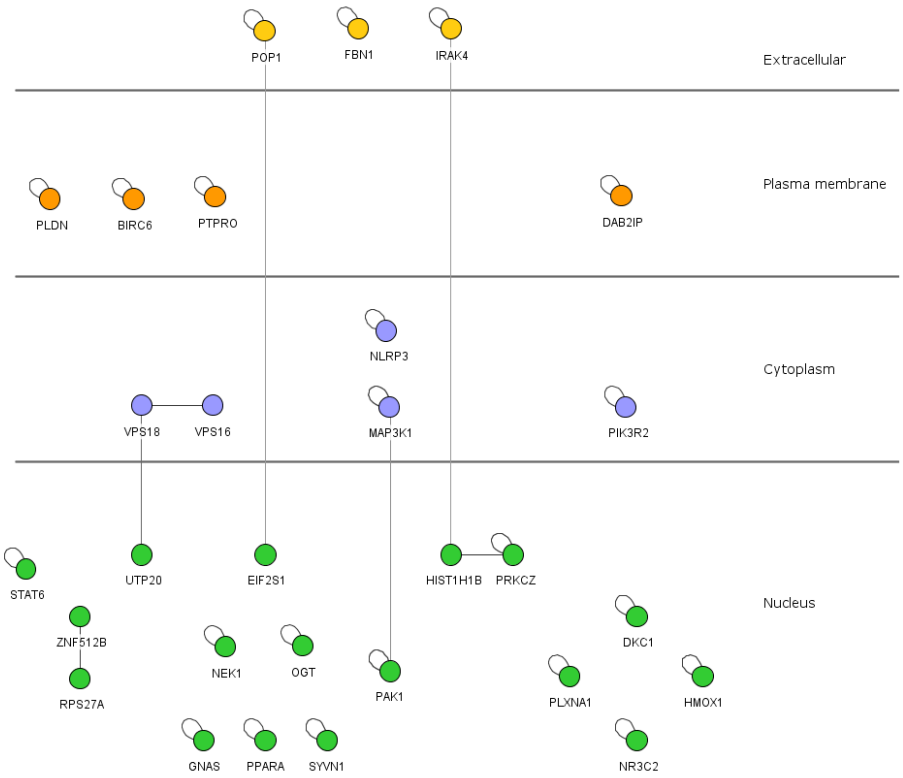

Figure 4. 5. Protein-protein interactions between the proteins expressed on the MHC I sites of VLP-treated monocyte-derived macrophages

More than 65% of reported interactions were physical associations.

4.9. SUPPLEMENTAL DATA

Supplemental Table 4. 1. Number of peptides identified with different dopants or dopant compositions used to enhance MS ionization efficiency

Dopant	Pressure (bar)	Formic acid (0.1% v/v)	# Peptides	Avg score (MaxQuant)	Avg signal intensity (MaxQuant)
None	0.0	No	56	28.4	28100
Methanol	0.3	No	85	42.8	66000
Acetone	0.3	No	32	14.9	12200
Acetonitrile	0.3	No	98	73.2	380000
MET/ACN (1:1 v/v)	0.3	No	89	55.0	120000
MET/ACE (1:1 v/v)	0.3	No	70	28.8	42900
ACE/ACN (1:1 v/v)	0.3	No	76	34.1	65400
Methanol	0.3	Yes	81	41.5	78000
Acetone	0.3	Yes	39	16.0	22000
Acetonitrile	0.3	Yes	90	71.6	240000
MET/ACN (1:1 v/v)	0.3	Yes	82	56.1	145000
MET/ACE (1:1 v/v)	0.3	Yes	76	28.2	42500
ACE/ACN (1:1 v/v)	0.3	Yes	73	31.3	58400

Note: Method optimization was performed using human serum digest from donor C, as described below. ACN: acetonitrile; ACE: acetone; MET: methanol.

Serum (2 µL) was delipidated (5 volume ice-cold acetone), denatured (50 mM DTT, 60 C, 30 min), alkylated (150 mM IAM, 25°C, 30 min, dark) and digested with sequencing-grade trypsin (Promega, Madison, WI; 1:40 w/w).

Digest peptides were cleaned on C18 reverse-phase solid-phase extraction (SPE) Macro spin columns (Harvard Apparatus, Holliston, MA) following manufacturer's instructions, and evaporated to dryness under vacuum (120 min, 37°C).

Peptides were reconstituted in 0.1% formic acid (60 µL) and analyzed (20 µL) as described in the manuscript.

Supplemental Table 4.2. 1. Number and relative abundance of protease-specific cleavage patterns identified in the MHC-I peptides from VLP-treated and control samples

	cathepsins	caspases	calpains	MMPs	granzymes	meprin	other peptidases
# in VLP	266	20	60	291	12	24	91
% in VLP	35%	3%	8%	38%	2%	3%	12%
# in CO	105	4	18	79	3	5	34
% in CO	42%	2%	7%	32%	1%	2%	14%

VLP: virus-like particles; CO: soluble HA control.

Supplemental Table 4.2. 2. Number and relative abundance of cathpesin-specific and matrix metalloprotinase-specific cleavage patterns identified in the MHC-I peptides from VLP-treated and control samples

	Cat B	Cat D	Cat E	Cat G	Cat K	Cat L	Cat S	Cat V	Cat X
# in VLP	10	25	1	1	67	62	47	53	0
% in VLP	4%	9%	0%	0%	25%	23%	18%	20%	0%
# in CO	6	18	1	1	21	23	16	19	0
% in CO	6%	17%	1%	1%	20%	22%	15%	18%	0%
% Avg	5%	13%	1%	1%	23%	23%	16%	19%	0%

	MMP-1	MMP-2	MMP-3	MMP-7	MMP-8	MMP-9	MMP-10	MMP-11
# in VLP	42	42	31	31	1	1	44	0
% in VLP	14%	14%	11%	11%	0%	0%	15%	0%
# in CO	11	11	8	8	1	1	14	0
% in CO	14%	14%	10%	10%	1%	1%	18%	0%
% Avg	14%	14%	10%	10%	1%	1%	16%	0%

	MMP-12	MMP-13	MMP-20	MMP-26	mMMP-1	mMMP-2	mMMP-4	mMMP-6
# in VLP	0	1	0	1	31	4	31	31
% in VLP	0%	0%	0%	0%	11%	1%	11%	11%
# in CO	0	1	0	0	8	0	8	8
% in CO	0%	1%	0%	0%	10%	0%	10%	10%
% Avg	0%	1%	0%	0%	10%	1%	10%	10%

VLP: virus-like particles; CO: soluble HA control.

Supplemental Table 4.2. 3. Number and relative abundance of cleavage patterns from other important proteases identified in the MHC-I peptides from VLP-treated and control samples

	calpain-2	calpain-3	granzyme A	granzyme B	granzyme K	granzyme M	meprin alpha	meprin beta	SENP1 peptidase
# in VLP	30	30	0	10	1	1	5	19	0
% in VLP	10%	10%	0%	3%	0%	0%	2%	7%	0%
# in CO	9	9	0	3	0	0	0	5	0
% in CO	11%	11%	0%	4%	0%	0%	0%	6%	0%
% Avg	11%	11%	0%	4%	0%	0%	1%	6%	0%

	SENP2 peptidase	SENP6 peptidase	SENP8 peptidase	otubain-1	legumain	blomycin hydrolase	dipeptidyl peptidase I	aspartyl aminopeptidase
# in VLP	0	0	0	0	16	0	34	10
% in VLP	0%	0%	0%	0%	5%	0%	12%	3%
# in CO	0	0	0	0	13	1	8	3
% in CO	0%	0%	0%	0%	16%	1%	10%	4%
% Avg	0%	0%	0%	0%	11%	1%	11%	4%

	paracaspase	RCE1 peptidase	aminopeptidase A	aminopeptidase B	aminopeptidase N	aminopeptidase P1
# in VLP	0	0	5	17	1	1
% in VLP	0%	0%	2%	6%	0%	0%
# in CO	0	0	2	6	0	1
% in CO	0%	0%	3%	8%	0%	1%
% Avg	0%	0%	2%	7%	0%	1%

	aminopeptidase P2	aminopeptidase P3	thimet oligopeptidase	cytosolic carboxypeptidase 1
# in VLP	0	1	0	4
% in VLP	0%	0%	0%	1%
# in CO	0	0	0	0
% in CO	0%	0%	0%	0%
% Avg	0%	0%	0%	1%

	leukotriene A4 hydrolase	cytosol alanyl aminopeptidase	endoplasmic reticulum aminopeptidase 1
# in VLP	2	0	0
% in VLP	1%	0%	0%
# in CO	0	0	0
% in CO	0%	0%	0%
% Avg	0%	0%	0%

VLP: virus-like particles; CO: soluble HA control.

Supplemental Table 4.3. Complete list of MHC-I-associated peptides identified in the VLP-treated and control samples

Sequence	Mass	Protein names	PEP	Sample	Term	Treatment
ALNFLHERGIIYR	1600.8838	Protein kinase C zeta type	1.0E-02	3	Internal	VLP
APDPTRDYFSLMD	1526.6711	Iron-sulfur cluster co-chaperone protein HscB, mitochondrial	1.0E-02	3	Internal	VLP
CMNGGSCSDDHCL	1340.4254	Fibrillin-1	1.0E-02	3	N-term	VLP
CPCDADNTISCHP	1374.5003	Multiple epidermal growth factor-like domains protein 11	1.0E-02	3	Internal	VLP
DFVDVQ	721.3283	Probable E3 ubiquitin-protein ligase HERC6	1.2E-02	8	Internal	VLP
EADVEGIQYKTLR	1520.7835	Nucleoporin Nup37	1.0E-02	3	Internal	VLP
EKKNKRPDIKKVQ	1609.9628	Interleukin-1 receptor-associated kinase 4	1.0E-02	3	C-term	VLP
ELPSNILLVRLLDGIKQR	2076.2419	E3 ubiquitin-protein ligase SH3RF1	2.2E-03	6	N-term	CO
EQPTTLSMPLLM	1359.6778	Enolase-like protein ENO4	9.3E-03	0	Internal	VLP
ERGWSTPPKCRSTIS	1703.8413	Complement factor H-related protein 2	2.2E-04	6	Internal	CO
ERQRRKKIIRDHG	1690.9816	Transcriptional adapter 2-alpha	1.0E-02	3	Internal	VLP
EYCRNDWSMWKVF	1762.7596	Dynactin-associated protein	1.0E-02	3	Internal	VLP
FDFEDVFVKIPQA	1553.7766	NADH dehydrogenase [ubiquinone] 1 alpha subcomplex subunit 9, mitochondrial	1.0E-02	3	Internal	VLP
FFGLLFWCIAFFH	1646.8108	Inward rectifier potassium channel 4	1.0E-02	3	Internal	VLP
FGCRHFS	852.3701	Uracil-DNA glycosylase	1.6E-04	6	C-term	CO
FHWKQEE	1002.4559	Signal transducer and activator of transcription 6	8.9E-04	0	Internal	VLP
FIELIPTVLRARASGIDLTA	2155.2365	Solute carrier family 22 member 10	1.4E-02	1	Internal	VLP
FILEPRLLIQQRK	1653.0090	Hermansky-Pudlak syndrome 3 protein	1.0E-02	3	Internal	VLP
FLHLKKAAIVFQK	1541.9446	Unconventional myosin-X	1.0E-02	3	Internal	VLP

FLPPVIKYTIRMS	1563.8847	ATP-binding cassette sub-family A member 12	1.0E-02	3	Internal	VLP
FMFNF	704.2992	Piwi-like protein 1	1.0E-02	6	Internal	CO
FNHTM	648.2690	Myosin-14;Synaptotagmin-like protein 1;Synaptotagmin-like protein 2;Myosin-9;Myosin-11;Myosin-10	1.0E-02	6	Internal	CO
FQYDKYVNVFYKF	1759.8610	Zinc finger protein 430	1.0E-02	3	Internal	VLP
GCDLVSW	778.3320	Integral membrane protein GPR155	3.0E-03	6	C-term	CO
GGPILPKKPPVKP	1326.8387	Targeting protein for Xklp2	1.0E-02	3	Internal	VLP
GGSFAVWGGLFSM	1314.6067	Mitochondrial import inner membrane translocase subunit Tim17-A	1.0E-02	3	Internal	VLP
GLSCRFYQHKFPE	1610.7664	Eukaryotic translation initiation factor 2 subunit 1	1.0E-02	3	N-term	VLP
GLVGAIAYAGLLG	1173.6758	GPI ethanolamine phosphate transferase 3	1.0E-02	3	Internal	VLP
GLVLKSRAKHHAI	1428.8678	Calmegin	1.0E-02	3	Internal	VLP
GRNEQFPV	945.4668	Small subunit processome component 20 homolog	9.8E-08	7	Internal	VLP
GVASTKSKQNHSK	1370.7266	Ran-binding protein 10	1.0E-02	3	Internal	VLP
HCVNM	602.2305	Sodium channel protein type 3 subunit alpha	1.0E-02	6	Internal	CO
HEFSW	704.2918	Carboxylesterase 3;Sodium/hydrogen exchanger 10	1.0E-02	6	Internal	CO
HPDLLQLPRDLEQ	1572.8260	Inverted formin-2	1.0E-02	3	Internal	VLP
HTGELPYECKECG	1464.6014	Zinc finger protein 546	1.0E-02	3	Internal	VLP
HWFSH	712.3081	Glycolipid transfer protein domain-containing protein 2;Valine--tRNA ligase, mitochondrial	1.0E-02	6	N-term	CO
HYVYQ	708.3231	Zinc finger protein 608	1.0E-02	6	Internal	CO

IAEMMFGF	944.4136	SUMO-interacting motif-containing protein 1	6.8E-06	5	Internal	CO
IFILLLVFVLIIR	1571.0578	Protein sidekick-2	1.0E-02	3	Internal	VLP
IKLLCEGLLH	1137.6580	NACHT, LRR and PYD domains-containing protein 3	2.0E-05	0	Internal	VLP
ILILRQIMALRVM	1568.9622	Glypican-4;Secreted glypican-4	1.0E-02	3	Internal	VLP
ILRKMWTRHKKKS	1711.0192	Uncharacterized protein C8orf46	1.0E-02	3	Internal	VLP
IPFVPLILKDLTF	1514.9112	Rap guanine nucleotide exchange factor-like 1	1.0E-02	3	Internal	VLP
IRYKKLLSLLTFA	1564.9705	Mitogen-activated protein kinase kinase kinase 1	1.0E-02	3	Internal	VLP
ITSELPVLQD	1113.5918	Cohesin subunit SA-1	1.2E-02	0	N-term	VLP
KAVKPKAAKPKAA	1306.8449	Histone H1.5	1.0E-02	3	Internal	VLP
KELILDKVY	1119.6540	Zinc finger C2HC domain-containing protein 1C	1.2E-02	4	Internal	CO
KHKEL	653.3861	Spectrin beta chain, non-erythrocytic 5;40S ribosomal protein S19;Putative STAG3-like protein 4;Coiled-coil domain-containing protein 152;Transcription factor Spi-B;Adenosine kinase;Centrosomal protein of 44 kDa;E3 ubiquitin-protein ligase MYLIP;Rab11 family-interacting protein 2;Gamma-taxilin;Serine palmitoyltransferase 3;Paternally-expressed gene 3 protein;Golgin subfamily B member 1	1.0E-02	6	Internal	CO
KKFNARRKLKGAI	1528.9678	Calcium/calmodulin-dependent protein kinase type II subunit alpha;Calcium/calmodulin-dependent protein kinase type II subunit delta;Calcium/calmodulin-	1.0E-02	3	Internal	VLP

		dependent protein kinase type II subunit beta				
KLEEYETLFKCQE	1658.7862	Disabled homolog 2-interacting protein	1.0E-02	3	Internal	VLP
KNAIRKLCS	1031.5910	Olfactory receptor 4C13;Olfactory receptor 4C46	6.2E-03	8	C-term	VLP
KPVLEELISARIR	1522.9195	Probable cation-transporting ATPase 13A4	1.0E-02	3	Internal	VLP
KRALKLQQKRQKE	1653.0162	Biogenesis of lysosome-related organelles complex 1 subunit 6	1.0E-02	3	Internal	VLP
KRVPFPIGIAIPF	1453.8809	Death domain-containing protein 1	1.0E-02	3	Internal	VLP
KYEGKHKRKKRRK	1741.0700	Putative uncharacterized protein encoded by LINC00467	1.0E-02	3	Internal	VLP
KYLTFLLVVTILI	1534.9738	Acetylcholine receptor subunit gamma	1.0E-02	3	Internal	VLP
LALLLHKGILAVS	1346.8650	Zinc transporter ZIP1	1.0E-02	3	Internal	VLP
LDSIASVVVPIII	1337.8170	Cysteine-rich motor neuron 1 protein;Processed cysteine-rich motor neuron 1 protein	1.0E-02	3	C-term	VLP
LEQEMGF	852.3688	Serine/threonine-protein kinase Nek1	7.6E-04	8	C-term	VLP
LEVALTLIDSWCKDHSYVIA	2275.1559	ER membrane protein complex subunit 8	1.5E-02	7	Internal	VLP
LGFCLPLYLICYR	1572.8197	Large neutral amino acids transporter small subunit 4	1.0E-02	3	C-term	VLP
LGKVKITKSGFLT	1390.8548	Putative acyl-coenzyme A thioesterase 6	1.0E-02	3	Internal	VLP
LHTRPPRFQRDFV	1667.9008	Nocturnin	1.0E-02	3	Internal	VLP
LIVCIERATRLVK	1512.9174	H/ACA ribonucleoprotein complex subunit 4	1.0E-02	3	Internal	VLP
LLPCTAQQQQQQQQQLPAL	2291.1692	R3H domain-containing protein 2	3.8E-23	5	Internal	CO
LPPRSLQVLLLLL	1473.9647	Plexin-A1	1.0E-02	3	N-term	VLP

LQQQKAKLEAKLH	1533.8991	Baculoviral IAP repeat-containing protein 6	1.0E-02	3	Internal	VLP
LRADLERAKRKLE	1596.9424	Myosin-13	1.0E-02	3	Internal	VLP
LRLRGGAKKRKKK	1538.0369	Ubiquitin-40S ribosomal protein S27a;Ubiquitin;40S ribosomal protein S27a	1.0E-02	3	Internal	VLP
LRLRHLRRPRVAR	1698.0866	Lysophosphatidic acid receptor 5	1.0E-02	3	Internal	VLP
LSKAIESGDTDLVF	1493.7613	Vacuolar protein sorting-associated protein 16 homolog	1.5E-02	0	Internal	VLP
LSSAIQVAGAPLV	1224.7078	mRNA-decapping enzyme 1A	1.0E-02	3	Internal	VLP
LSSDVLTLLIKQY	1491.8548	Lon protease homolog, mitochondrial	4.1E-03	5	Internal	CO
LVGDELWVVMEYL	1564.7847	Serine/threonine-protein kinase PAK 1;Serine/threonine-protein kinase PAK 3	1.0E-02	3	Internal	VLP
LYDRPASYKKK	1367.7561	Platelet-derived growth factor receptor alpha	3.3E-07	4	Internal	CO
MECCQ	612.1706	Espin-like protein	1.0E-02	6	Internal	CO
MEHTN	630.2432	Tubulin alpha chain-like 3;Forkhead box protein P1	1.0E-02	6	Internal	CO
METHN	630.2432	Matrix metalloproteinase-24;Processed matrix metalloproteinase-24;Beta-1,4-N-acetylgalactosaminyltransferase 3	1.0E-02	6	Internal	CO
MFKCW	713.3029	Follistatin-related protein 5	1.0E-02	6	N-term	CO
MFSHQ	648.2690	TRPM8 channel-associated factor 1;Constitutive coactivator of PPAR-gamma-like protein 2	1.0E-02	6	C-term	CO
MFSQQ	639.2687	Cip1-interacting zinc finger protein;Nuclear receptor coactivator 2	1.0E-02	6	N-term	CO

MFWGH	676.2792	SKI family transcriptional corepressor 1	1.0E-02	6	Internal	CO
MLQVLRLMVGVQV	1484.8571	Calcineurin B homologous protein 2	1.0E-02	3	Internal	VLP
MVMHN	630.2618	Uncharacterized protein KIAA1551;Niban-like protein 1	1.0E-02	6	Internal	CO
NFSKRRKVAEITG	1504.8474	Son of sevenless homolog 2;Son of sevenless homolog 1	1.0E-02	3	Internal	VLP
NKRQLERR	1098.6370	Unconventional myosin-XVIIIa	1.1E-02	7	Internal	VLP
NRENHKNENVLTVT	1666.8387	DDB1- and CUL4-associated factor 17	2.7E-03	0	Internal	VLP
PAAPWLLLGVLLL	1374.8639	NFAT activation molecule 1	1.0E-02	3	N-term	VLP
PAVKYFFDFLDEQ	1617.7715	Plexin-B2	1.0E-02	3	Internal	VLP
PFFTN	624.2908	Matrix-remodeling-associated protein 5;Cadherin-23	1.0E-02	6	Internal	CO
PFSSNIANIPRDLVDEILEE	2270.1430	SHC SH2 domain-binding protein 1-like protein	1.4E-02	7	Internal	VLP
PGAARLPSRVARL	1362.8208	UDP-N-acetylglucosamine/UDP-glucose/GDP-mannose transporter	1.0E-02	3	N-term	VLP
PIVVSKPVTVSRP	1377.8344	Zinc finger protein 512B	1.0E-02	3	Internal	VLP
PLLLYILAAKTLIL	1554.0160	Small integral membrane protein 11	3.0E-31	4	Internal	CO
PPALPPKPPKAKP	1336.8231	Phosphatidylinositol 3-kinase regulatory subunit beta	1.0E-02	3	Internal	VLP
PPKKIKTPKGTLP	1403.8864	Axonemal dynein light chain domain-containing protein 1	1.0E-02	3	N-term	VLP
PRHMRRRAMSHNV	1646.8470	Ribonucleases P/MRP protein subunit POP1	1.0E-02	3	Internal	VLP
QEMCC	612.1706	E3 ubiquitin-protein ligase Praja-1	1.0E-02	6	C-term	CO
QFSQM	639.2687	Uncharacterized protein KIAA1551	1.0E-02	6	Internal	CO
QGTDDGPSLGAQD	1259.5266	Testis-expressed sequence 33 protein	1.0E-02	3	Internal	VLP
QKVRPLARWKGQL	1578.9471	Vacuolar protein sorting-associated protein 18 homolog	1.0E-02	3	Internal	VLP

QQRLG	600.3344	Cip1-interacting zinc finger protein;Tubulin polyglutamylase complex subunit 1;Progestin and adipoQ receptor family member 9;Ig-like V-type domain-containing protein FAM187A;Neuronal pentraxin-2;Protein C-ets-1;E3 ubiquitin-protein ligase RNF25;Coiled-coil domain-containing protein 149;Molybdenum cofactor biosynthesis protein 1;Cyclic pyranopterin monophosphate synthase;Cyclic pyranopterin monophosphate synthase accessory protein;Lon protease homolog, mitochondrial;Laminin subunit alpha-4;Pericentrin;Laminin subunit alpha-5	1.0E-02	6	Internal	CO
QRAPILRPAFVPH	1500.8678	RNA-binding protein 42	1.0E-02	3	Internal	VLP
QVVKWAKVLPGFKN	1612.9453	Mineralocorticoid receptor	8.3E-03	1	Internal	VLP
RCKNRYTNILPYD	1654.8250	Receptor-type tyrosine-protein phosphatase O	1.0E-02	3	Internal	VLP
REEKYPLRGTDPL	1572.8260	Protein ALEX	1.0E-02	3	Internal	VLP
RGLSPRKLLEHVA	1474.8732	Signal-induced proliferation-associated protein 1	1.0E-02	3	Internal	VLP
RHRDFLTNDAKFK	1646.8641	Putative SMEK homolog 3	1.0E-02	3	Internal	VLP
RIVLNGIDLKAFL	1470.8922	UDP-N-acetylglucosamine--peptide N-acetylglucosaminyltransferase 110 kDa subunit	1.0E-02	3	Internal	VLP
RKRKKEKKKKKHR	1777.1751	Nucleolar protein of 40 kDa	1.0E-02	3	Internal	VLP
RMSNVYSKAAVSI	1424.7446	Patched domain-containing protein 3	1.0E-02	3	Internal	VLP

RNFQLLVITHDED	1598.8053	DNA repair protein RAD50	1.0E-02	3	C-term	VLP
RRMLHLPSL	1121.6492	Methyltransferase-like protein 12, mitochondrial	3.9E-06	4	N-term	CO
RVCNSYW	926.4069	Dual oxidase 1	9.3E-03	8	Internal	VLP
RVKGVTIVKPIVY	1470.9286	YEATS domain-containing protein 4	1.0E-02	3	N-term	VLP
RYQIINGLRRFEIE	1805.9901	Sphingomyelin phosphodiesterase 4	1.2E-02	4	Internal	CO
SFNKLIVNGRRLNV	1628.9475	Pre-mRNA-splicing factor RBM22	1.2E-02	1	Internal	VLP
SLIAEVLVKILKK	1452.9643	Secretoglobin family 1D member 2	1.0E-02	3	Internal	VLP
SNSPRDWRTITYTN	1709.8121	UPF0258 protein KIAA1024	3.0E-03	1	Internal	VLP
SQAPLLRWVLTLS	1482.8558	Heme oxygenase 1	1.0E-02	3	C-term	VLP
SVAILLYLTRKYK	1566.9497	Glutathione S-transferase theta-1	1.0E-02	3	Internal	VLP
SVKEPSKTAKQKR	1485.8627	Centrosomal protein of 78 kDa	1.0E-02	3	Internal	VLP
SYCRNPLCE	1083.4477	Transmembrane protein 39B	2.2E-03	4	N-term	CO
SYTLEDLDREFMD	1632.6978	UDP-glucuronosyltransferase 1-8	1.0E-02	3	Internal	VLP
TGETFVKLVVRLM	1491.8483	Dedicator of cytokinesis protein 1	5.9E-05	4	Internal	CO
THCAW	616.2428	SCO-spondin	1.0E-02	6	Internal	CO
THMGW	630.2584	NADH-ubiquinone oxidoreductase chain 2	1.0E-02	6	Internal	CO
TISLNISIIFLFL	1492.8905	Sodium/potassium/calcium exchanger 5	1.0E-02	3	Internal	VLP
TMGHW	630.2584	Midasin	1.0E-02	6	N-term	CO
TMGHW	630.2584	Midasin	1.4E-02	8	N-term	VLP
TMNHF	648.2690	Sperm flagellar protein 2	1.0E-02	6	Internal	CO
TPMKLMKTVMTVLGAFVVCW	2254.1750	Lysophosphatidic acid receptor 3	1.1E-39	4	Internal	CO
TPMKLMKTVMTVLGAFVVCW	2254.1750	Lysophosphatidic acid receptor 3	4.4E-05	5	Internal	CO
TSQCSFSSTIVHV	1394.6500	Period circadian protein homolog 1	1.0E-02	3	Internal	VLP
TSVETVTELTEFA	1425.6875	Peroxisome proliferator-activated receptor alpha	1.0E-02	3	Internal	VLP

TTDPEPHLEELGH	1473.6736	Pyruvate dehydrogenase E1 component subunit alpha, testis-specific form, mitochondrial	1.0E-02	3	C-term	VLP
TTEKSLKMVQQ	1291.6806	Afamin	8.9E-03	0	Internal	VLP
VENVPPVISTPHH	1424.7412	AP-3 complex subunit mu-1	1.0E-02	3	Internal	VLP
VGPVQEE	756.3654	A-kinase anchor protein 1, mitochondrial	5.5E-05	8	Internal	VLP
VIISSSILLLGTLLI	1554.0008	Leptin receptor	2.1E-08	0	Internal	VLP
VIISSSILLLGTLLI	1554.0008	Leptin receptor	2.0E-77	1	Internal	VLP
VIISSSILLLGTLLI	1554.0008	Leptin receptor	2.8E-08	2	Internal	VLP
VIISSSILLLGTLLI	1554.0008	Leptin receptor	4.7E-297	3	Internal	VLP
VIISSSILLLGTLLI	1554.0008	Leptin receptor	3.9E-100	4	Internal	CO
VIISSSILLLGTLLI	1554.0008	Leptin receptor	2.0E-167	5	Internal	CO
VLRRIKVTFLDTV	1558.9559	Autophagy-related protein 2 homolog A	1.0E-02	3	N-term	VLP
VNHQN	610.2823	Homeobox protein Hox-D10	1.0E-02	6	Internal	CO
VRDDPRIQHCRRM	1680.8413	Nebulin-related-anchoring protein	1.0E-02	3	Internal	VLP
WDPVM	646.2785	Solute carrier family 35 member F5	1.0E-02	6	C-term	CO
WENQF	722.3024	Transmembrane 9 superfamily member 4	1.0E-02	6	Internal	CO
WEPSD	632.2442	Piezo-type mechanosensitive ion channel component 2	1.0E-02	6	Internal	CO
WEQGW	704.2918	Nucleotide exchange factor SIL1;N-terminal kinase-like protein	6.6E-04	6	Internal	CO
WHCTG	602.2271	SCO-spondin	1.0E-02	6	Internal	CO
WKEKKKKKKPIQE	1697.0352	RalA-binding protein 1	1.0E-02	3	Internal	VLP
WKVPP	625.3588	Alpha-mannosidase 2x	1.0E-02	6	Internal	CO
WLAEDRVDFMERS	1652.7617	E3 ubiquitin-protein ligase synoviolin	1.0E-02	3	Internal	VLP

WLPAL	598.3479	GPI ethanolamine phosphate transferase 3;Vacuolar-sorting protein SNF8;Putative inactive carboxylesterase 4;Isthmin-2;Metal transporter CNNM1;Adenylate cyclase type 4;Cilia- and flagella-associated protein 54;Protein SZT2	1.0E-02	6	Internal	CO
WPPFC	648.2730	Otogelin	1.0E-02	6	Internal	CO
WQANM	648.2690	Putative adenosylhomocysteinase 2	1.0E-02	6	Internal	CO
WQEGW	704.2918	Presequence protease, mitochondrial	1.0E-02	6	Internal	CO
YDYLN	686.2912	Activin receptor type-1C;Cadherin-19;Cadherin-3;Cadherin-1;E-Cad/CTF1;E-Cad/CTF2;E-Cad/CTF3;Cadherin-2;Cadherin-4	1.0E-02	6	Internal	CO
YEDDEEEGEDEEE	1615.5169	Nucleosome assembly protein 1-like 5	1.0E-02	3	Internal	VLP
YFTYW	778.3326	Inactive rhomboid protein 2	2.6E-03	6	Internal	CO
YHEAW	704.2918	CTP synthase 1	1.0E-02	6	Internal	CO
YHVQC	648.2690	Multidrug resistance-associated protein 4	1.0E-02	6	Internal	CO
YKRLEIYLEPLKD	1678.9294	Protrudin	1.0E-02	3	Internal	VLP
YLGSPFWIHQAVR	1572.8201	Thrombopoietin receptor	1.0E-02	3	Internal	VLP
YNASW	639.2653	Group 3 secretory phospholipase A2	1.0E-02	6	Internal	CO
YRTMTGLDTPVLMV	1595.8051	Oxidation resistance protein 1	1.0E-02	0	Internal	VLP
YSCKC	602.2193	Disintegrin and metalloproteinase domain-containing protein 28;Slit homolog 2 protein;Slit homolog 2 protein N-product;Slit homolog 2 protein C-product;Neurogenic locus notch homolog protein 1;Notch 1 extracellular truncation;Notch 1 intracellular domain;Sushi, von	1.0E-02	6	Internal	CO

		Willebrand factor type A, EGF and pentraxin domain-containing protein 1				
YSHGW	648.2656	Kallikrein-2	1.2E-04	6	Internal	CO
YSSYGF	722.2912	Arylsulfatase H	1.6E-08	6	Internal	CO

VLP: virus-like particles; CO: soluble HA control.

Supplemental Table 4.4. 1. Gene ontology analysis of MHC-I-associated peptides identified in VLP-treated samples

GO - molecular function		#	percent
1	translation regulator activity	1	1.20%
2	binding	31	36.00%
3	receptor activity	6	7.00%
4	structural molecule activity	3	3.50%
5	signal transducer activity	7	8.10%
6	catalytic activity	29	33.70%
7	transporter activity	9	10.50%

GO - biological process		#	percent
1	cellular component organization or biogenesis	17	8.90%
2	cellular process	55	28.60%
3	localization	16	8.30%
4	reproduction	1	0.50%
5	biological regulation	19	9.90%
6	response to stimulus	18	9.40%
7	developmental process	11	5.70%
8	rhythmic process	1	0.50%
9	multicellular organismal process	8	4.20%
10	biological adhesion	3	1.60%
11	locomotion	2	1.00%
12	metabolic process	38	19.80%
13	immune system process	3	1.60%

GO - cellular component		#	percent
1	cell junction	2	2.10%
2	membrane	17	17.50%
3	macromolecular complex	19	19.60%
4	extracellular matrix	1	1.00%
5	cell part	33	34.00%
6	organelle	24	24.70%
7	extracellular region	1	1.00%

GO - protein class		#	percent
1	transporter	6	9.80%
2	transmembrane receptor regulatory/adaptor protein	1	1.60%
3	membrane traffic protein	1	1.60%
4	chaperone	1	1.60%
5	oxidoreductase	4	6.60%
6	cell adhesion molecule	1	1.60%
7	enzyme modulator	7	11.50%
8	lyase	1	1.60%
9	transfer/carrier protein	5	8.20%
10	transferase	1	1.60%
11	transcription factor	6	9.80%
12	nucleic acid binding	12	19.70%
13	receptor	6	9.80%
14	calcium-binding protein	3	4.90%
15	cytoskeletal protein	1	1.60%
16	signaling molecule	2	3.30%
17	extracellular matrix protein	3	4.90%

GO - pathway		#	percent
1	Axon guidance mediated by netrin	1	1.30%
2	Axon guidance mediated by semaphorins	2	2.50%
3	Apoptosis signaling pathway	2	2.50%
4	JAK/STAT signaling pathway	1	1.30%
5	Angiogenesis	5	6.30%
6	Ionotropic glutamate receptor pathway	1	1.30%
7	Interleukin signaling pathway	2	2.50%
8	5HT2 type receptor mediated signaling pathway	1	1.30%
9	Alzheimer disease-amyloid secretase pathway	1	1.30%
10	Integrin signalling pathway	3	3.80%
11	Insulin/IGF pathway-protein kinase B signaling cascade	1	1.30%
12	Insulin/IGF pathway-mitogen activated protein kinase kinase/MAP kinase cascade	1	1.30%
13	Inflammation mediated by chemokine and cytokine signaling pathway	5	6.30%
14	Hypoxia response via HIF activation	1	1.30%
15	p53 pathway	1	1.30%
16	p53 pathway feedback loops 2	1	1.30%
17	Heterotrimeric G-protein signaling pathway-Gq alpha and Go alpha mediated pathway	1	1.30%
18	Wnt signaling pathway	2	2.50%
19	VEGF signaling pathway	2	2.50%

20	Thyrotropin-releasing hormone receptor signaling pathway	1	1.30%
21	Toll receptor signaling pathway	2	2.50%
22	Ras Pathway	3	3.80%
23	FGF signaling pathway	3	3.80%
24	T cell activation	4	5.00%
25	TGF-beta signaling pathway	1	1.30%
26	Oxytocin receptor mediated signaling pathway	1	1.30%
27	TCA cycle	1	1.30%
28	Endothelin signaling pathway	2	2.50%
29	EGF receptor signaling pathway	5	6.30%
30	Cytoskeletal regulation by Rho GTPase	2	2.50%
31	PI3 kinase pathway	2	2.50%
32	Circadian clock system	1	1.30%
33	PDGF signaling pathway	3	3.80%
34	Histamine H1 receptor mediated signaling pathway	1	1.30%
35	Nicotinic acetylcholine receptor signaling pathway	4	5.00%
36	B cell activation	1	1.30%
37	Muscarinic acetylcholine receptor 1 and 3 signaling pathway	1	1.30%
38	CCKR signaling map	2	2.50%
39	Pyruvate metabolism	1	1.30%
40	Gonadotropin-releasing hormone receptor pathway	5	6.30%

Supplemental Table 4.4. 2. Gene ontology analysis of MHC-I-associated peptides identified in control samples

GO - molecular function		#	percent
1	binding	10	34.50%
2	receptor activity	3	10.30%
3	structural molecule activity	1	3.40%
4	signal transducer activity	1	3.40%
5	catalytic activity	10	34.50%
6	transporter activity	4	13.80%

GO - biological process		#	percent
1	cellular component organization or biogenesis	5	6.80%
2	cellular process	20	27.00%
3	localization	4	5.40%
4	reproduction	3	4.10%
5	biological regulation	8	10.80%
6	response to stimulus	5	6.80%
7	developmental process	6	8.10%
8	multicellular organismal process	6	8.10%
9	biological adhesion	1	1.40%
10	locomotion	2	2.70%
11	metabolic process	14	18.90%

GO - cellular component		#	percent
1	membrane	9	24.30%
2	macromolecular complex	3	8.10%
3	extracellular matrix	2	5.40%
4	cell part	13	35.10%
5	organelle	9	24.30%
6	extracellular region	1	2.70%

GO - protein class		#	percent
1	transporter	3	11.50%
2	hydrolase	11	42.30%
3	enzyme modulator	3	11.50%
4	transfer/carrier protein	2	7.70%
5	ligase	1	3.80%
6	transferase	1	3.80%
7	receptor	2	7.70%
8	cytoskeletal protein	2	7.70%

9	signaling molecule	1	3.80%

GO - pathway		#	percent
1	De novo pyrimidine ribonucleotides biosythesis	1	10.00%
2	Angiogenesis	1	10.00%
3	Integrin signalling pathway	1	10.00%
4	Alzheimer disease-presenilin pathway	1	10.00%
5	Inflammation mediated by chemokine and cytokine signaling pathway	1	10.00%
6	Wnt signaling pathway	1	10.00%
7	TGF-beta signaling pathway	1	10.00%
8	PDGF signaling pathway	1	10.00%
9	Cytoskeletal regulation by Rho GTPase	1	10.00%
10	Nicotinic acetylcholine receptor signaling pathway	1	10.00%

Supplemental Table 4.5. Complete list of interactions reported between the MHC-I-associated peptides identified in the VLP-treated sample

queryXref	idgroup	fullname	species	type	Num Public	PMIDs	Source DBIds	Interactor Types
Q9NR09	174777	BIRC6 physically associates with BIRC6	Homo sapiens	physical association	1	15200957	BIOGRID-677890	protein - protein
Q13233	480411	Colocalization of MAP3K1 and MAP3K1	Homo sapiens	colocalization	1	11784851	BIOGRID-715707	protein - protein
Q13153	262306	Colocalization of PAK1 and PAK1	Homo sapiens	colocalization	1	11804587	BIOGRID-317166	protein - protein
Q99575	453327	Colocalization of POP1 and EIF2S1	Homo sapiens	colocalization	1	22939629	BIOGRID-747199	protein - protein
O75691	191501	Colocalization of VPS18 and UTP20	Homo sapiens	colocalization	1	22939629	BIOGRID-749016	protein - protein
Q9H269	191504	Colocalization of VPS18 and VPS16	Homo sapiens	colocalization	1	22939629	BIOGRID-742948	protein - protein
Q5VWQ8	73625	DAB2IP interacts with DAB2IP	Homo sapiens	self interaction	1	12813029	EBI-6692336; EBI-6692328	protein - protein
O60832	181555	DKC1 physically associates with DKC1	Homo sapiens	physical association	1	21931644	BIOGRID-855408	protein - protein
P35555	7886	FBN1 physically interacts with FBN1	Homo sapiens	physical interaction	1	25034023	EBI-9636797	protein - protein
P84996	224015	GNAS physically interacts with GNAS	Homo sapiens	physical interaction	1	7797570	BIOGRID-316551	protein - protein

P16401	74615	HIST1H1B physically interacts with IRAK4	Homo sapiens	physical interaction	1	15927069	BIOGRID-632455	protein - protein
P09601	445292	HMOX1 associates with HMOX1	Homo sapiens	association	1	12500973	BIOGRID-275144	protein - protein
P09601	445296	HMOX1 physically associates with HMOX1	Homo sapiens	physical association	4	15522396, 12500973, 15049686, 15525643	BIND-305590; BIND-113193; BIND-109660; BIND-113194; BIND-108893; BIND-163782	protein - protein
Q13153	480376	MAP3K1 physically interacts with PAK1	Homo sapiens	physical interaction	1	12228228	BIOGRID-720318	protein - protein
Q13233	480407	MAP3K1 physically associates with MAP3K1	Homo sapiens	physical association	1	11784851	BIOGRID-715706	protein - protein
Q13233	480406	MAP3K1 physically interacts with MAP3K1	Homo sapiens	physical interaction	1	11784851	BIOGRID-715696	protein - protein
Q96PY6	374443	NEK1 physically associates with NEK1	Homo sapiens	physical association	1	14690447	EBI-696022	protein - protein
Q96P20	94819	NLRP3 physically associates with NLRP3	Homo sapiens	physical association	2	23582325, 25686105	EBI-6910800; IDB-	protein - protein

							2061346; IDB-1631978	
P08235	23852	NR3C2 physically associates with NR3C2	Homo sapiens	physical association	1	15967794	BIND-330717	protein - protein
O15294	111243	OGT physically associates with OGT	Homo sapiens	physical association	2	10753899, 15361863	BIND-302861; BIOGRID-281374	protein - protein
Q13153	262276	PAK1 associates with PAK1	Homo sapiens	association	1	10975528	BIOGRID-317167	protein - protein
Q13153	262282	PAK1 physically associates with PAK1	Homo sapiens	physical association	1	11804587	BIOGRID-317165	protein - protein
Q13153	262280	PAK1 physically associates with PAK1	Homo sapiens	physical association	3	11804587, 10975528, 16278681	BIND-87589; BIND-87591; BIOGRID-317168; BIND-87590; BIOGRID-740069	protein - protein
Q13153	262297	Phosphorylation of 22000 by 65610	Homo sapiens	phosphorylation	1	12228228	IDB-117542	protein - protein
Q9NWZ3	15782	Phosphorylation of 28022 by 28022	Homo sapiens	phosphorylation	1	17141195	IDB-113326	protein - protein
Q9NWZ3	15788	Phosphorylation of 28022 by 28022	Homo sapiens	phosphorylation reaction	1	21220427	IDB-190153	protein - protein

Q13153	262275	Phosphorylation of 65610 by 65610	Homo sapiens	phosphorylation	3	10995762, 10980699, 7618083	IDB-117340; IDB-117288; IDB-117293	protein - protein
Q05513	154766	Phosphorylation of 86108 by 86108	Homo sapiens	phosphorylation reaction	2	11078718, 15665819	IDB-118776; IDB-120715; IDB-120711	protein - protein
O00459	281833	PIK3R2 physically associates with PIK3R2	Homo sapiens	physical association	1	19380743	BIOGRID-726260	protein - protein
Q9UL45	22023	PLDN physically interacts with PLDN	Homo sapiens	physical interaction	2	16189514, 15102850	BIOGRID-120528; BIOGRID-251821; BIND-215902	protein - protein
Q9UIW2	296459	PLXNA1 physically associates with PLXNA1	Homo sapiens	physical association	2	15187088, 11239433	BIOGRID-315776; BIOGRID-251225	protein - protein
Q99575	453320	POP1 physically associates with POP1	Homo sapiens	physical association	1	15096576	BIND-153546; BIND-151564; BIOGRID-251885	protein - protein
Q07869	56019	PPARA physically associates with PPARA	Homo sapiens	physical association	1	11698662	BIND-102382	protein - protein

Q05513	154703	PRKCZ physically interacts with HIST1H1B	Homo sapiens	physical interaction	1	8663071	BIOGRID-860019	protein - protein
Q05513	154751	PRKCZ physically interacts with PRKCZ	Homo sapiens	physical interaction	5	21911421, 21624955, 19920073, 15665819, 7588787	BIOGRID-569256; BIOGRID-565828; BIOGRID-608713; BIND-209434; BIOGRID-818000	protein - protein
Q16827	205345	PTPRO associates with PTPRO	Homo sapiens	association	1	15978577	MINT-62307; MINT-62298; EBI-7669477; EBI-7670237	protein - protein
Q96KM6	47048	RPS27A interacts with ZNF512B	Homo sapiens	physical association	1	15231748	BIND-149778; BIOGRID-834395	protein - protein
P42226	127111	STAT6 physically associates with STAT6	Homo sapiens	physical association	1	8085155	BIND-185448	protein - protein
Q86TM6	319336	SYVN1 physically associates with SYVN1	Homo sapiens	physical association	3	19864457, 21149444, 24366871	BIOGRID-573717; BIOGRID-592993; BIOGRID-938384	protein - protein

Q86TM6	319335	SYVN1 physically interacts with SYVN1	Homo sapiens	physical interaction	3	16289116, 12646171, 23867461	BIOGRID-696288; BIOGRID-463073; BIOGRID-882679	protein - protein
Q9H269	191494	VPS16 interacts with VPS18	Homo sapiens	physical association	1	11382755	BIOGRID-301758; BIOGRID-301755	protein - protein

Chapter 5: A novel serological assay for influenza based on DiD fluorescence dequenching that is free from observer bias and potentially automatable – A proof of concept study

Alexander I. Makarkov [a,b,1], Aakash R. Patel [b,1], Valentine Bainov [c], Brian J. Ward [b]

[a] Division of Experimental Medicine, Department of Medicine, McGill University, 1001 Décarie Street, Montréal, Québec H4A 3J1, Canada

[b] Research Institute of McGill University Health Centre, Glen Site, 1001 Décarie Street, Montréal, Québec H4A 3J1, Canada

[c] ConKor Systems Ltd., High Tech Park, Kibbutz Saar, Mail to P.O. Box 3047, Nahariya, Israel

[1] These authors contributed equally.

Adapted from *Vaccine*, with permission from Elsevier, Copyright © 2018 Elsevier Ltd. Makarkov AI, Patel AR, Bainov V, Ward BJ. A novel serological assay for influenza based on DiD fluorescence dequenching that is free from observer bias and potentially automatable - A proof of concept study. Vaccine. 2018;36(30):4485-93.

5.1. PREFACE

Work described in the previous chapters have focused on understanding the robust and diverse immunogenicity of the plant-derived VLP that elicit strong and cross-reactive antibody responses against both seasonal and pandemic influenza strains in animal models and clinical trials. Our experiments demonstrated that H1-VLP-exposed APCs can present HA-derived antigenic peptides in the association with MHC I molecules. Further, we attempted to develop a novel method for assessment of the humoral immune response to influenza vaccines that would measure the titers of 'functional' antibodies and has the potential to become a fully automated and observer bias-free assay. We used the phenomenon of DiD fluorescence dequenching to study fusion of DiD-labelled VLPs with endosomal membranes in U-937 cells and human MDM (chapter 2). In the following chapter, we describe the performance of a serological assay based on DiD fluorescence dequenching with three influenza strains included in the seasonal influenza

vaccine by comparing the DiD dequenching antibody titers with those measured by the conventional HAI and MN techniques.

5.2. ABSTRACT

Background: Serum hemagglutination inhibition (HAI) and microneutralization (MN) antibodies are often used as a correlate of protection for influenza. However, these manual assays are labor-intensive and difficult to standardize due to variability in biologic reagents used and subjective interpretation of the results.

Methods: Sera with known HAI and MN titers were used to assess a novel test based on the inhibition of fluorescence 'dequenching'. Whole influenza virions (A/California/07/2009 (H1N1), A/Hong Kong/4801/2014 (H3N2) and B/Brisbane/60/2008) labelled with 1,1′-dioctadecyl-3,3,3′,3′-tetramethylindodicarbocyanine perchlorate (DiD) were exposed to serial dilutions of serum and mixed with turkey red blood cells followed by acidification of the media (pH 5.0–5.5). The H1N1 and B/Brisbane strains were high hemagglutinating while the H3N2 strain had low hemagglutinating activity. In some experiments, labelled virions were subjected to repetitive freeze-thaw cycles prior to use in the assay.

Results: In the absence of detectable HAI/MN antibodies, there were consistent and substantial increases from baseline DiD fluorescence upon acidification. Sera with known high titer HAI/MN antibodies reduced or completely prevented DiD dequenching at low dilutions with progressive increases in fluorescence at higher dilutions, which permitted a reproducible assignment of an antibody 'titer' based on baseline and acidified DiD fluorescence values. The 'titers' measured by the DiD dequenching assay were highly correlated with HAI/MN results for the H1N1 and B strains (Spearman's correlation coefficients (r_s) 0.874 to 0.946, $p < 10^{-7}$ to 10^{-35}). Correlations with HAI/MN titres for the low-hemagglutinating H3N2 strain tested were lower but remained statistically significant (r_s 0.547–0.551, $p < 0.004$). Freeze-thawing of the DiD pre-stained virus stocks had no significant impact on the results of the assay.

Conclusions: The DiD dequenching assay may be a labour-saving and more objective alternative to the classic serologies. This novel assay could theoretically be standardized across laboratories using pre-stained virions and has the potential to be fully automated.

5.3. INTRODUCTION

Over the last 75 years, a large number of serologic tests have been introduced to assess the humoral response to natural influenza infection and influenza vaccination (1). Among the most important are the hemagglutination inhibition (HAI) and microneutralization (MN) assays that have slowly become embedded as 'reference' assays over the last half-century (2–4). For better or worse (5), these assays have been widely used as a surrogate for protection to both license and compare vaccines (4). It is likely that many hundreds of thousands if not millions of HAI and MN assays are performed every year in reference, industry and academic laboratories around the globe.

Despite its obvious utility, the HAI and MN assays are not simple assays to perform for a number of reasons. First, these assays use a number of biologic reagents such as red blood cells from various species (e.g. turkey, horse, guinea pig), either live or inactivated viruses grown in hens' eggs or tissue culture (e.g. Madin-Darby canine kidney (MDCK) cells), virus-like particles produced in various systems and receptor destroying enzyme (RDE from Vibrio cholerae culture supernatant). Although some aspects of these assays can be automated, they are typically read visually and are therefore subject to large operator bias (6). These characteristics make the classical serological assays very difficult to standardize. Despite substantial effort over decades (7–10), the variance in Geometric Mean Titers (GMT) between industry, academic and public health laboratories performing HAI testing for example can still be stubbornly high (e.g. 80-fold variation in one recent study) (9). Although the use of international standard sera (9) and standardizing methodologies can improve reproducibility (10,11), there is still considerable residual variability between laboratories even when both methodologies and reagents are harmonized (12).

Herein we present the results of a proof-of-concept study that targeted the least automatable step in the standard serological tests: the visual reading and interpretation of the assay. To do this, we exploited dequenching of fluorescence of DiD pre-labeled influenza virions (13–15). Hemagglutinin (HA)-mediated fusion of such virions with turkey red blood cells (RBC) under acid conditions permits diffusion of the fluorescent dye into a larger membrane area and release of fluorescence (up to 40-fold from baseline). In natural influenza infection, the viral envelope fuses with host cell membranes in late endosomes where acidification drives conformational changes in the HA protein that are required for fusion (16). Theoretically, the

pre-incubation of labeled virions with different dilutions of immune serum should prevent such dequenching to a greater or lesser extent depending upon the antibody titer. We tested this novel assay with three different DiD-labeled influenza viruses included in the 2016–2017 vaccine, e.g. A/California/07/2009 (H1N1), A/Hong Kong/4801/2014 (H3N2) and B/Brisbane/60/2008. We observed near perfect correlation between the DiD dequenching and classical HAI and MN results with the influenza H1N1 and B strains. Correlations with the low-agglutinating H3N2 strain were lower but were still highly significant. Results were not changed by repeated freeze-thaws of the DiD-labeled virions.

5.4. MATERIALS AND METHODS

5.4.1. Participants and serum samples

Serum samples collected from a subset of adult healthy volunteers group participating in an influenza vaccination clinical trial (clinicaltrials.gov: NCT03150537) were used in this project. Study participants were immunized with a commercial 2016–2017 trivalent split virion influenza vaccine (Fluviral, GlaxoSmithKline Inc., Mississauga, ON) containing the following antigens: A/California/07/2009 (H1N1), A/Hong Kong/4801/2014 (H3N2) and B/Brisbane/60/2008. Paired sera collected prior to (day 0) and at day 21 after vaccination were tested for antibodies against the targeted H1N1 (n = 72), H3N2 (n = 26) and B strains (n = 24).

5.4.2. Conventional antibody tests

HAI titers were determined as previously described (12). Briefly, influenza virus stocks were prepared in MDCK cells (ATCC CCL-34). A/California/07/2009(H1N1), A/Hong Kong/4801/2014 (H3N2) and B/Brisbane/60/2008 (B_{Bris})-like viruses were provided by the National Microbiology Laboratory (Winnipeg, MB). Serum samples were treated with receptor-destroying enzyme (RDE, Denka Seiken, Tokyo, Japan), heat-inactivated (56°C for 30 min) and further diluted to 1:10 with phosphate-buffered saline (PBS, Wisent, Saint-Jean-Baptiste, QC). 2-fold serial dilutions in PBS (starting at 1:10) of 25 µL serum samples in 96-well V-bottom plates (Corning, Kennebunk, ME) were incubated with 25 µL (4 hemagglutination units) of the virus for 30 min at room temperature (RT). 50 µL of 0.5% RBCs in PBS from turkey whole blood (Lampire Biological Laboratories, Pipersville, PA) were added, and the reaction mixture was

incubated for a further 30 min at RT. Wells were examined visually for inhibition of hemagglutination, as indicated by the appearance of well-defined RBC 'buttons' or teardrop formation upon plate tilting. HAI titer was determined as the highest dilution of serum that completely prevented hemagglutination.

MN titers were determined as previously described (17). Briefly, MDCK cells were seeded into flat-bottom 96-well plates (Corning, Corning, NY) in HyClone SFM4MegaVir medium (MegaVir, Thermo Scientific, Waltham, MA) to achieve confluent cell monolayers. 2-fold serial dilutions of tested sera starting at 1:10 in MegaVir were incubated with 100 50% tissue culture infective doses (TCID50) of the virus for 2 h at 37 °C with 5% CO_2. Serum/virus mixture was then added to MDCK cells in MegaVir medium with 1 × TPCK (tolylsulfonyl phenylalanyl chloromethyl ketone)-treated trypsin (Sigma-Aldrich, St. Louis, MO). After 3 h at 37°C with 5% CO_2, medium in each well was refreshed with MegaVir medium with 0.75 × TPCK-treated trypsin (1 × TPCK-treated trypsin for H1N1 strain). MDCK cells were examined for the presence of cytopathic effect at day 3 to 5 of the experiment, and MN titer was defined as the highest serum dilution allowed retaining a confluent cell monolayer. The lower limit of detection (LOD) of both of these assays was 1:10.

5.4.3. DiD labeling of influenza virions

Influenza viruses (H1N1, H3N2 and B_{Bris} as above) were propagated in MDCK cells. Culture supernatants were collected at peak cytopathic effect and virions were purified from cell debris by ultracentrifugation (Optima XPN-90 ultracentrifuge with SW 32 Ti rotor, Beckman Coulter, Brea, CA) on 15% – 20% – 30% OptiPrep Density Gradient Medium (Sigma-Aldrich) at 174,000 × g for 3 h at 4°C. Virions were stained with the lipophilic dye 1,1′-dioctadecyl-3,3,3′,3′-tetramethylindodicarbocyanine perchlorate (DiD, Thermo Fisher Scientific, Eugene, OR) at a concentration of 20 µg/mL for 30 min at RT and then purified from free dye by gel filtration columns (PD MiniTrap G-25, GE Healthcare, Buckinghamshire, UK). To test the efficiency of DiD self-quenching, different virus preparations were loaded with DiD at concentrations ranging from 1.25 to 80 µg/mL. DiD-stained virus stocks were either used the same day or stored at −80°C until used. Some aliquots were subjected to up to two freeze-thaw cycles prior to use.

5.4.4. DiD dequenching assay

Serum samples were heat-inactivated, treated with RDE (as above) and serially diluted 2-fold (starting at 1:10) in 5% Bovine Serum Albumin (BSA, Sigma-Aldrich) in PBS (for additional buffering capacity) in 96-well Nunclon Delta black flat-bottom plates (Thermo Fisher Scientific, Roskilde, Denmark), 25 µL/well. DiD-labeled virus was diluted in 5% BSA in PBS (8 hemagglutination units/50 µL) and added to the serum dilutions, 25 µL/well. Plates were incubated at RT for 30 min before the addition of 50 µL/well of 0.5% turkey RBC in PBS with 5% BSA. After a further 30 min incubation at RT, baseline DiD fluorescence was measured using an Infinite 200 PRO spectrophotometer (Tecan, Männedorf, Switzerland) at 644 nm excitation and 680 nm emission wavelengths. The serum/DiD-stained virus/RBC reaction mixture was then acidified by adding 35 µL/well of 0.19% hydrochloric acid (HCl, Fisher Scientific Canada, Ottawa, ON) in PBS to achieve a pH between 5.0 and 5.5. Plates were incubated for 20 min at 37°C with 5% CO_2, and fluorescence was remeasured using the same spectrophotometer settings. To establish the magnitude of full DiD dequenching, Triton X-100 (Sigma-Aldrich) at final concentration 1% was added to the DiD-labelled viral inoculum in some experiments. Fluorescence was expressed as arbitrary units (a.u.). Baseline and acidified DiD fluorescence intensity curves were then plotted and examined visually. Serum titers for all assays are reported as reciprocals of the highest dilution considered to be 'positive' in each assay and assignment of the DiD dequenching assay titers was performed independently by two individuals (A.I.M., A.R.P.) blinded to the HAI/MN titers of the samples. The LOD of the dequenching assay was also 1:10.

5.4.5. Automated titer assignment in the dequenching assay

Although most curves were easy to interpret visually, we wanted to develop an algorithm (Microsoft Excel-based) for assigning titers to see if this subjective element of the assay could also be eliminated. Individual data sets consisting of the baseline $B(d)$ and acidified $A(d)$ DiD fluorescence readings for eight serial serum dilutions were analyzed where $d = \{1{:}\,10, 1{:}\,20, 1{:}\,40, 1{:}\,80, 1{:}\,160, 1{:}\,320, 1{:}\,640, 1{:}\,1280\}$.

We used three empirically defined thresholds selected for fitting the calculation results to the conventional HAI titers:

$$th_1 = 0.25; th_2 = 2.8; th_3 = 0.9.$$

We defined $minA$ and $minB$ values as:

$$minB = MIN\{B(d)\};\ minA = MIN\{A(d) > minB\},$$

We normalized $A(d)$ and defined its derivative:

$$r(d) = \frac{A(d) - minA}{minA}$$

$$r'(d) = \text{IF } r(d) \leq th_1 \text{ THEN } \frac{\Delta r}{\Delta d} \text{ ELSE } 0$$

Next, we attempted to classify each data set using the following two criteria:

C_1 — Acidified readings are too high above the baseline readings

$$C_1 = \frac{minA}{minB} \leq th_2$$

C_2 — It is possible to characterize the acidified fluorescence reading values as a U-shaped curve of $r(d)$ with expressed left arch, nearly horizontal plateau in the middle and (present in some cases) small right arch. We aimed to locate the beginning of the left arch L as

$$C_2 = \exists L \mid r'(d_{L-1}) \equiv 0, r'(d_L) > 0$$

The DiD dequenching assay antibody titer of a given serum sample was then determined through falling into one of the three categories:

Category	Description	C1	C2	Result of the calculation
1	'Too high above the base line' case	TRUE	any	<10
2	U-shaped curve detected	FALSE	TRUE	IF $r(d_{L+1}) > th_3$THEN $L+1$ ELSE $L+2$
3	Left slope without horizontal plateau	FALSE	FALSE	$\min(i \mid r(d_i) > th_3)$

5.4.6. Statistical analysis

Statistical analyses were performed using GraphPad Prism 6.0 software. We calculated Spearman rank correlation coefficients for antibody titers between log-transformed HAI or MN titers and DiD dequenching assay results. We also created linear regression plots for visual

presentation of the data. For statistical analyses, we assigned a value of 1:5 to antibody titers below the LOD for each assay. To examine differences in titers determined by the different methods, we applied two-way ANOVA followed by Tukey's multiple comparisons post-test. The absolute (a.u.) and fold-increase fluorescence values were presented as mean ± standard error mean.

5.5. RESULTS

5.5.1. Anti-H1N1 titers in the DiD dequenching assay

Baseline fluorescence of the DiD-labelled virus/RBC mixture pre-incubated with either PBS (control) or any dilution of human serum was consistently low (23.5 ± 0.15 a.u., Fig. 5.1). Acidification of the DiD-stained virions/RBCs mixture after pre-incubation with either PBS or HAI/MN-negative serum resulted in up to ~40-fold (mean fold increase 20.21 ± 0.71) increase of DiD fluorescence at all tested serum dilutions (Fig. 5.1A). However, when DiD-labelled virions were incubated with HAI/MN-positive samples, acidified fluorescence values formed a U or L-shaped curve, with a descending left arch that evolved into a near horizontal low plateau at or near the baseline (non-acidified) curve. As the antibody titer of the test serum increased, the point at which the descending left arch approached the baseline curve was pushed further to the left (i.e. higher serum dilutions, Fig. 5.1B–D). The point of intersection was readily apparent by visual inspection permitting the confident determination of the serum dilution (±1 dilution) at which the plateau phase of acidified fluorescence curve approached/merged with the baseline fluorescence curve. The visually-assigned DiD titers were strongly correlated with both the known HAI and MN titers (Spearman's Rank Correlation Coefficients (r_s) 0.945 and 0.946, respectively – p values on Fig. 5.1E and F). Of note, visual agglutination of RBCs was impaired in the presence of BSA that was included in the DiD assay reaction mixture (Suppl. Fig. 5.1A). Despite this interference with hemagglutination, the DiD dequenching assay performed well, possibly due to the irreversible and rapid nature of the interaction between fully 'armed' HA molecules with RBC membranes under acid conditions even with such interactions are sporadic.

Intra-assay and inter-operator reproducibility of the DiD dequenching assay were assessed using a test-set of 12 samples with widely varied HAI titers. The DiD titers obtained by the two operators who performed all steps of the assay independently on different days were

highly correlated ($r_s = 0.944$, Fig. 5.1G). The intra-assay reproducibility between technical replicates was very high (Suppl. Fig. 5.1B). When Triton X-100 was added to the DiD-stained virus inoculum, destruction of the viral envelope resulted in a massive increase in the DiD fluorescence intensity. When virions were labeled with dye concentrations between 10 and 40 µg/mL, background fluorescence was low, and Triton-released fluorescence was 420- to 570-fold higher (data not shown). Thus, both DiD labeling and self-quenching were highly efficient suggesting that any minor variations in DiD concentration used for virion labeling would be unlikely to influence assay performance.

5.5.2. DiD dequenching assay performance with a low-agglutinating H3N2 strain

Background fluorescence of the DiD-labelled H3N2 virus/RBC mixture was also consistently low (20.94 ± 0.39 a.u., Suppl. Fig. 5.2). Acidification of the reaction mixture again resulted in an increase of DiD fluorescence in PBS samples up to ~7-fold (mean fold increase 4.7 ± 0.26, Suppl. Fig. 5.2A); a difference that was clearly less prominent than observed with the high-agglutinating H1N1 influenza strain ($p < 0.0001$). In the presence of immune sera, acidified fluorescence values were lower than the PBS controls and, similar to the H1N1 assay, serum dilution curves adopted either an L or shallow U shape with a clear horizontal low plateau. Unlike the H1N1 assay however, fluorescence intensities only rarely dropped all the way down to baseline levels, even at the lowest dilutions of sera with high HAI/MN titres (Suppl. Fig. 5.2B and C). In a small number of samples, the baseline and acidified fluorescence curves were almost parallel with the acidified curve slightly above the baseline curve (Suppl. Fig. 5.2D). The dilution at which the acidified curve broke into a horizontal plateau or showed a clear lowest point was considered as the DiD assay titer in H3N2 data set. The visually-assigned H3N2 DiD titers were still correlated with the known HAI and MN titers but the agreement was less robust ($r_s = 0.551$ and 0.547 respectively; both $p < 0.004$ – Fig. 5.2A and B). A striking observation with the H3N2 strain was that some samples had very high DiD titers despite having almost no detectable HAI or MN antibodies.

5.5.3. DiD dequenching assay performance with influenza B_{Bris} strain

The DiD dequenching assay performed well for anti-B antibodies using DiD-labelled B_{Bris}. The baseline fluorescence (20.87 ± 0.09 a.u.) and acidified control (PBS or negative serum)

curves were similar to what we observed in the H1N1 assay. Up to ~22-fold (mean fold increase 9.19 ± 0.71) fluorescence increase was detected upon acidification. The acidified curves closely resembled those seen for H1N1 and titers could be assigned easily by visual inspection (±1 dilution). Correlations between the DiD dequenching assays and the results of HAI and MN tests were slightly lower than those seen with H1N1 but were still very high ($r_s = 0.891$ and 0.874, respectively – Fig. 5.3A and B).

5.5.4. DiD dequenching assay using labeled virions subjected to freeze-thawing cycles

Because preparation of the DiD-stained virions required multiple steps that could introduce hard-to-control variables (e.g. virus stock concentration and purity, efficiency and uniformity of DiD labeling, ultracentrifugation etc.), we decided to assess large-scale production with frozen storage of DiD-stained virus (−80°C for 72 h) as well as the robustness of this reagent subjected to freeze-thaw cycles. When a large batch of DiD-labeled B_{Bris} was used in repeated assays after 1 or 2 freeze-thaw cycles, the baseline and acidified curves were unchanged, and the correlation between the results using freshly-labeled DiD virions and the once- or twice-frozen and thawed virions was excellent ($r_s = 0.807$ and 0.850 respectively – Fig. 5.4A and B).

5.5.5. Automated assignment of DiD dequenching assay titers

Similar to conventional HAI and MN assays, the visual interpretation of DiD dequenching results can introduce a performance bias. To reduce the risk of such bias, we developed a simple algorithm using the baseline and acidified DiD fluorescence curves and simple rules to automate the process of titer assignment. When this algorithm was applied to the set of H1N1 curves, there was a strong positive correlation between the automated and visually-assigned titers ($r_s = 0.944$ – Fig. 5.5A), and the automated titers remained highly correlated with the known HAI and MN values ($r_s = 0.910$ and 0.911, respectively – Fig. 5.5B and C). Also, the correlation between technical replicates of the DiD assay performed in duplicate was almost perfect when titers were assigned using the automated algorithm, further supporting the excellent reproducibility of the assay (Suppl. Fig. 5.3). The performance of the algorithm was tested with both lower (pre-vaccination) and higher titer (post-vaccination) samples from the same individuals, and the strong correlations with the conventional HAI data were maintained across

the spectrum of titers ($r_s = 0.837$ and 0.810, respectively – Fig. 5.5D and E). Using automated titers, the DiD dequenching assay results tended to be slightly lower than the MN values as has been previously reported for HAI titers by us (18) and others (19,20). In contrast, visual DiD assay titers appeared to be one serum dilution lower than the conventional HAI and automated DiD assay titers (Fig. 5.5F). Importantly, using titers determined visually or assigned by the algorithm, the seroprotection rates (SPR) and seroconversion rates (SCR) for H1N1 based on the DiD dequenching assays were essentially identical with those determined with the classical HAI and MN tests (Fig. 5.5G).

5.6. DISCUSSION

The HAI and MN assays are important tools for the evaluation of the immune response to natural influenza infection and influenza vaccination. In the context of vaccination, HAI titers are routinely used as a surrogate for protection, to compare products and, in certain situations, to license new products (4). Unfortunately, this assay has been very difficult to standardize due to the need for multiple biological reagents and a subjective read-out that can introduce substantial operator bias (1,5,9). In this paper, we present a pilot, proof-of-concept study that introduces a new method for measuring serum antibodies based on the phenomenon of the fluorescence dequenching. When influenza virions are 'loaded' with a sufficiently high concentration of the lipophilic fluorescent dye DiD, self-quenching of fluorescence occurs. When these DiD-labeled virions fuse with unstained cell membranes, the DiD molecules are free to diffuse into the larger lipid membrane area and quenching is eased; resulting in much greater fluorescence. The increased fluorescence with dequenching is proportional to fusion progression (21). This phenomenon has been used to study endocytosis of influenza virions and has shown that acidification of the endosomal compartment is required for the conformational changes of the influenza HA protein that drive fusion of the viral envelope with the endosomal membrane (13–15,22), and that the speed of fusion is dependent upon the density of HA on the virus surface (23). In our assay, we induced the same conformational change in the viral HA by adding HCl to the reaction mixture leading to fusion of the viral envelope with the RBC membranes.

For viruses that exhibit strong hemagglutination such as influenza H1N1 and B strains used in this study, the HAI and DiD dequenching assays likely measure antibodies that are very similar in character; a supposition that is supported by strong correlation between the assays

(r_s = 0.891–0.945). As the name suggests, antibodies measured in the classical HAI target the viral HA protein, interfering with binding to its sialic acid receptors and preventing the agglutination of RBCs from different animal species (24). However, the spectrum of antibodies assessed in the DiD dequenching assay is likely to be broader than the classical HAI since interference could theoretically occur at the time of HA binding to its receptors, during the conformational changes associated with acidification or during fusion. As a result, the DiD dequenching titer may provide a more complete picture of antibody functionality than the HAI titer, especially for viruses with low ability to induce agglutination of RBCs. It is tempting to speculate that the dequenching assay may be closer in nature to the MN assay in detecting 'functional' antibodies (i.e. interference with binding, internalization and fusion with host membranes, release of the viral genome into the cytosol) (24). Although DiD and MN titers were strongly correlated for the high-agglutinating strains (r_s = 0.874–0.946), the correlation was considerably lower for the low-agglutinating H3N2 strain (r_s = 0.547). This observation and the fact that some sera with very high DiD tires had low or absent MN titres raise the interesting possibility that the DiD and MN assays measure distinct subsets of functional antibodies. Importantly, GMT values measured in the visually-interpreted DiD dequenching assay using the influenza H1N1 strain were generally one dilution lower than those determined with the conventional HAI for this particular data set. Clearly the testing of much larger numbers of sera in settings where efficacy can be assessed will be required to begin to predict what level of DiD antibodies might correlate with clinical protection (3,24).

As noted above, high inter- and intra-laboratory variability limits the usefulness of both the HAI and MN assays (1,12). This poor reproducibility is attributable at least in part to difficulties in standardizing the required biological reagents (5,12). Some of these same reagents and methods are used in the DiD dequenching assay (e.g. viral propagation and purification, sources of RBCs), and this assay has several unique steps that could also be sources of unwanted variability (e.g. DiD staining, purification post-staining, etc.). In an effort to eliminate confounding from these assay-specific issues, we assessed the robustness of DiD-labelled viruses to freezing and to repeated freeze-thaw cycles. We were reassured to find that performance of the DiD dequenching assay was not significantly different using pre-labelled virus that had been stored at −80°C for up to three days or even subjected to two freeze-thaw cycles. These observations raise the possibility of centralized production and distribution of a standard reagent,

significantly reducing the variability of one of the test's major components. Although the preparation of labelled virus stocks would lead to additional costs related to the dye itself, purification of labelled virions etc., these costs are small (~ US$3.80 per sample tested) with no economies of scale. It is likely that reductions in labor through automation, centralized production of labelled viruses and/or the use of other, less expensive lipophilic dyes could more than compensate for these extra costs.

One of the most vulnerable aspects of the conventional serological assays and, by far, the most difficult to automate (25,26) is the subjectivity inherent in the visual reading and interpretation of results. To address this challenge, we used a panel of sera with known HAI and MN titers to develop a predictive algorithm based on baseline and acidified DiD fluorescence at 8 serial serum dilutions. When we tested this algorithm using 72 paired sera collected before and 21 days after vaccination, and H1N1 virus, the titers measured with DiD dequenching assay were strongly correlated with HAI and MN titers across the broad range of measured titers. Assembling these results as GMT, SCR and SPR, the conventional HAI and the DiD dequenching assay with algorithmic interpretation were very similar, suggesting that DiD dequenching test has the potential to be developed as a fully automated assay that would minimize performance bias and support high throughput.

The current study has several limitations. These include the relatively small number of samples studied (n = 72) and the fact that only three influenza strains were tested: A/California/07/2009 (H1N1), A/Hong Kong/4801/2014 (H3N2) and B/Brisbane/60/2008. Further validation of the DiD dequenching assay will need to include other influenza strains and perhaps particularly those with a reduced ability to induce hemagglutination (27,28). Testing with a much larger number of samples would also permit refinement of the relatively simple algorithm that we used to assign DiD dequenching titers. The current work focused on DiD but many other lipophilic dyes are available with different properties that could potentially be exploited to further refine this assay (21,29).

In conclusion, we have developed a novel method to measure 'functional' anti-influenza antibodies based on DiD fluorescence dequenching that closely parallels the results of classical serologic assays for influenza: HAI and MN. While the correlation with the classical assays was near perfect for strains exhibiting strong hemagglutination, agreement was lower with an H3N2 strain that has low hemagglutinating ability. The observation that some subjects have high

apparent DiD titers for this H3N2 strain despite having low or even absent HAI/MN titers raises the possibility that at least some of the antibody functionality assessed by this novel assay is distinct from that measured by the classical tests. This work also raises obvious questions regarding the potential use of dequenching in serologic assays for other enveloped viruses that fuse with host cell membranes as a part of their life-cycle (e.g. Paramyxoviruses, Flaviviruses, HIV among others). Future work will determine the flexibility of this assay and, most important, whether or not it can be successfully automated. An assay that measures functional antibodies and that can be fully-automated would be an important advance in standardizing influenza serologic testing.

5.7. ACKNOWLEDGEMENTS

We thank Dr. Li Xing for helpful discussions during planning of experiments, guidance and assistance with purification of the viruses. We also thank Sidrat Rahman for technical assistance.

5.8. REFERENCES

1. Trombetta CM, Montomoli E. Influenza immunology evaluation and correlates of protection: a focus on vaccines. Expert Rev Vaccines. 2016;15(8):967–76.
2. Hobson D, Curry RL, Beare AS, Ward-Gardner A. The role of serum haemagglutination-inhibiting antibody in protection against challenge infection with influenza A2 and B viruses. J Hyg (Lond). 1972;70(4):767–77.
3. Trombetta C, Perini D, Mather S, Temperton N, Montomoli E. Overview of Serological Techniques for Influenza Vaccine Evaluation: Past, Present and Future. Vaccines. 2014;2(4):707–34.
4. Weir JP, Gruber MF. An overview of the regulation of influenza vaccines in the United States. Influenza Other Respi Viruses. 2016;10(5):354–60.
5. Ward BJ, Pillet S, Charland N, Trepanier S, Couillard J, Landry N. The establishment of surrogates and correlates of protection: Useful tools for the licensure of effective influenza vaccines? Hum Vaccines Immunother. 2018;14(3):647–56.
6. Truelove S, Zhu H, Lessler J, Riley S, Read JM, Wang S, et al. A comparison of hemagglutination inhibition and neutralization assays for characterizing immunity to seasonal influenza A. Influenza Other Respi Viruses. 2016;10(6):518–24.
7. Stephenson I, Heath A, Major D, Newman RW, Hoschler K, Junzi W, et al. Reproducibility of serologic assays for influenza virus A (H5N1). Emerg Infect Dis. 2009;15(8):1252–9.
8. Wood JM, Gaines-Das RE, Taylor J, Chakraverty P. Comparison of influenza serological techniques by international collaborative study. Vaccine. 1994;12(2):167–74.
9. Wood JM, Major D, Heath A, Newman RW, Höschler K, Stephenson I, et al. Reproducibility of serology assays for pandemic influenza H1N1: Collaborative study to evaluate a candidate WHO International Standard. Vaccine. 2012;30(2):210–7.
10. Wood JM, Montomoli E, Newman RW, Daas A, Buchheit K-H, Terao E. Collaborative study on influenza vaccine clinical trial serology - part 2: reproducibility study. Pharmeur Bio Sci Notes. 2011;2011(1):36–54.
11. Laurie KL, Engelhardt OG, Wood J, Heath A, Katz JM, Peiris M, et al. International Laboratory Comparison of Influenza Microneutralization Assays for A(H1N1)pdm09, A(H3N2), and A(H5N1) Influenza Viruses by CONSISE. Clin Vaccine Immunol.

2015;22(8):957–64.

12. Zacour M, Ward BJ, Brewer A, Tang P, Boivin G, Li Y, et al. Standardization of Hemagglutination Inhibition Assay for Influenza Serology Allows for High Reproducibility between Laboratories. Clin Vaccine Immunol. 2016;23(3):236–42.
13. Chu VC, McElroy LJ, Chu V, Bauman BE, Whittaker GR. The avian coronavirus infectious bronchitis virus undergoes direct low-pH-dependent fusion activation during entry into host cells. J Virol. 2006;80(7):3180–8.
14. Nunes-Correia I, Eulálio A, Nir S, Düzgünes N, Ramalho-Santos J, Pedroso de Lima MC. Fluorescent probes for monitoring virus fusion kinetics: comparative evaluation of reliability. Biochim Biophys Acta. 2002;1561(1):65–75.
15. Stegmann T, Morselt HW, Scholma J, Wilschut J. Fusion of influenza virus in an intracellular acidic compartment measured by fluorescence dequenching. Biochim Biophys Acta. 1987;904(1):165–70.
16. Fontana J, Steven AC. Influenza virus-mediated membrane fusion: Structural insights from electron microscopy. Archives of Biochemistry and Biophysics. 2015;581:86–97.
17. Yam KK, Gupta J, Brewer A, Scheifele DW, Halperin S, Ward BJ, et al. Unusual patterns of IgG avidity in some young children following two doses of the adjuvanted pandemic H1N1 (2009) influenza virus vaccine. Clin Vaccine Immunol. 2013;20(4):459–67.
18. Verschoor CP, Singh P, Russell ML, Bowdish DME, Brewer A, Cyr L, et al. Microneutralization Assay Titres Correlate with Protection against Seasonal Influenza H1N1 and H3N2 in Children. PLoS One. 2015;10(6):e0131531.
19. Hsu JP, Zhao X, Chen MI-C, Cook AR, Lee V, Lim WY, et al. Rate of decline of antibody titers to pandemic influenza A (H1N1-2009) by hemagglutination inhibition and virus microneutralization assays in a cohort of seroconverting adults in Singapore. BMC Infect Dis. 2014;14(1):414.
20. Veguilla V, Hancock K, Schiffer J, Gargiullo P, Lu X, Aranio D, et al. Sensitivity and specificity of serologic assays for detection of human infection with 2009 pandemic H1N1 virus in U.S. populations. J Clin Microbiol. 2011;49(6):2210–5.
21. Chu VC, McElroy LJ, Bauman BE, Whittaker GR. Fluorescence dequenching assays of coronavirus fusion. In: Advances in Experimental Medicine and Biology. 2006;581:241–6.

22. Jakubcová L, Hollý J, Varečková E. The role of fusion activity of influenza A viruses in their biological properties. Acta Virol. 2016;60(2):121–35.
23. Clague MJ, Schoch C, Blumenthal R. Delay time for influenza virus hemagglutinin-induced membrane fusion depends on hemagglutinin surface density. J Virol. 1991;65(5):2402–7.
24. Reber A, Katz J. Immunological assessment of influenza vaccines and immune correlates of protection. Expert Review of Vaccines. 2013;12:519–36.
25. Nguyen M, Fries K, Khoury R, Zheng L, Hu B, Hildreth SW, et al. Automated Imaging and Analysis of the Hemagglutination Inhibition Assay. J Lab Autom. 2016;21(2):287–96.
26. Wilson G, Ye Z, Xie H, Vahl S, Dawson E, Rowlen K. Automated interpretation of influenza hemagglutination inhibition (HAI) assays: Is plate tilting necessary? PLoS One. 2017;12(6):e0179939.
27. Mögling R, Richard MJ, Vliet S van der, Beek R van, Schrauwen EJA, Spronken MI, et al. Neuraminidase-mediated haemagglutination of recent human influenza A(H3N2) viruses is determined by arginine 150 flanking the neuraminidase catalytic site. J Gen Virol. 2017;98(6):1274–81.
28. Hu Z, Jiao X, Liu X. Antibody Immunity Induced by H7N9 Avian Influenza Vaccines: Evaluation Criteria, Affecting Factors, and Implications for Rational Vaccine Design. Front Microbiol. 2017;8:1898.
29. Klymchenko AS, Kreder R. Fluorescent Probes for Lipid Rafts: From Model Membranes to Living Cells. Chem Biol. 2014;21(1):97–113.

5.9. FIGURES AND FIGURE LEGENDS

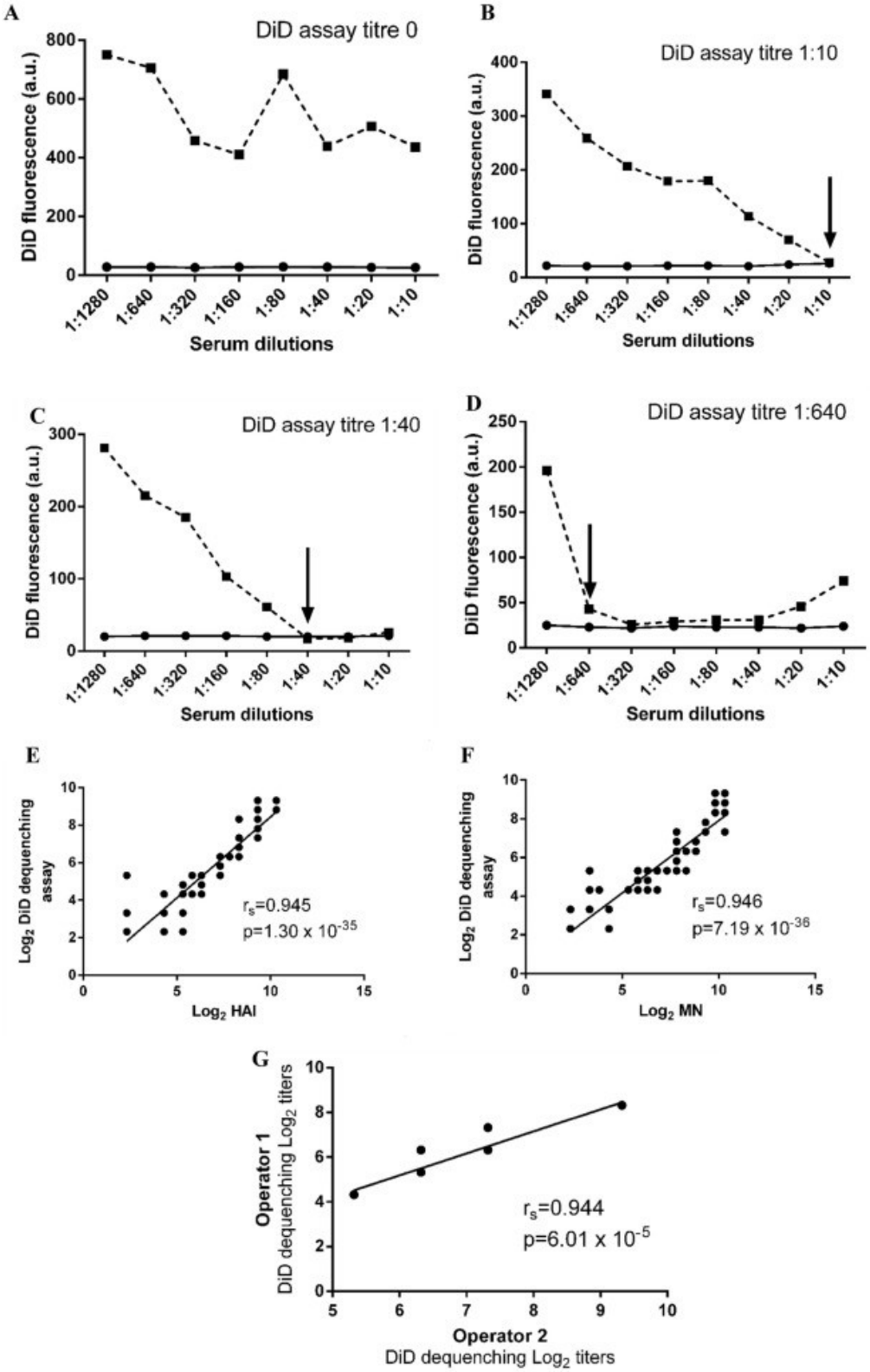

(legend on next page)

Figure 5. 1. Anti-influenza A (H1N1) serum antibody titers determined with DiD dequenching assay

(A) to (D) – examples of baseline (solid line) and acidified (dotted line) DiD fluorescence curves. (A) – undetectable serum antibodies. (B), (C) and (D) – serum antibody titers 1:10, 1:40 and 1:640, respectively (indicated with arrows). (E), (F) – linear regression plots show correlation between Log_2-transformed antibody titers determined with DiD dequenching assay and HAI (E) or MN (F); n = 72. (G) – linear regression plot shows correlation between Log_2-transformed antibody titers determined with DiD dequenching assay independently by two operators; n = 12.

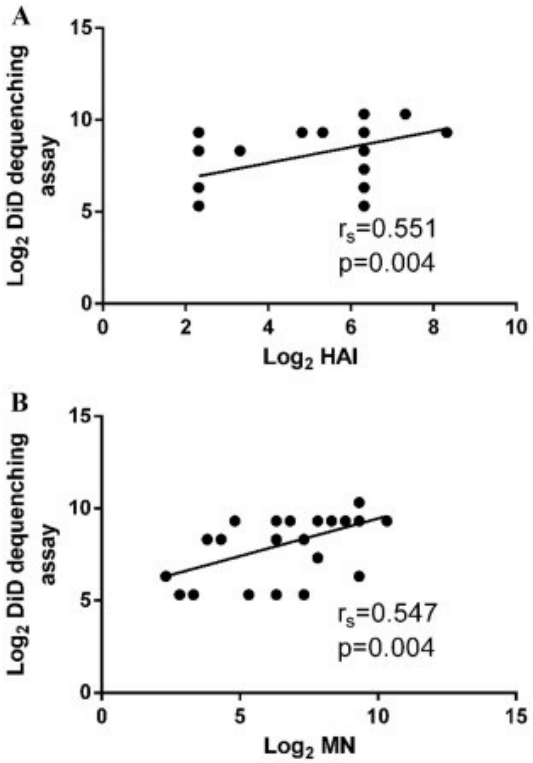

Figure 5. 2. Anti-influenza A (H3N2) serum antibody titers determined with DiD dequenching assay

Linear regression plots show correlation between Log_2-transformed antibody titers determined with DiD dequenching assay and HAI (A) or MN (B); n = 26.

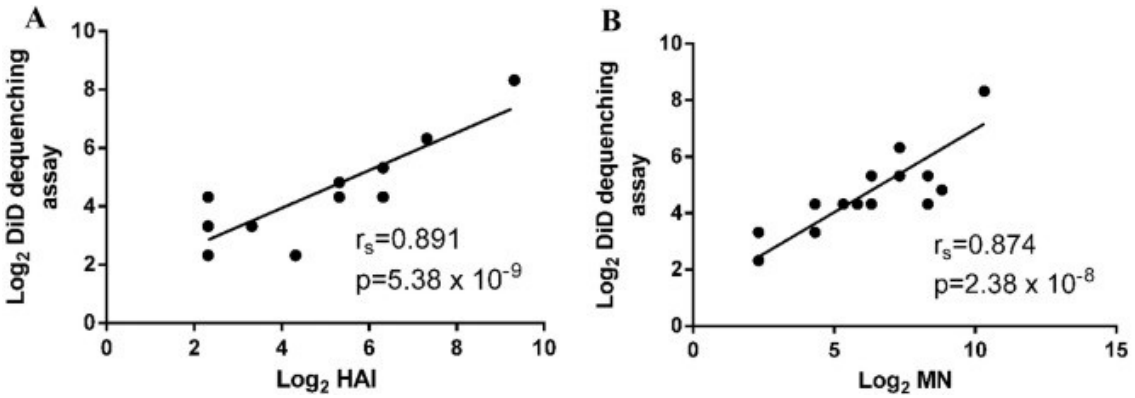

Figure 5. 3. Anti-influenza B (B_{Bris}) serum antibody titers determined with DiD dequenching assay

Linear regression plots show correlation between Log_2-transformed antibody titers determined with DiD dequenching assay and HAI (A) or MN (B); n = 24.

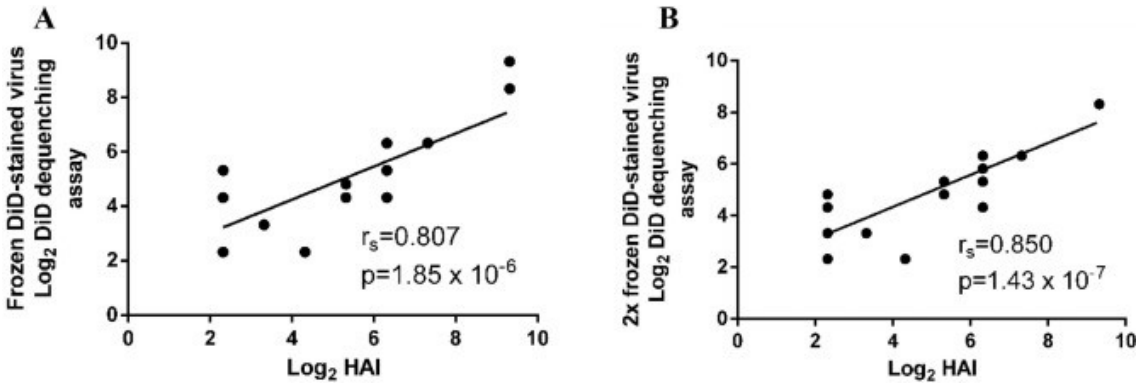

Figure 5. 4. DiD dequenching assay with DiD-stained influenza B (B_{Bris}) virus preparations subjected to repeated freeze-thawing cycles

Linear regression plots show correlation between Log_2-transformed antibody titers determined with DiD dequenching assay and HAI. (A) DiD pre-stained virions subjected to a single freeze-thawing cycle (n = 24). (B) DiD pre-stained virions subjected to two freeze-thawing cycles (n = 24).

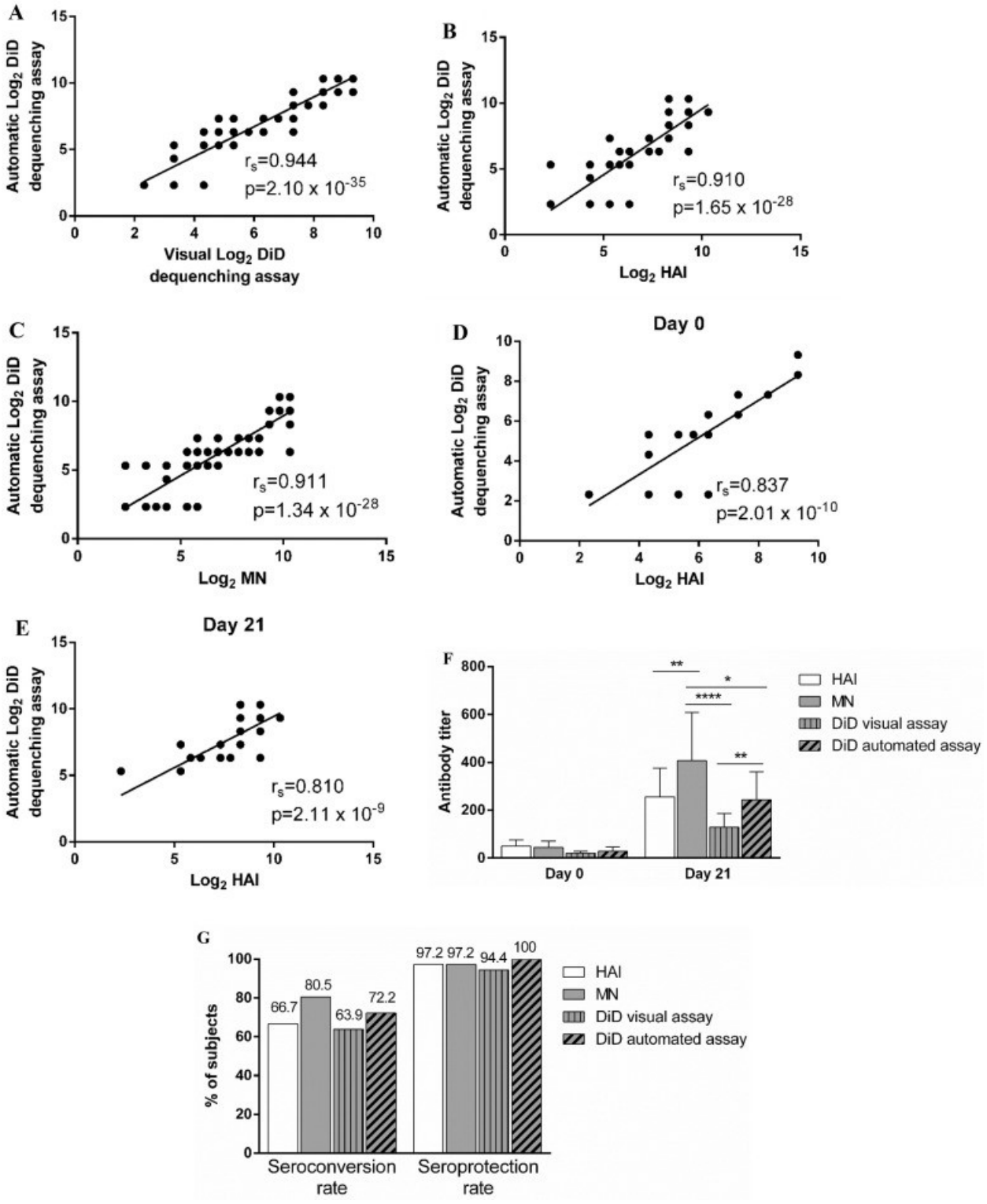

(legend on next page)

Figure 5. 5. Anti-influenza A (H1N1) serum antibody titers determined with automated DiD dequenching assay

(A), (B), (C), (D), (E) – linear regression plots show correlation between Log_2-transformed antibody titers determined by automated and visual interpretation of the DiD dequenching assay, n = 72 (A); automated DiD dequenching assay and HAI (B) or MN (C), n = 72; automated DiD dequenching assay and HAI prior to vaccination, day 0, n = 36 (D), and at day 21 post-vaccination, n = 36 (E). (F) – serum antibody titers determined with HAI, MN, visual and automated DiD dequenching assays (n = 72, paired samples). GMT and 95% confidence intervals are shown. * – $p < 0.05$; ** – $p < 0.01$; **** – $p < 0.0001$. (G) – SCRs and SPRs determined with HAI, MN, visual and automated DiD dequenching assays (n = 72, paired samples).

5.10. SUPPLEMENTARY MATERIAL

A novel serological assay for influenza based on DiD fluorescence dequenching that is free from observer bias and potentially automatable - a proof of concept study

Alexander I. Makarkov, Aakash R. Patel, Valentine Bainov, Brian J. Ward

A

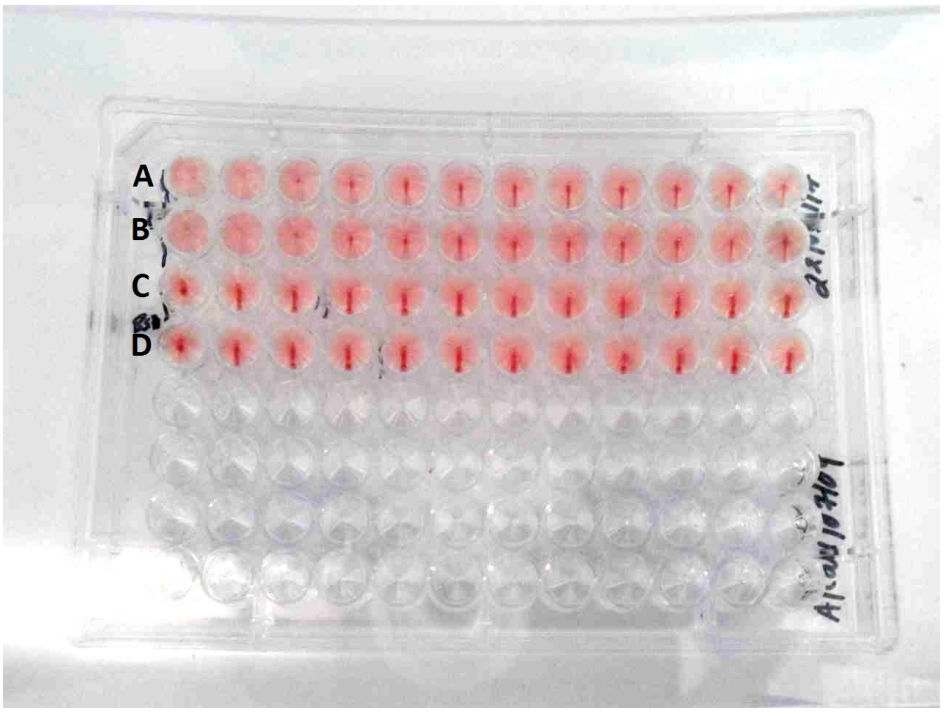

B

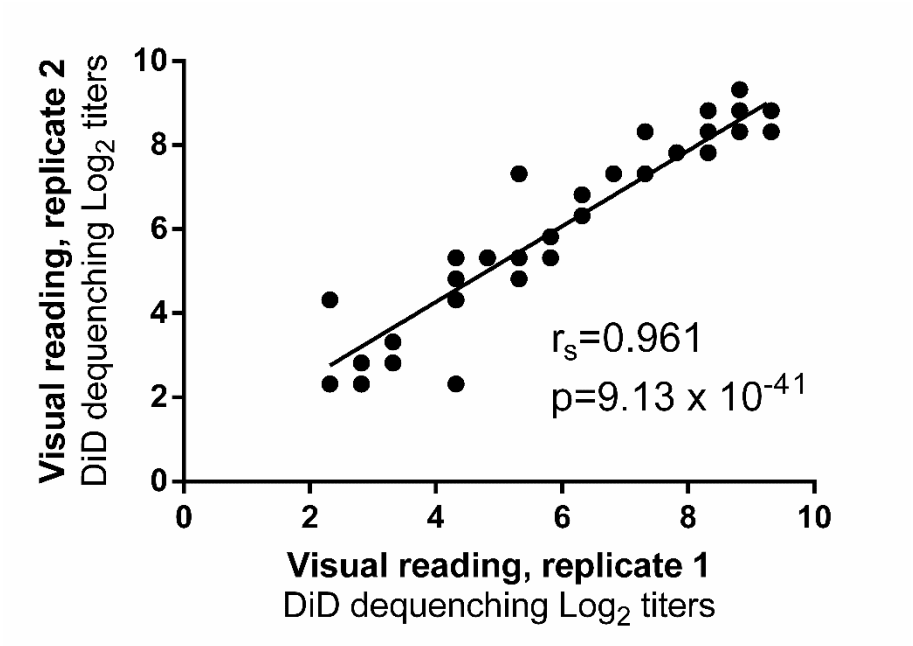

Supplemental Figure 5. 1. Anti-H1N1 titers in the DiD dequenching assay

(A) - example of H1N1 virus titration with the standard buffer (row A and B) and in the presence of 5% BSA (row C and D). Addition of BSA affected the agglutination of RBCs. (B) –

(legend continued on next page)

reproducibility of DiD dequenching assay. Linear regression plot shows correlation between technical replicates of the DiD dequenching assay performed in duplicate. Log_2-transformed antibody titers presented; n=72, in duplicate.

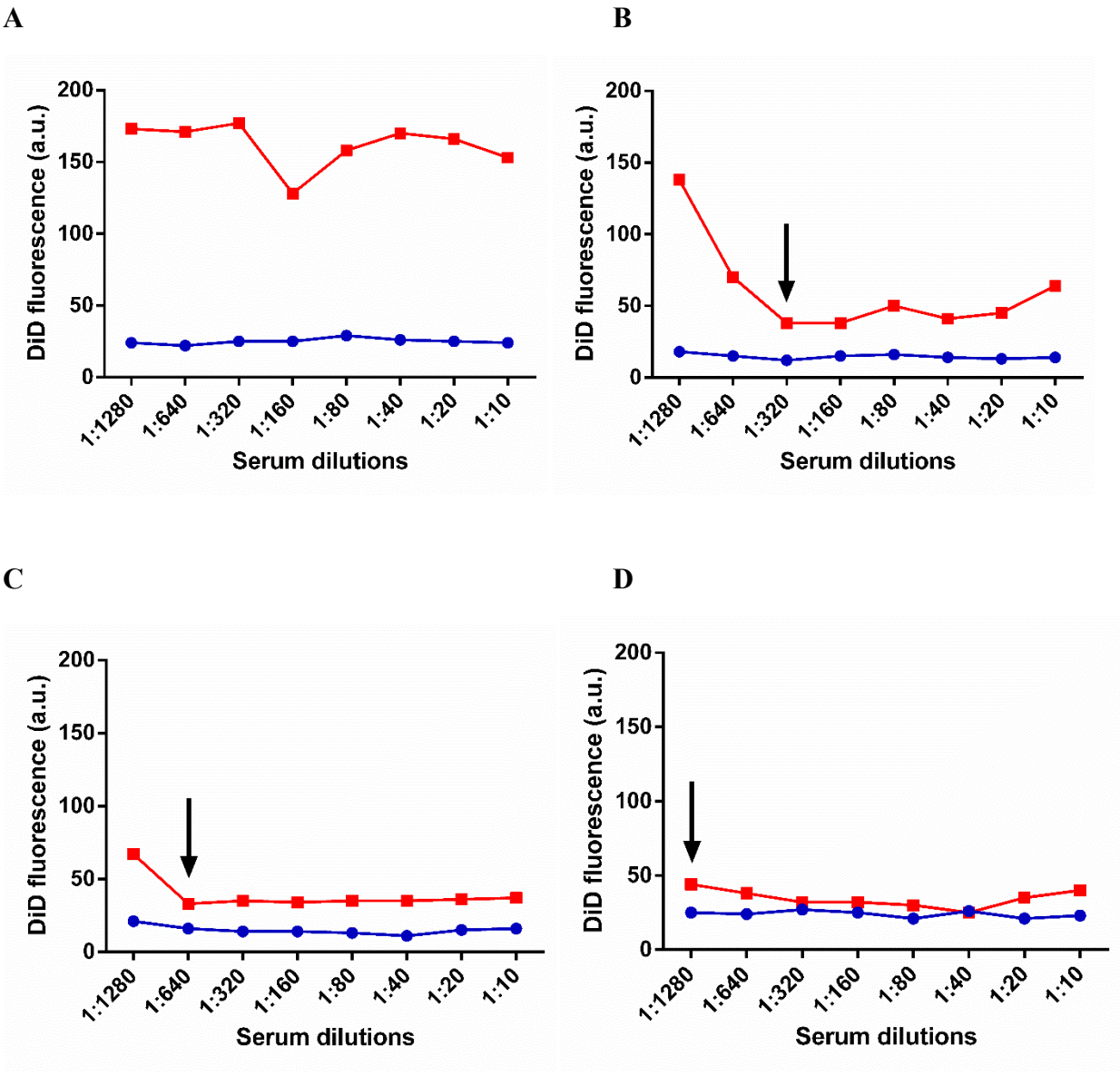

Supplemental Figure 5. 2. DiD dequenching assay performance with low-agglutinating influenza H3N2 strain

(A) to (D) – examples of baseline (blue line) and acidified (red line) DiD fluorescence curves. (A) – PBS control, undetectable antibody titer. (B), (C) and (D) – serum antibody titers 1:320, 1:640 and 1:1280, respectively (indicated with arrows).

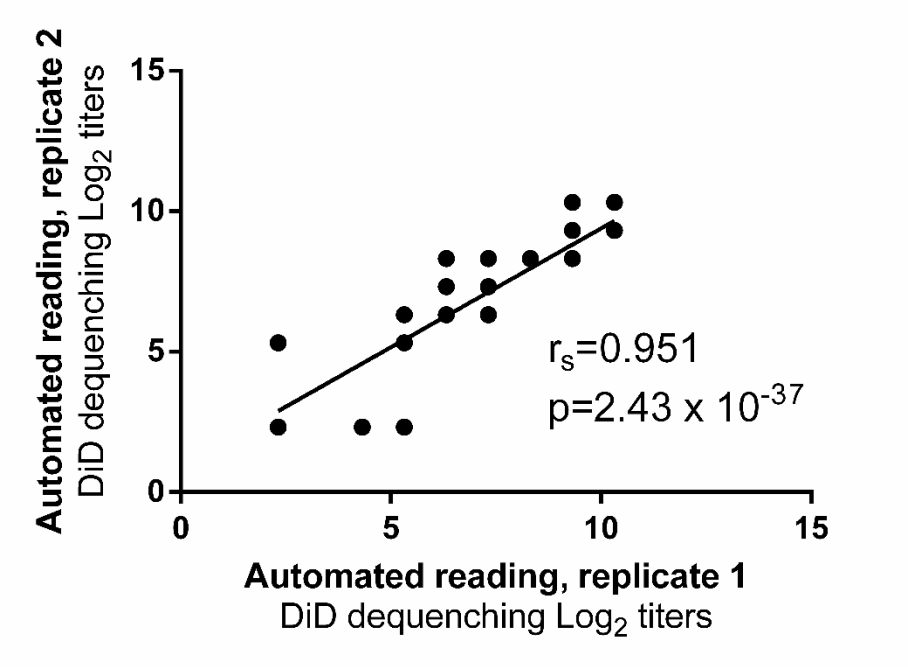

Supplemental Figure 5. 3. Automated assignment of DiD dequenching assay titers

Reproducibility of DiD dequenching assay. Linear regression plot shows correlation between technical replicates of the DiD dequenching assay performed in duplicate. Log_2-transformed automatically assigned antibody titers presented; n=72, in duplicate.

Chapter 6: General discussion

The influenza vaccine market is large and growing rapidly, with 140–170 million doses distributed annually in the United States during the last 5 years (1). This corresponds to US$ 1.8 billion in 2016, representing about 13% of the overall US vaccine market (2). The US market forecast for influenza vaccines by 2021 reaches US$ 2.4 billion, representing roughly a 4.5% compound annual growth rate (CAGR) (2). Globally, the influenza vaccine market value is estimated at US$ 3.3 billion in 2018, with the CAGR of 6.93%; hence anticipated growth up to US$ 4.6 billion by 2023 (3). The market is currently dominated by the IIV products for adults and LAIV in the pediatric segment (1,2). However, the LAIV was not recommended in the US for the 2017–18 season due to poorly-understood concerns about its effectiveness (4). Recombinant influenza vaccines licensed in the US include only two products (Flublok™ and Flublok™ Quadrivalent, manufactured by Protein Sciences) that have only recently entered the market; however, their market share was less than 1% in 2017-18 (2,4).

The plant-derived VLP vaccine bearing influenza HA developed by Medicago is a highly promising candidate. The HAs expressed by Medicago in plant cells as recombinant proteins are structurally identical to those in the circulating influenza stains (5–7). The use of recombinant technology allows major limitations of the egg-based vaccine production to be overcome; most importantly the mismatch between HA antigenic structure in the vaccine strain and the wild type influenza viruses resulting in a reduced vaccine effectiveness (VE). For example, altered glycosylation of HA on the egg-adapted influenza strains can strongly affect immunogenicity. This is the reason that antibodies elicited in ferrets and humans immunized with the egg-adapted 2016–2017 H3N2 vaccine strain failed to effectively neutralize the circulating H3N2 viruses (8). During the most recent 2017-18 influenza season, the adjusted VE in Canada was 42% overall, and 31% in adults 20–64 years old. The adjusted VE against influenza A (H3N2) was 17% overall, and only 10% in adults 20–64 years old. Importantly, 49% of the influenza cases were caused by type A viruses, and among them 92% were attributable to the H3N2 viruses (9). Low VE against influenza A (H3N2) strain was also reported in the US (10) and Australia (11).

Plant-based production of VLPs does not depend on embryonated hens' eggs, so manufacturing cannot be disrupted by supply issues or variability of the virus growth in eggs (12–14). Importantly, plant-based VLP production allows rapid, low cost and large-scale

manufacturing of the influenza vaccine, which is a major advantage compared to the only currently licensed recombinant vaccines that are produced in insect cells (6,7,15). VLPs are non-living so the VLP manufacturing process provides a safer environment for operators than working with live viruses to make either IIV or LAIV (6,7,16).

The immunogenicity profiles differ between the major vaccine types. IIVs typically elicit stronger serum antibody response than LAIV, whereas cell-mediated immune responses to IIV are low or undetectable (17–20). Plant-derived VLPs have been shown to induce robust antibody production both in animal models and in humans (6,21–24). Hodgins *et al.* (25) recently demonstrated the superiority of H1-VLPs in triggering a humoral immune response in mice compared to a monovalent split virion vaccine of the same influenza strain. Healthy volunteers vaccinated with VLP-based monovalent A/California/7/09 (H1N1) or quadrivalent seasonal influenza vaccine also mount a long-term polyfunctional and cross-reactive $CD4^+$ T cell response, mainly represented by transitional and effector memory subsets. This $CD4^+$ T cell response to the VLP-based vaccines was significantly greater than to commercial IIV comparators (21,24).

LAIV, in contrast to IIV, triggers a cytotoxic immune response mediated primarily by $CD8^+$ T cells (19,20,26,27). It is generally accepted that this effect of LAIV depends on replication on the live virus in infected cells with direct MHC I-restricted presentation of the virus-derived antigens (20,28,29). Although cell-mediated cytotoxicity helps to eliminate virus-infected cells and therefore can't prevent infection, disease severity and duration as well as the risk of complications and the viral spread are greatly reduced in individuals who develop a strong $CD8^+$ T cell immunity (30–32). A vaccine capable of inducing a $CD8^+$ T cell response might be particularly beneficial for the elderly. The naïve CD8 T cells pool declines with age, in parallel with other immune mechanisms (33,34). However, the longevity of memory $CD8^+$ T cells may help to maintain a robust recall immune response against influenza even in aged individuals. Most people are exposed to at last one influenza strain by the age of 15, either through natural infection or vaccination (35,36). In animal studies, $CD8^+$ T cell memory has been found to be life-long if the priming occurs early in life, and influenza-specific $CD8^+$ T cells have been shown to persist for at least 13 years in humans (37). If a vaccine can elicit even a modest $CD8^+$ T cell response, it may help to maintain the memory pool over time (30,38). Monovalent H1-VLPs have been shown to trigger a detectable polyfunctional $CD8^+$ T cell

response in healthy adults but this effect did not reach statistical significance compared to placebo group (21).

In summary, plant-derived VLPs possess a number of immunological features that make them a unique vaccine candidate. These characteristics could be attributable to the delivery of antigen in the form of nanoparticles that bear influenza HA trimers in an immunologically-relevant array (6,7,39). Plant lipids forming the VLP envelope, residual plant proteins, contamination with *Agrobacterium* lipopolysaccharide or other factors that are difficult to identify could potentially shape the anti-HA immune responses elicited by VLPs (5,6). Therefore, it was of great interest to study the mechanisms underlying the unusual immunogenicity of the plant-derived VLPs, and this interest led to the primary objectives of this thesis. The diversity of immune responses elicited by these novel vaccine candidates encouraged a re-evaluation of the 'standard' approaches used for the laboratory assessment of the vaccine efficacy (40–42). The correlates of protection currently used for vaccine licensure and their limitations were discussed in Chapter 1.3.2. In this project, we attempted to develop at least one new method to evaluate functional serological response to influenza vaccines.

6.1 MAIN FINDINGS

This thesis presents major findings from experiments designed to explain the broad immunogenicity profile of plant-derived VLPs bearing influenza HA through the study of interactions between the VLPs and human APCs. In our first mechanistic study, we looked at the interplay between DiD-labeled VLPs and U-937 cells or primary human MDMs. Cell surface binding of the fluorescent VLPs became apparent within minutes. Pre-treatment of U-937 cells or MDMs with sialidases abolished binding. Moreover, empty vesicles (VLPs that do not bear HA or any other protein on their surface) (39) did not significantly interact with the APCs, suggesting that HA-VLPs bind to target cells in sialic acid-dependent manner. VLPs bound to cell membranes were rapidly internalized, and this internalization occurred at 37°C but not at 4°C, suggesting an energy-dependent uptake mechanism. The dynamin inhibitor Dynasore™ completely prevented VLPs endocytosis by U-937 cells and demonstrated partial inhibitory effect in MDM, indicating an important role for dynamin-dependent endocytic pathways. After internalization, DiD-labelled VLPs partially colocalized with the LysoSensor Green fluorescent

signal, suggesting that a portion of the internalized VLPs had been delivered into acidified endosomal compartment whereas other VLPs had remained in compartment(s) at pH close to neutral. Some of the DiD-labeled VLPs fused with endosomal membranes of target cells, as made apparent by the robust increase of DiD fluorescence intensity (fluorescence dequenching). We observed a striking difference in the binding and uptake of H1- vs. H5-VLPs by U-937 cells and MDMs: H5-VLPs interacted with these cells with several fold greater efficiency than the H1-bearing particles. Finally, exposure of MDMs to H1-VLPs resulted in a dose-dependent proliferative response of autologous PBMCs upon co-culturing *in vitro*, whereas H5-VLPs did not cause any PBMCs proliferation. Since all PBMC donors had most likely been exposed to H1N1 antigens (i.e. infection, vaccination or both) but had not had previous exposure to H5 antigens, the recall immune response to H1 but not H5 epitopes triggered the PBMCs proliferation. In summary, we looked at key stages of the VLP interactions with APCs such as surface binding, internalization, endosomal acidification and endosomal fusion, antigen processing and presentation, and observed a great similarity to what we know about wild-type influenza virus interactions with target cells. These results were published in the August 2017 issue of *Vaccine* and are presented in Chapter 2 of this thesis.

The rapid and massive internalization of HA-VLPs by human MDMs prompted us to study the mechanisms of VLPs uptake as well as to compare them with the soluble HA uptake. We quantified the fluorescence intensity of immunolabelled H1 and found that the internalization of H1-VLPs became apparent at 5 min of exposure and reached a plateau at 10-15 min. The 15 min pulse exposure of MDMs to H1-VLPs resulted in ~ 3-fold greater intracellular accumulation of HA compared to soluble H1 protein. The H1-VLP uptake mechanisms were CME, CIE, macropinocytosis and, probably, phagocytosis. In contrast, soluble H1 was internalized almost exclusively by CME. MDMs pulsed with soluble H1 had almost completely lost detectable HA immunofluorescence at 45 min, indicating that the protein was handled in a high-degradative endosomal compartment. In contract, a portion of endosomes in MDMs pulsed with H1-VLPs retained the fluorescence at 45 min whereas other endosomes appeared to lose signal. These observations suggested that H1 proteins delivered on VLPs underwent bidirectional trafficking in MDMs: endosomes that lost the HA signal likely representing a high-degradative compartment and endosomes that retained the HA immunofluorescence were likely low-degradative and preserved the protein in non-denatured form. Image colocalization analysis revealed that HA

initially colocalized with the early endosomal marker Rab5 and was later delivered into recycling $Rab11^+$ endosomes in MDMs exposed to H1-VLPs; the VLP-delivered HA fluorescence also colocalized with MHC I fluorescent signal. Segmentation ICCS analysis of HA-positive endosomes revealed a substantial increase in HA colocalization with Rab5 and Rab11 markers at 45 min, suggesting protein retention in static early and/or recycling endosomes.

We hypothesized that the diversity of HA-VLP uptake mechanisms and bidirectional endosomal trafficking of HA in MDMs might favor both MHC II- and MHC I-restricted presentation of the VLP-delivered antigens. Although there are strong evidences of MHC II-restricted HA presentation, including the induction of $CD4^+$ T cell response and robust antibody secretion following VLP vaccination in both animal models and human trials, MHC I-restricted presentation of HA delivered in the form of VLPs had not been convincingly demonstrated. To test our hypothesis, we treated MDMs with either H1-VLPs or soluble H1, immunoprecipitated the MHC I – peptide complexes from the MDM lysates, and analyzed eluted peptides using high-resolution tandem mass spectrometry. No confident HA-derived peptides were detected in the lysate of MDMs exposed to soluble H1. In contrast, 115 HA-derived MHC I-associated peptides were found in MDMs treated with H1-VLPs, contributing to HA sequence coverage of 12-89%; eight of these peptides were detected in more than one donor. Thus, we were able to confirm HA cross-presentation by human MDMs *in vitro* when these cells were exposed to H1-VLPs but not to soluble H1. The results of these VLP internalization and endosomal trafficking experiments, as well as the proteomics studies are described in Chapter 3 of the thesis and in a manuscript that has been submitted to *npj Vaccines* (under review – July 23, 2018).

We also analyzed the MHC I-restricted peptides derived from host proteins in human MDMs exposed to H1-VLPs with cells treated with soluble H1 serving as controls. A total of 109 host-derived MHC-I peptides were identified in HA-VLP-treated MDMs, two of which were also detected in control samples. The peptides unique to VLP treatment were 13 amino acids long on average, slightly more basic and hydrophilic, and predominantly arose through the proteolysis by matrix metalloproteinases and cathepsins. The proteins associated with these peptides were primarily involved in cellular, metabolic and regulatory processes, and activated several pathways including inflammation stimulation and attenuation, response to stimuli, innate and adaptive immunity, CME, protein synthesis and endo-lysosomal degradation. These results

are described in Chapter 4 of the thesis and in a manuscript that has been submitted to *Molecular & Cellular Proteomics.*

In the course of these mechanistic studies, a wide range of techniques were applied or developed including the DiD dequenching assay described above. Since influenza viruses fusion with host cell membranes is a critical event in the virus life-cycle, it occurred to us that the dequenching phenomenon might permit the development of a novel method to evaluate the serologic response to influenza vaccination/infection. In the dequenching-based serological assay, we mixed DiD-labeled wild-type influenza virions with red blood cells (± serum dilutions) and measured DiD fluorescence intensity at baseline and after acidification of the reaction mixture. We observed a robust increase of the DiD fluorescence intensity in the absence of antibodies, and a great reduction of DiD dequenching in the presence of immune sera. This new assay allowed us to determine antibody titers against three influenza strains in serum samples collected from vaccinated individuals. The dequenching assay titers correlated perfectly with HAI and MN titers when high-hemagglutinating H1N1 and B influenza viruses were used, and a moderate correlation was observed with the low-hemagglutinating H3N2 influenza strain. We believe that this dequenching assay measures functional antibodies that may interfere with several key steps in viral invasion including binding to target cells, HA conformational change and/or viral envelope-cell membrane fusion. These results were published in the journal *Vaccine* and are presented in Chapter 5 of the thesis.

6.2 FUTURE PERSPECTIVES

In this thesis, we described significant aspects of the plant-derived VLP interactions with human APCs that shed the light on their unusual immunogenicity. These results clearly show that the HA-VLPs are promising influenza vaccine candidates. More importantly however, this body of work has defined a number of important directions for further studies some of which are discussed below:

6.2.1 Exploring the mechanisms of immunogenicity of plant-derived HA-bearing VLPs

We have demonstrated cross-presentation of influenza HA delivered in the form of VLPs by human MDMs. Indeed, the ability of macrophages to cross-present exogenous antigens with appropriate stimulation has been previously shown in many studies (43–45). Although our initial

focus was MDM and we observed endosomes with a cross-presentation compartment phenotype (46–48), it is generally acknowledged that DCs are better cross-presenting cells than macrophages (49–51). Therefore, it appears reasonable to reproduce the imaging and proteomics cross-presentation studies described above using human MDDC.

6.2.1.1 HA-VLPs processing and presentation by human DCs

In preliminary experiments, we have observed a rapid and massive uptake of H1-VLPs by immature primary human MDDCs; soluble H1 internalization was much less prominent (Fig. 6.1A – 6.1C). At 45 min of H1-VLPs pulse exposure, MDDCs retained mostly non-denatured HA that often re-distributed to the cell periphery, suggesting predominant handling by the recycling endosomal pathway (Fig. 6.1A and 6.1C), similar to our findings in the MDM model. Conventional colocalization analysis revealed partial colocalization of HA with Rab5 and Rab7 endosomal markers at 15 min, which were both significantly reduced at 45 min (Fig. 6.1D). The HA colocalization with MHC I molecules was high at 15 min and remained at quite a substantial level at 45 min (Fig. 6.1E). Although we have not yet studied the recycling endosomal compartment in MDDC, a massive reduction of the HA colocalization with Rab5 and Rab7 markers at 45 min argues for delivery of the antigen into the recycling endosomes. On the other hand, the endosomal trafficking kinetics that we established in the MDM model may differ from MDDCs. Nevertheless, based on the retention of undegraded HA in MDDCs at 45 min and the HA colocalization with MHC I, we expect that MDDCs will also be capable of HA cross-presentation when HA is delivered in the form of VLPs. Further work will help to address this question, and should include at least:

- Characterization of kinetics of the HA-VLPs endosomal trafficking in MDDCs;
- MDDCs imaging and detailed characterization of their recycling endosomal compartment using Rab11, Rab4, Rab35, Arf6 and other markers (52);
- Conventional colocalization and segmentation ICCS analyses of HA-positive endosomes;
- Immunopeptidomics studies of HA-derived peptides in MDDCs.

It is important to mention that the MDDC model might not be as successful as MDMs in evaluating HA cross-presentation. When DC are discussed as potent cross-presenting cells, it is often with the ‘classical’ cytosolic pathway in mind (53–55). However, our MDM observations suggest that endosomal cross-presentation mechanisms may be active. Moreover, macrophages

produce large amounts of reactive oxygen species upon their activation. These reactive oxygen species prevent acidification of early endosomes and help to preserve non-degraded antigen over time, which is beneficial for endosomal cross-presentation (56,57). Finally, DCs are highly heterogeneous, and different subsets exhibit different cross-presentation potential (58–60). Thus, MDDCs are not necessarily the 'best' model to study HA cross-presentation.

6.2.1.2 Cross-priming of naïve CD8$^+$ T cells and stimulation of the influenza HA-specific CD8$^+$ T cell memory pool. Human MDDC interactions with autologous CD8$^+$ T cells in vitro

Our proteomic approach allowed us to demonstrate processing and cross-presentation of HA by human MDMs. However, these results provided a 'snapshot' of the generation and editing the MHC I-restricted peptides. Some of these peptides had an optimal length for binding to the MHC I molecules with high affinity and probably for expression on the surface of APC. However, other peptides were much longer, and most likely represented the intermediary peptide pool that needed to be further trimmed before optimal biding to MHC I molecules was achieved. The discovery of HA-derived peptides co-immunoprecipitated with MHC I does not necessarily mean that these peptides will inevitably reach the surface of APC and be presented to antigen-specific T-cells.

To begin to address this issue, we have attempted to stimulate the HA-specific pool of human CD8$^+$ T cells by co-culturing with autologous MDDCs pulsed with quadrivalent seasonal VLP-based vaccine. A licensed trivalent split virion vaccine was used as comparator. We found that exposure of MDDC to VLP resulted in the induction of IFN-γ, IL-2 and/or TNF-α production by autologous CD8$^+$ T cells from some donors; however, CD8$^+$ T cells from other donors responded to the stimulation by MDDC exposed to split vaccine (data not shown). These differences may be attributable to the fact that this model relies on the cytokine production by pre-existing memory T cells persisting after the natural influenza infection or vaccination. In addition, the HA-VLPs we used had only a single viral antigen (i.e. HA), whereas the split vaccine was composed of many influenza proteins including those known to contain a number of conserved MHC I-restricted epitopes (NP, M1 and others) (61–63).

Unexpectedly, we found that co-culturing of VLP-pulsed MDDCs with autologous CD8$^+$ T cells led to a dose-dependent formation of multicellular clusters (Fig. 6.2.A and 6.2C).

MDDCs treatment with the split vaccine did not cause formation of cell clusters (Fig. 6.2B and 6.2C). The CD8 fluorescence intensity of these complexes was an order of magnitude higher than single T cells, suggesting that each cluster contained multiple T cells. The MDDCs (detected by CD209/DC-SIGN expression) were also found in these complexes (Fig. 6.2D). These results echo recently published work by Hendin *et al.* (64) who observed formation of PBMC clusters upon *in vitro* incubation with H1- but not H5-VLPs. The main difference between these two experimental systems was that free VLPs were absent from the MDDC – $CD8^+$ T cell culture. Thus, cluster formation in the later model could be caused either by VLPs bound to but not yet internalized by MDDCs, or by VLP-induced changes in the phenotype/functional status of MDDCs themselves.

The impact of the VLP-treated MDDC on $CD8^+$ T cells was most prominent in the cells incorporated into the multicellular clusters; single T cells examined by flow cytometry were only weekly affected by exposure to the VLP-pulsed MDDCs. In this context, several major questions need to be addressed:

- What is the mechanism of cell cluster formation?
- Is the cluster formation a reversable phenomenon?
- Do $CD8^+$ T cells incorporated into the clusters remain viable and functional?
- Does the *in vitro* clustering of lymphocytes co-cultured with VLP-pulsed MDDCs have any *in vivo* significance?
- What kind of (immunologically relevant) biological processes are triggered by cluster formation?

The most convincing way to prove the ability of VLP-based vaccine to cross-prime and activate human $CD8^+$ T cells is the *ex vivo* induction of antigen-specific responses of lymphocytes obtained from VLP-vaccinated individuals. The formation of multicellular clusters can be avoided if T cells are stimulated *ex vivo* with HA-derived peptide pool. Landry *et al.* (21) observed a polyfunctional $CD8^+$ T cell responses after H1-VLP vaccination; however, the difference between VLP-vaccinated and placebo groups was not statistically significant, probably because the blood samples were collected 201 days after immunization. Peak $CD8^+$ T cell responses are typically observed one to two weeks during influenza infection (65,66), therefore, it would be more informative to collect the blood samples at earlier time points.

The Medicago plant-based production platform allows producing VLPs bearing different proteins (6,22,67). Making VLPs that express the influenza core proteins that have been shown to elicit a robust $CD8^+$ T cell response in other systems (30,63,68) may be considered in the long term.

6.2.1.3 VLP-induced programmed cell death may boost the adaptive immune responses, facilitate antigen delivery and cross-presentation by the neighboring APCs

The role of programmed cell death mechanisms in the innate defense against influenza was discussed in Chapter 2.1.2.5. Importantly, cell death can strongly shape 'downstream' adaptive immune responses (69–71). The first study that demonstrated the importance of apoptosis in cross-presentation of exogenous antigens by non-infected DCs was performed with influenza infected monocytes (72). Recently, Chatziandreou *et al.* (73) demonstrated that footpad injection of inactivated H1N1 virus caused rapid death of the subcapsular and medullary macrophages in the draining lymph nodes that was essential to elicit the humoral immune response against the influenza vaccine.

It is generally agreed that influenza-induced programmed cell death requires virus replication or at least the presence of viral RNA in the dying cell (73–76). Therefore, we did not anticipate seeing the induction of apoptosis in immune cells exposed to plant-derived VLPs that lack viral RNA. Unexpectedly, we observed a substantial number of apoptotic body-like objects (77) in the supernatant of human MDDCs exposed to H1-VLPs; some of which appeared to interact with the neighboring MDDCs (Fig. 6.3A). Importantly, the surface of these apoptotic body-like objects was covered by HA as revealed by immunostaining, suggesting that they may facilitate antigen presentation upon engulfment by the neighboring MDDCs.

To explore these observations, we studied the apoptogenic effect of VLPs in U-937 cell model. Both H1- and H5-VLPs caused a substantial increase in the number of Annexin V-positive U-937 cells upon 30 min exposure. Co-staining with PI also showed the increase in late apoptotic and secondary necrotic cell numbers (Fig. 6.3B and 6.3C). Next, we studied the effect of VLP-based quadrivalent influenza vaccine on Caspase 3 and 7 activity in U-937 cells. The 30 min exposure of cells with VLP-based vaccine resulted in a substantial induction of apoptosis and secondary necrosis that became apparent at HA concentrations ≥5.0 μg/mL. In contrast, split

virion vaccine used as control in these experiments had a minimal effect on U-937 cells viability over the range of HA concentrations tested (1.0 - 15.0 µg/mL) (Fig. 6.3D).

We believe that these results may help to explain the broad spectrum of immune responses elicited by VLP-based vaccines and, in particular, HA cross-presentation (see Chapter 3 of the thesis). Further work is needed to address some important questions:

- What is the mechanism of apoptosis induction by non-replicating and viral RNA-free VLPs?
- Is apoptosis the only programmed cell death pathway induced by VLPs; i.e. is there any contribution of necroptosis or other pathways?
- Does the *in vitro* induction of programmed cell death upon VLP exposure have any *in vivo* significance?
- What are immunological consequences of the VLP-induced program cell death (i.e. T cell priming vs. tolerization, antigen cross-presentation etc.)?

A substantial reduction in peripheral blood leukocyte numbers due to cell apoptosis was observed after mice immunization with the whole virion IIV (78). It is of great interest to see whether VLP-based vaccines have a similar effect and, if so, what impact might this have on vaccine immunogenicity.

6.2.1.4 VLP fusion with cell membranes may facilitate the innate and adaptive immune responses, and favor the cytosolic cross-presentation pathway

To enter a cell, all viruses must cross a membrane either at the cell surface or within endosomal compartments. For most enveloped viruses, this key step in the replication cycle is executed when the viral envelope fuses with cell membranes (79–82). In many cases, the physical act of viral entry into a cell is sufficient to alert the cell to the presence of an invading pathogen. Both viral and VLP envelope fusion with cell membranes can trigger expression of type I IFNs and/or ISGs (83–86).

Holm *et al.* (87) reported that herpes simplex virus type 1-derived VLPs that lack viral capsid and genomic material were able to fuse with primary mouse and human cells, and these fusion events induced a type I IFN response and up-regulated the expression of ISGs. The responses to these VLPs were dependent on STING but did not require TLR or RIG-I-like signaling. Later, the same group reported that influenza A viruses can evade the innate response

triggered by the viral envelope fusion with endosomal membranes through an interaction between STING and a conserved region of the HA fusion peptide that antagonizes interferon production (88).

We have demonstrated robust fusion of plant-derived VLPs with endosomal membranes in U-937 cells and human MDMs (Chapter 2 of this thesis) by DiD fluorescence dequenching. However, in contrast to the native influenza viruses, prevention of endosomal acidification with ammonium chloride or chloroquine did not affect either the shape or the amplitude of the DiD dequenching curve (data not shown). These findings suggest that VLP fusion with endosomal membranes may not require acidification and HA conformation changes. One may speculate that plant lipids have weaker hydrophobic interactions within the phospholipid bilayer and can more easily fuse with the mammalian cell membranes.

We do not yet know whether or not plant-derived VLP fusion with endosomal membranes can trigger type I IFN secretion. If so, the stronger innate response elicited by VLPs may enhance the adaptive immunity against influenza (89–91). In addition, massive VLP fusion with endosomal membranes may cause significant perturbations of the endosomal membrane lipids leading to release of the antigenic material into the cytosol, a prerequisite for the cytosolic cross-presentation pathway (49,92,93). Finally, activation of STING can strongly enhance the cross-presentation capacity of APCs (94,95).

6.2.2 Plant-derived VLPs as a targeted delivery system

In recent years, multidisciplinary research efforts in the field of nanomedicine led to the development of a variety of nanoparticle-based carrier systems that were potentially suitable for targeted delivery of prophylactic and therapeutic agents (96–98). Synthetic nanocarriers can also protect the cargo from early degradation in biological environments, establish an antigen reservoir for stimulation of adaptive immune responses, ensure targeting the desirable cell populations, enhance the uptake of antigens and adjuvants by APCs, and facilitate endosomal release of an antigen and stimulate its cross-presentation in the cytosol (99–102).

Medicago's plant-derived VLPs can be thought of as biological nanoparticles that have been developed as antigen delivery vectors for influenza HA protein (6,7,103,104). VLPs demonstrated exciting potential for eliciting robust and diverse immune responses, and can be

designed to enable their visualization and tracking, expression of specific components of pathogens and targeting the desirable cell populations (16,67,105,106).

6.2.2.1 Endocytic cell receptors for plant-derived HA-bearing VLPs

A number of proteins, most of which are C-type lectin receptors, have been proposed to play a role in cell entry by influenza viruses (Chapter 1.2.2.1.1.2 of this thesis). To date however, none has been confirmed to be the 'true' influenza virus receptor. HA serves as the principal intermediary between influenza virions and target cells (79,107,108), and therefore the HA-bearing VLPs may utilize the same cell entry pathways as the viruses.

To address this hypothesis, we used mannan, a complex polymer of mannose residues that has been shown to interfere with influenza virus binding to mannose-specific C-type lectin receptors such as MR and DC-SIGN/L-SIGN (109). We observed a massive inhibition of the H1-VLPs (Fig. 6.4A) and H5-VLPs (Fig. 6.4B) binding and internalization by U-937 cells in the presence of mannan. These experiments suggested that either MR or DC-SIGN may serve as the entry receptor for HA-bearing VLPs on U-937 cells. Next, we applied DiD-labelled H5-VLPs in a mixture with anti-DC-SIGN monoclonal antibody (clone 120612) at 4°C (to prevent receptor internalization upon antibody binding) and again found a strong blocking effect of the antibody on the VLPs' surface binding (Fig. 6.4C).

These preliminary results suggest that, indeed, MR or DC-SIGN may facilitate VLP binding and endocytosis by U-937 cells. However, we believe that it is unlikely that only one or two molecules ultimately serve as the receptors for influenza virus or HA-VLP entry into target cells. Rather, it seems likely that multiple molecules act in concert to facilitate HA-mediated uptake. Different cell types may utilize alternative entry receptors, and the ligand – receptor binding specificity can be affected by the type of HA (i.e. H1-, H3-, H5- or H7-VLPs) or through the HA glycosylation profile. Moreover, modified HA glycosylation on the VLPs may help to target them to the specific entry receptor and cell type, achieving the desirable immune responses. Therefore, studying the influenza entry receptors has both fundamental and practical implications. We can apply different blocking agents such as polysaccharides or monoclonal antibodies against the putative entry receptors, or try to down-regulate the expression of these receptors; however, proteomic methods like those we used to study the MHC I-restricted

immunopeptidome (Chapters 3 and 4 of this thesis) may be more efficient in characterizing the influenza virus/HA-VLP endocytic receptor pool.

6.2.2.2 Plant-derived VLPs as intracellular delivery nanocarriers

We observed a rapid and massive internalization of plant-derived HA-bearing VLPs by U-937 cells, primary human MDMs and MDDCs (Chapters 2, 3 and 6.2.1.1). This prompted us to test VLPs as nanocarriers for a cargo intracellular delivery. We used STAT6 inhibitory peptide (STAT6-IP) – cell penetrating peptide construct (110) as a model cargo for 'loading' the HA-VLPs.

In our preliminary experiments, H1-VLPs incubation with nine-arginine-based STAT6-IP resulted in a physical association of the peptide with VLPs that was detected by Western blotting (Fig. 6.5). These results offer the intriguing possibility of using plant-derived VLPs for targeted intracellular delivery of bioactive molecules that have the potential to modify the magnitude and shift the Th1/Th2-balance of immune responses.

6.2.3 The establishment of novel correlates of protection against influenza

The influenza vaccine landscape is rapidly changing with introducing new products that differ from the 'traditional' vaccines by the nature of antigen (LAIV, viral vectors, VLPs), origin of immunogen (DNA, RNA, recombinant proteins), adjuvants, manufacturing platform (insect and mammalian cell-based vaccines, plant-derived VLPs) (12,68,111,112). Novel vaccine candidates eliciting broadly-neutralizing and cross-reactive serum anti-HA antibodies as well as mucosal IgA, antibodies targeting NA and influenza core proteins, and cell-mediated immunity are under development (20,26,113,114). However, vaccine licensure is primarily based on the traditional serological assays described in Chapter 1.3.2 of this thesis. Alternative methods for the assessment of immunogenicity are needed to meet the challenge arising from rapidly expanding vaccine development and manufacturing programs (40–42).

6.2.3.1 Advancement in serological assessment of the influenza vaccine response

We proposed a novel serological assay for influenza based on DiD fluorescence dequenching upon fusion of the labelled virions with RBC membranes (Chapter 5 of the thesis). We believe that the DiD dequenching-based assay may be measuring different types of

functional antibodies such as those that prevent binding of virions to target cells or interfere with the HA conformation change and viral envelope fusion with target cells. After comparing the results obtained with high-agglutinating vs. low-agglutinating influenza strains, we think that the informativeness of DiD dequenching assay can be increased by a more detailed evaluation of the curves generated (i.e. the angle between descending part and plateau of the acidified curve, the distance between the non-acidified curve and the plateau of acidified curve etc.), and that the mathematical examination of the curves could be made more accurate. To achieve these goals, a number of additional experiments should be performed, namely:

- Testing the assay performance with more high-agglutinating and low-agglutinating influenza strains;
- Increasing the number of samples to at least 100 – 200 for each virus strain;
- Comparing the DiD dequenching assay titers not only with HAI and MN titers but also with total serum anti-influenza IgG (measured by ELISA);
- Drawing the DiD fluorescence curves with narrowed serum dilution steps (i.e. 30 dilution points within the range 1:10 to 1:1280).

Based on these data, we may be able to develop a unified algorithm for interpretation of the results that would perform equally well with any influenza strain and provide insight into the type of protective anti-influenza antibodies measured.

6.3 CONCLUDING REMARKS

We live in an exciting time. The novel preventive and therapeutic approaches create tremendous hope for full control of the influenza infection. In this thesis, we explored the mechanisms of immunogenicity of plant-derived influenza HA-bearing VLP-based vaccine candidate developed by Medicago Inc. Unlike many other vaccines, these plant-derived VLPs can elicit a broad spectrum of immune responses, including robust production of antibodies that are cross-reactive, and transitional and effector memory $CD4^+$ T cells that are polyfunctional and also cross-reactive. The main finding of this thesis is that influenza HA delivered in the form of VLPs can be cross-presented by human APCs. This observation is, however, only the starting point for further studies of the mechanisms underlying the unusual immunological features of VLPs.

6.4 REFERENCES

1. Mohn KG-I, Smith I, Sjursen H, Cox R. Immune responses after live attenuated influenza vaccination. Hum Vaccin Immunother. 2018;14(3):571–8.
2. KPMG LLP. Succeeding in a commoditised market. Lessons from the US influenza vaccine market. 2017. Available from: https://assets.kpmg.com/content/dam/kpmg/uk/pdf/2017/05/influenza-vaccines-rethinking-life-sciences.pdf
3. PR Newswire Association LLC. Global Influenza Vaccine Markets 2017-2023 - Major Players for the $4.6 Bn Market are Seqirus, GlaxoSmithKilne, Sanofi Pasteur, and Merck Sharp & Dohme. 2017. Available from: https://www.prnewswire.com/news-releases/global-influenza-vaccine-markets-2017-2023---major-players-for-the-46-bn-market-are-seqirus-glaxosmithkilne-sanofi-pasteur-and-merck-sharp--dohme-300573165.html
4. Grohskopf LA, Sokolow LZ, Broder KR, Walter EB, Bresee JS, Fry AM, et al. Prevention and Control of Seasonal Influenza with Vaccines: Recommendations of the Advisory Committee on Immunization Practices — United States, 2017–18 Influenza Season. MMWR Recomm Reports. 2017;66(2):1–20.
5. Le Mauff F, Mercier G, Chan P, Burel C, Vaudry D, Bardor M, et al. Biochemical composition of haemagglutinin-based influenza virus-like particle vaccine produced by transient expression in tobacco plants. Plant Biotechnol J. 2015;13(5):717–25.
6. D'Aoust MA, Lavoie PO, Couture MMJ, Trépanier S, Guay JM, Dargis M, et al. Influenza virus-like particles produced by transient expression in Nicotiana benthamiana induce a protective immune response against a lethal viral challenge in mice. Plant Biotechnol J. 2008;6(9):930–40.
7. D'Aoust MA, Couture MMJ, Charland N, Trépanier S, Landry N, Ors F, et al. The production of hemagglutinin-based virus-like particles in plants: A rapid, efficient and safe response to pandemic influenza. Plant Biotechnol J. 2010;8(5):607–19.
8. Zost SJ, Parkhouse K, Gumina ME, Kim K, Diaz Perez S, Wilson PC, et al. Contemporary H3N2 influenza viruses have a glycosylation site that alters binding of antibodies elicited by egg-adapted vaccine strains. Proc Natl Acad Sci. 2017;114(47):201712377.
9. Skowronski DM, Chambers C, De Serres G, Dickinson JA, Winter AL, Hickman R, et al.

Early season co-circulation of influenza a(H3N2) and b(yamagata): Interim estimates of 2017/18 vaccine effectiveness, Canada, January 2018. Eurosurveillance. 2018;23(5).

10. Flannery B, Chung JR, Belongia EA, McLean HQ, Gaglani M, Murthy K, et al. Interim estimates of 2017–18 seasonal influenza vaccine effectiveness — United States, February 2018. Am J Transplant. 2018;18(4):1020–5.
11. Sullivan SG, Chilver MB, Carville KS, Deng Y-M, Grant KA, Higgins G, et al. Low interim influenza vaccine effectiveness, Australia, 1 May to 24 September 2017. Eurosurveillance. 2017;22(43).
12. Lambert LC, Fauci AS. Influenza Vaccines for the Future. N Engl J Med. 2010;363(21):2036–44.
13. Milián E, Kamen AA. Current and emerging cell culture manufacturing technologies for influenza vaccines. BioMed Research International. 2015;2015:1–11.
14. Houser K, Subbarao K. Influenza vaccines: Challenges and solutions. Cell Host Microbe. 2015;17(3):295–300.
15. Moro PL, Winiecki S, Lewis P, Shimabukuro TT, Cano M. Surveillance of adverse events after the first trivalent inactivated influenza vaccine produced in mammalian cell culture (Flucelvax®) reported to the Vaccine Adverse Event Reporting System (VAERS), United States, 2013-2015. Vaccine. 2015;33(48):6684–8.
16. Marsian J, Lomonossoff GP. Molecular pharming-VLPs made in plants. Current Opinion in Biotechnology. 2016;37:201–6.
17. Chotpitayasunondh T, Thisyakorn U, Pancharoen C, Pepin S, Nougarede N. Safety, humoral and cell mediated immune responses to two formulations of an inactivated, split-virion influenza A/H5N1 vaccine in children. PLoS One. 2008;3(12):e4028.
18. Christensen D, Christensen JP, Korsholm KS, Isling LK, Erneholm K, Thomsen AR, et al. Seasonal influenza split vaccines confer partial cross-protection against heterologous influenza virus in ferrets when combined with the CAF01 adjuvant. Front Immunol. 2018;8:1928.
19. He X-S, Holmes TH, Zhang C, Mahmood K, Kemble GW, Lewis DB, et al. Cellular Immune Responses in Children and Adults Receiving Inactivated or Live Attenuated Influenza Vaccines. J Virol. 2006;80(23):11756–66.
20. Jang YH, Seong BL. Cross-protective immune responses elicited by live attenuated

influenza vaccines. Yonsei Med J. 2013;54(2):271–82.

21. Landry N, Pillet S, Favre D, Poulin JF, Trépanier S, Yassine-Diab B, et al. Influenza virus-like particle vaccines made in Nicotiana benthamiana elicit durable, poly-functional and cross-reactive T cell responses to influenza HA antigens. Clin Immunol. 2014;154(2):164–77.
22. Pillet S, Racine T, Nfon C, Di Lenardo TZ, Babiuk S, Ward BJ, et al. Plant-derived H7 VLP vaccine elicits protective immune response against H7N9 influenza virus in mice and ferrets. Vaccine. 2015;33(46):6282–9.
23. Pillet S, Aubin É, Trépanier S, Poulin JF, Yassine-Diab B, Ter Meulen J, et al. Humoral and cell-mediated immune responses to H5N1 plant-made virus-like particle vaccine are differentially impacted by alum and GLA-SE adjuvants in a Phase 2 clinical trial. npj Vaccines. 2018;3:3.
24. Pillet S, Aubin É, Trépanier S, Bussière D, Dargis M, Poulin JF, et al. A plant-derived quadrivalent virus like particle influenza vaccine induces cross-reactive antibody and T cell response in healthy adults. Clin Immunol. 2016;168:72–87.
25. Hodgins B, Yam KK, Winter K, Pillet S, Landry N, Ward BJ. A single intramuscular dose of a plant-made virus-like particle vaccine elicits a balanced humoral and cellular response and protects young and aged mice from influenza H1N1 virus challenge despite a modest/absent humoral response. Clin Vaccine Immunol. 2017;24(12):1–14.
26. Wong S-S, Webby RJ. Traditional and New Influenza Vaccines. Clin Microbiol Rev. 2013;26(3):476–92.
27. Hoft DF, Babusis E, Worku S, Spencer CT, Lottenbach K, Truscott SM, et al. Live and inactivated influenza vaccines induce similar humoral responses, but only live vaccines induce diverse T-cell responses in young children. J Infect Dis. 2011;204(6):845–53.
28. Spitaels J, Roose K, Saelens X. Influenza and Memory T Cells: How to Awake the Force. Vaccines. 2016;4(4):33.
29. Clemens E, van de Sandt C, Wong S, Wakim L, Valkenburg S. Harnessing the Power of T Cells: The Promising Hope for a Universal Influenza Vaccine. Vaccines. 2018;6(2):18.
30. Grant EJ, Quinõnes-Parra SM, Clemens EB, Kedzierska K. Human influenza viruses and CD8+T cell responses. Curr Opin Virol. 2016;16:132–42.
31. Sridhar S, Begom S, Bermingham A, Hoschler K, Adamson W, Carman W, et al. Cellular

immune correlates of protection against symptomatic pandemic influenza. Nat Med. 2013;19(10):1305–12.

32. Wang Z, Wan Y, Qiu C, Quiñones-Parra S, Zhu Z, Loh L, et al. Recovery from severe H7N9 disease is associated with diverse response mechanisms dominated by CD8+ T cells. Nat Commun. 2015;6:6833.
33. Pera A, Campos C, López N, Hassouneh F, Alonso C, Tarazona R, et al. Immunosenescence: Implications for response to infection and vaccination in older people. Maturitas. 2015;82(1):50–5.
34. Johnstone J, Millar J, Lelic A, Verschoor CP, Walter SD, Devereaux PJ, et al. Immunosenescence in the nursing home elderly. BMC Geriatr. 2014;14(1):50.
35. Van Braeckel-Budimir N, Harty JT. Influenza-induced lung T rm: Not all memories last forever. Immunol Cell Biol. 2017;95(8):651–5.
36. Pizzolla A, Nguyen THO, Sant S, Jaffar J, Loudovaris T, Mannering SI, et al. Influenza-specific lung-resident memory t cells are proliferative and polyfunctional and maintain diverse TCR profiles. J Clin Invest. 2018;128(2):721–33.
37. van de Sandt CE, Hillaire MLB, Geelhoed-Mieras MM, Osterhaus ADME, Fouchier RAM, Rimmelzwaan GF. Human Influenza A Virus-Specific CD8+ T-Cell Response Is Long-lived. J Infect Dis. 2015;212(1):81–5.
38. Valkenburg SA, Venturi V, Dang THY, Bird NL, Doherty PC, Turner SJ, et al. Early priming minimizes the age-related immune compromise of CD8+ T cell diversity and function. PLoS Pathog. 2012;8(2):e1002544.
39. Lindsay BJ, Bonar MM, Costas-Cancelas IN, Hunt K, Makarkov AI, Chierzi S, et al. Morphological characterization of a plant-made virus-like particle vaccine bearing influenza virus hemagglutinins by electron microscopy. Vaccine. 2018;36(16):2147–54.
40. Ward BJ, Pillet S, Charland N, Trepanier S, Couillard J, Landry N. The establishment of surrogates and correlates of protection: Useful tools for the licensure of effective influenza vaccines? Hum Vaccines Immunother. 2018;14(3):647–56.
41. Reber A, Katz J. Immunological assessment of influenza vaccines and immune correlates of protection. Expert Review of Vaccines. 2013;12:519–36.
42. McCullers JA, Huber VC. Correlates of vaccine protection from influenza and its complications. Hum Vaccines Immunother. 2012;8(1):34–44.

43. Bernhard CA, Ried C, Kochanek S, Brocker T. CD169 + macrophages are sufficient for priming of CTLs with specificities left out by cross-priming dendritic cells. Proc Natl Acad Sci. 2015 Apr 28;112(17):5461–6.
44. Brayer J, Cheng F, Wang H, Horna P, Vicente-Suarez I, Pinilla-Ibarz J, et al. Enhanced CD8 T cell cross-presentation by macrophages with targeted disruption of STAT3. Immunol Lett. 2010;131(2):126–30.
45. Dinter J, Duong E, Lai NY, Berberich MJ, Kourjian G, Bracho-Sanchez E, et al. Variable Processing and Cross-presentation of HIV by Dendritic Cells and Macrophages Shapes CTL Immunodominance and Immune Escape. PLoS Pathog. 2015;11(3):1–22.
46. Adiko AC, Babdor J, Gutiérrez-Martínez E, Guermonprez P, Saveanu L. Intracellular transport routes for MHC I and their relevance for antigen cross-presentation. Front Immunol. 2015;6:1–11.
47. Mintern JD, Macri C, Villadangos JA. Modulation of antigen presentation by intracellular trafficking. Curr Opin Immunol. 2015;34:16–21.
48. Zou L, Zhou J, Zhang J, Li J, Liu N, Chai L, et al. The GTPase Rab3b/3c-positive recycling vesicles are involved in cross-presentation in dendritic cells. Proc Natl Acad Sci U S A. 2009;106(37):15801–6.
49. Blander JM. Regulation of the Cell Biology of Antigen Cross Presentation. Annu Rev Immunol. 2018;36:717-53.
50. Gutiérrez-Martínez E, Planès R, Anselmi G, Reynolds M, Menezes S, Adiko AC, et al. Cross-presentation of cell-associated antigens by MHC class I in dendritic cell subsets. Front Immunol. 2015;6:363.
51. Norbury CC. Defining cross presentation for a wider audience. Curr Opin Immunol. 2016;40:110–6.
52. Kobayashi H, Fukuda M. Arf6, Rab11 and transferrin receptor define distinct populations of recycling endosomes. Commun Integr Biol. 2013;6(5):10–3.
53. Segura E, Durand M, Amigorena S. Similar antigen cross-presentation capacity and phagocytic functions in all freshly isolated human lymphoid organ–resident dendritic cells. J Exp Med. 2013;210(5):1035–47.
54. Zehner M, Marschall AL, Bos E, Schloetel JG, Kreer C, Fehrenschild D, et al. The Translocon Protein Sec61 Mediates Antigen Transport from Endosomes in the Cytosol for

Cross-Presentation to CD8$^+$ T Cells. Immunity. 2015;42(5):850–63.

55. Zehner M, Burgdorf S. Regulation of antigen transport into the cytosol for cross-presentation by ubiquitination of the mannose receptor. Molecular Immunology. 2013;55:146–8.

56. Savina A, Jancic C, Hugues S, Guermonprez P, Vargas P, Moura IC, et al. NOX2 Controls Phagosomal pH to Regulate Antigen Processing during Crosspresentation by Dendritic Cells. Cell. 2006;126(1):205–18.

57. Mantegazza AR, Savina A, Vermeulen M, Pérez L, Geffner J, Hermine O, et al. NADPH oxidase controls phagosomal pH and antigen cross-presentation in human dendritic cells. Blood. 2008;112(12):4712–22.

58. Segura E, Amigorena S. Cross-presentation by human dendritic cell subsets. Immunology Letters. 2014;158:73–8.

59. Joffre OP, Segura E, Savina A, Amigorena S. Cross-presentation by dendritic cells. Nature Reviews Immunology. 2012;12:557–69.

60. Segura E, Amigorena S. Cross-Presentation in Mouse and Human Dendritic Cells. Advances in Immunology. 2015;127:1–31.

61. Soema PC, Kompier R, Amorij JP, Kersten GFA. Current and next generation influenza vaccines: Formulation and production strategies. Eur J Pharm Biopharm. 2015;94:251–63.

62. Nafziger AN, Pratt DS. Seasonal influenza vaccination and technologies. J Clin Pharmacol. 2014;54(7):719–31.

63. Grant EJ, Chen L, Quinones-Parra S, Pang K, Kedzierska K, Chen W. T-Cell Immunity to Influenza A Viruses. Crit Rev Immunol. 2014;34(1):15–39.

64. Hendin HE, Pillet S, Lara AN, Wu CY, Charland N, Landry N, et al. Plant-made virus-like particle vaccines bearing the hemagglutinin of either seasonal (H1) or avian (H5) influenza have distinct patterns of interaction with human immune cells in vitro. Vaccine. 2017;35(19):2592–9.

65. Lawrence CW, Ream RM, Braciale TJ. Frequency, specificity, and sites of expansion of CD8+ T cells during primary pulmonary influenza virus infection. J Immunol. 2005;174(9):5332–40.

66. Hillaire MLB, van Trierum SE, Bodewes R, van Baalen CA, van Binnendijk RS, Koopmans MP, et al. Characterization of the Human CD8+ T Cell Response following

Infection with 2009 Pandemic Influenza H1N1 Virus. J Virol. 2011;85(22):12057–61.

67. Young KR, Arthus-Cartier G, Yam KK, Lavoie PO, Landry N, D'Aoust MA, et al. Generation and characterization of a trackable plant-made influenza H5 virus-like particle (VLP) containing enhanced green fluorescent protein (eGFP). FASEB J. 2015;29(9):3817–27.
68. Berlanda Scorza F, Tsvetnitsky V, Donnelly JJ. Universal influenza vaccines: Shifting to better vaccines. Vaccine. 2016;34(26):2926–33.
69. Yatim N, Cullen S, Albert ML. Dying cells actively regulate adaptive immune responses. Nat Rev Immunol. 2017;17(4):262–75.
70. Garg AD, Dudek-Peric AM, Romano E, Agostinis P. Immunogenic cell death. Int J Dev Biol. 2015;59(1–3):131–40.
71. Hartmann BM, Albrecht RA, Zaslavsky E, Nudelman G, Pincas H, Marjanovic N, et al. Pandemic H1N1 influenza A viruses suppress immunogenic RIPK3-driven dendritic cell death. Nat Commun. 2017;8(1):1931.
72. Albert ML, Sauter B, Bhardwaj N. Dendritic cells acquire antigen from apoptotic cells and induce class I-restricted CTLs. Nature. 1998;392(6671):86–9.
73. Chatziandreou N, Farsakoglu Y, Palomino-Segura M, D'Antuono R, Pizzagalli DU, Sallusto F, et al. Macrophage Death following Influenza Vaccination Initiates the Inflammatory Response that Promotes Dendritic Cell Function in the Draining Lymph Node. Cell Rep. 2017;18(10):2427–40.
74. Tran AT, Cortens JP, Du Q, Wilkins JA, Coombs KM. Influenza Virus Induces Apoptosis via BAD-Mediated Mitochondrial Dysregulation. J Virol. 2013;87(2):1049–60.
75. Shim J, Kim J, Tenson T, Min J-Y, Kainov D. Influenza Virus Infection, Interferon Response, Viral Counter-Response, and Apoptosis. Viruses. 2017;9(8):223.
76. Downey J, Pernet E, Coulombe F, Divangahi M. Dissecting host cell death programs in the pathogenesis of influenza. Microbes Infect. 2018; doi: 10.1016/j.micinf.2018.03.005.
77. György B, Szabó TG, Pásztói M, Pál Z, Misják P, Aradi B, et al. Membrane vesicles, current state-of-the-art: Emerging role of extracellular vesicles. Cellular and Molecular Life Sciences. 2011;68:2667–88.
78. Ato M, Takahashi Y, Fujii H, Hashimoto S ichi, Kaji T, Itamura S, et al. Influenza A whole virion vaccine induces a rapid reduction of peripheral blood leukocytes via

interferon-α-dependent apoptosis. Vaccine. 2013;31(17):2184–90.
79. Fontana J, Steven AC. Influenza virus-mediated membrane fusion: Structural insights from electron microscopy. Archives of Biochemistry and Biophysics. 2015;581:86–97.
80. Matlin KS, Reggio H, Helenius A, Simons K. Infectious entry pathway of influenza virus in a canine kidney cell line. J Cell Biol. 1981;91(3 Pt 1):601–13.
81. Harrison SC. Viral membrane fusion. Virology. 2015;479-480:498–507.
82. Marsh M, Helenius A. Virus entry: Open sesame. Cell. 2006;124:729–40.
83. Hare D, Mossman KL. Novel paradigms of innate immune sensing of viral infections. Cytokine. 2013;63(3):219–24.
84. Schoggins JW, Randall G. Lipids in innate antiviral defense. Cell Host and Microbe. 2013;14:379–85.
85. Paladino P, Cummings DT, Noyce RS, Mossman KL. The IFN-Independent Response to Virus Particle Entry Provides a First Line of Antiviral Defense That Is Independent of TLRs and Retinoic Acid-Inducible Gene I. J Immunol. 2006;177(11):8008–16.
86. Noyce RS, Taylor K, Ciechonska M, Collins SE, Duncan R, Mossman KL. Membrane Perturbation Elicits an IRF3-Dependent, Interferon-Independent Antiviral Response. J Virol. 2011;85(20):10926–31.
87. Holm CK, Jensen SB, Jakobsen MR, Cheshenko N, Horan KA, Moeller HB, et al. Virus-cell fusion as a trigger of innate immunity dependent on the adaptor STING. Nat Immunol. 2012;13(8):737–43.
88. Holm CK, Rahbek SH, Gad HH, Bak RO, Jakobsen MR, Jiang Z, et al. Influenza A virus targets a cGAS-independent STING pathway that controls enveloped RNA viruses. Nat Commun. 2016;7:1–9.
89. Le Bon A, Tough DF. Links between innate and adaptive immunity via type I interferon. Current Opinion in Immunology. 2002;14:432–6.
90. Tough DF. Type I Interferon as a Link Between Innate and Adaptive Immunity through Dendritic Cell Stimulation. Leuk Lymphoma. 2004;45(2):257–64.
91. Vatner RE, Janssen EM. STING, DCs and the link between innate and adaptive tumor immunity. Molecular Immunology. 2017: doi: 10.1016/j.molimm.2017.12.001.
92. Cruz FM, Colbert JD, Merino E, Kriegsman BA, Rock KL. The Biology and Underlying Mechanisms of Cross-Presentation of Exogenous Antigens on MHC-I Molecules. Annu

Rev Immunol. 2017;35(1):149–76.

93. Dingjan I, Verboogen DRJ, Paardekooper LM, Revelo NH, Sittig SP, Visser LJ, et al. Lipid peroxidation causes endosomal antigen release for cross-presentation. Sci Rep. 2016;6:1–12.

94. Lirussi D, Ebensen T, Schulze K, Trittel S, Duran V, Liebich I, et al. Type I IFN and not TNF, is Essential for Cyclic Di-nucleotide-elicited CTL by a Cytosolic Cross-presentation Pathway. EBioMedicine. 2017;22:100–11.

95. Ahn J, Xia T, Rabasa Capote A, Betancourt D, Barber GN. Extrinsic Phagocyte-Dependent STING Signaling Dictates the Immunogenicity of Dying Cells. Cancer Cell . 2018;33(5):862–873.e5.

96. Silva JM, Vandermeulen G, Oliveira VG, Pinto SN, Rodrigues C, Salgado A, et al. Development of functionalized nanoparticles for vaccine delivery to dendritic cells: a mechanistic approach. Nanomedicine. 2014;9(17):2639–56.

97. Yameen B, Choi W Il, Vilos C, Swami A, Shi J, Farokhzad OC. Insight into nanoparticle cellular uptake and intracellular targeting. J Control Release. 2014;190:485–99.

98. Li Z, Sun L, Zhang Y, Dove AP, O'Reilly RK, Chen G. Shape Effect of Glyco-Nanoparticles on Macrophage Cellular Uptake and Immune Response. ACS Macro Lett. 2016;5(9):1059–64.

99. Petrizzo A, Conte C, Tagliamonte M, Napolitano M, Bifulco K, Carriero V, et al. Functional characterization of biodegradable nanoparticles as antigen delivery system. J Exp Clin Cancer Res. 2015;34(1):114.

100. Kuhn DA, Vanhecke D, Michen B, Blank F, Gehr P, Petri-Fink A, et al. Different endocytotic uptake mechanisms for nanoparticles in epithelial cells and macrophages. Beilstein J Nanotechnol. 2014;5(1):1625–36.

101. Zaki NM, Tirelli N. Gateways for the intracellular access of nanocarriers: a review of receptor-mediated endocytosis mechanisms and of strategies in receptor targeting. Expert Opin Drug Deliv. 2010;7(8):895–913.

102. Zhang J, Zhang X, Liu G, Chang D, Liang X, Zhu X, et al. Intracellular trafficking network of protein nanocapsules: Endocytosis, exocytosis and autophagy. Theranostics. 2016;6(12):2099–113.

103. Scotti N, Rybicki EP. Virus-like particles produced in plants as potential vaccines. Expert

Rev Vaccines. 2013;12(2):211–24.

104. Chen Q, Lai H. Plant-derived virus-like particles as vaccines. Hum Vaccines Immunother. 2013;9(1):26–49.
105. Kim HS, Jeon JH, Lee KJ, Ko K. N-glycosylation modification of plant-derived virus-like particles: An application in vaccines. Biomed Res Int. 2014;2014:249519.
106. Steele JFC, Peyret H, Saunders K, Castells-Graells R, Marsian J, Meshcheriakova Y, et al. Synthetic plant virology for nanobiotechnology and nanomedicine. Wiley Interdiscip Rev Nanomedicine Nanobiotechnology. 2017;9(4):1–18.
107. Luo M. Influenza virus entry. Adv Exp Med Biol. 2012;726:201–21.
108. Byrd-Leotis L, Cummings RD, Steinhauer DA. The interplay between the host receptor and influenza virus hemagglutinin and neuraminidase. International Journal of Molecular Sciences. 2017;18:1541.
109. Londrigan SL, Tate MD, Brooks AG, Reading PC. Cell-surface receptors on macrophages and dendritic cells for attachment and entry of influenza virus. J Leukoc Biol. 2012;92(1):97–106.
110. McCusker CT, Wang Y, Shan J, Kinyanjui MW, Villeneuve A, Michael H, et al. Inhibition of Experimental Allergic Airways Disease by Local Application of a Cell-Penetrating Dominant-Negative STAT-6 Peptide. J Immunol. 2007;179(4):2556–64.
111. Tregoning JS, Russell RF, Kinnear E. Adjuvanted influenza vaccines. Hum Vaccines Immunother. 2018;14(3):550–64.
112. Sautto GA, Kirchenbaum GA, Ross TM. Towards a universal influenza vaccine: Different approaches for one goal. Virol J. 2018;15(1):1–12.
113. Barría MI, Garrido JL, Stein C, Scher E, Ge Y, Engel SM, et al. Localized mucosal response to intranasal live attenuated influenza vaccine in adults. J Infect Dis. 2013;207(1):115–24.
114. Mcelhaney JE, Coler RN, Baldwin SL. Immunologic correlates of protection and potential role for adjuvants to improve influenza vaccines in older adults. Expert Review of Vaccines. 2013;12:759–66.

6.5 FIGURES AND FIGURE LEGENDS

A

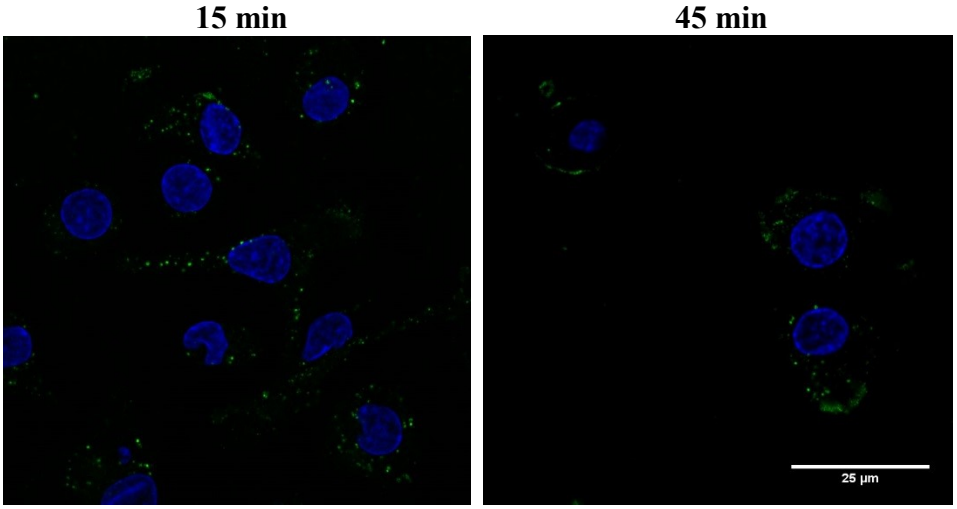

B

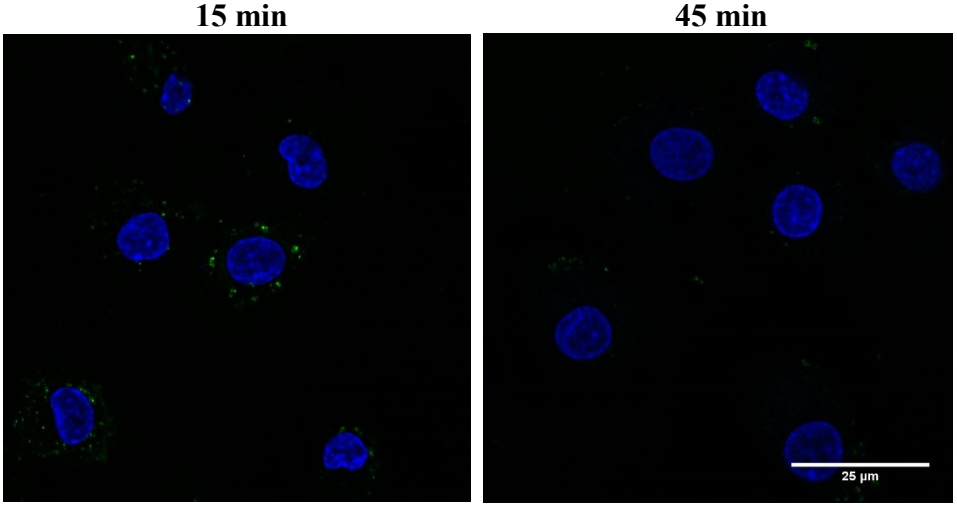

C

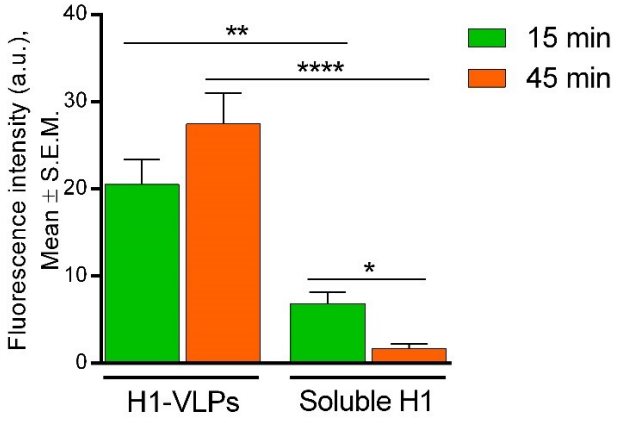

D

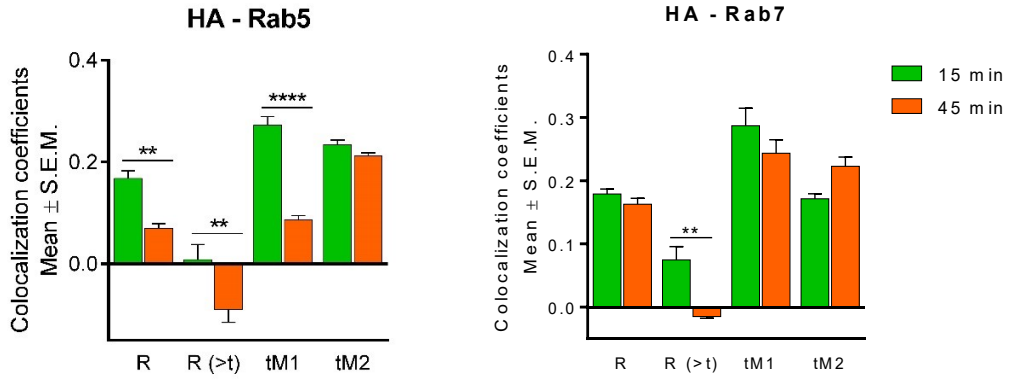

E

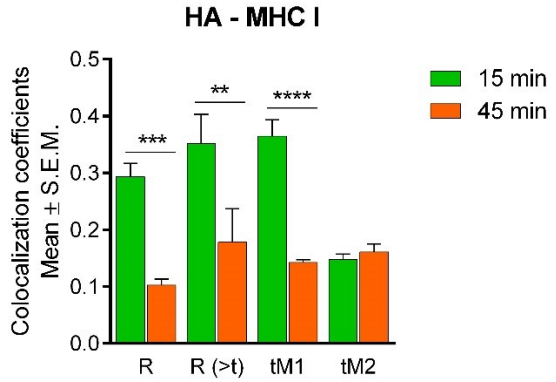

Figure 6. 1. Intracellular HA distribution in primary human MDDCs exposed to H1-VLPs or soluble H1

(A) and (B) Representative images of MDDCs pulsed (15 min) with either H1-VLPs (A) or soluble H1 (B) at 15 min and 45 min. Green: immunofluorescent staining of HA, blue: nuclei stained with DAPI. (C) HA internalization and degradation by MDDCs pulsed (15 min) with either H1-VLPs or soluble H1. The amount of internalized protein was evaluated by the intensity of HA immunofluorescence per cell area on confocal microscopy images at 15 min and 45 min; 35 cells per group were analyzed. (D) and (E) Analysis of HA colocalization with endosomal markers Rab5 and Rab7 (D) or MHC I (E) in MDDCs pulsed (15 min) with H1-VLPs at 15 min and 45 min; 6 cell-defined ROIs/images per group were analyzed. * $p<0.05$, ** $p<0.01$, *** $p<0.001$, **** $p<0.0001$.

Contribution of authors: these experiments were planned, performed, and the results were analyzed by Alexander I. Makarkov.

A

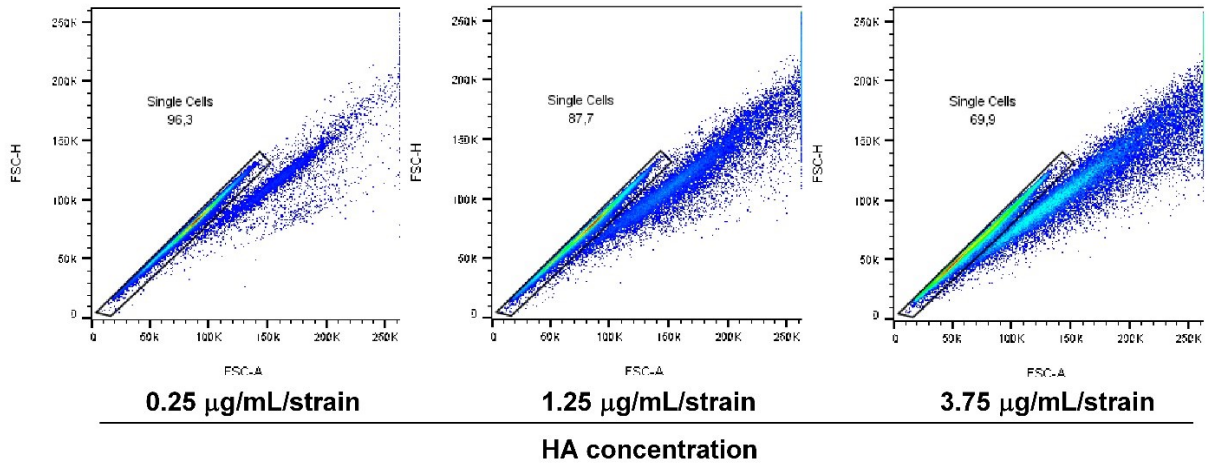
Single Cells
96,3
Single Cells
87,7
Single Cells
69,9
FSC-H
FSC-A
0.25 µg/mL/strain
1.25 µg/mL/strain
3.75 µg/mL/strain
HA concentration

B

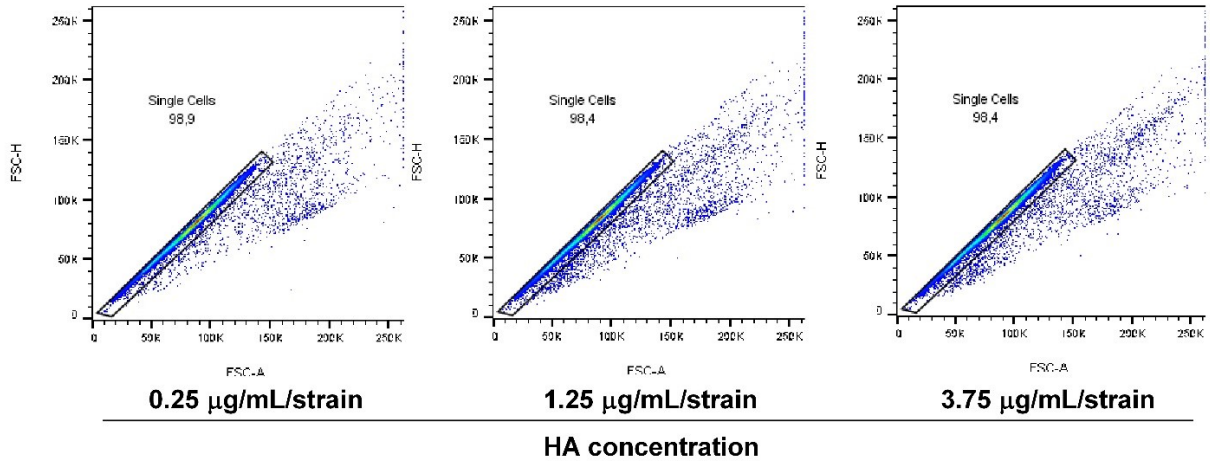
Single Cells
98,9
Single Cells
98,4
Single Cells
98,4
FSC-H
FSC-A
0.25 µg/mL/strain
1.25 µg/mL/strain
3.75 µg/mL/strain
HA concentration

C

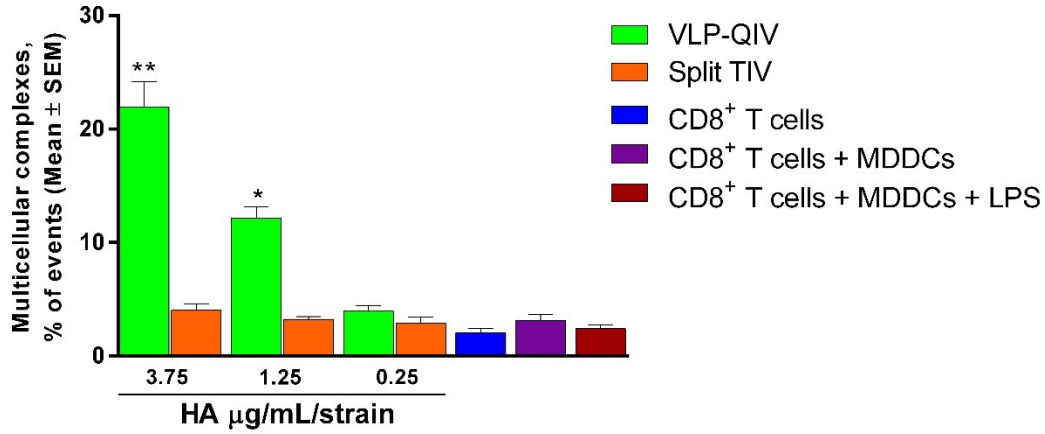
Multicellular complexes,
% of events (Mean ± SEM)
30
20
10
0
**
*
3.75
1.25
0.25
HA µg/mL/strain
VLP-QIV
Split TIV
CD8+ T cells
CD8+ T cells + MDDCs
CD8+ T cells + MDDCs + LPS

D

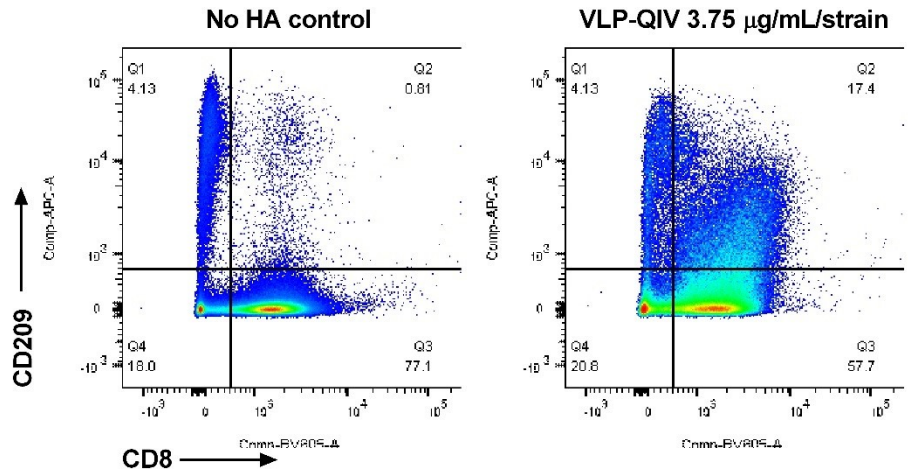

Figure 6. 2. MDDCs exposure to quadrivalent seasonal VLP-based vaccine caused formation of multicellular clusters upon MDDCs co-culturing with autologous $CD8^+$ T cells

(A) and (B) Single cell population vs. multicellular $CD8^+$ T cell – MDDC complexes formed upon MDDCs exposure to quadrivalent seasonal VLP-based (A) or trivalent split virion vaccine (B) at concentrations 0.25, 1.25 or 3.75 μg/mL/strain (by HA content). (C) Number of multicellular cluster events after $CD8^+$ T cells co-culturing with MDDCs pulsed with enter quadrivalent seasonal VLP-based or trivalent split virion vaccine. Controls: non-stimulated $CD8^+$ T cells; $CD8^+$ T cells co-cultured with non-stimulated MDDCs; $CD8^+$ T cells co-cultured with MDDCs stimulated by *E. coli* lipopolysaccharide (LPS). Based on 5 experiments; * $p<0.05$, ** $p<0.01$, compared to non-stimulated $CD8^+$ T cells. (D) Multicellular clusters formed upon co-culturing of $CD8^+$ T cells with MDDCs pulsed with quadrivalent seasonal VLP-based vaccine express both CD8 and CD209 markers. $CD8^+$ T cells co-cultured with non-stimulated MDDCs – left; $CD8^+$ T cells co-cultured with MDDCs pulsed with quadrivalent seasonal VLP-based vaccine at concentration 3.75 μg/mL/strain (by HA content) - right.

Contribution of authors: these experiments were planned, performed, and the results were analyzed by Alexander I. Makarkov.

A

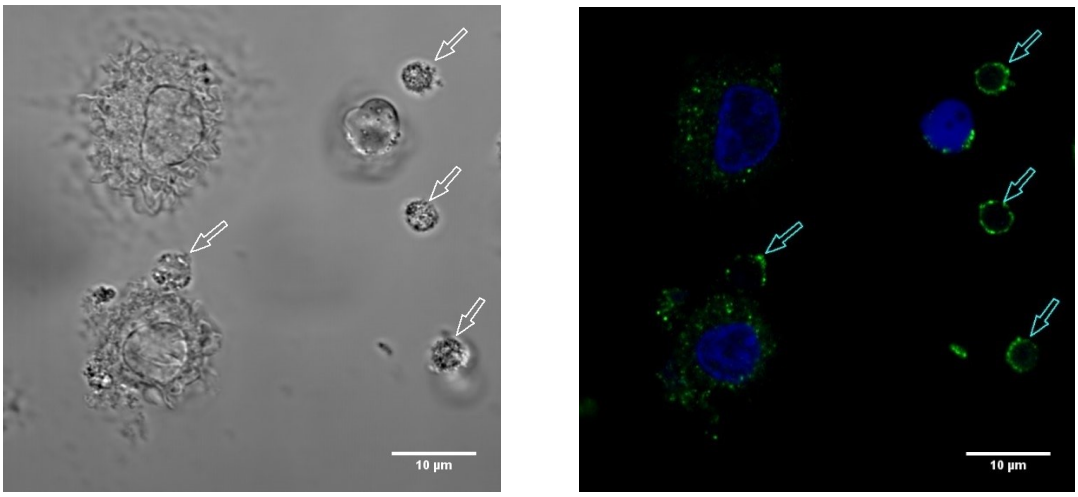
10 µm
10 µm

B

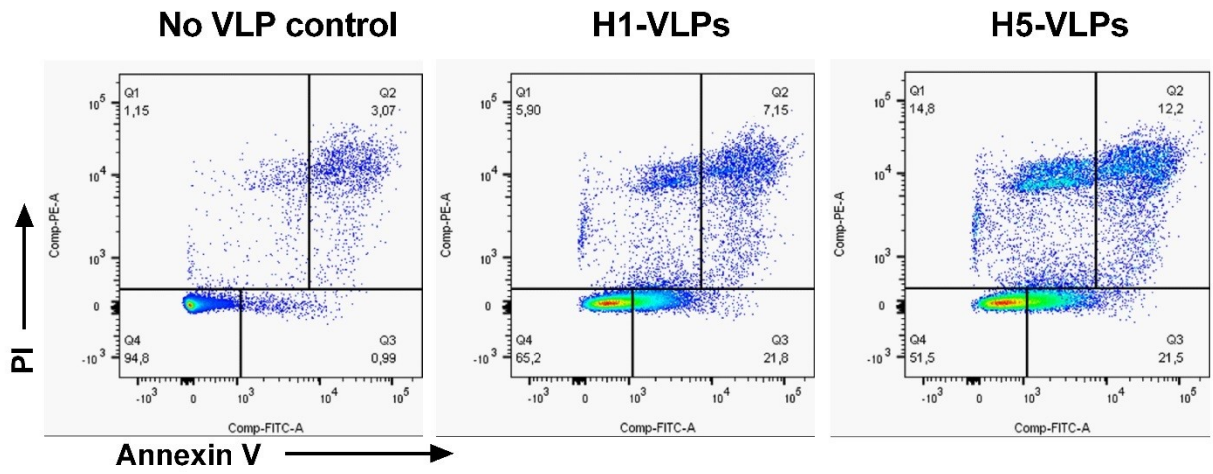
No VLP control
H1-VLPs
H5-VLPs
PI
Annexin V
Comp-PE-A
Comp-FITC-A
Q1 1,15
Q2 3,07
Q4 94,8
Q3 0,99
Q1 5,90
Q2 7,15
Q4 65,2
Q3 21,8
Q1 14,8
Q2 12,2
Q4 51,5
Q3 21,5

C

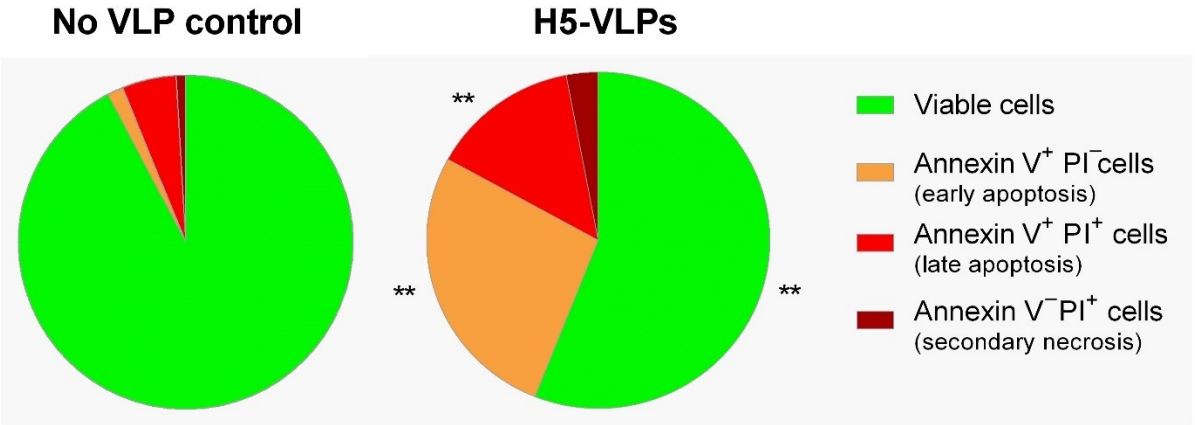
No VLP control
H5-VLPs
**
**
**
Viable cells
Annexin V+ PI− cells
(early apoptosis)
Annexin V+ PI+ cells
(late apoptosis)
Annexin V− PI+ cells
(secondary necrosis)

D

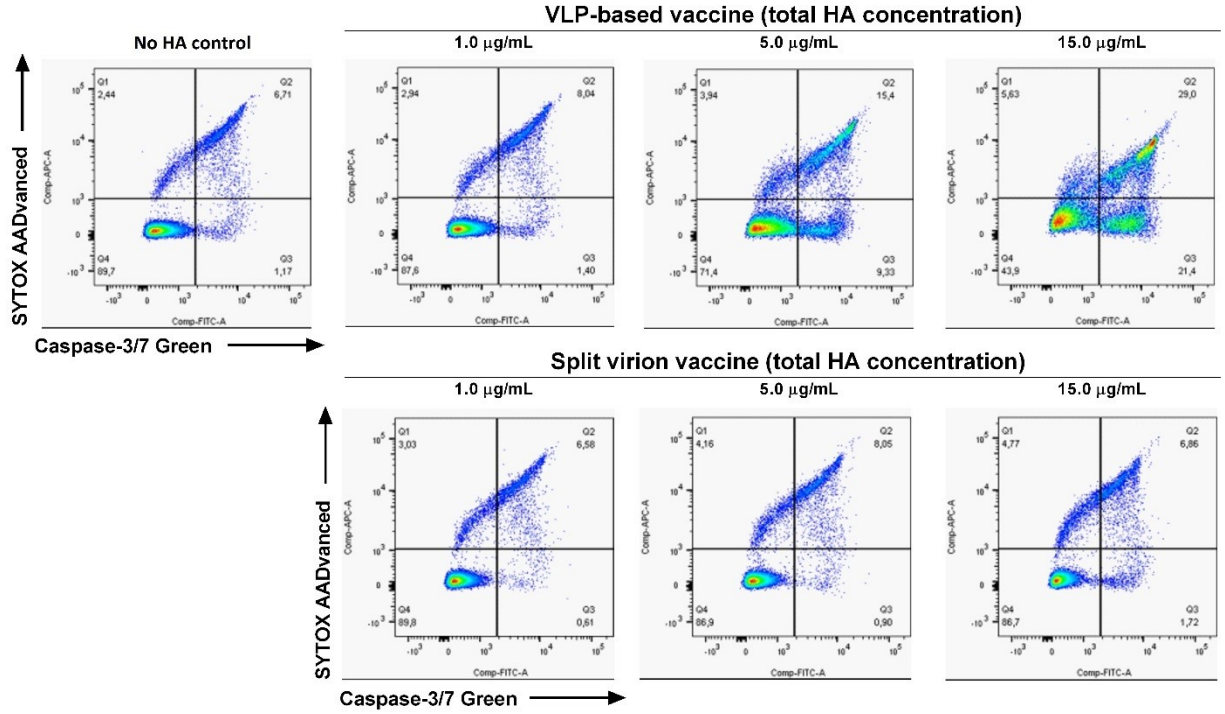

Figure 6. 3. Plant-derived VLPs induce apoptosis of human MDDCs and U-937 cells

(A) MDDCs exposed to H1-VLPs for 45 min. A number of apoptotic body-like objects (indicated by arrows) are seen on the bright field image (left). Accumulation of HA on the surface of apoptotic body-like objects, some of which are interacting with MDDC (right). Green: immunofluorescent staining of HA, blue: nuclei stained with DAPI. (B) U-937 cells exposed to H1- or H5-VLPs (15 µg/mL) for 30 min exhibit different stages of apoptosis. Annexin V and propidium iodide (PI) staining, flow cytometry. (C) H5-VLPs (15 µg/mL, 30 min exposure) caused apoptosis of U-937 cells. Quantification of early apoptotic (Annexin V^+PI^-), late apoptotic (Annexin V^+PI^+) and secondary necrotic (Annexin V^-PI^+) cells. Based on 5 experiments; ** $p<0.01$, compared to U-937 cells that were not exposed to VLPs. (D) U-937 cells apoptosis assessment using CellEvent™ Caspase-3/7 Green flow cytometry assay. U-937 cells exposed to VLP-based quadrivalent influenza vaccine (1.0 to 15.0 µg/mL) for 30 min show dose-dependent increase in the number of early and late apoptotic events. Split virion quadrivalent influenza vaccine did not affect the U-937 cells viability.

Contribution of authors: these experiments were planned, performed, and the results were analyzed by Alexander I. Makarkov.

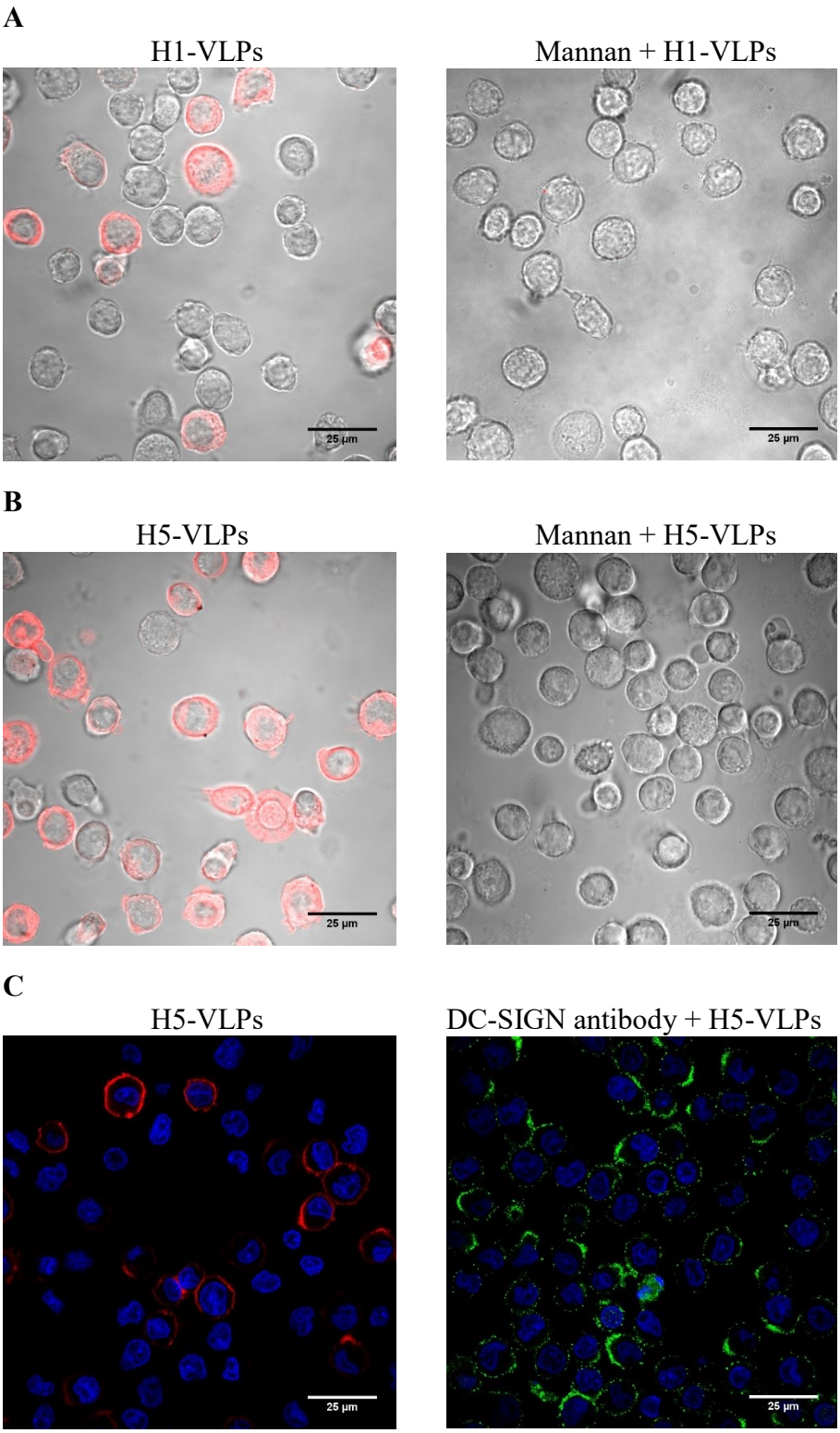

Figure 6. 4. Endocytic cell receptors for plant-derived HA-bearing VLPs

(A) and (B) Representative images of U-937 cells treated with DiD-labelled H1-VLPs (A) or

(legend continued on next page)

H5-VLPs (B) alone (left) or in the presence of mannan (right). Red: DiD-labeled VLPs. (C) Representative images of U-937 cells treated with DiD-labelled H5-VLPs alone (left) or in the mixture with anti-DC-SIGN blocking antibody (right) at 4°C. Red: DiD-labeled VLPs, green: immunofluorescent staining of DC-SIGN, blue: nuclei stained with DAPI.
Contribution of authors: these experiments were planned, performed, and the results were analyzed by Dr. Sabrina Chierzi and Alexander I. Makarkov.

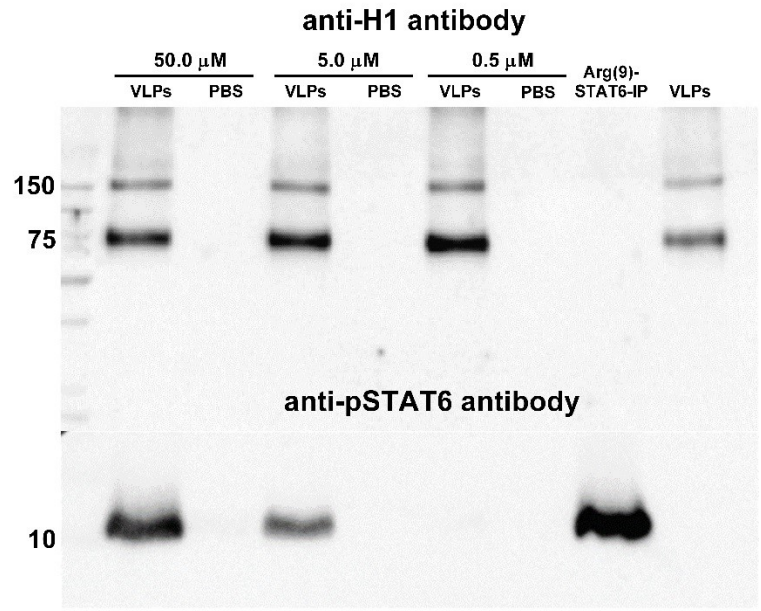

Figure 6. 5. H1-VLPs 'loaded' with STAT6 inhibitory peptide (STAT6-IP)

H1-VLPs were incubated with STAT6-IP (50.0, 5.0 and 0.5 μM) one hour at room temperature and then purified by centrifugation. Western blotting revealed the HA (75 kDa and 150 kDA dimers) and STAT6-IP (~ 10 kDa) bands in VLP samples 'loaded' with STAT6-IP at concentrations 50.0 and 5.0 μM.

Contribution of authors: these experiments were planned, performed, and the results were analyzed by Lingrui Meng and Alexander I. Makarkov.